Rôle des facteurs de transcription Eos et Helios dans la biologie des cellules T régulatrices

Katarzyna Polak

UNIVERSITÉ DE STRASBOURG

ÉCOLE DOCTORALE des Sciences de la Vie et de la Santé
IGBMC - CNRS UMR 7104 - Inserm U 964

THÈSE **présentée par :**

Katarzyna POLAK

soutenue le : 15 Octobre 2015

pour obtenir le grade de : **Docteur de l'université de Strasbourg**
Discipline : Sciences du vivant
Spécialité : Aspects moléculaires et cellulaires de la biologie

Role of the Eos and Helios transcription factors in regulatory T cell biology

Rôle des facteurs de transcription Eos et Helios dans la biologie des cellules T régulatrices

Thèse dirigée par:

Dr. Susan Chan,	DR, Inserm, IGBMC, Illkirch

Rapporteur interne:

Pr. Sylviane Muller	DR, CNRS, IBMC, Strasbourg

Rapporteurs externes:

Dr. Maria-Cristina Cuturi	DR, Inserm, ITUN, Nantes
Dr. Jean-Christophe Bories	DR, Inserm, IUH, Paris

ACKNOWLEDGMENTS

First of all, I wish to thank my PhD supervisors, Susan Chan and Philippe Kastner for accepting me in the lab and for their mentorship over the last four years. Susan, my direct PhD advisor, I want to thank for reading my thesis manuscript and always pointing in the good direction.

I would like to thank my jury members, Pr. Sylviane Muller, Dr. Maria-Cristina Cuturi and Dr. Jean-Christophe Bories, for agreeing to evaluate my work and discuss it during the thesis defense.

I wish to greatly acknowledge the HEM_ID network, for providing a great PhD training and possibility to attend international meetings and workshops, during which I could present my work. Special thanks are for my HEM_ID colleagues and fellows, for all the scientific contributions and social interactions. I am really happy I have met you all.

Patricia, thank you for welcoming me warmly in the lab and helping to accommodate in Strasbourg, for helping me with so many things, teaching how to handle mice, and organize my work. I'm extremely grateful for all your help.

I also wish to thank Claudine, responsible for the flow cytometry platform, for all the advice, patience, trusting with her precious machines in front of which I spent a considerable part of my PhD… and the cookies!

Sanjay, I am very grateful for helping me out to set up the colitis experiment and advising during the past few months. I would also like to thank everyone from IGBMC and ICS animal facilities, especially to Sylvie, William, Michael and Nadine for taking care of the mice and all the precious help they provided.

I want to thank all the past and present members of the lab, Alejandra, Apostol, Deepika, Jérôme, Marie-Pierre, Clément, Stephanie, Ujjwal, Beate, Attila, Patricia, Isma, Peggy, Marie, Gaëtan, Célestine, Rose-Marie, Marie for creating a great atmosphere in the lab. I would like to thank especially Rose and Deepika who were my first teachers in the lab and also great friends, on whom I can always count. Marie and Gaëtan, thank you for your support and interesting discussions, Isma and Clement, for being the best bench neighbors and friends. Attila thanks for all the help and fun, peculiar discussions and for entertaining (!) during lunch time.

Colleagues and friends, thank you for being there and making my PhD an amazing time: Anna, Iskander, Anastazja, Damien, Aurelia, Shilpy, Ira, Alexey, Claire, Nico, Léa, Isabelle, Anne-Sophie, Heena, Katerina, Vova, Firas, Pierre-Etienne, Grigory, Ismail, JoLi, Benjamin. Thank you guys! Anna and Iskander, we started together and we finish together, but the adventure will continue! Ana thanks for being a friend and for the distraction at the gym during the last months.

Finally, I wish to thank my parents for all their encouragement and support.

Ben, of course thank you for reading and then… reading again my thesis manuscript. For always being there for me and cheering me up, for making the four years of my PhD such a beautiful adventure.

TABLE OF CONTENTS

LIST OF FIGURES AND TABLES

LIST OF ABBREVIATIONS

Ab	Antibody
ABC	ATP-Binding Cassette
Ag	Antigen
AHR	Aryl Hydrocarbon Receptor
APC	Antigen Presenting Cell
ATRA	All Trans Retinoic Acid
aTreg	activated regulatory T cell
BCR	B-Cell Receptor
BM	Bone Marrow
BMDC	Bone Marrow-derived Dendritic Cell
BMT	Bone Marrow Transplantation
BrdU	Bromodeoxyuridine (5-bromo-2'-deoxyuridine)
BSA	Bovine Serum Albumin
CCR	Chemokine Receptor
CD	Cluster of Differentiation
CFC	Colony Forming Cell assay
CFSE	5-CarboxyFluorescein N-Succinimidyl Ester
ChIP	Chromatin Immunoprecipitation
ChIP-seq	Chromatin Immunoprecipitation with sequencing
CLP	Common Lymphoid Progenitor
CMP	Common Myeloid Progenitor
CNS	Central Nervous System
CNS1	Non-Coding Sequence-1
CtBP	C-terminal Binding Protein
CtIP	CtBP Interacting Protein
CTLA-4	Cytotoxic T Lymphocyte-Associated protein 4
DAPI	4'6-Diamidino-2-Phenylindole
DBD	DNA Binding Domain
DC	Dendritic Cell
DEC-205	Dendritic and Epithelial Cells, 205 kDa, multilectin endocytic receptor
dKO	double Knock-Out
DLL4	Delta-Like Ligand 4
DN	Double Negative ($CD4^-CD8^-$)
DNA	Deoxyribonucleic Acid
DP	Double Positive ($CD4^+CD8^+$)
DT	Diphtheria Toxin
DTR	Diphtheria Toxin Receptor
EAE	Experimental Autoimmune Encephalomyelitis
ECM	Extra Cellular Matrix
ES	Embryonic Stem cells
ETP	Early Thymic Precursor
EUCOMM	European Conditional Mouse Mutagenesis Program
FACS	Fluorescence Activated Cell Sorting
FBS	Fetal Bovine Serum (equivalent to Fetal Calf Serum)
FCS	Fetal Calf Serum
FDG	Fluorescein-Di-3-D-Galactopyranoside
FL	Full Length
GFP	Green Fluorescent Protein

GM-CSF	Granulocyte-Macrophage Colony-Stimulating Factor
GMP	Granulocyte-Macrophage Progenitor
GvHD	Graft versus Host Disease
H2B	Histone 2B
H3K27me3	tri-methylation of lysine 27 on histone H3
HDAC	Histone Deacetylase
He	Helios
HE	Hematoxylin Eosin
HSC	Hematopoietic Stem Cell
IBD	Inflammatory Bowel Disease
ICS	Institut Clinique de la Souris
IFN	Interferon
Ik	Ikaros
IL	Interleukin
IL-2R/IL-7R	Interleukin 2/7 Receptor
IPEX	Immune dysregulation, Polyendocrinopathy, Enteropathy, X-linked
IRES	Internal Ribosome Entry Site
iTreg	induced regulatory T cell
KLRG1	Killer-cell Lectin like Receptor G1
KO	Knock-Out
LAG-3	Lymphocyte-Activation Gene 3
LCR	Locus Control Region
Lin	Lineage
LK	$Lineage^{-}c\text{-}Kit^{+}$
LMPP	Lymphoid Primed Multipotent Progenitor
LSK	$Lineage^{-}Sca1^{+}c\text{-}Kit^{+}$
LT-HSC	Long-Term Hematopoietic Stem Cell
mAb	monoclonal Antibody
MEP	Megakaryocyte-Erythroid Progenitor
MHC	Major Histocompatibility Complex
miRNA	micro RNA
MPP	Multipotent Progenitor cells
mRNA	messenger Ribonucleic Acid
MS	Multiple Sclerosis
mTOR	mammalian Target Of Rapamycin
NCS	Neocarzinostatin
NFAT	Nuclear Factor of Activated T cells
NK	Natural Killer cell
NKG2A	inhibitory NK cell receptor G2A
NKT	Natural Killer T cell
NOD	Non-Obese Diabetic mice
Nrp1	Neuropilin-1
nTreg	natural regulatory T cell
NuRD	Nucleosome Remodeling Complex
pA	poly Adenylation
PB	Peripheral Blood
PBS	Phosphate Saline Buffer
PC-HC	Pericentromeric Heterochromatin
PCR	Polymerase Chain Reaction
PD-1	Programmed Death 1

PKC	Protein Kinase C
p-MHC	peptide-MHC complex
Pol II	Polymerase II
PRC2	Polycomb Repressive Complex 2
P-TEFb	Positive Transcriptional Elongation Factor b
pTreg	peripheral regulatory T cell
RA	Retinoic Acid
RAG-1/2	Recombination Activating Gene 1/2
RFP	Red Fluorescent Protein
rhIL	recombinant human Interleukin
rmIL	recombinant mouse Interleukin
RNA	Ribonucleic Acid
ROS	Reactive Oxygen Species
RT	Room Temperature
RT-PCR	Reverse Transcription - PCR
RT-qPCR	Real Time - quantitative PCR
SA	Splice Acceptor
SCF	Stem Cell Factor
SCID	Severe Combined Immuno-Deficiency
SCP	Stem Cell Factor
shRNA	short hairpin RNA
siRNA	small interfering RNA
SLAM	Signaling Lymphocytic Activation Molecule
SP	Side Population
SP	Single Positive ($CD4^+$ or $CD8^+$)
SPF	Specific Pathogen Free
ST-HSC	Short-Term Hematopoietic Stem Cell
SWI/SNF	SWItch/Sucrose Non-Fermentable nucleosome remodeling complex
T-ALL	T cell Acute Lymphoblastic Leukemia
TCR	T Cell Receptor
TF	Transcription Factor
Tfh	follicular helper T cell
Tg	Transgenic
TGF	Transforming Growth Factor
Th	helper T cell
TLR	Toll-Like Receptor
TNFRSF	TNF receptor super family
TNF-α	Tumor Necrosis Factor α
TPO	Thrombopoietin
Treg	regulatory T cell
tTreg	thymic regulatory T cell
UTR	Un-Translated Region
WT	Wild Type
ZF	Zinc Finger
Zn-finger	Zinc Finger

CHAPTER I INTRODUCTION AND LITERATURE REVIEW

The main objective of my thesis was to understand the roles of the Eos and Helios transcription factors in regulatory T cell biology. During my PhD I have also studied the role of Eos in hematopoietic stem cells. While setting up the necessary experimental procedures and establishing the mouse lines, I have also participated in a project related to the mechanisms of Ikaros mediated gene silencing in T cells.

In this chapter I will review the literature concerning subjects discussed in the thesis manuscript in a concise and synthetic way, giving the background necessary to the interpretation of the presented results.

I will first give a general introduction to the selected aspects of hematopoiesis and introduce them according to the hematopoietic hierarchy. Thus, I will start with a description of the hematopoietic stem cell compartment and then T cell lineage development. My main focus will be on regulatory T cells, which I will describe next. Unless otherwise indicated, hematopoiesis will be discussed in the context of mouse biology.

Further, I will present the Ikaros family of transcription factors. The literature review in this part will give both general and more precise information about the members discussed in this manuscript, namely Eos, Helios and to a lesser extent, Ikaros. I will then go back to the main subject of my PhD, regulatory T cells, and review the recent findings concerning the mechanisms of their regulation. In particular, I will discuss the current knowledge concerning roles of Eos and Helios in regulatory T cell biology. This chapter will finish with presenting the aims of study.

I.1 Hematopoietic stem cells and their progeny

Hematopoiesis is a process responsible for generating all types of blood cells. The most important characteristic of hematopoiesis is its continuity, as it starts early during the embryogenesis and persists throughout the life of an individual. Hematopoiesis can be also described as a hierarchical process with an infrequent hematopoietic stem cell (HSC) on its top (Fig.I.1).

Hematopoietic stem cell is characterized by an ability to self-renew. It can continuously give rise to progeny, first pluripotent and more restricted progenitors, then terminally differentiated mature cells of all blood cell lineages (Katayama et al., 1993; Orkin, 2000). Between all the steps of differentiation there are numerous stages of commitment, however the closer it is to the bottom end of the hematopoietic hierarchy, the more the cells lose their self-renewal potential. Long-term HSCs (LT-HSCs) possess the highest self-renewal potential and are followed by short-term HSCs and then multipotent progenitors (MPPs). It is believed that cells with multipotent progenitor potential give rise to two distinct lineages, myeloid and lymphoid. The myeloid lineage through common myeloid progenitor cells (CMPs) will give rise to erythrocytes, megakaryocytes, macrophages and granulocytes (neutrophils, eosinophils, basophils). The lymphoid lineage through common lymphoid progenitor cells (CLPs) will in turn give rise to B cells, T cells, natural killer cells (NK cells) and dendritic cells (DC cells) (Akashi et al., 2000; Kondo et al., 1997). It is noteworthy that this view is simplified and other sub-populations of progenitor cells may exist. The commitment to the lymphoid and myeloid lineage is not exclusively due to a straightforward separation into those two branches. An additional population of progenitor cells with both myeloid and lymphoid potential has been identified. This population, named lymphoid primed multipotent progenitor (LMPP) and shown to express the tyrosine kinase receptor Flt3, can give rise to monocytes, granulocytes, B or T cells but lack the potential to produce erythroid and megakaryocytic lineages (Adolfsson et al., 2005; Naik et al., 2013).

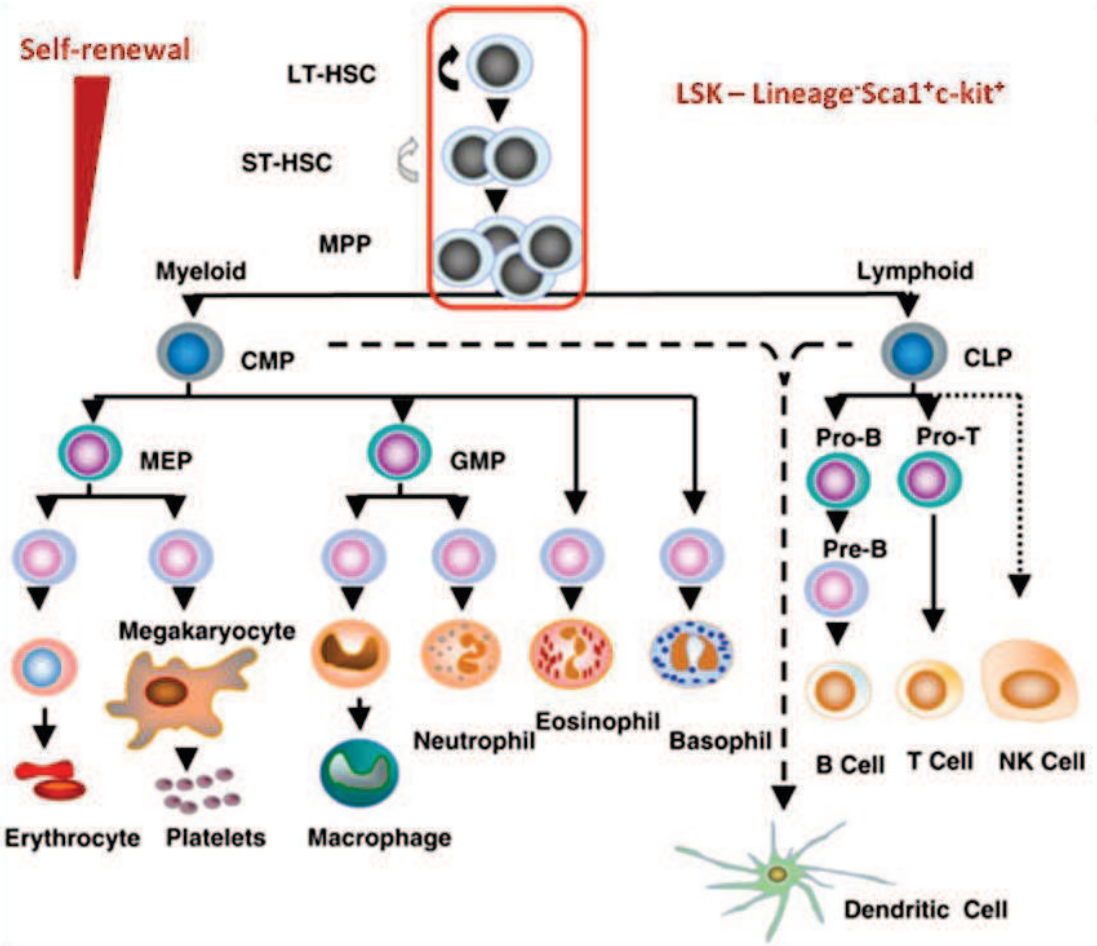

Figure I.1. Hierarchical organization of the hematopoietic system. Adapted from Larsson and Karlsson, 2005. HSC – hematopoietic stem cell; LT-HSC - long-term HSC; ST-HSC - short-term HSC; MPP - multipotent progenitor; CMP - common myeloid progenitor; CLP - common lymphoid progenitor; MEP - megakaryocyte/erythroid progenitor; GMP -granulocyte/macrophage progenitor. Population distinguished in red is highly enriched in hematopoietic stem and progenitor cells and comprises LT-HSC, ST-HSC and MPP. It can be identified as Lin^-, $Sca\text{-}1^+$, $c\text{-}kit^+$. Lin – lineage. Red triangle on the left indicates decreasing self-renewal potential during subsequent steps of lineage commitment. In a different model, the LMPP (lymphoid primed multipotent progenitors) population arises from MPP and differentiates further into CLP and GMP. CMP is depicted here as a progeny of the MPP population.

I.1.1 Identification and characterization of HSCs

LT-HSC in the bone marrow can differentiate into ST-HSC and further into MPP and committed progeny, or self-renew to maintain the pool of stem cells. HSCs found in the bone marrow or at any other anatomical site can be definitively identified only experimentally, as being capable of completely reconstituting the hematopoietic system of ablated host animals (Uchida et al., 1994). Destruction of the host bone marrow, usually by whole body irradiation, is necessary to provide a niche in the bone marrow for recipient cells and protect from graft rejection. More recently, non-irradiated immunodeficient mice with functionally impaired and fewer endogenous HSCs were also proposed as hosts for HSC engraftment

(Waskow et al., 2009; Cosgun et al., 2014). In a transplantation assay HSC can be not only identified, but also characterized, by analyzing its efficiency to contribute to the blood production. The activity of the transplanted cells can be evaluated by analyzing peripheral blood or bone marrow at different time points. The contribution of the cell of interest to the reconstitution of hematopoietic system can be verified as the recipient and donor cells carry different alleles of the CD45 antigen (CD45.1, CD45.2) (Spangrude et al., 1988). In a similar manner the functionality of the cells of interest can be assessed more precisely and quantitatively by comparing them with WT competitor cells (transplanted at the same time into host mice to ensure their survival) (Harrison, 1980). In both cases, the level of chimerism can be calculated from the percentage of donor and recipient cells (and competitors) after analyzing by flow cytometry (Fig.I.2).

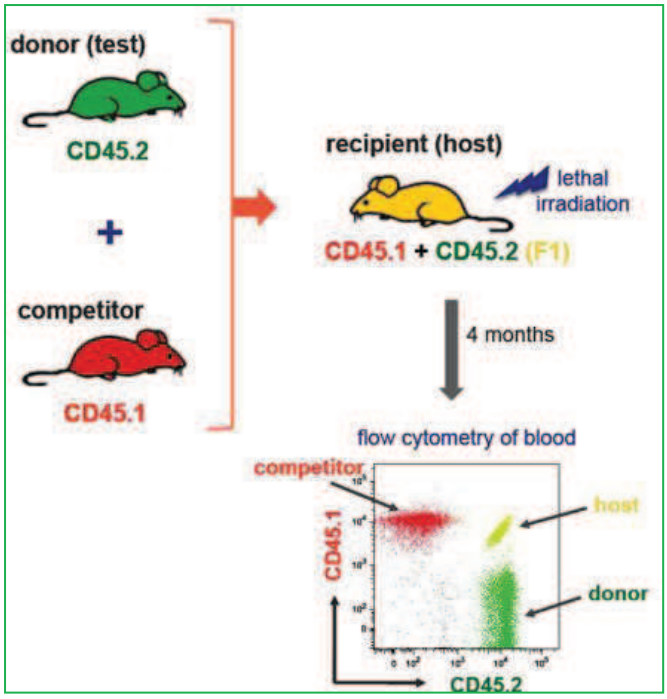

Figure I.2. Identification and functional characterization of HSCs by transplantation assay. From Bersenev 2011. The competitive transplantation assay evaluates the contribution of hematopoietic stem cells of given origin to the reconstitution of the hematopoietic compartment. Total bone marrow cells or purified HSCs from donor mice are injected into lethally irradiated recipient mice together with competitor WT cells. In this experimental set-up donor cells are $CD45.2^+$, recipient cells are $CD45.1^+CD45.2^+$ and competitor cells are $CD45.1^+$ which distinguishes those populations by flow cytometry.

Finally, with the help of transplantation assays LT-HSCs can be also distinguished from ST-HSCs and multipotent progenitors. The two latter populations can reconstitute the hematopoietic system for a short period of time, whereas only LT-HSCs can maintain hematopoiesis for a period of time longer than 4 months (Morrison and Weissman, 1994; Zhong et al., 1996; Purton and Scadden, 2007).

Due to the advancement in cell isolation and flow cytometry techniques, HSCs can be also phenotypically identified (Table I.1). HSCs and progenitor cells are highly enriched in a population defined as $Lineage^-Sca1^+c\text{-}Kit^+$ (LSK), where lineage stands for markers representing all mature cell types (e.g. B220, CD4, CD8, CD3, Gr1, CD11b, CD11c).

The LSK population represents around 0,1% of the total bone marrow cells (Ikuta and Weissman, 1992; Spangrude et al., 1988). LT-HSCs, ST-HSCs and MPPs are found within the LSK population. The most potent in terms of self-renewal and reconstitution capacity, LT-HSCs constitute only around 10% of LSK cells. LT-HSCs, ST-HSCs and MPPs can be classically identified by the expression of CD34 and Flk2 (also known as CD135 or Flt3) (Osawa et al., 1996; Adolfsson et al., 2005; Yang et al., 2005). SLAM (Signaling Lymphocytic Activation Molecule) molecules were also proposed to identify HSC and progenitor cells and recently have been the most commonly used markers to define LT-HSCs (LSK $CD150^{+}CD48^{-}$) (Kiel et al., 2005; Oguro et al., 2013). More committed progenitors, namely CLPs, CMPs and their descendents MEPs and GMPs can also be precisely identified (Table I.1) (Kondo et al., 1997; Akashi et al., 2000).

Marker phenotype	Cell type
SP^{LSK}	Long-term HSCs (LT-HSC)
LSK $Flk2^{-}CD34^{-}$	Long-term HSCs
LSK $CD150^{+}CD48^{-}$	Long-term HSCs
LSK $CD150^{+}CD48^{-}$	(Fetal liver) HSCs
LSK Flk-$2^{+}CD34^{+}$	Short-term HSC (ST-HSC) and multipotent progenitors (MPP) progenitor cells (MMP)
LSK Flk-$2^{-}CD34^{+}$	Short-term HSC (ST-HSC)
$Lin^{-}IL7r\alpha^{+}$c-$Kit^{+}Sca\text{-}1^{+}$	Common lymphoid progenitors (CLP)
$Lin^{-}IL7r\alpha^{-}$c-$Kit^{+}Sca\text{-}1^{-}$	Myeloid progenitors
$Lin^{-}Il7r\alpha^{-}$c-$Kit^{+}Sca\text{-}1^{-}CD34^{+}CD16/32^{-}$	Common myeloid progenitor (CMP)
$Lin^{-}Il7r\alpha^{-}$c-$Kit^{+}Sca\text{-}1^{-}CD34^{-}CD16/32^{-}$	Megakaryocyte–erythrocyte (MEP)
$Lin^{-}Il7r\alpha^{-}$c-$Kit^{+}Sca\text{-}1^{-}CD34^{+}CD16/32^{+}$	Granulocyte-macrophage progenitors (GMP)

Table I.1. Phenotypic identification of hematopoietic stem and progenitor cells. Adapted from Mayle et al., 2013. Most commonly used markers identifying HSC and progenitor cells. Cell populations can be analyzed by flow cytometry and identified by the expression of the indicated cell surface markers. LSK , $Lineage^{-}Sca1^{+}$c-Kit^{+}. SP, side population.

Other properties of HSCs can be used to identify and isolate them. HSCs are characterized by the presence of highly active membrane transport pumps that can efflux certain dyes and maintain only its low levels. Classically, Hoechst 33342 that binds to the DNA of living cells is used. During analysis, when Hoechst is displayed in a specific manner HSCs appear in the side of the fluorescent profile as a “side population” (SP) (Goodell et al., 1996).

All of the described phenotypic characteristics of HSC and progenitor cells allow for their identification and isolation with high purity. Purified cells can be then used in different experimental systems and their properties can be evaluated in detail.

I.1.2 Properties and choices of a hematopoietic stem cell

The hematopoietic stem cell compartment can be regulated by both cell-intrinsic and external mechanisms. The first one comprises signaling pathways and their downstream effectors and transcription factors. External mechanisms include signals from the BM niche, extracellular matrix (ECM), cell-cell interactions and growth factors. All those signals can in turn be affected by many processes including stress, inflammation or aging. As a result, different outcomes and choices are plausible for a hematopoietic stem cell (Fig.I.3). In this chapter I would like to discuss selected properties of hematopoietic stem cells.

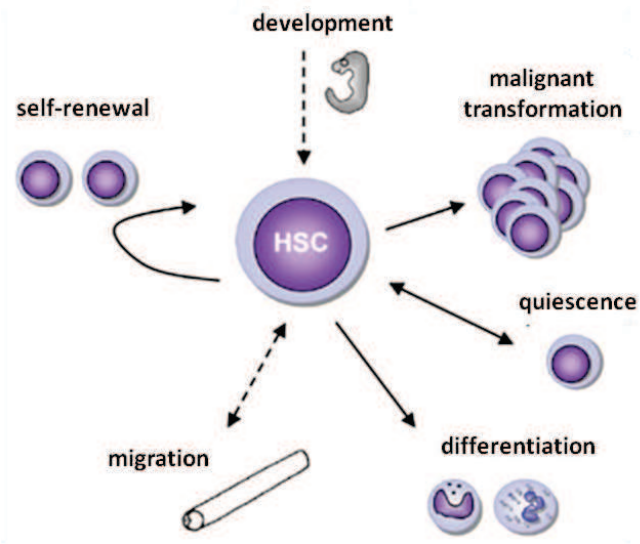

Figure I.3. Different outcomes of hematopoietic stem cell regulation. From Larsson and Karlsson, 2005. Depending on internal or external signals, the hematopoietic stem cell awaits different fates. It can remain a HSC in a self-renewal process, after symmetric or asymmetric division. It can remain quiescent or undergo differentiation. It can also migrate out of the BM niche into the circulation and home to peripheral organs (or migrate back to the BM). Under unfavorable conditions HSC can undergo apoptosis. HSC can also be subjected to malignant transformation and clonal expansion leading to a hematopoietic malignancy.

Self-renewal and differentiation

HSC is at the top of the hematopoietic hierarchy. Thus, any defect or imbalance in the hematopoietic stem cell fate will potentially affect all its progeny. The HSC must balance between the self-renewal as the necessity to maintain the pool of stem cells and a potential for malignant transformation. HSC self-renewal can be defined as an ability to maintain or expand stem cell numbers after cellular division. Division can give rise to another HSC cell with high self-renewal potential or a daughter cell that will undergo differentiation and become committed. Experimentally, classical or serial transplantation assays can demonstrate the capacity for self-renewal. Donor BM or purified HSC populations can be engrafted into recipient mice and even though this is accompanied by a functional decline of HSC in serial

transplantations and is limited in number (4-6 times), donor HSC can be still phenotypically identified in recipient mice (Harrison et al., 1978; Kamminga et al., 2005). This is a case even with a single HSC providing a long-term multi-lineage reconstitution of hematopoietic system (Osawa et al., 1996). In a more direct way HSC self-renewal was demonstrated by retroviral tagging of HSC clones transplanted into primary and secondary recipient mice (Dick et al., 1985; Lemischka et al., 1986). Studies with single-cell cultures of HSCs followed by transplanting the expanded cells into irradiated recipients also showed self-renewal capacity and that one HSC can give rise to at least one daughter HSC (Ema et al., 2005; Nakauchi et al., 2001).

Quiescence and proliferation

Self-renewal in HSC compartment must be accompanied by another fundamental property: quiescence. Quiescence is a dormant, non-cycling state characteristic of stem cells. It is thought that quiescence protects HSCs from functional exhaustion or DNA damage, and enables maintenance of lifelong hematopoiesis. Quiescence of hematopoietic stem cells must be then tightly controlled by intrinsic and extrinsic factors to provide a balance between cells in the G0 phase and cells entering the cell cycle (Fig.I.4). Using different methods of measurement it has been demonstrated that a vast majority of HSCs are quiescent with very few being in the cell-cycle at once (Goodell et al., 1996; Passegué et al., 2005). At the same time the majority of those dormant stem cells do enter the cell cycle and divide once over a period of a few (5-6) months (Wilson et al., 2008). Attempts were also made to estimate, with dilution assays, BrdU labeling or H2B-GFP tagging combined with mathematical modeling, the frequency with which a single HSC divides, and it was proposed that it occurs, 18, 5 or 20 times per lifetime of a laboratory mouse respectively, depending to the mentioned methods (Takizawa et al., 2011; Wilson et al., 2008; Foudi et al., 2009). Although in the steady-state, the HSC remains mainly dormant, its proliferation can be activated, for example, during BM transplantation and chemotherapy, after TLR stimulation, IFN-α stimulation or by IFN-γ during chronic infection (Trumpp et al., 2010; Nagai et al., 2006; Essers et al., 2009; Baldridge et al., 2010).

Decades ago, it was shown that cells can divide a limited number of times and that at certain point reach their maximum turnover, named the “Hayflick limit” and become senescent mostly due to telomere shortening (Hayflick and Moorhead, 1961; Olovnikov, 1973). Transplantation assays also showed that proliferation leads to the exhaustion of the HSC pool (Harrison and Astle, 1982; Kamminga et al., 2006). Interestingly, knock-out studies with mice deficient for p21, Gfi1 or Pten show that the mutant HSCs are characterized

by increased cell-cycle entry and a loss of HSC functionality (Cheng et al., 2000; Hock et al., 2004; Zhang et al., 2006).

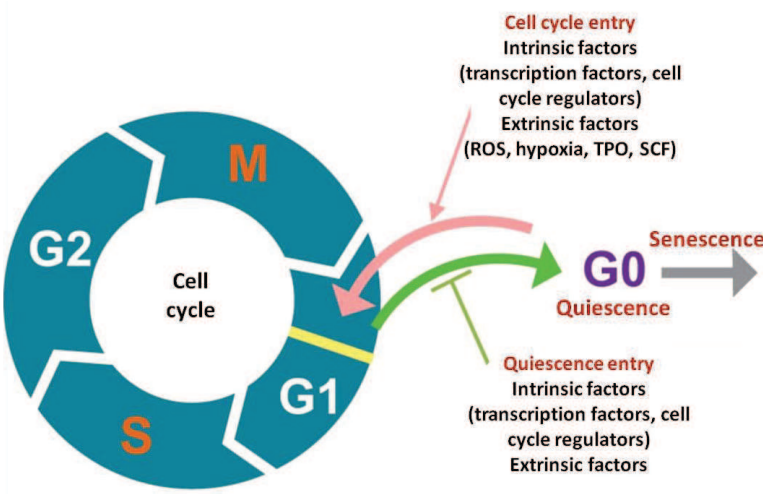

Figure I.4. Quiescence and cell cycle entry regulation. Adapted from Nakamura-Ishizu et al., 2014. Hematopoietic stem cells are primarily dormant but can enter the cell cycle and go through its 4 phases: G1 phase, S phase, G2 phase and M phase and divide. Dormant, non-dividing cells enter the G0 phase but are able to enter the cell cycle again or become quiescent. After reaching a limit in divisions cells can also enter senescence. ROS, reactive oxygen species; SCF, stem cell factor; TPO, thrombopoietin.

Migration end engraftment

Hematopoietic stem and progenitor cells are constantly migrating between the peripheral blood and bone marrow in the adulthood. This process occurs not only during inflammation or engraftment followed by myeloablation, but also during homeostasis, and is controlled by a large number of chemokines, chemoattractants or adhesion molecules. Cells from the circulation seed in the bone marrow and at the same time are replaced by cells mobilized from the BM. HSCs migrate even within the BM, especially after losing quiescence, when they move toward specialized proliferative niches. During homeostasis, HSCs can be additionally found in several non-lymphoid and lymphoid organs. Mobilization from the BM can be also facilitated by tissue damage, stress signals or infection (Mazo et al., 2011). Irrespectively of the underlying reason of the engraftment, its efficiency will largely depend on the BM niche availability. The BM niche is a morphological structure within the bone marrow that provides a microenvironment controlling HSC properties. HSC niches in the bone marrow are rare, thus the necessity to empty them, for example by irradiation, before manipulation (Bhattacharya et al., 2006; Morrison and Scadden, 2014).

Finally, those selected characteristics show that when analyzing HSC activity one should consider a broad spectrum of phenotypical and functional aspects.

I.1.3 Regulatory mechanisms

A big spectrum of factors important for HSC regulation have been identified, including cytokines, growth factors, transcription factors and chromatin modifiers. Signaling pathways are a bridge between those different components, integrating various signals and transmitting them to downstream effectors. Concerning cytokines and growth factors, a big effort was put into discovering those implicated in HSC development. The importance of TPO, SCF, IL-3 and IL-6 have been demonstrated, hence those factors are now used for *in vitro* HSC expansion and cultivation (Nakauchi et al., 2001; Blank et al., 2008). Several signaling pathways were also implicated in HSC regulation including Smad, Notch, Wingless-type (Wnt) and Sonic hedgehog (Shh). Signaling pathways as well as transcription factors or epigenetic modifiers play important but different roles, regulating steady-state hematopoiesis or HSC development. Figure I.5 in a simplified way depicts examples of intrinsic factors regulating the HSC compartment. However, it must be mentioned that their roles are much more complex and very often context dependent, with different factors and pathways being implicated in different HSC functions at the same time (Cullen et al., 2014; Göttgens, 2015). In addition, the recent advancement in high-throughput analysis has made it possible to look at the HSC compartment from a global perspective. Integration of transcriptomic, proteomic and methylome data has revealed a whole regulatory network of a few hundred transcription factors and also non-coding RNAs that operate specifically in HSCs (Cabezas-Wallscheid et al., 2014). Function of many of these single factors is known, but not always their detailed mechanisms of action or protein partners. Roles of many more are yet to be discovered, in regard to HSC fate decisions, or responses to stress and aging.

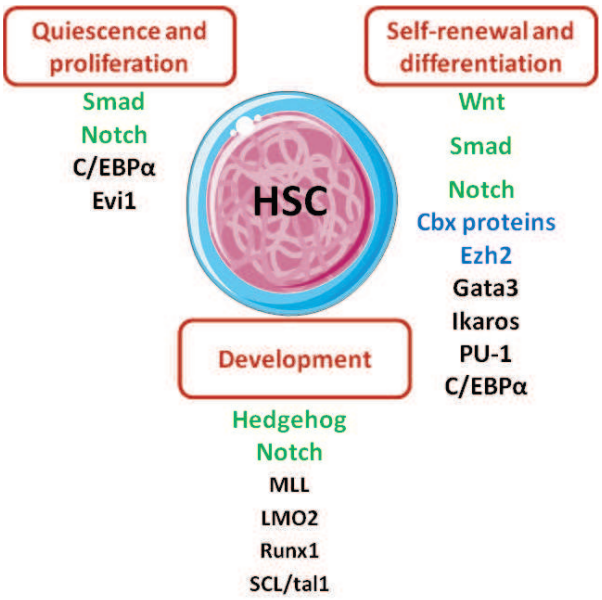

Figure I.5. Intrinsic regulation of HSCs. All properties of HSCs including development, quiescence, proliferation, self-renewal and differentiation undergo regulation. Examples of signaling pathways (green), components of Polycomb group (blue) and transcription factors (black) controlling indicated HSC functions.

I.2 The T cell lineage

In this section, I describe the T cell development in the thymus and its regulation. I also discuss the T cell activation and subset specification, while restricting to the αβ T cell lineage.

I.2.1 T cell development in the thymus

T cell precursors leave the bone marrow niche and migrate through blood using a chemotaxis process to reach the thymus for maturation (Love and Bhandoola, 2011) (Fig.I.6).

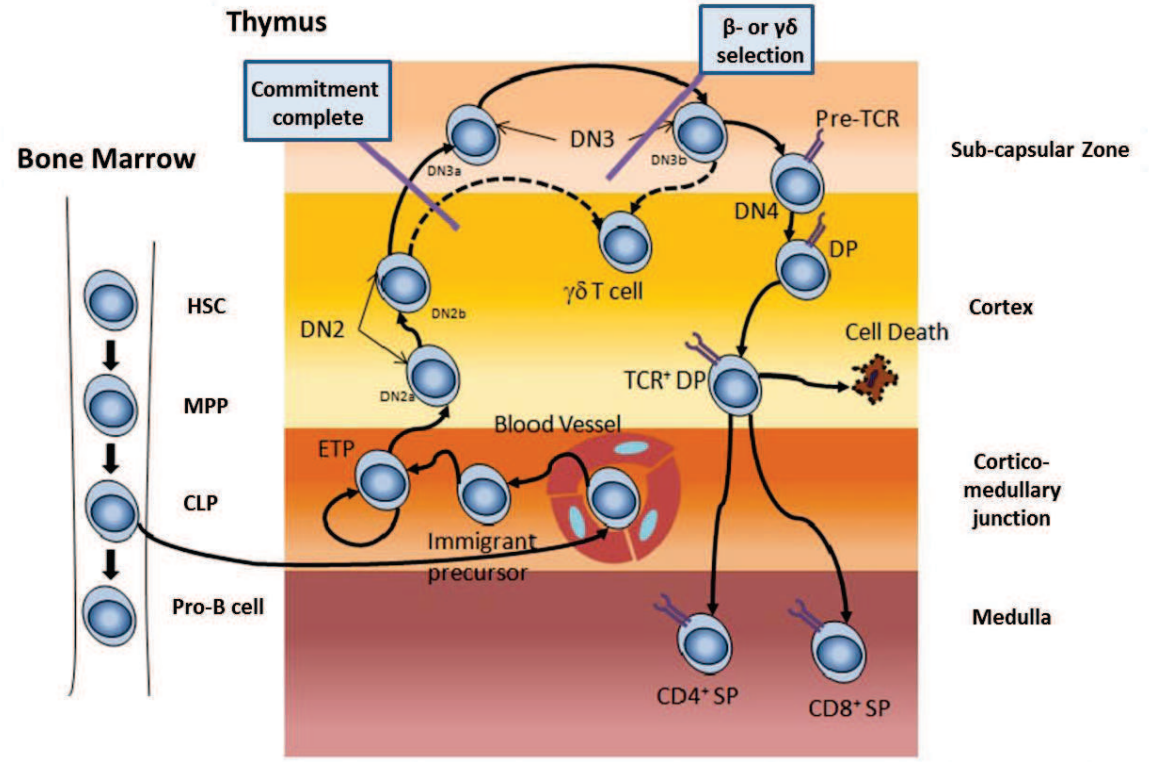

Figure I.6. T cell development. Adapted from Litt et al., 2013. Early thymic progenitor cells (ETP) derived through differentiation from HSC (hematopoietic stem cell), MPP (multipotent progenitor) and CLP (common lymphoid progenitor) seed in the thymus. They arrive through circulation near the cortico-medullary junction. They subsequently migrate and differentiate from double negative (DN) to double positive (DP) and single positive (SP) stages. Markers distinguishing main DN to SP populations are presented in Figure I.7. DN2a-DN2b can be distinguished by Kit, CD44 and DN3a-DN3b by pre-TCR and CD25. The distinct microenvironments of the thymus are indicated on the right. Commitment to the T-cell lineage occurs between the DN2b and DN3a stages. Cells during differentiation undergo β or γδ selection and positive/negative selection at the DP stage, which if not successful can lead to cell death. β or γδ selection occurs during the accumulation of the DN3 T cells in the subcapsular zone. Positive and negative selection takes place in the thymic cortex.

Interestingly, the identity of these progenitors is controversial. First, common lymphoid progenitors can leave the BM and seed the thymus. They express high levels of

interleukin-7 receptor (IL-7R), low levels of the tyrosine kinase receptor c-Kit and are restricted to the lymphoid lineage (Serwold et al., 2009; Schlenner et al., 2010). Second, lymphoid-primed multipotent precursors, can also reach the thymus and differentiate. They express lower levels of IL-7R, but high levels of c-Kit, and have both lymphoid and myeloid potential (Serwold et al., 2009; Schlenner et al., 2010). These progenitors develop into early thymic progenitor cells (ETPs) and double negative 1 (DN1), which have an IL-7R^{low}c-Kit^{hi} phenotype. Subsequent steps of T cell differentiation are characterized by the expression of CD3, CD4, CD8, CD25 and CD44. The earliest stages are called DN as cells do not express the markers, CD4 and CD8, but express differentially CD25 and CD44 (Fig.I.7). DN1 cells develop into IL-7R^{hi}c^{-}Kit^{hi} DN2 cells before committing to the T cell lineage (Heinzel et al., 2007). This commitment can be defined by the expression of several gene products, including Rag-1 and Rag-2 (Recombination Activating Genes) necessary for TCR rearrangement, CD3 that forms the TCR assembly complex itself or components of the TCR signaling (e.g. LCK, ZAP70). They become activated in DN2 cells initiating the T cell lineage commitment process that will we completed in DN3a stage (Masuda et al., 2007; Tabrizifard et al., 2004; Taghon et al., 2005).

Progression to DN3 and finally DN4 stages is also accompanied by the down-regulation of c-Kit receptor. Differentiation from DN1-DN4 occurs in a thymic microenvironment, which supports developing T cells with cytokines, including the c-Kit receptor ligand and IL-7, growth factors, and Notch ligands, particularly Delta-like ligand 4 (DLL4) (Takahama, 2006). The latter one is absolutely crucial. Notch signaling is required for T cell commitment and important for T cell proliferation. Aberrations in this pathway may lead to development of leukemias (Aster et al., 2011). After a Notch ligand interacts with the cell-surface receptor Notch1, proteolytic cleavage will release the intracellular Notch1. It will bind then to the transcription factor RBPJ (also named CSL) and complex with transcriptional co-activators to drive the expression of Notch target genes (Radtke et al., 2013). At early steps of thymocyte development cells will start to rearrange their TCR receptor, which will also trigger specific signaling. The subsequent stages of T cell development will be then divided into TCR- and Notch- dependent events. For αβ T cells, TCRβ rearrangement is usually initiated at the DN3a stage, and then the development becomes Notch-independent (Yui and Rothenberg, 2014). TCRβ will be expressed on the cell surface as a pre-TCR (TCRβ with invariant pre-Tα) and its signaling will initiate β-selection and inhibit further the *TCRβ* gene rearrangement via allelic exclusion, trigger progressive down-regulation of CD25, proliferation and differentiation. Notch signaling is necessary for

β-selection as well, but once the cell passes it, it becomes Notch-independent and shut down expression of Notch target genes (Ciofani et al., 2006; Maillard et al., 2006). Cells that become double positive (DP - $CD4^+CD8^+$) will have a unique TCRβ chain and will finally rearrange the TCRα locus (von Boehmer and Fehling, 1997; Cantrell, 2002). When the DP cells express fully functional heterodimeric αβTCR receptor, they will go through another round of selection, this time based on the TCR recognition (positive and negative selection). Thymic microenvironment will provide contact with p-MHCI/II complexes (peptide - major histocompatibility complexes I and II) and according to specificity and affinity of the TCR this will trigger the differentiation of $CD4^+CD8^+$ T cells into single positive (SP) $CD4^+$, $CD8^+$ or natural killer T cells (NKT cells) (Starr et al., 2003). Following selection, αβ T cells will migrate from the thymus to secondary lymphoid organs to carry out their functions (Ciofani and Zúñiga-Pflücker, 2010).

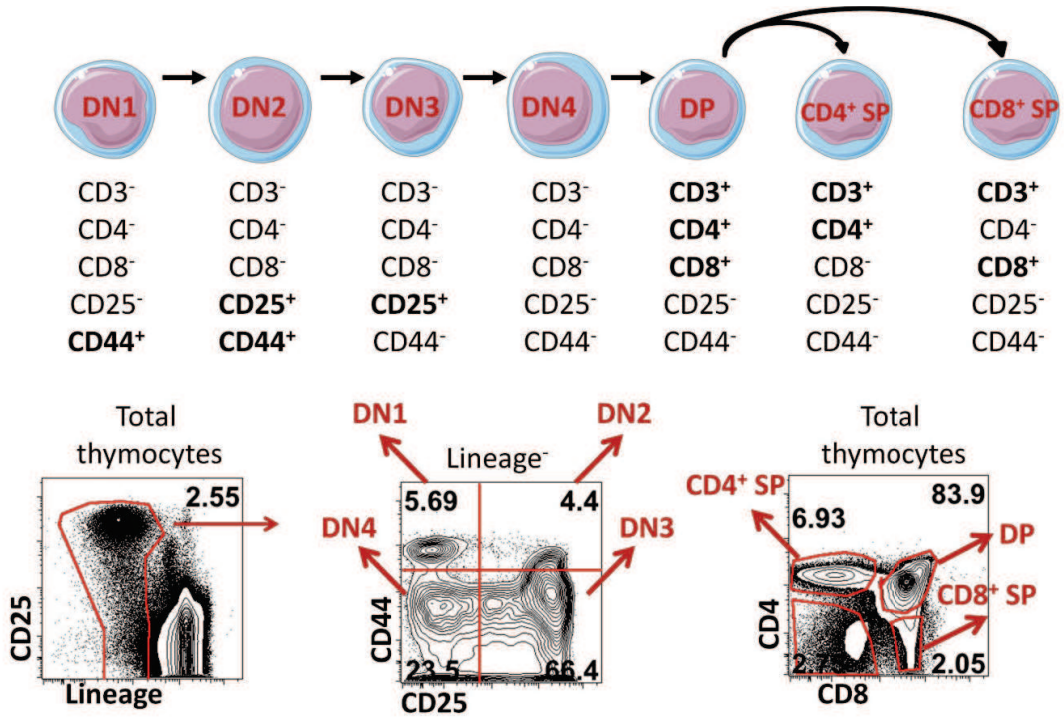

Figure I.7. Phenotypic identification of T cell developmental stages. Markers distinguishing main DN to SP populations are presented below each subset. On the bottom example of flow cytometry analysis to distinguish DN-SP cells. Classically, to obtain DN staining cells are gated as lineage negative (to exclude markers of mature cells like CD3, CD4, CD8, Gr1, CD11b, etc.). Staining with CD44 and CD25 allow then to distinguish DN1-DN4 subsets. CD4 and CD8 staining of thymocytes gives a profile where ~80% of cell will have a DP phenotype and the remaining populations will be $CD4^+$, $CD8^+$ or double negative.

I.2.2 Pathways and genes governing T cell development

It was mentioned that the Notch pathway is required for T cell development and several stages of T cell differentiation are absolutely Notch dependent. To be more precise,

thymocyte development is blocked in the absence of Notch1 protein (Radtke et al., 1999). Notch signaling participates in the early fate decisions of progenitor cells and influences the lymphoid versus myeloid specification (Pui et al., 1999). Finally, aberrant Notch activation leads to development of hematological malignancies both in mice and human (Pear et al., 1996; Weng et al., 2004). Over the years a network of other regulatory factors was identified to drive T cell development. Particularly, T cell differentiation depends on numerous transcription factors that have a stage-specific pattern of expression (Fig.I.8).

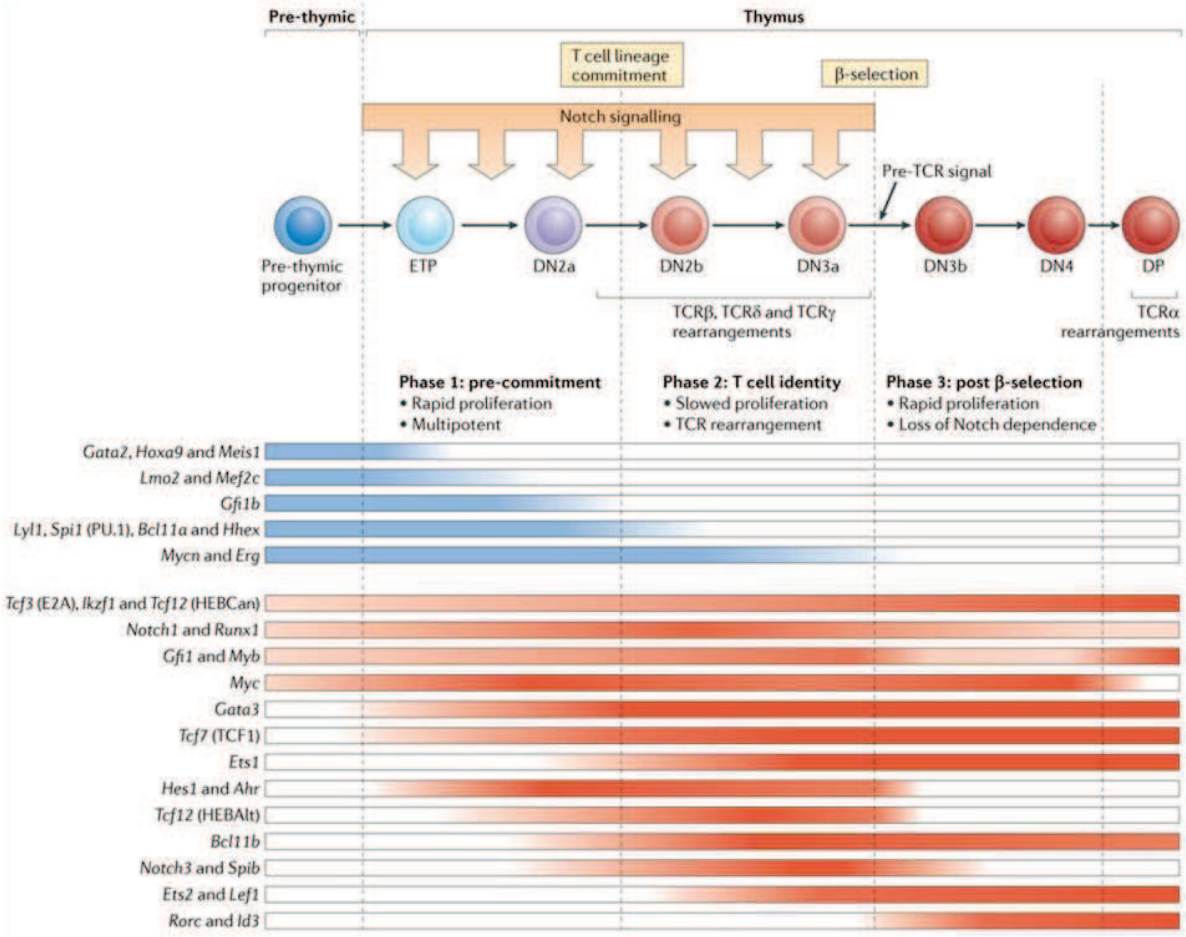

Figure I.8. Expression of transcription factors during T cell development. Adapted from Yui and Rothenberg, 2014. A group of transcription factors (in blue) is expressed in lymphoid progenitors and early T cell precursors and are responsible for the pre-commitment to the T cell lineage (Phase 1). Another group of genes (in red) is crucial for establishing the T cell identity and carrying out the subsequent steps of differentiation. This will require slowed proliferation and initiation of TCR rearrangement (Phase 2). After β-selection specific genes will in turn control the switch to rapid proliferation and loss of Notch dependency (Phase 3). Finally, up-regulation of CD4 and CD8 must be controlled, followed by proliferation arrest necessary for TCRα rearrangements.

Many of the genes presented in Fig.I.8 are critical for T cell development as their inactivation or overexpression in murine models may have a dramatic effect on this process (Yui and Rothenberg, 2014). Many others along with their protein partners regulate every

step of T cell differentiation. Another level of complexity is added by their downstream effectors and epigenetic modifications.

I.2.3 T cell activation

In a classical model two signals are necessary for a proper T cell activation (Lafferty and Cunningham, 1975). The first one is initiated when an antigen presented by a specialized cell (APC; antigen presenting cell) and bound to a MHC complex will interact with a TCR causing a cascade of intracellular events (Fig.I.9).

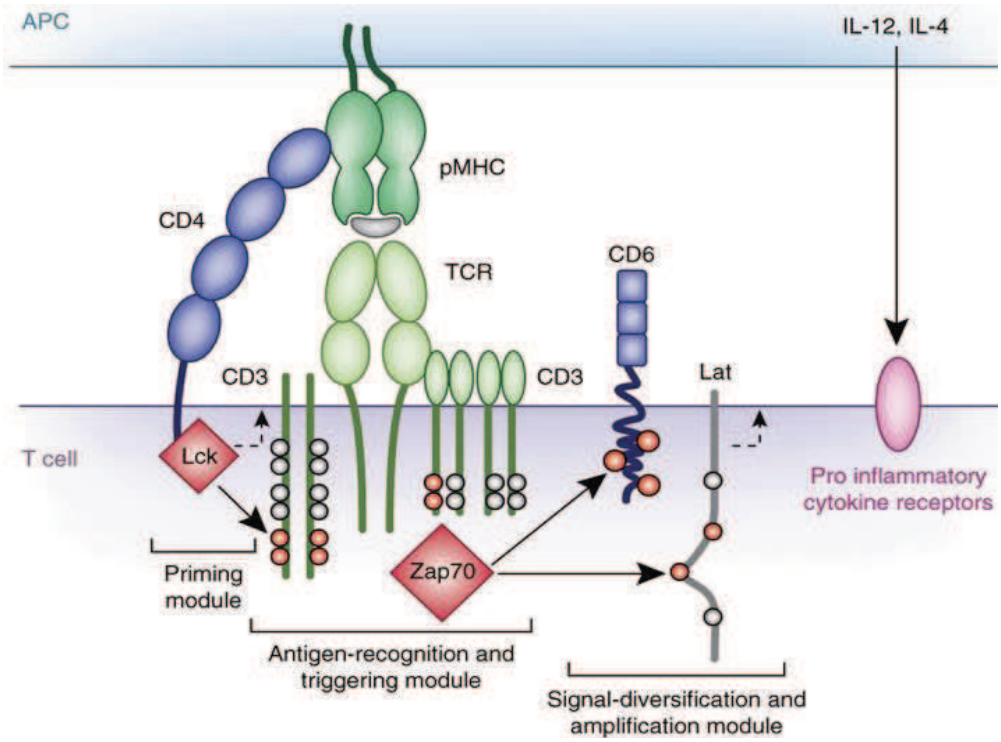

Figure I.9. TCR signaling. Adapted from Malissen et al., 2014. In this model TCR signaling is separated into 3 modules. The priming module comprise CD4 or CD8 that recognize peptide-MHC class II or class I complexes (p-MHC) respectively, and is associated with the tyrosine kinase Lck. Binding of the p-MHC associated with CD4/CD8 to the TCR, within the antigen-recognition module, triggers phosphorylation of CD3 by Lck. Those events lead to the recruitment of Zap70 which will in turn phosphorylate specific intracellular residues of CD6 and Lat, composing the third signal-diversification and amplification module. Finally, the cells will also be primed by cytokines from APCs (IL-12, IL-14) or the cellular microenvironment that can further stimulate lineage specification.

The TCR heterodimer signaling is associated with CD3 subunits, which may contain immunoreceptor tyrosine-based activation motifs. Those motifs can be phosporylated by Lck kinase. Lck is associated with intracellular segments of CD4 or CD8 co-receptors and can phosphorylate CD3 segments after TCR/p-MHC/co-receptor initial interaction (Hogquist and Jameson, 2014; Malissen et al., 2014). This will be followed by a subsequent activation of the cytosolic tyrosine kinase Zap70 which will phosphorylate the intracellular domain of the

adaptor protein Lat (Roncagalli et al., 2014). Lat will provide a "hub" for downstream effectors and form a multiprotein complex. Among other proteins it will recruit a cytosolic adaptor SLP-76 necessary for T cell activation (Roncagalli et al., 2010). Recruitment of SLP-76 will in turn depend on the phosphorylation of CD6, by Zap70 (Roncagalli et al., 2014).

T cell activation through only the TCR leads to anergy (Jenkins and Schwartz, 1987). Thus, additional priming is required for T cells to be fully active in physiological conditions. This second signal is delivered in a form of co-stimulatory or co-inhibitory interactions, which balance the level of T cell activation and allow for proliferation, migration and carrying out effector functions. The best known co-stimulatory interaction occurs between CD28 on a T cell and B7 proteins (CD80 or CD86) on the APC (June et al., 1987; Linsley et al., 1990). T cell activation can be inhibited when B7 molecules bind to CTLA4 (cytotoxic T lymphocyte-associated protein) which has a higher affinity for B7 (Linsley et al., 1990). Other co-inhibitory interactions can be mediated for example by PD-1 and its receptors (Freeman et al., 2000; Okazaki et al., 2002).

I.2.4 T cell lineage diversification

Following differentiation, additional stimulation enables T cells to acquire distinct effector phenotypes and functions such as cytotoxicity or the production of various cytokines.

$CD8^+$ T cells recognize antigens in a MHC class I-restricted manner and diversify into specific subsets that are not very well defined. In the literature one can find descriptions of $CD8^+$ Tc1, Tc2 or Tc17 cells, where "c" indicates cytotoxic cell. However, more frequently CD8 T cells are described phenotypically by the expression of cell surface markers and their functionality. Thus, they comprise cytotoxic T cells, which play a role in the direct killing of malignant or infected cells, and $CD8^+$ suppressor T cells, which inhibit immune responses in a specific manner (Shrikant et al., 2010).

$CD4^+$ T cells recognize antigen in a MHC class II-restricted manner and mainly produce cytokines that affect target cells or stimulate other lymphocytes. Effector $CD4^+$ and $CD8^+$ T cells can disappear after antigenic clearance, but some may persist and acquire a memory phenotype. Memory T cells can live for years in lymphoid organs and peripheral tissues, and due to their lower activation threshold, can trigger efficient and fast response upon re-encounter with antigen (Broere et al., 2011; Luckheeram et al., 2012). Memory T cells of both $CD8^+$ and $CD4^+$ origin can be phenotypically distinguished by the expression of cell surface markers, where a $CD44^{hi}CD45R(B)^-CD62L^-$ profile can define a memory T cell and $CD44^-CD45R(B)^+CD62L^+$ can identify a naïve T cell (Desbarats et al., 1999).

The differentiation of naïve T cells to effector cells requires factors from the cell microenvironment, mainly cytokines. Cytokines can in turn trigger a signaling cascade that will activate specific transcription factors, which determine precisely the differentiation program. Naïve $CD4^+$ T cells can diversify into T helper 1 (Th1), Th2, Th17 and regulatory T (Treg) cells (Fig.I.10). They can also give rise to T follicular helper (Tfh) cells, Th9 and Th22 subsets (Zhou et al., 2009).

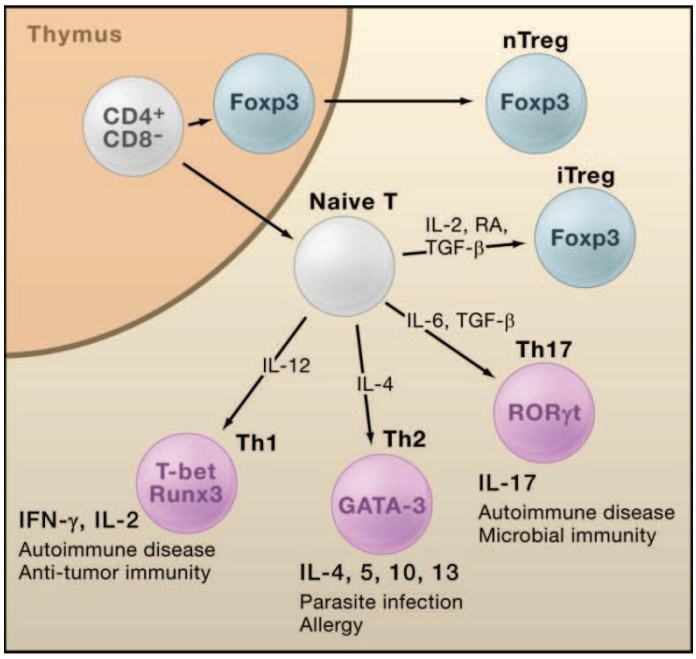

Figure I.10. Diversification of $CD4^+$ T cells. Adapted from Sakaguchi et al., 2008. Figure present examples of cytokines and transcription factors, which participate in the differentiation of $CD4^+$ T cells into effector T cells and Treg cells. Generated T cell subsets also produce cytokines and play distinct roles in immune responses (indicated below differentiated cells). nTreg, natural Treg; iTreg, induced Treg; RA, retinoic acid.

Concerning the Th populations, mainly the pattern of cytokine expression defines their identity. For example, Th1 cells are known to produce IFNγ and fight intracellular microorganisms. Their differentiation is driven mainly by IFNγ and IL-12 and the T-bet transcription factor (Zhou et al., 2009). The Th2 subset requires at least IL-4, Stat6 and the Gata3 transcription factor for differentiation, and is characterized by the secretion of IL-4, IL-5 and IL-13. Its function is to control immune responses to extracellular parasites and allergies (Paul and Zhu, 2010). Polarization into the Th17 lineage requires the RORγt transcription factor and cytokines, including IL-6, IL-21 and IL-23. Th17 cells play a role in immune responses mainly against extracellular bacteria and fungi, and to carry-out their function, they secrete IL-17A, IL-17F and IL-22 (Chen et al., 2007). Treg cells are responsible for the suppression of immune responses and for mediating several aspects of immunological tolerance. They can arise in the thymus, or in the periphery, in a process also dependent on a distinct transcriptional program and cytokine milieu which will be reviewed in detail in the following sections.

I.3 Regulatory T cells – a brief history

Regulatory T cells are T lymphocytes specialized in the suppression and maintenance of immune self tolerance. Self tolerance can be roughly divided into central and peripheral. The former stems from events taking place in central lymphoid organs, thus for T cells it is acquired in the thymus. Developing thymocytes that will recognize self antigens presented by thymic APCs with strong affinity will be eliminated during negative selection. This process, however, has its limitations. Autoreactive T cells can escape from the thymus, and removing all of the self-reactive ones during negative selection would actually leave an organism with a relatively small repertoire of cross-reactive T cells. Thus, other mechanisms supporting central tolerance must be employed. In this regard, peripheral tolerance is acquired after maturation and emigration from the thymus and can be achieved for example by anergy or active suppression of effector T cells. The latter can be attributed greatly to regulatory T cells.

It was demonstrated over four decades ago that there are cells within the thymus able to suppress autoimmunity. Neonatal thymectomy in mice led to the development of oophoritis (ovarian autoimmune disease) which could in turn be prevented by a thymic graft (Nishizuka and Sakakura, 1969). Soon after, in early 1970s, Gershon and colleagues proposed for the first time the existence of a distinct population of "suppressor T cells" able to inhibit antibody responses (Gershon and Kondo, 1970; Gershon et al., 1972). Later on, it was proposed that a cell can possess both, a helper and suppressor phenotype, and was named "hermaphrocyte" (Gershon et al., 1977). This observation is being brought to life again recently, and described as Treg cell plasticity. Interestingly, in those early studies $CD8^+$ T cells (identified at the time by the Ly or Lyt nomenclature) were already described to have suppressive potential (Cantor et al., 1978; Green et al., 1983). During the next years, regulatory T cells were also identified as cells of $CD4^+$ origin able to protect from organ specific autoimmunity induced either by thymectomy or reconstitution of lymphopenic animals with naïve T cells. Thus, post-thymectomy autoimmune oophoritis, could be prevented by Lyt-1^+ ($CD4^+$) T cells from whole thymus or spleen grafts (Sakaguchi et al., 1982). Athymic rats injected with donor $CD45RB^{hi}$ $CD4^+$ (but not $CD45RB^{low}$ $CD4^+$) T cells developed a severe wasting disease. When co-injected with a mixture of both populations, animals were protected from the wasting disease, suggesting that $CD45RB^{low}$ $CD4^+$ cells are the suppressive ones in the experimental system used (Powrie and Mason, 1990). Similar results were obtained with a model of a wasting disease induced in SCID (Severe Combined

Immuno-Deficiency) mice (Morrissey et al., 1993). Interestingly, autoimmune disease (again oophoritis) could be adoptively transferred to another healthy recipient, and again, be prevented by reconstituting mice with total splenocytes. The same study showed also that both effector and suppressive T cells are CD4 positive (Smith et al., 1991). Finally, a few years later Treg cells were identified as $CD4^+$ T cells expressing CD25, and able to protect from autoimmune disease (Sakaguchi et al., 1995). In the 1990s, a "scurfy" mutation (named after the skin phenotype) leading to a fatal lymphoproliferative disorder was discovered in mice (Godfrey et al., 1991). Later, this mutation was found to be localized within the gene encoding the Foxp3 (Forkhead box P3) transcription factor, and mutations or deficiencies in Foxp3 caused early onset, severe and highly aggressive autoimmune disorders in both humans and mice (Bennett et al., 2001; Brunkow et al., 2001). Soon after, Foxp3 was identified as a key regulatory factor and a marker of Treg cells (Fontenot et al., 2003; Hori et al., 2003; Khattri et al., 2003).

These breakthrough discoveries initiated more studies that followed. Combined with advancements in molecular and cellular biology they gave us a vast knowledge about Treg cell biology. Now, the development of Treg cells, their diversification into distinct subsets, mechanisms of action and regulation are better understood. In the next sections, I will review these aspects of the Treg cell compartment.

I.3.1 Origins of Treg cells

The first evidence that regulatory T cells originate from the thymus came from the early studies. Neonatal thymectomy performed at day 3 but not at day 7 led to the development of autoimmune syndrome in mice (Nishizuka and Sakakura, 1969). In combination with several other studies, this was the first indication that thymus not only contains a population of suppressive T cells, but also that thymus derived suppressor T cells migrate from the thymus early after birth and play essential roles in self-tolerance (Asano et al., 1996). However, conventional T cells, particularly $CD4^+CD25^-Foxp3^-$ can also differentiate in the periphery and acquire a $CD4^+CD25^+Foxp3^+$ Treg phenotype and functional properties (Apostolou and von Boehmer, 2004). Those studies established an essential principle in the Treg field. Treg cells have two described origins, the thymus and the periphery. A specific nomenclature was built accordingly, with thymic Treg cells commonly referred to as "natural" or "thymic" (nTreg or tTreg respectively), and Treg cells induced in the periphery or in other conditions as "peripheral" or "induced" (pTreg, iTreg respectively).

Moreover, regulatory T cells can originate from both $CD4^+$ and $CD8^+$ T cell lineages (Fig.I.11).

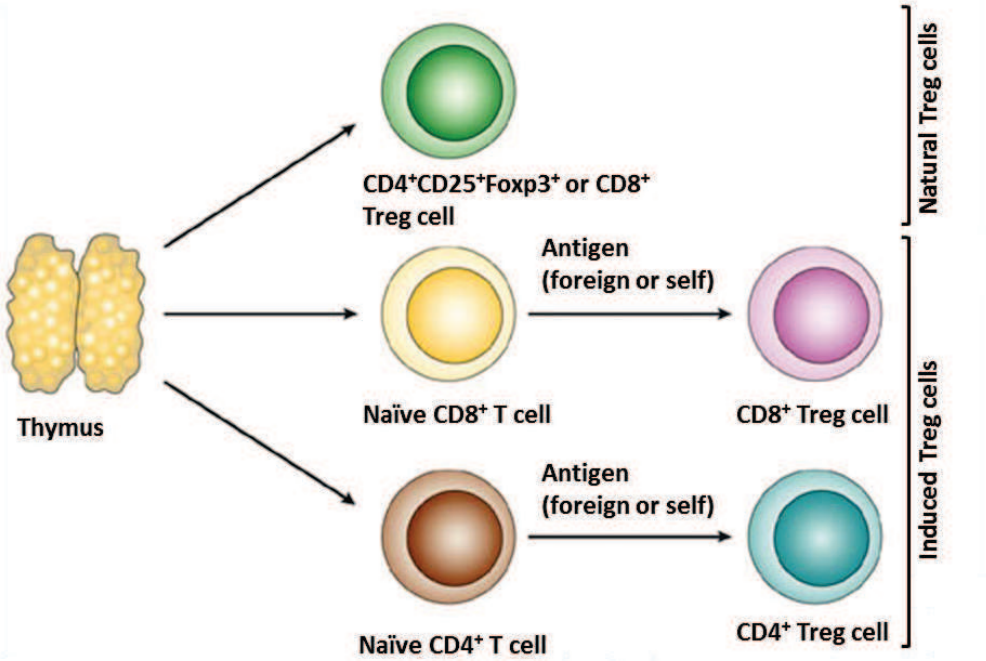

Figure I.11. Origins of regulatory T cells. Schematic representation, adapted from Mills, 2004. The best characterized Treg cells originate in the thymus and express the cell-surface marker CD25 and the transcriptional factor Foxp3. $CD4^+CD25^+Foxp3^+$ migrate from the thymus and constitute ~10% of peripheral $CD4^+$ T cells in normal mice. Populations of $CD8^+$ T cells were also described as natural Treg cells. Antigen specific conventional $CD4^+$ or $CD8^+$ T cells can be also induced in the periphery with the help of antigen presenting cells, IL-2, TGFβ signaling or other factors.

I.3.1.1 Thymic Treg cells

Among the different subsets of regulatory T cells, the best characterized are $CD4^+$ T cells that express CD25 and the transcription factor Foxp3, with most of the studies related to Treg development using the $CD4^+CD25^+Foxp3^+$ population. In this context, a two-step model of Treg cell development in the thymus was proposed (Burchill et al., 2008; Lio and Hsieh, 2008) (Fig.I.12).

First, $CD4^+$ T cells require high affinity interactions between the TCR and peptide-MHC class II complexes, presented on thymic epithelial cells (Aschenbrenner et al., 2007). A big proportion of T cells generated in TCR transgenic mice, co-expressing a specific TCR and its antigen at the same time, are functional $Foxp3^+$ Treg cells (Jordan et al., 2001; Aschenbrenner et al., 2007). Likewise, the TCR repertoire of Treg cells largely overlaps with self-reactive T cells, confirming the model where cells that possess a TCR with high self-reactivity are not always eliminated, but can become Treg cells (Hsieh et al., 2006; Pacholczyk et al., 2006; Wong et al., 2007). Similar to a classical model of T cell activation,

Treg cells require other signals for proper diversification, including the CD28-B7 co-stimulation (Tang et al., 2003; Tai et al., 2005).

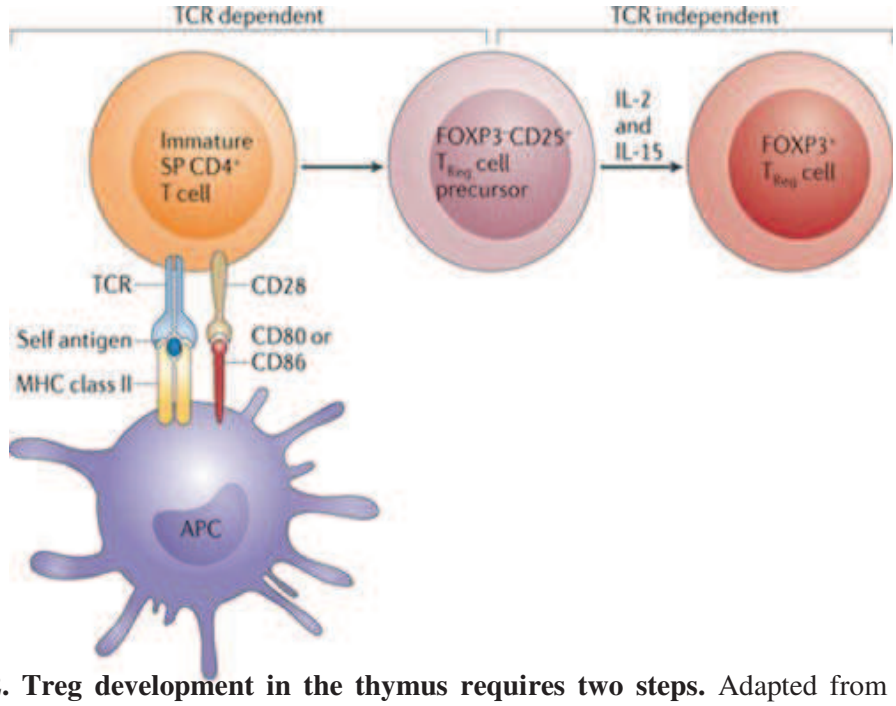

Figure I.12. Treg development in the thymus requires two steps. Adapted from Hsieh et al., 2012. During positive selection in the thymus, T cells recognize self antigens presented by MHC class II molecules in the presence of co-stimulatory signals (CD28 and CD80 or CD86). If the antigen is recognized with high level of self-reactivity, some of the cells undergoing selection are primed to become Treg cells (Treg precursors). The TCR signal leads then to the activation of several transcriptional changes and the remodeling of the Foxp3 locus which become inducible by IL-2 signaling. At this point, the Treg cell precursor does not require further TCR stimulation for the expression of Foxp3, but cytokine signals mediated mainly by IL-2, or possibly IL-15.

Second, after the TCR signal, IL-2 is important to complete the Treg development (Burchill et al., 2008; Lio and Hsieh, 2008). The requirement for IL-2 can be supported by defects in Treg cells lacking IL-2 receptors or IL-2 signaling transducers Jak3 or STAT5 (Burchill et al., 2007; Sakaguchi et al., 2008; Soper et al., 2007). Recent studies revealed that antigen presenting dendritic cells residing in the thymus provide both the antigen and IL-2 for developing Treg cells (Weist et al., 2015). Moreover, Treg cells already existing within the thymus, or recirculating from the periphery, can inhibit the development of new Treg cells by limiting the IL-2 supply (Weist et al., 2015; Thiault et al., 2015). Finally, the commitment to the nTreg lineage in the thymus is TGF-β independent, but TGF-β signaling appears to be crucial to promote Treg survival by antagonizing T cell negative selection (Ouyang et al., 2010).

I.3.1.2 Alloantigen specific Treg cells

It is well established that naturally occurring autoreactive $CD4^+$ regulatory T cells control immune responses. These cells undergo positive selection within the thymus and appear in the periphery as committed Treg cells. Alloantigen specific Treg cells could be also generated in the thymus. This could result from a combined effect of a big TCR diversity and its high cross-reactivity. Alloantigen could also enter the thymus and mediate the positive selection of alloreactive $CD4^+$ Treg cells, but not many studies support the essential role of the thymus in de novo generation of alloreactive Treg cells. However, this can certainly occur in the periphery (Wood and Sakaguchi, 2003).

Existence of alloantigen specific Treg cells is particularly important in transplantation biology. Fully functional $CD4^+CD25^+Foxp3^+$ Treg cells prevent allograft rejection and can be generated or induced after exposure to alloantigen both *in vivo* (Bushell et al., 1995; Hara et al., 2001) and *ex vivo* (Feng et al., 2008a, 2008b). Alloantigen specific $CD4^+Foxp3^+$ can be also found locally after pancreatic islet transplantation and their presence and expansion is specifically promoted after pre-treatment of recipient mice with tolerogenic DCs and anti-CD3 antibody (Baas et al., 2014). Also, treatment with an immunosuppressive agent can promote allograft tolerance and protect rats from autoimmune disease in the central nervous system (CNS) specifically by inducing Treg cells (Chiffoleau et al., 2002; Duplan et al., 2006). A more recent study provided evidence that allograft protective $Foxp3^+$ Treg cells can develop *in vivo,* by both conversion of conventional $CD4^+$ T cells and expansion of endogenous, naturally occurring $CD4^+$ Treg cells (Francis et al., 2011).

I.3.1.3 Induced Treg cells

Under specific conditions conventional T cells can differentiate in the periphery into iTreg cells, which will perform distinct functions. Mechanisms and requirements for iTreg development have been extensively documented for the most abundant $CD4^+$ Treg cells, thus the examples below will concern this subset. Certainly, less is known about the $CD8^+$ iTreg cell populations. To avoid confusion, I review the recent findings about those cells in the following section where the distinct Treg subsets are discussed.

Both *in vivo* and *in vitro* data concerning iTreg cell generation suggest the importance of appropriate TCR signaling and co-stimulation, along with TGF-β1, IL-2 and retinoic acid (RA) (Fig.I.13).

Induced Treg cells can develop after exposure to antigens following intravenous injection, peptide infusion with minipumps or administration of non-depleting anti-CD4

antibodies (Thorstenson and Khoruts, 2001; Apostolou and von Boehmer, 2004; Cobbold et al., 2004). Similarly, oral administration of antigen can mediate iTreg cell differentiation and oral tolerance (Mucida et al., 2005).

Peripheral induction of Treg cells can be accomplished by TGF-β, which maintains Treg cell suppressive potential and stable expression of Foxp3 (Marie et al., 2005; Zheng et al., 2010). TGF-β1 deficient mice have significantly reduced numbers of peripheral Treg cells, but not thymic ones, and this is associated with Foxp3 down-regulation and defective suppressive activity of Treg cells. Foxp3 induction by TGF-β1 in iTreg cells is mediated by epigenetic modifications, namely by the release from the inhibitory effect of DNA methylation and the acquisition of histone acetylation (Luo et al., 2008; Josefowicz et al., 2009; Tone et al., 2008).

The necessity for IL-2 in the induction of iTreg cells is not clear. It appears that *in vivo,* its presence is not absolutely required for the generation of iTreg cells, but is rather needed to promote their survival, proliferation and $Foxp3^+$ Treg lineage stability (Fontenot et al., 2005a; D'Cruz and Klein, 2005; Chen et al., 2011).

The generation of iTreg cells at specific locations, like the lamina propria of the small intestine, is also dependent on DCs secreting RA (Coombes et al., 2007; Sun et al., 2007). To a lesser extent, RA can induce Foxp3 by down-regulating the receptor for IL-6, a cytokine which negatively regulates Foxp3. However, the main role of RA in inducing iTreg cells and Foxp3 expression would be by an indirect mechanism involving the negative regulation of the $CD4^+CD44^{hi}$ cell population (partially through the secretion of IL-4, IL-21 and IFNγ) that in turn inhibits TGF-β1 mediated T cell conversion (Hill et al., 2008).

The development of iTreg cells in un-manipulated mice can be also stimulated by commensal bacteria (Round and Mazmanian, 2010; Atarashi et al., 2011). The induction of Treg cells can be observed during colitis resolution in lymphopenic hosts (Haribhai et al., 2009). More recently iTreg cell development has been demonstrated to occur locally in non mucosal tissues, for example in the eye (Zhou et al., 2012; McPherson et al., 2013).

Conventional $CD4^+$ Treg cells isolated from lymphoid organs can be also induced to express Foxp3 *in vitro,* in the presence of TGF-β1 and IL-2 (Chen et al., 2003; Davidson et al., 2007). An efficient protocol to induce $CD4^+CD25^+Foxp3^+$ regulatory cells *in vitro* from naïve T cells with anti-CD3 antibody stimulation (plate bound), anti-CD28 antibody stimulation (soluble) and TGF-β1 was also proposed (Fantini et al., 2007).

These examples support the biological importance of generating iTreg cells from $CD4^+$ T cell lineage.

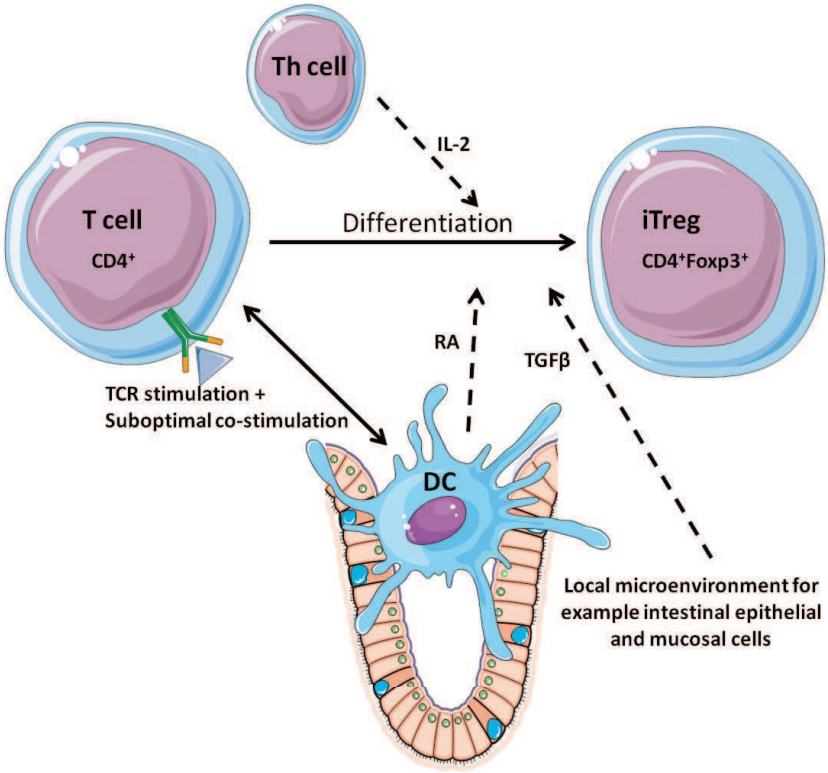

Figure I.13. iTreg development in peripheral tissues. An example of $CD4^+Foxp3^+$ iTreg cell development in the intestinal tissues. Conventional $CD4^+$ T cell requires antigenic TCR stimulation and co-stimulation together with cytokines and growth factors to become a $CD4^+Foxp3^+$ Treg cell. Retinoic acid (RA) can be provided by a dendritic cell (DC) residing in the local microenvironment. TGF-β1 can be also produced by DC or cells forming the local microenvironment. IL-2 can be supplied by conventional helper T cells (Th).

I.3.2 Phenotypical and functional Treg subsets

It this section I discuss the phenotypical characteristics of $CD4^+$ and $CD8^+$ Treg cells and give examples of their markers to illustrate the big heterogeneity of Treg cell lineage.

I.3.2.1 $CD4^+$ Treg cells

Omics approaches have allowed a detailed analysis of Treg cells, and a distinct Treg cell "signature" has been proposed (Fig.I.14) (Hill et al., 2007; Feuerer et al., 2009). Various subsets of Treg cells have been identified by differential expression of cell surface and intracellular markers. Many of them are co-expressed on Treg cells and delineate sub-populations with different functions and tissue localization. In addition, some of the markers are constitutively expressed in Treg cells while some need to be activated.

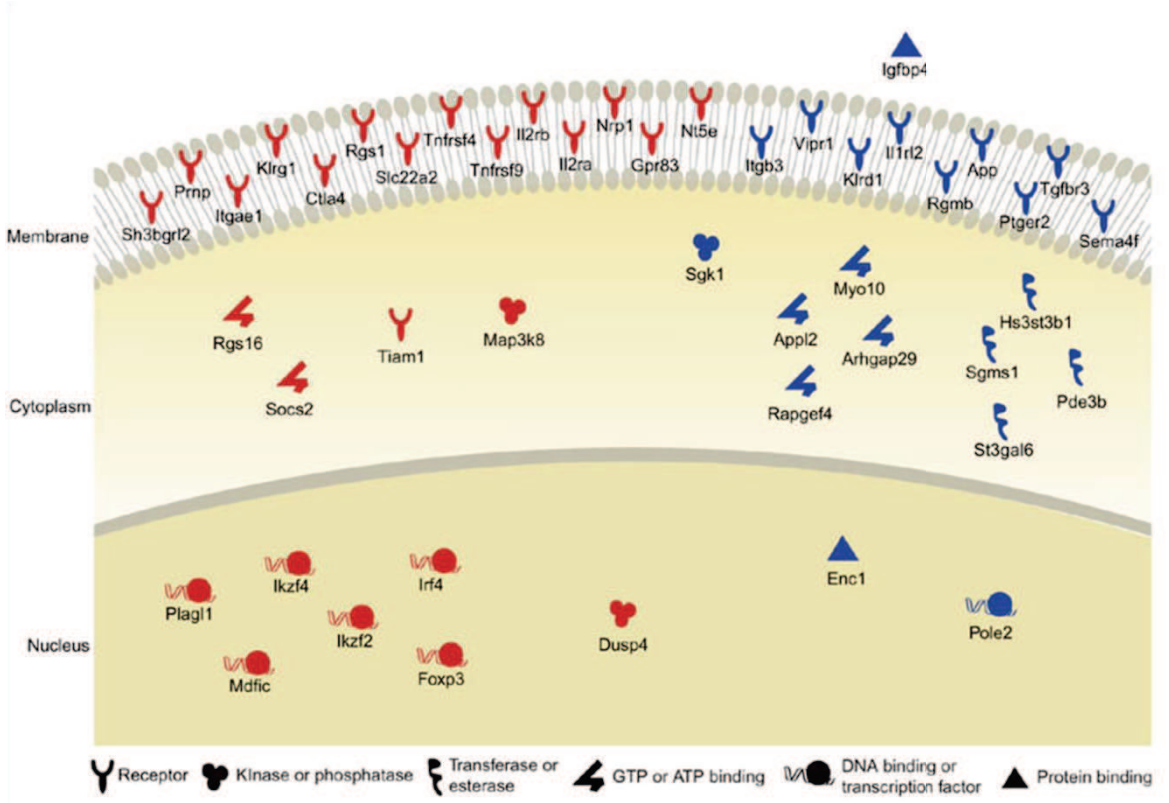

Figure I.14. Gene signature of resting Treg cells. Adapted from Feuerer et al., 2009. Most differentially expressed genes defining Treg signature from Hill et al., 2007 are presented. Red and blue color indicate up-regulated and down-regulated genes, respectively, in resting Treg cells from the spleen and lymph nodes, compared to conventional T cells. The cellular localization of gene products is indicated on the left and their functions are presented as symbols (bottom legend).

Treg cells express a panel of co-stimulatory/co-inhibitory molecules (CD28, CTLA-4, and PD-1 etc.), TNF receptor super family (TNFRSF) members (TNFR2, GITR, OX40, etc.), chemokine receptors (CCR2, CCR4, CCR5, etc.) and others which give specific properties to the cell. On the top of the well known CD25, Treg cells have several activation markers, including CD69, CD38, CTLA-4, OX-40, CD62L, GITR or CD103.

Some of the markers (e.g. CTLA-4, GITR, CD103, OX-40) have higher levels of expression on Treg cells than activated T cells, giving an advantage to Treg cells in performing their suppressive functions. For example, CD103 is an $\alpha_E\beta_7$ integrin which directs lymphocytes to their E-cadherin ligand expressed on epithelial cells (Cepek et al., 1994). According to its principal role, the expression of CD103 on Treg cells gives these cells an advantage to more easily access and reside in peripheral tissues and to prolong their interactions with other cells during ongoing inflammation (Huehn et al., 2004; Schön et al., 1999). It is supported by the fact that, $CD103^+$ Treg cells have a higher suppressive activity than their $CD103^-$ counterparts i*n vitro* (Lehmann et al., 2002). $CD4^+CD103^+$ Treg cells are

also functional *in vivo* and actively participate in ameliorating the GvHD (Graft versus Host disease) in a mouse model (Zhao et al., 2008). After adoptive transfer to lymphopenic hosts $CD4^+CD103^-$ Treg cells can acquire the CD103 expression and a transcriptional profile resembling gut Treg cells, which are mostly $CD103^+$ (Feuerer et al., 2010).

Moreover, CD103 is expressed on 20-30% of $Foxp3^+$ cells in secondary lymphoid organs but its levels are even higher at other locations, including the lung, skin and lamina propria of the gut (Huehn et al., 2004; Stephens et al., 2007). Similar to CD103, the expression of the chemokine receptor CCR4 correlates with Treg tissue specific localization. $CCR4^+$ Treg cells are found in peripheral lymphoid organs and non-lymphoid organs like the skin, but not in the thymus (Sather et al., 2007). The importance of CCR4 in Treg compartment was demonstrated by specific abrogation of CCR4 expression in $Foxp3^+$ cells. CCR4 deficient Treg cells performed normally and were fully functional *in vitro*. However, loss of CCR4 led also to a severe, inflammatory and tissue specific disease in the skin and lungs, indicating impaired homing of $Foxp3^+$ cells to these locations (Sather et al., 2007).

In addition, markers like Klrg1, Nrp1 and PD-1 emerged more recently, and were proposed to define functionally distinct Treg cells (Wei et al., 2006; Feuerer et al., 2009; Chen and Oppenheim, 2011). However, a strict classification is difficult to make, as many of the Treg subsets co-exist at the same time and express similar markers. For example the co-inhibitory receptor killer-cell lectin like receptor G1 (Klrg1) that can be expressed on NK cells and antigen-experienced T cells, has been found on a proportion of Treg cells in the periphery. In the literature $Klrg1^+$ Treg cells are often described as a subset lacking the CD25 or Foxp3 expression. However, $CD25^+$ and $Klrg1^+$ subsets largely overlap and ~60% of $CD4^+Klrg1^+$ Treg cells express CD25, and conversely, ~6% of $CD4^+CD25^+$ cells express Klrg1. Nonetheless, purified $CD4^+CD25^-Klrg1^+$ cells have suppressive potential, even higher than $CD4^+CD25^+Klrg1^-$ cells (Beyersdorf et al., 2007; Feuerer et al., 2010). In addition, $CD4^+Klrg1^+$ cells have a phenotype and transcriptional profile of activated and short-lived Treg cells expressing elevated levels of Treg suppressive molecules. Thus, it was proposed that $Klrg1^+$ Treg cells are a terminally differentiated subset of Treg cells (Cheng et al., 2012; Feuerer et al., 2010). Finally, the expression of Klrg1 together with the CD62L and CD69 activation markers have been proposed to distinguish Treg subsets with different functionality, migration abilities, proliferation and survival (Fig.I.15) (Beyersdorf et al., 2007; Cheng et al., 2012).

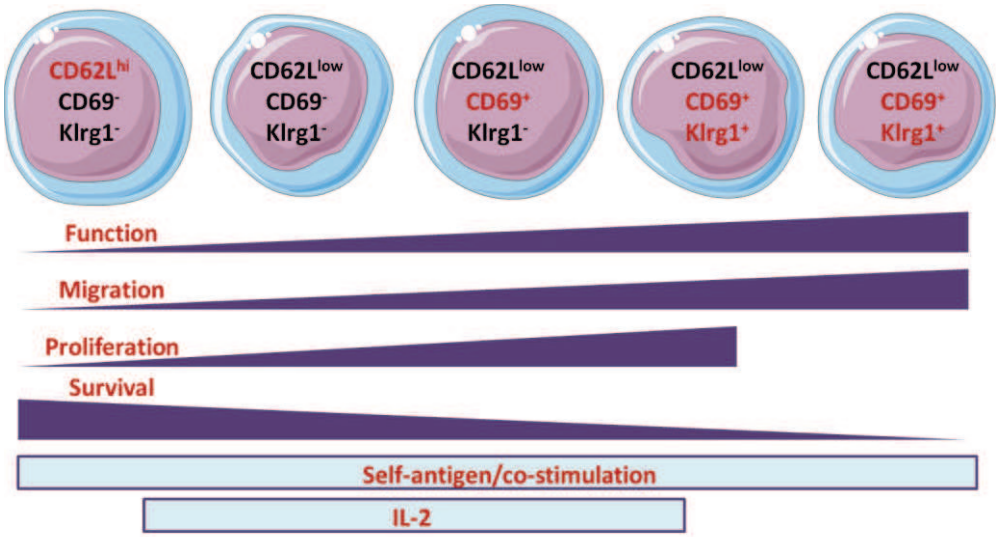

Figure I.15. Development and functional characteristics of Klrg1$^+$ Treg cells. Adapted from (Yuan et al., 2014). CD62L is a known adhesion molecule (L-selectin) expressed on T cells and regulating their trafficking between lymph nodes. CD62L^{hi} cells are considered as naïve and CD62L^{low} as memory/effector cells. CD69 expressed on T cells acts as a costimulatory molecule in proliferation and cytokine secretion. It marks recently activated T cells. Terminally differentiated Klrg1$^+$ cells express low levels of CD62L but do express CD69. They are short-lived and prone to undergo apoptosis. Functional properties of presented subsets were evaluated based on genome-wide gene expression profiling. Function was assessed by the expression of Treg effector molecules, including Fgl2, IL-10 or IL-35. Markers such as Ki-67 or Bcl-2 indicated proliferative activity and apoptosis prone cells, respectively. Chemokine receptors were indicative of migration properties.

I selected these few examples of markers to highlight the particular functional and phenotypical heterogeneity of Treg cells. As depicted in Figure I.14, there are many molecules that are supposed to be characteristic of Treg cells. However, in the current literature, it is difficult to identify what could be the specific role of some of them in Treg cells. At the same time, other markers were proposed to define distinct Treg subsets. Still, many of the observations are based only on a correlation between the expression and function (e.g. CD103$^+$ Treg cells versus CD103$^-$ counterparts, Klrg1 expression correlating with CD62L and CD69, expression of CD103 or CCR4 at distinct anatomical location). In addition, markers identified to differentiate between subsets are often overlapping (e.g. CD25 and Klrg1), making it difficult to precisely categorize cells into distinct populations.

Finally, it is possible that the acquisition of specific extracellular and intracellular markers is a response to different microenvironmental cues and a manifestation of Treg cell lineage plasticity.

I.3.2.2 CD8$^+$ Treg cells

CD8$^+$ Treg cells can also exhibit suppressive functions, but in comparison to CD4$^+$ Treg cells, much less attention has been given to those cells and their biological significance. However, they have also emerged as important players in immune regulation and several subsets have been identified. Nevertheless, still very little is known about their regulation and development.

Phenotypically, several subsets of CD8$^+$ Treg cells can also be distinguished by the expression of cell surface and intracellular marker (Fig.I.16). Moreover, according to their origin, CD8$^+$ Treg cell can be induced and naturally occurring. In the next paragraphs I discuss the best studied populations known today.

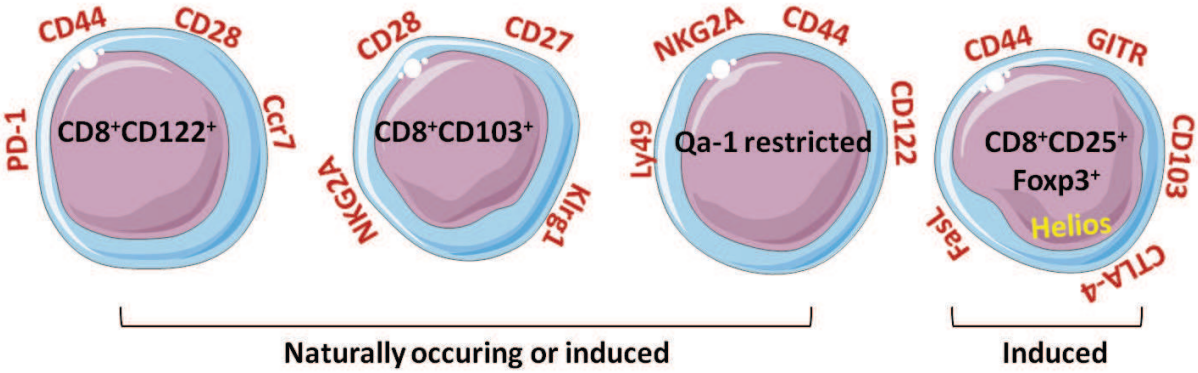

Figure I.16. Phenotypical subsets of CD8$^+$ Treg cells. Based on Koch et al., 2008; Beres et al., 2012; Dai et al., 2014. The presented four types of CD8$^+$ Treg subsets are most frequently described in the literature. Except for the cell surface or intracellular markers (e.g. Foxp3) that categorize them into a given subset (in black), CD8$^+$ Treg cells express other characteristic factors (cell surface in red, intracellular in yellow). The last population of CD8$^+$CD25$^+$Foxp3$^+$ is barely detectable in un-manipulated mice and it is generally accepted that is induced mainly under allogeneic conditions. Populations defined as CD8$^+$CD122$^+$, CD8$^+$CD103$^+$ and Qa-1 restricted can be found as such in immunologically naïve mice, hence the term "naturally occurring". However, it is also known that they can be specifically induced, like the CD8$^+$CD103$^+$ population, which can be generated after alloantigen stimulation.

One of the first phenotypically characterized populations of CD8$^+$ Treg cells was identified as being able to suppress immune responses exclusively after recognition of the MHC class I product, Qa-1. Those cells can suppress the development and relapse of EAE and mice deficient in Qa-1 restricted CD8$^+$ T cells have elevated responses to self antigens (Jiang et al., 1995; Hu et al., 2004). Recently, Qa-1 restricted CD8$^+$ Treg cells were shown to suppress CD4$^+$ Tfh cells (Kim et al., 2010). Phenotypic analysis of those cells revealed that

they are confined to a small population of $CD8^+CD44^+CD122^+Ly49^+$ cells that constitute around 3-5% of $CD8^+$ T cells (Kim et al., 2011).

Recently, human $CD8^+CD103^+$ T cells were identified as alloantigen specific Treg cells. $CD8^+CD103^+$ cells can be induced *in vitro* by alloantigen stimulation, are highly suppressive, act in a cell-cell contact dependent manner and can secrete IL-10 (Uss et al., 2006). $CD8^+CD103^-$ T cells can also differentiate into $CD8^+CD103^+Foxp3^+$ T cells after *in vitro* stimulation with either alloantigens or TGF-β, and $CD8^+CD103^+$ Treg cells contribute to a liver allograft tolerance (Lu et al., 2009). Another study showed that rapamycin, an immunosuppressive compound and inhibitor of mTOR pathway (mammalian Target Of Rapamycin), can induce the *in vitro* generation of $CD8^+CD103^+$ Treg cells after stimulation with alloantigen and enhance their suppressive capacity (Uss et al., 2007). Thus, it is proposed today that CD8 and CD103 can define a distinct subset of Treg cells.

Un-manipulated mice possess also a population of $CD8^+CD122^+$ T cells that can function as regulatory cells. CD122 constitutes an IL-2/IL-15 receptor β chain. CD122 deficient mice have increased number of activated T cells and present a severe immune hyper-responsiveness, elevated granulopoiesis and suppressed erythropoiesis (Suzuki et al., 1995, 1999). However, the transfer of $CD8^+CD122^+$ cells into CD122 deficient neonates prevents the appearance of activated T cells, and $CD8^+CD122^+$ cells can suppress activated conventional $CD4^+$ and $CD8^+$ T cell both *in vivo* and *in vitro* (Rifa'i et al., 2004). $CD8^+CD122^+$ Treg cells recognize activated T cells mainly via the classical MHC class I/TCR interaction and suppress their proliferation by secretion of IL-10 and in a CD28 co-stimulation dependent manner (Endharti et al., 2005; Rifa'i et al., 2008; Shi et al., 2008). In addition, they can also release IFN-γ and TGF-β to suppress $CD4^+$ T cell activation (Mangalam et al., 2012).

In healthy humans and mice, $CD8^+CD25^+Foxp3^+$ cells constitute approximately 0,1% and 0,4% of peripheral $CD8^+$ T cells, respectively (Churlaud et al., 2015). $CD8^+CD25^+Foxp3^+$ regulatory T cells can differentiate from $CD8^+CD25^-$ cells after *in vitro* stimulation with a staphylococcal enterotoxin B antigen. Those cells can suppress cytokine production and proliferation of T cells in a cell-cell dependent manner. They can secrete IL-10 together with TGF-β1, and express classical Treg molecules including CTLA-4, GITR, granzyme A/B, perforin and CD28 (Mahic et al., 2008). $CD8^+Foxp3^+$ cells were also identified in autoimmune disorders, particularly in lupus prone mice and patients with multiple sclerosis (Hahn et al., 2005; Frisullo et al., 2010). $CD8^+Foxp3^+$ Treg cells were also

suggested to play a role in tumor immune escape in prostate and colorectal cancer tissues (Kiniwa et al., 2007; Chaput et al., 2009).

Finally, in 2012, $CD8^+Foxp3^+$ Treg cells were implicated in allogeneic stem cell transplantation and GvHD biology (Robb et al., 2012; Sawamukai et al., 2012; Beres et al., 2012). Those studies showed that $CD8^+Foxp3^+$ Treg cells are induced specifically in an alloantigen specific manner. In a bone marrow transplantation model, it was clear that the emergence of $CD8^+Foxp3^+$ Treg cells is correlated positively with the level of MHC- (and/or minor histocompatibility antigens) mismatch disparity between the recipient and the donor. In syngeneic conditions, $CD8^+Foxp3^+$ Treg cells could not be generated (Beres et al., 2012; Robb et al., 2012). Treg cells induced *in vivo* in allogeneic conditions expressed the Treg markers CD25, CD44, GITR, CD103, PD-1, FasL, CTLA-4, and interestingly, the Helios transcription factor. They were also fully functional and could suppress the proliferation of $CD4^+$ and $CD8^+$ T cells (Beres et al., 2012). Another study provided an elegant protocol to induce $CD8^+CD25^+Foxp3^+$ cells *in vitro,* using allogeneic bone marrow-derived dendritic cells, TGF-β1, IL-2 and RA. The generated cells suppressed $CD4^+$ and $CD8^+$ T cell proliferation and cytokine production. Adoptive transfer of the *in vitro* induced cells protected mice from skin allograft rejection (Lerret et al., 2012).

In summary, a population of $CD8^+CD25^+Foxp3^+$ Treg cells emerged recently as biologically relevant, as demonstrated by numerous *in vivo* studies. However, in contrast to their counterparts of $CD4^+$ origin, very little is known about the molecular mechanisms involved in the differentiation and suppression activity of those cells.

I.3.3 Mechanisms of suppression

Regardless of the phenotype and affiliation with $CD4^+$ or $CD8^+$ lineage, different Treg cell subsets share similar mechanisms of suppression. In general, these mechanisms can be grouped in four main types: suppression by inhibitory cytokines, cytolysis, metabolic disruption and modulation of dendritic cells (Fig.I.17). In this section I describe examples for each type of the suppression mechanism.

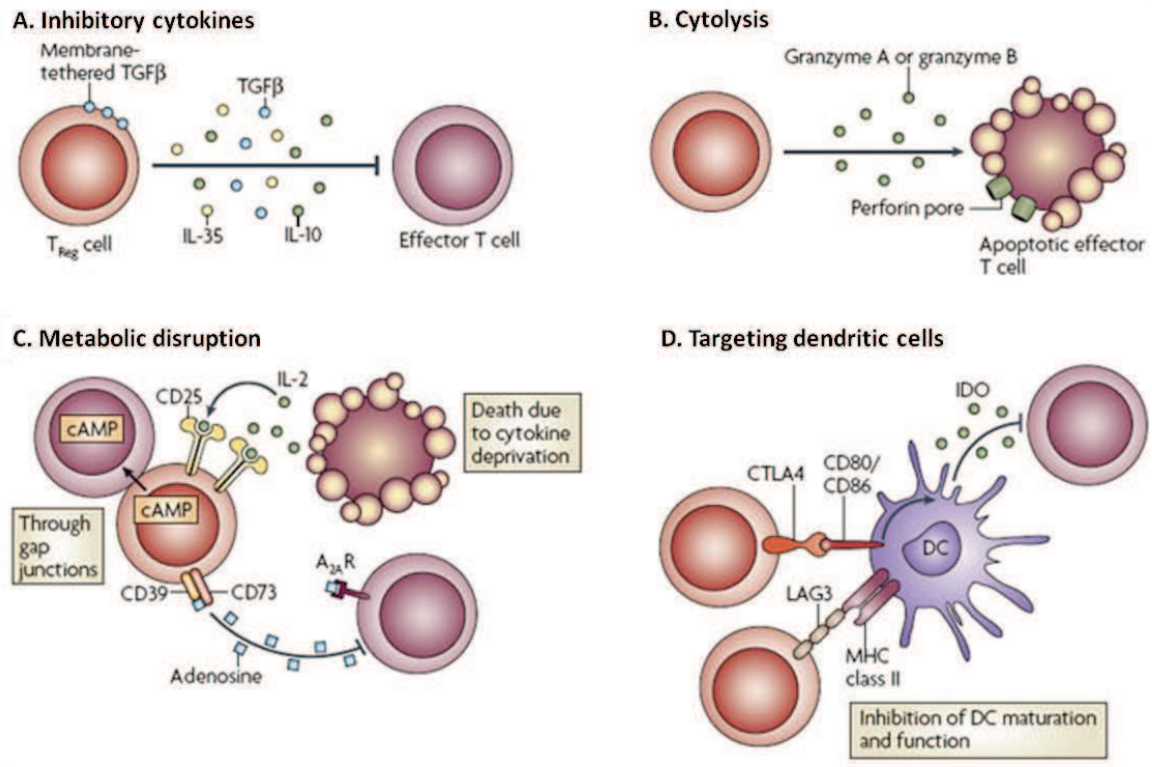

Figure I.17. Main mechanisms of Treg cell mediated suppression. Adapted from Vignali et al., 2008. A. Upon activation Treg cells can secrete inhibitory cytokines including IL-10, IL-35 and TGF-β. B. Cytolysis can be mediated by granzymes A or B and perforin. C. Metabolic disruption is mainly mediated by T cell deprivation of the important survival cytokine – IL-2, through its receptor present on Treg cells (CD25). Co-expression of ectonucleotides CD73 and CD39 lead to the production and release of adenosine, which is recognized by A2A receptor on T cells and triggers the production of cyclic AMP (cAMP). As a result, proliferation and cytokine production by effector T cell can be inhibited. D. Targeting of dendritic cells includes mechanisms impairing DC maturation and/or function, for example, Lag3 interaction with MHC-class-II molecules, CTLA-4–CD80/CD86-co-inhibitory interaction and induction of indoleamine 2,3-dioxygenase (IDO), an immunosuppressive molecule produced by DCs.

Concerning the first mechanism, it is accepted that inhibitory cytokines, including IL-10, IL-35 and TGF-β play a crucial role in Treg mediated suppression. However, they do not always act in synergy and blocking one of them does not necessarily abrogate Treg suppressive potential, indicating that Treg cells can probably use more than one mechanism at the same time (Kullberg et al., 2005). The role of TGF-β was documented *in vivo* in several studies and one particularly elegant, showed that cells that cannot properly respond to TGF-β signaling (they bear a dominant negative version of TGF-β receptor) can escape Treg mediated suppression (Powrie et al., 1996; Fahlén et al., 2005). IL-10 and IL-35 were also shown to be important *in vivo* to suppress effector T cells and many Treg subsets utilize them against target cells (Asseman et al., 1999, 2000; Collison et al., 2007).

Treg cells can also target effector T cells by cytolysis using molecules like granzyme B. A study by Gondek et al. showed, for the first time, that Treg cells have a cytolytic capacity, which is granzyme-B dependent, but perforin independent. Authors used granzyme-B deficient mice and observed that Treg cells ($CD4^+CD25^+$) are defective in suppressing effector $CD4^+$ T cells (Gondek et al., 2005). Granzyme-B and perforin dependent suppression was observed during Treg cell activity against B cells (Zhao et al., 2006). Both mechanisms proved to be crucial also *in vivo*, particularly for Treg mediated suppression of anti-tumor immunity (Cao et al., 2007).

Another mechanism possibly underlying the Treg mediated suppression is often referred to as metabolic disruption, and can be mediated by T cell deprivation of important "nutrients", including cytokines or amino acids. This mechanism was studied most extensively in regards to IL-2. Thornton et al. were the first to suggest, in a study where $CD4^+CD25^+$ cells suppressed the proliferation of effector T cells by specifically inhibiting the production of IL-2, that the suppression was not cytokine mediated but rather dependent on cell-cell contact (Thornton and Shevach, 1998). This mechanism was more recently confirmed by another group, who showed that cytokine deprivation by Treg cells leads to T cell apoptosis through suppression of cytokine-dependent signaling in responder T cells (Pandiyan et al., 2007). However, experiments with human Treg cells showed no requirement for cytokine deprivation, or cytokine participation whatsoever, in Treg mediated suppression (Oberle et al., 2007). One interesting study carried out few years later linked the IL-2 deprivation with TGF-β mediated suppression. In a transwell system that separated Treg cells from effector T cells, these authors showed that TGF-β contributed to Treg suppression under IL-2 depriving condition, suggesting that mechanisms involving cytokine deprivation and cytokine release can act together (Wang et al., 2010).

Finally, Treg cells can suppress effector T cells indirectly, by modulating dendritic cell function. Lymphocyte activation gene-3 (Lag-3) is a CD4-related transmembrane protein expressed by Treg cells that binds MHC class II molecules on APCs. During interaction between Treg cell and DC, Lag-3 engagement with MHC class II can inhibit DC activation (Liang et al., 2008). Treg cells can also down-modulate B7 molecules on DCs in a CTLA-4-dependent manner, increasing suppression of T-cell activity through stripping APCs from co-stimulatory ligands. The co-inhibitory interaction between CTLA-4 on Treg cells and CD80/CD86 on DCs can also promote the production of indoleamine 2,3-dioxygenase (IDO), a molecule that modulates tryptophan catabolism and triggers generation of pro-apoptotic metabolites that suppress effector T cell function (Fallarino et al., 2003; Oderup et al., 2006).

I.4. Ikaros family of transcription factors

The Ikaros family of transcription factors comprises Ikaros (*Ikzf1*), Helios (*Ikzf2*), Aiolos (*Ikzf3*), Eos (*Ikzf4*) and Pegasus (*Ikzf5*) and is crucial for hematopoiesis. In this chapter I will introduce this family of closely related proteins. In each section my focus will be on Eos and Helios, which I studied during my thesis. I will also mention Ikaros, the founding and the best characterized member of the family.

I.4.1 Discovery and evolution

The discovery of Ikaros proteins started in the early 1990s. Ikaros is the founding member of the family. Interestingly, it was first identified as a protein controlling the transcription of the terminal deoxynucleotidyltransferase (*Tdt*) gene and was called LyF-1 (Lo et al., 1991). One year later, a second lab re-discovered this protein bound to the CD3δ gene (*Cd3d*) in T cells, where it was given its present name – Ikaros (Georgopoulos et al., 1992). The next family members were named according to the Greek mythology, as initiated. Aiolos and Helios were discovered as new dimerization partners of Ikaros (Morgan et al., 1997; Kelley et al., 1998; Hahm et al., 1998). Eos was identified in a screen for genes induced in cultured neuronal cells (Honma et al., 1999). Another study designed to find new Ikaros family proteins, also identified Eos, as well as the fifth member of the family, Pegasus (Perdomo et al., 2000).

From the evolutionary point of view, the Ikaros family is thought to originate from a single primordial gene, possibly related to the Hunchback gene (*Hb*). This ancestor gene underwent its first duplication before the transition from urochordates/lower vertebrates to higher vertebrates and subsequently gave rise to all five members through duplications coinciding with the “emergence” of adaptive immunity, at around 450 million years ago (John et al., 2009).

I.4.2 Protein structure

Ikaros proteins are characterized by the presence of highly conserved C2H2-type zinc fingers (ZF or Zn-fingers). All Ikaros family members have two characteristic sets of Zn-finger domains: a C-terminal which forms a dimerization domain and a N-terminal which forms a DNA binding domain (DBD) (Molnár and Georgopoulos, 1994; Rebollo and Schmitt, 2003). Ikaros, Helios, Aiolos and Eos have a DBD formed by four Zn-fingers, whereas Pegasus has only three Zn-fingers at the N-terminus (Fig.I.18) (Molnár and Georgopoulos, 1994; Perdomo et al., 2000). This common protein structure is also

characterized by high protein sequence similarity. For example, Eos and Helios share 83,3% of the overall protein sequence, Eos and Aiolos - 82,4% and Eos with Ikaros - 72% (Honma et al., 1999).

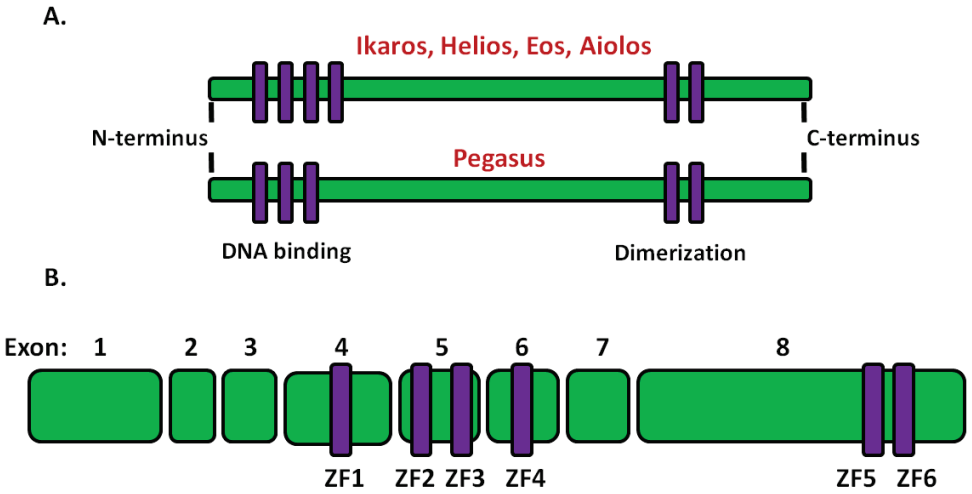

Figure I.18. Schematic structure of Ikaros family proteins. A. Ikaros, Helios, Aiolos and Eos share the general organization of the protein. At the N-terminus they possess a DNA binding domain composed of 4 zinc fingers (violet blocks) and a dimerization domain at the C-terminus composed of two zinc fingers. Pegasus has only 3 zinc fingers forming the DNA binding motif. B. Schematic representation of exons (green blocks) encoding the zinc fingers (ZF). The presented structure is based on the example of *Ikzf4* gene, encoding Eos, which has 8 exons.

Zn-fingers proteins need usually two or three fingers in a DBD domain for DNA recognition and stable binding (Wolfe et al., 2000). For example, in case of Ikaros, Zn-fingers 2 and 3 are sufficient for stable binding and recognition of the consensus binding site, whereas fingers 1 and 4 seem to modulate binding to specific genomic sites (Cobb et al., 2000; Georgopoulos et al., 1994; Koipally et al., 2002). A recent study has proposed that the first and fourth Zn-fingers of Ikaros contribute also to the functionality of Ikaros during hematopoiesis, and that ZF1 is required for generation of full-length Ikaros protein, whereas ZF4 is necessary for tumor suppressor function (Schjerven et al., 2013). All together, this suggests that the N-terminal Zn-fingers are crucial components of Ikaros proteins, regulating different biological functions and genes.

Zn-fingers 5 and 6 of the Ikaros family proteins form the dimerization domain, necessary for the interactions of the proteins with themselves and other family members (Hahm et al., 1998; Morgan et al., 1997; Perdomo et al., 2000). For example, Eos can form homodimers or heterodimers with all family members, but only in a form of a full length (FL) protein. Deletion of the C-terminal part of the protein abrogates interactions with Ikaros family proteins (Honma et al., 1999). In addition, the C-terminal dimerization domain is

required for protein function and stability, as mutations in the last two Zn-fingers can impair the ability to bind DNA and activate transcription (Sun et al., 1996).

Alternative splicing can generate multiple isoforms of Ikaros proteins. Their common feature is the presence of the C-terminal Zn-fingers, but they differ in the composition of the N-terminal Zn-fingers. For example, there are several known isoforms of Ikaros, which can be roughly divided into two groups (Fig.I.19A). The first one is characterized by the presence of at least two zinc fingers in the DBD of the protein and is capable of DNA binding. The second lacks more than two Zn-fingers in the DBD, and cannot bind DNA (Molnár and Georgopoulos, 1994).

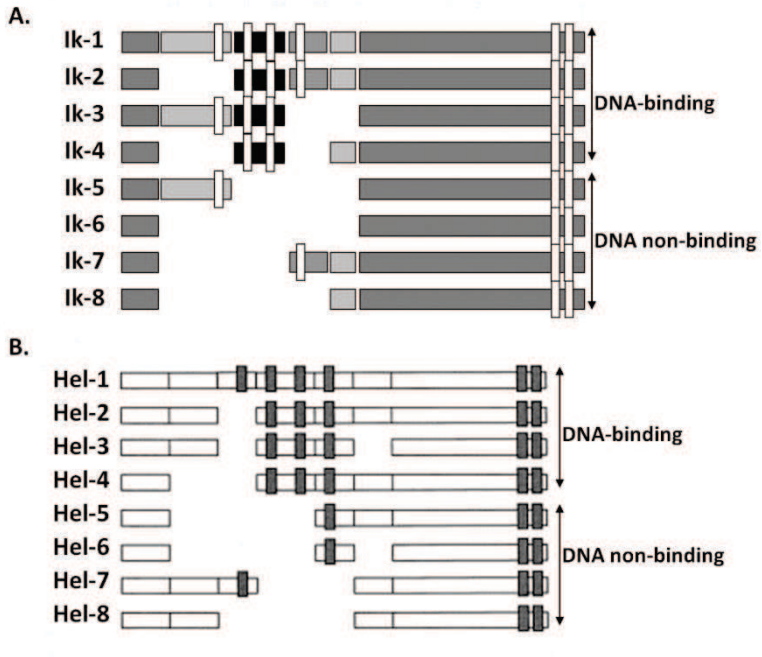

Figure I.19. Isoforms of Ikaros and Helios. Examples of isoforms of Ikaros and Helios**.** Adapted from Ezzat and Asa, 2008 and Nakase et al., 2002. Examples of Ikaros (A) and Helios isoforms (B) that can possess the DNA binding activity or due to the loss of N-terminal Zn-fingers lack the DNA-binding activity. White or grey vertical bars represent zinc fingers. Horizontal blocks depict protein coding exons.

Similarly, Helios has several identified isoforms that can bind DNA or not, depending on the composition of the DBD (Fig.I.19B) (Nakase et al., 2002). Interestingly, only some isoforms of Ikaros and Helios are expressed during normal hematopoiesis. The full length Ikaros (Ik-1 isoform) and Ik-2 (lacking exon 2 and the first Zn-finger) are abundantly expressed in normal hematopoietic cells. Ikaros isoforms lacking other Zn-fingers are less abundant and are mainly detected in malignant cells (Hahm et al., 1998; Molnár and Georgopoulos, 1994; Payne et al., 2003). Likewise, the Helios isoforms Hel-1 and Hel-2 are found in healthy cells, whereas the remaining ones are detected in malignant cells, particularly from patients with T cell leukemias (Fujii et al., 2003; Nakase et al., 2002).

Ikaros proteins can bind to DNA as dimers or possibly multimers. In this regard, different complexes may be formed between the FL protein and the isoforms, resulting in diverse functionality (Fig.I.20) (Morgan et al., 1997; Westman et al., 2003). For example,

Ikaros isoforms lacking Zn-fingers 2 and 3 can heterodimerize with DNA-binding isoforms, and operate in a dominant-negative manner. Those dominant-negative (DN) isoforms can negatively affect the DNA binding and transcriptional activity of the functional proteins (Sun et al., 1996; Li et al., 2011). This in turn is an effect of different nuclear localization potential of Ikaros isoforms. Ikaros DN isoforms do not enter the nucleus and are retained in the cytoplasm, where they cannot activate transcription (Sun et al., 1996; Molnár and Georgopoulos, 1994).

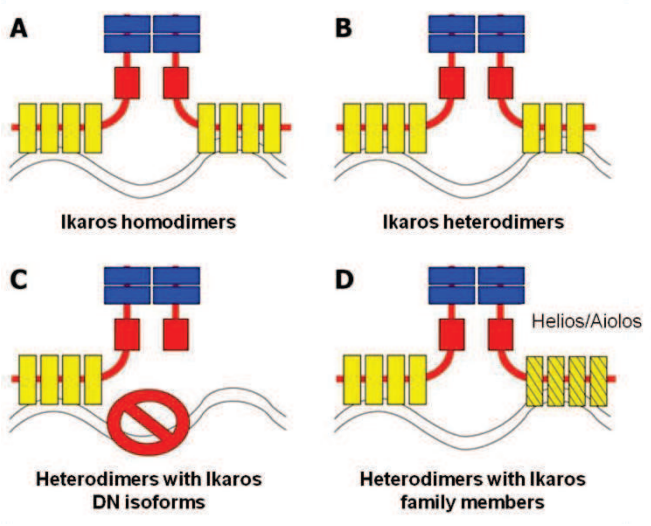

Figure I.20. Possible interactions between Ikaros isoforms and Ikaros family proteins. Adapted from (Li et al., 2011). The activity of Ikaros can be controlled by the type of complex it forms with its isoforms or other family members. Examples of possible complexes are presented. A. Homodimers of full length (FL) Ikaros protein; B. Heterodimers of FL Ikaros with isoforms that have the DNA-binding activity; C. Heterodimers of FL Ikaros with dominant-negative (DN) isoforms are retained in the cytoplasm, thus they cannot bind DNA; D. Heterodimers of FL Ikaros with other family members (here Helios or Aiolos).

Contrary to Helios and Ikaros, only a FL Eos protein has been detected so far (Honma et al., 1999; Perdomo et al., 2000). However, the *Ikzf4* locus can potentially generate 8 alternative transcripts, from which 3 may be protein coding (Fig.I.21), and all having the DNA-binding and homo/hetero-dimerization potential.

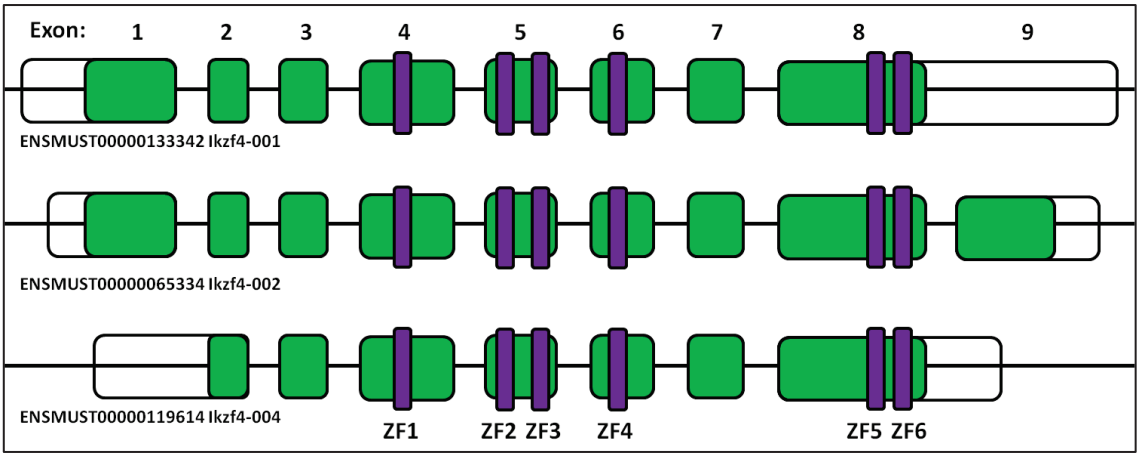

Figure I.21. *Ikzf4* protein coding transcripts. Schematic representation of protein coding transcripts of *Ikzf4* gene. Green blocks indicate exons, violet vertical bars indicate zinc fingers (ZF), empty blocks are UTR (Un-Translated Region), and lines show intronic regions. Ikzf4-001 encodes the identified full length Eos protein. Prediction of protein coding transcripts is based on Ensembl and VEGA/Havana genes (ensemble.org). Nomenclature presented on the left comes from the Ensembl genome browser.

I.4.4 Expression in the hematopoietic system

Ikaros family proteins are detected throughout hematopoiesis, starting from the most immature HSC to mature cells of the lymphoid and myeloid lineages. Below, I briefly summarize what is known about the expression of Ikaros, Eos and Helios in the hematopoietic system.

Ikaros expression is restricted mainly to sites of hematopoiesis. It can be detected in the developing mouse embryo, in the fetal liver and in the embryonic thymus (Georgopoulos et al., 1992). In the adult, Ikaros is expressed in the LT-HSCs and can be detected as cells differentiate through ST-HSCs and MPPs. It is highly expressed again in the lymphoid progenitors and B cell precursors as well as maturing thymocytes (Georgopoulos et al., 1994; Klug et al., 1998). Within the T cell lineage, Ikaros is most highly expressed in DP cells. Ikaros can be also found in progenitors and mature cells of the myeloid lineage. Finally, Ikaros is expressed in almost all types of hematopoietic cells (Klug et al., 1998).

Eos was first found to be expressed in the developing nervous system, but also in the embryonic thymus in the mouse (Honma et al., 1999). In man, it was found mainly in skeletal muscles and brain, with lower expression in the heart, kidney, liver, thymus and spleen (Perdomo et al., 2000). Eos can be detected in many hematopoietic populations from both lymphoid and myeloid lineages. It is highly expressed in self-renewing populations, including embryonic stem (ES) cells, LT-HSC, ST-HSCs and MPPs and its levels decrease as cells become more committed. The highest levels of Eos are then found in the T cell lineage, with relatively high expression in DN2 and DN3 cells, $CD8^+$ T cells, and a peak of expression in

$CD4^+$ T cells in the thymus (Papathanasiou et al., 2009). Within the T cell lineage, Eos is mostly expressed in Treg cells, where its high levels are found both at the protein and mRNA level (ImmGen Database, Hill et al., 2007; Rieder et al., 2015; Sharma et al., 2013). This pattern of expression, especially in the HSC and progenitor cells, as well as in T cells, resembles that of Helios.

Helios expression can be detected at various sites of embryonic hematopoiesis, in adult HSCs and in mature cells, where it is mainly restricted to lymphoid cells (Hahm et al., 1998; Kelley et al., 1998). In more detail, early Helios expression can be detected in LT-HSCs followed by decreasing levels in ST-HSCs, MPPs and more committed progenitors. It again peaks throughout T cell development in the thymus, with high levels detected in DP cells, $CD4^+$ and $CD8^+$ T cells. The highest levels of Helios, both in the thymus and the periphery, can be found in Treg cells (Papathanasiou et al., 2009; Sugimoto et al., 2006).

I.4.5 Mechanisms of transcriptional regulation

Ikaros family proteins can repress or activate gene expression through different mechanisms. However, to perform this regulatory function they must first bind to their target genes. The N-terminal Zn-fingers of all Ikaros family members are responsible for sequence specific DNA-binding. The binding motif identified for Ikaros, Helios, Aiolos and Eos contains the core sequence “tGGGAa” (Honma et al., 1999; Kelley et al., 1998; Molnár and Georgopoulos, 1994; Morgan et al., 1997). Only Pegasus has an “atypical” “GNNNGNNG” DNA binding sequence, probably due to a different organization of the N-terminal Zn-fingers (Fig.I.17) (Perdomo et al., 2000).

In the following section I give examples of the mechanisms used by Ikaros family proteins, namely Ikaros, Helios and Eos, to regulate gene expression.

- **Ikaros**

In lymphocytes, Ikaros localizes to pericentromeric heterochromatin (PC-HC), where it regulates the expression of its target genes (Fig.I.22A/B). (Brown et al., 1997; Gurel et al., 2008). Transcriptional gene activation can be mediated by the SWI/SNF (SWItch/Sucrose Non-Fermentable) chromatin remodeling complex, through mechanisms including histone acetylation (Wurster and Pazin, 2012). Ikaros associates with SWI/SNF complex to regulate gene expression in T cells and erythroid progenitors (Kim et al., 1999; O’Neill et al., 2000). Ikaros can also initiate gene transcription by allowing long-range chromatin interactions in the human β-globin locus. In addition, Ikaros regulates gene expression through promoting transcription initiation and elongation mechanisms. In erythroid cells it recruits Brg1 (the

catalytic subunit of the SWI/SNF complex), Gata-1, Pol II (Polymerase II) and importantly, Cdk9 – the catalytic subunit of the positive transcription elongation factor (P-TEFb) to the human γ-globin encoding gene, eventually activating its transcription (Bottardi et al., 2011).

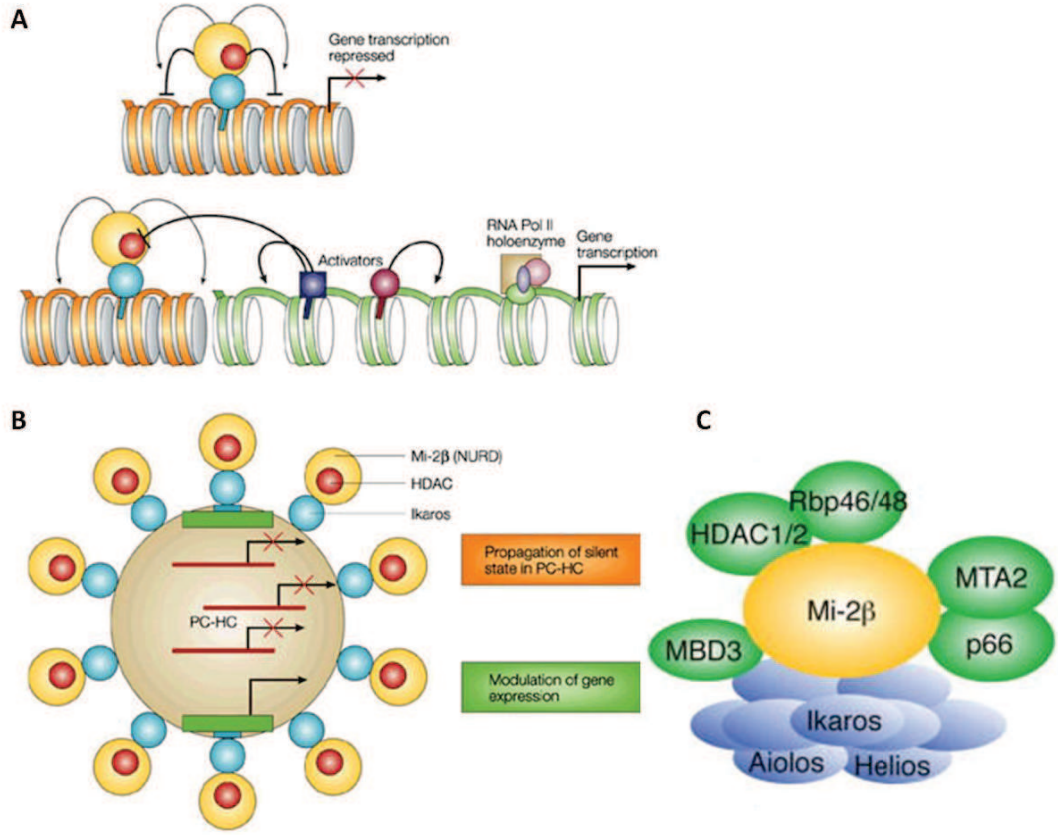

Figure I.22. Mechanisms of gene repression by Ikaros proteins. Adapted from (Georgopoulos, 2002; Yoshida and Georgopoulos, 2014). A and B. Ikaros transcription factor (blue) co-localizes with pericentromeric heterochromatin PC-HC (depicted by orange nucleosomes or the ring of balls). Ikaros and the NuRD complex (orange balls, with Mi-2β as the core) containing the histone deacetylases (HDAC, red balls) characterize repressed genes (orange nucleosomes). Transcriptional activators can also access target genes and recruit histone modifiers that promote the transcriptionally open (permissive) chromatin state (green nucleosomes). C. Composition of the NuRD complex, containing Class I histone deacetylases (HDAC1/2) and the ATP-dependent chromatin remodeler Mi-2β, through which it can bind with Ikaros family proteins.

Ikaros can mediate gene suppression through several mechanisms. It can associate with co-repressors, including C terminal binding protein (CtBP) or CtBP interacting protein (CtIP), which can repress transcription independently of histone modifications (Koipally and Georgopoulos, 2000, 2002a). In addition, Ikaros associates with components of chromatin remodeling complexes to repress the expression of its target genes in a histone deacetylase dependent manner. It binds Mi-2β, a catalytic subunit of the nucleosome remodeling and deacetylase complex (NuRD) (Fig.I.22) (Kim et al., 1999; Zhang et al., 2012). Ikaros can also bind to the subunits of Sin3 complex, containing histone deacetylases HDAC1 and

HDAC2 or directly associate with these deacetylases (Koipally et al., 1999; Koipally and Georgopoulos, 2002b).

During thymocyte development Ikaros is highly expressed in DP cells, where it represses the expression of Notch-target genes, for example *Hes1*. Interestingly, this repression is accompanied by a decrease in the trimethylation of lysine 27 on histone 3 (H3K27me3) in Ikaros deficient cells (Dumortier et al., 2006; Kleinmann et al., 2008). This suggests that Ikaros regulates gene repression also via Polycomb Repressive Complex 2 (PRC2), which is responsible for the deposition of the H3K27me3 repressive chromatin mark (Rea et al., 2000).

All together, a considerable amount of data show the role of Ikaros in mediating gene regulation through its association with different protein partners, yet still little is known about Ikaros molecular functions and mechanisms as transcription factor.

- **Eos**

So far, it has been shown that Eos may act as a transcriptional repressor in the hematopoietic system (Hu R et al., 2007; Yu HC et al., 2011; Pan F et al., 2009) or as a transcriptional activator outside of the hematopoietic system (Bao J et al., 2004; Yeung F et al., 2011).

Mechanisms facilitating Eos mediated gene activation are not well defined. In muscle cells, Eos is required for the expression of miR-499, and knock-down of Eos with siRNA (small interfering RNA) abrogates its expression (Yeung et al., 2012). In neuronal cells, Eos induces the expression of PSD-95 (postsynaptic density protein-95) *in vivo* through an unknown pathway (Bao et al., 2004). Those studies do not provide a mechanism of gene expression activation. Therefore, it is not clear if the observed effects actually require active participation of Eos.

Concerning the transcriptional repression activity, Eos can recruit and bind co-repressors CtBP and Sin3a, for example in osteoclast precursors (Perdomo and Crossley, 2002; Hu et al., 2007). In Treg cells, Eos binds to Foxp3 and associates with CtBP, initiating epigenetic changes, including DNA methylation, that leads to gene repression (Pan et al., 2009). Eos can also negatively regulate the expression of γ-globin encoding gene during erythroid differentiation, through inhibition of the interaction between the LCR (locus control region) and the gene promoter (Yu et al., 2011). Eos has also the capacity to bind histone deacetylases HDAC1 and HDAC2 as well as components of the NuRD complex *in vitro*, however, the biological relevance of this finding is not well understood (Koipally and Georgopoulos, 2002b).

- **Helios**

The functions of Helios and its mechanisms of action as a transcription factor are largely unknown. It has a potential to activate gene expression, but this was shown only in an *in vitro* system, where it could drive the expression of a reporter gene (Kelley et al., 1998).

Similar to Ikaros, Helios co-localizes with PC-HC, suggesting its active role in gene repression (Kelley et al., 1998). Helios can also bind components of the NuRD and Sin3 histone deacetylase complexes, HDAC1 and HDAC2, as well as co-repressors CtBP and CtIP implicated in gene repression (Koipally and Georgopoulos, 2002b; Sridharan and Smale, 2007). However, examples for Helios mediated gene repression during hematopoiesis are not well documented and do not always indicate an active role of Helios. For example, in Treg cells loss of Helios expression leads to the increase in IL-2 production and is associated with an increase in H3 acetylation. Thus, it was proposed that Helios, through binding to the *Il2* promoter, induces epigenetic modifications, including histone deacetylation (Baine et al., 2013). However, the exact mechanism in this system and identity of possible protein partners recruited by Helios, are two points that need to be resolved.

I.5. Regulation of the Treg cell lineage

For a long time, Treg cells have been described and defined by the expression of the Foxp3 transcription factor. In this section, two aspects of Treg cell regulation are described. First, I discuss the importance of Foxp3 in $CD4^+$ Treg cells and provide examples of Foxp3-mediated gene regulation mechanisms. Second, I discuss why Foxp3 alone is not sufficient to confer the Treg cell genetic signature and functional properties.

I.5.1 Crucial role of the Foxp3 transcription factor

Many studies provided evidence for the critical role of Foxp3 in the development and function of Treg cells. The $CD4^+CD25^+$ Treg cells constitutively expressing the Foxp3 transcription factor are required to maintain immune homeostasis and to prevent from immune responses that can be potentially harmful (Sakaguchi et al., 2008; Rudensky, 2011). Treg cells migrate to the sites of ongoing inflammation and respond by limiting excessive immune reactions by targeting mainly helper T cells, including Th1, Th2, Th17 and Tfh cells, and it is known today that they can suppress them in a Foxp3 dependent manner (Chaudhry et al., 2009; Fyhrquist et al., 2012; Koch et al., 2009; Linterman et al., 2011).

Mutations in the human *FOXP3* gene lead to the development of defective Treg cells and to the appearance of the IPEX syndrome (immune dysregulation, polyendocrinopathy, enteropathy, X-linked syndrome), together with autoimmune and inflammatory bowel disease (Bennett et al., 2001). Mice that carry a mutation or deletion of *Foxp3* fail to generate $CD4^+CD25^+$ Treg cells and develop systemic and lethal lymphoproliferative disorders (Brunkow et al., 2001; Fontenot et al., 2003; Godfrey et al., 1991).

Additionally, Foxp3 is not up-regulated in activated conventional $CD4^+CD25^-$ T cells, contrary to other classical markers which define Treg cells (Fontenot et al., 2003). At the same time, ectopic expression of Foxp3 is sufficient to up-regulate the expression of CD25, CTLA-4 or GITR and to repress production of effector cytokines (IL-2, IL-4, IFN-γ), while inducing suppressive potential in $CD4^+CD25^-$ T cells (Fontenot et al., 2003; Hori et al., 2003; Khattri et al., 2003). All together, these early studies established Foxp3 as a key phenotypic marker and a regulator of the Treg cell lineage.

I.5.2 Foxp3 mediated gene regulation in Treg cells

Foxp3 belongs to a Forkhead (FKH) family of transcription factors, which is characterized by the presence of a highly conserved FKH-binding domain (Kaufmann and Knöchel, 1996). Foxp3 protein has several functional domains facilitating transcriptional

regulation through interaction with protein partners, enabling the formation of Foxp3 homo-dimers or tetramers, and finally allowing binding to FKH motifs at Foxp3 target genes (Fig.I.23).

The suppressive function of Foxp3$^+$ Treg cells is facilitated by the activation of genes associated with suppressive functions, like *Ctla4* or *Tnfrsf18 (*encoding GITR*)*. At the same time, an intrinsic property of Treg cells is their anergy, as they do not normally proliferate and produce IL-2 after antigen stimulation without other signals. Thus, release of effector cytokines such as IL-2 or IFN-γ must be limited. With the help of omics approaches many more of Foxp3 target genes have been described. Foxp3 suppression of its targets was shown to be required for the normal function of Treg cells, as abnormal activity of these genes can result in autoimmunity (Marson et al., 2007). Furthermore, Foxp3 binding regions were identified for hundreds of genes and microRNAs (miRNAs). Interestingly, many of the Foxp3 bound genes were up- or down-regulated in Foxp3$^+$ Treg cells, indicating that Foxp3 is indeed a transcriptional repressor and activator (Zheng et al., 2007).

Concerning the Foxp3 mechanism of action, it can work in a DNA-binding complex with NFAT (nuclear factor of activated T cells) to regulate the transcription of several known target genes indispensable for Treg function, including *Il10* (Bettini and Vignali, 2009; Campbell and Ziegler, 2007). Repression of a number of genes is also dependent on Foxp3 interaction with other transcription factors, including Eos (Hill et al., 2007; Pan et al., 2009). Interestingly, transcription factors can also modulate the expression of Foxp3 itself. For example, the transcription factors Smad3 and NFAT are required for histone acetylation in the enhancer region of *Foxp3* gene and its induction (Tone et al., 2008).

Foxp3 can also mediate epigenetic modifications of its target genes, for example via an association with the histone acetyltransferases, Tip60 and p300, and the histone deacetylase HDAC7 (Li et al., 2007; Tao et al., 2007). Bettini et al. showed that Foxp3^{GFP} knock-in reporter mouse, which carries the N-terminal GFP-Foxp3 fusion protein, is a hypomorph characterized by the accelerated autoimmune diabetes, when introduced on a NOD (Non-Obese Diabetic) background. Foxp3^{GFP} mice have also functionally impaired nTreg compartment under inflammatory conditions and a defect in iTreg cell generation. Interestingly, Foxp3 was not able to interact with HDAC7, Tip60 and Eos protein partners, which in turn led to a loss of Foxp3-dependent epigenetic modifications, altered transcriptional signature and reduced Foxp3-dependent gene repression in Treg cells, for example of the *Il2* locus (Bettini et al., 2012).

The histone deacetylases HDAC3 and HDAC9 are also implicated in the regulation of Foxp3$^+$ Treg cell function. In murine models, loss of HDAC3 activity restores the production of IL-2 by nTreg cells and impairs their suppressive function *in vitro* and *in vivo*. This study determined also that HDAC3 and Foxp3 physically interact, and that HDAC3 expression can reduce *Il2* promoter activity. In addition, HDAC3 deficient T cells cannot differentiate into iTreg cells under polarizing conditions, finally implicating HDAC3 in the regulation of both nTreg and iTreg cells (Wang et al., 2015). Strikingly, loss of HDAC9 has an opposite effect, and increases numbers and the functionality of Foxp3$^+$ Treg cells in a model of colitis (de Zoeten et al., 2010).

In addition, Foxp3 can act by recruiting the histone methyltransferase Ezh2, the catalytic subunit of PRC2 complex, to direct the deposition of H3K27me3 repressive chromatin mark on genomic regions, in Treg cells activated under inflammatory conditions (Arvey et al., 2014).

A study from Rudra et al. from 2012, showed also that Foxp3 can form multiprotein complexes and identified protein partners associated with Foxp3, including chromatin remodeling complexes NuRD and SWI-SNF nucleosome remodeling complexes and many other transcription related factors. Interestingly, many of the genes encoding Foxp3 partners, were also direct targets of Foxp3 (Rudra et al., 2012). All together, it is clear that Foxp3 transcription factor regulates gene expression in tight cooperation with a number of factors and interaction with its protein partners is crucial for Foxp3-dependent gene regulation in Treg cells. Figure I.23 gives examples of known Foxp3 protein partners and their functions.

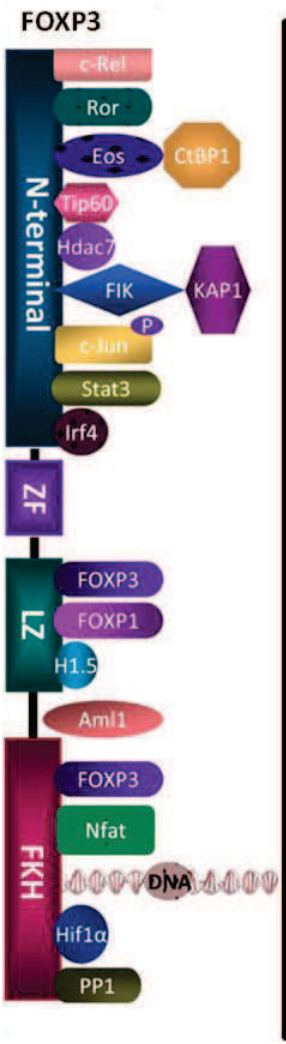

Interacts with	Foxp3 region	Function
c-Rel	Exon 1	Inhibition of NFκB. Nuclear translocation
RORγt, RORα	Exon2	Suppression of ROR-mediated IL17A
Eos/CtBP1	Proline rich region	Suppression of gene expression
TIP60/HDAC7	106-190	Oligomerization status. Transcriptional repression/activation
FIK/KAP1	106-198	Decrease IL2 and IFN- γ production
c-Jun	unknown	Alters subnuclear localization of c-Jun. Cell anergy
STAT3/IRF4	unknown	Modulate Treg effector functions
FOXP3	K250, K252	FOXP3 dimerization
FOXP1		Competition with FOXP3 homo-dimerization
H1.5	unknown	Repression of IL2 transcription
AML1/Runx	278-336	Repression of IL2 and IFN-γ production. Cell anergy
FOXP3(FKH domain)	364-374	FOXP3 dimerization
NFAT	Wing1, H2 helix	Repression of IL2 and up-regulation of CTLA-4, CD25
DNA	H3 helix	DNA binding
HIF1α	unknown	Promote FOXP3 degradation by the proteasome
PP1	S418	P-S418 is necessary for the function of FOXP3

Figure I.23. Examples of Foxp3 protein partners and their roles. Adapted from Lozano et al., 2013. *Foxp3* gene is located on the X chromosome and its protein product has several functional domains: N-terminal domain crucial for transcriptional repression, a zinc finger (ZF) and a leucine-zipper (LZ)-like motif mediating the formation of Foxp3 homo-dimers or tetramers, and the highly conserved C-terminal FKH (Forkhead) domain responsible for the DNA binding. Specific Foxp3 domains can interact with other protein partners (interaction presented on the left and exact Foxp3 region indicated in the table) and confer specific functions (right column of the table). Only examples of Foxp3 partners are presented.

I.5.3 Is Foxp3 sufficient to define Treg cells?

The concept that the $CD4^+$ Treg cell lineage is regulated exclusively by Foxp3 has been questioned by several studies and observations. Certainly, Foxp3 is important to establish the Treg transcriptional signature, but Treg lineage specification is also largely influenced by the TCR, IL-2 and TGF-β signaling pathways (Hill et al., 2007; Sugimoto et al., 2006). In the study by Hill et al., data from several gene expression profiles were combined, including those from conventional T cells and Treg cells, activated or resting. The analysis revealed a few hundred genes that are differentially expressed between Treg cells

and conventional T cells, and which compose a "Treg-cell signature". Strikingly, it became clear that this signature cannot be entirely attributed to Foxp3, because it contained gene clusters that are co-regulated with Foxp3, but not transactivated (induced after Foxp3 transduction in conventional T cells) by Foxp3 (Fig.I.24) (Hill et al., 2007).

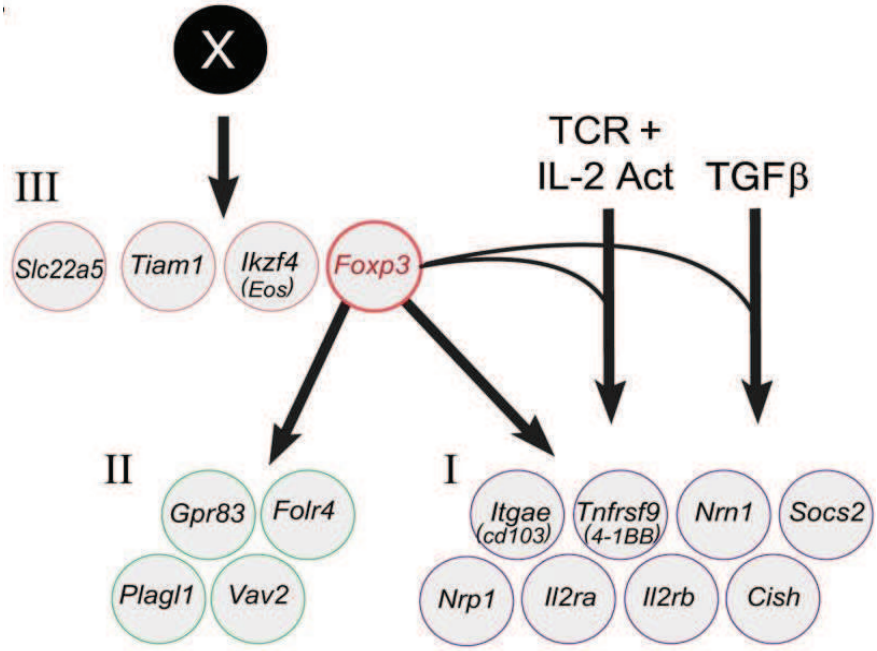

Figure I.24. Clusters of genes defining the Treg cell signature and their hierarchy. From (Hill et al., 2007). Cluster I indicates genes that can be transactivated by Foxp3 but they correlated poorly between the various datasets, probably because they are also influenced by signals delivered by TCR, IL-2 or TGF-β. Genes in clusters II and III are well correlating with Foxp3 but only genes from cluster II are transactivated by Foxp3 transduction, indicating that they are directly or indirectly regulated by Foxp3. Genes from cluster III cannot be transactivated by Foxp3 indicating another level of regulation that is yet to be discovered.

Another study by Samstein et al. analyzed Foxp3 occupancy at enhancer regions in Treg and conventional T cells. It showed that Foxp3 binds to enhancers in T cells, which are already occupied by its cofactors (e.g. Foxo1). In addition, these enhancer regions become accessible in $CD4^{+}Foxp3^{-}$ upon TCR activation, before Foxp3 expression, showing that during Treg cell differentiation Foxp3 is recruited to enhancers in a TCR-dependent manner (Fig.I.25). Overall, this suggested that other signals are necessary to establish the Treg signature (Samstein et al., 2012).

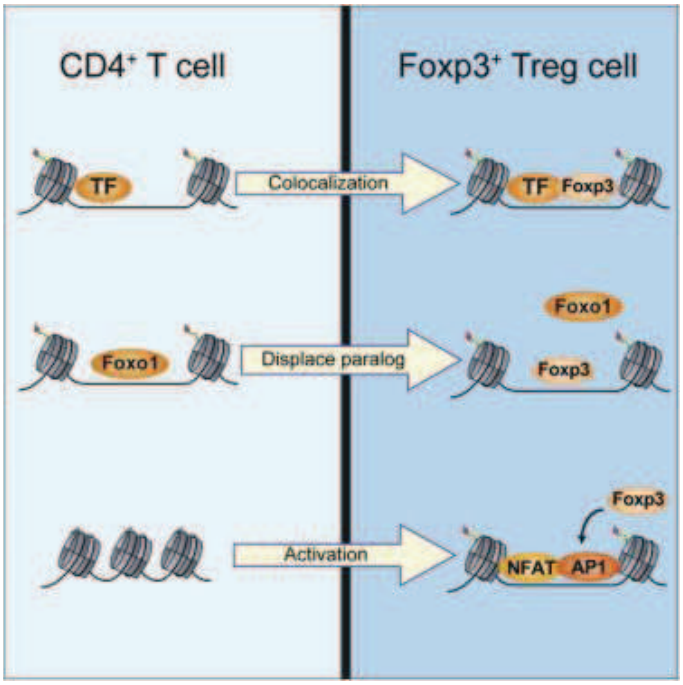

Figure I.25. Possible mechanisms of Foxp3 gene regulation at enhancer regions. From Samstein et al., 2012. Analysis of DNA sequences at Foxp3 binding sites to enhancers in T cells identified a Forkhead binding motif only in a small proportion of these regions, suggesting a presence of cofactors. In this regard, Foxp3 can bind to sites occupied by cofactors in precursor cells, for example Foxo1, a Forkhead family member (two top panels). Finally TCR signaling is required to establish the accessibility to the majority of Treg-specific enhancers. This occurs possibly through recruitment of AP-1, which forms complexes with NFAT, to control expression of target genes downstream of TCR signals (bottom panel).

In line with these studies, ectopic expression of Foxp3 in $CD4^+Foxp3^-$ T cells is not sufficient to establish a complete Treg transcriptional signature (Hill et al., 2007; Sugimoto et al., 2006). Another peculiar point is that human conventional T cells can express Foxp3 expression upon activation without acquiring suppressive functions (Allan et al., 2007; Miyara et al., 2009). Likewise, other studies that used non-functional Foxp3 showed that it is required mainly to maintain Treg cell effector functions, initiated by the TCR signaling, rather than to drive the lineage commitment (Gavin et al., 2007; Lin et al., 2007). Finally, another study, that combined both experimental approaches and sophisticated computational methods, clarified some of the mentioned observations. These authors showed that Foxp3 acts in synergy with a particular group of transcription factors to confer the Treg cell transcriptional signature. Those transcription factors included Eos, Irf4, Satb1, Lef1 and Gata1 (Fu et al., 2012).

These studies demonstrate the complexity in the regulation of the Treg cell lineage. In this regard, Foxp3 certainly plays an essential role, but is not driving alone the "Treg signature". Some subsets of Treg cells exist without Foxp3 (e.g. $CD8^+CD122^+$, $Klrg1^+$ Treg cells), and can still display the characteristic Treg properties, including suppressive activity mediated by mechanisms similar to $Foxp3^+$ Treg cells (for example production of IL-10). Thus, other molecular players or events must be participating in the differentiation and function of Treg cells.

I.6. Eos and Helios – biological functions

In this section I focus on two members of the Ikaros family, Eos and Helios. I briefly describe their known functions during hematopoiesis, and then review their roles in regulatory T cells.

I.6.1 Eos and Helios during hematopoiesis – a brief overview

Despite its discovery 16 years ago and known expression pattern, little is known about the function of Eos in the hematopoietic system. Eos has been mainly implicated in Treg cell function, which I will discuss in the next section. Apart from that, Eos plays a role in erythroid differentiation where it represses the expression of human γ-globin, and during osteoclast differentiation where it recruits corepressors to lineage specific genes in committed myeloid progenitors, through mechanisms described in chapter I.4.5 (Yu et al., 2011; Hu et al., 2007). In the T cell lineage, it was only recently observed that Eos may be required for IL-2 production by activated $CD4^+$ T cells, and implicated in Th17 lineage differentiation under inflammatory conditions (Rieder et al., 2015).

Helios was discovered one year before Eos, in 1998, and its functions are slightly better characterized. Helios is mainly implicated in the regulation of the lymphoid lineage. The expression of Helios in the B lineage is strongly reduced when compared to hematopoietic progenitors or HSCs, and consistent with that, transgenic mice expressing Helios specifically in B cells develop B cell lymphomas, suggesting that normal B cell function requires silencing of Helios (Dovat et al., 2005). Later studies provided clues for the mechanism behind these observations, and proposed that Helios may control the strength of B cell receptor (BCR) signaling in immature cells, through regulating the expression of signaling regulators, including protein kinase Cs (PKCs) (Alinikula et al., 2010; Kikuchi et al., 2011). Additionally, when full-length Helios is ectopically expressed in hematopoietic progenitors, T cell development is blocked at the $CD4^-CD8^-$ stage. Constitutive expression of a Helios DBD mutant protein leads to the development of T cell lymphomas, indicating the importance of Helios, also at early stages of T cell development (Zhang et al., 2007).

More recently, Helios was also proposed to act as a marker of strongly autoreactive $CD4^+$ T cells, as its expression is up-regulated during negative selection, and a marker of activated and proliferating T cells (Daley et al., 2013; Akimova et al., 2011). It was also implicated in Th2 and Tfh differentiation, but again rather as a marker, as its expression was up-regulated on differentiating cells and loss of Helios did not impair the effector T cell development (Serre et al., 2011). In addition, Helios appears to act as a tumor suppressor in

humans, as Helios dominant negative short isoforms are overexpressed in patients with T-cell acute lymphoblastic leukemias and lymphomas (Fujii et al., 2003; Nakase et al., 2002). More recently, alterations in *IKZF2* gene were also found in hypodiploid acute lymphoblastic leukemias (Holmfeldt et al., 2013).

I.6.2 Role in Treg cells

Both Eos and Helios are expressed in Treg cells and are implicated as modulators of Treg cell functions. They are also among the most differentially expressed genes between conventional T cells and Treg cells, when comparing available gene expression profile datasets (ImmGen Database). Additionally, the promoter regions of *Ikzf2* and *Ikzf4*, like other Treg genes *Ctla4* or *Il2rα*, are hypomethylated in Treg cells, which can indicate their stability in the Treg lineage (Ohkura et al., 2012).

I.6.2.1 Eos

The first study describing the role of Eos in Treg cells indicated it as a "critical mediator" of Treg cell function. Pan et al. demonstrated using ectopically expressed proteins in T cell lines that Eos interacts directly with Foxp3 and together with the CtBP co-repressor is required for histone modifications and methylation of *Il2* promoter, leading to gene repression. Moreover, knock-down of Eos through siRNA in purified $CD4^+CD25^+$ Treg cells abrogated the Treg suppressive potential *in vitro* and *in vivo,* in a colitis model (Pan et al., 2009). Later, findings from this study were indirectly confirmed. Eos can indeed bind to the N-terminal part of Foxp3, and loss of that interaction, which occurs in hypomorphic $Foxp3^{GFP}$ mice, leads to severely impaired nTreg cell functions and iTreg cell generation (Xiao et al., 2010; Bettini et al., 2012).

Interestingly, other studies also linked indirectly loss of Treg activity with decreased Eos expression. Down-regulation of Eos was observed in Treg cells isolated from the peripheral blood of patients with ongoing GvHD after stem cell transplantation, but not in Treg cells from patients accepting the graft (Ukena et al., 2012). In another study Eos, together with Nrp1, was implicated in maintaining T cell function during allograft rejection (Campos-Mora et al., 2015).

Nonetheless, those observations were really intriguing, because two independent studies showed later that Eos deficient mice have a normal Treg compartment, arguing that Eos is dispensable for Foxp3 mediated Treg functions (Fu et al., 2012; Rieder et al., 2015). However, what should be kept in mind from the study by Pan et al. is one of the final observations. In the colitis model, where gut inflammation was induced in $Rag2^{-/-}$ mice by

naïve $CD4^+$ T cells, Eos deficient Treg cell could actually develop effector T cell functions. This was demonstrated in a very elegant and simple manner, by injecting $Rag2^{-/-}$ mice with higher numbers of pure $CD4^+CD25^+$ Treg cells with Eos knock-down. Transfer of those cells actually induced colitis, although less severe than mediated by naïve T cells. Hence, the hypothesis that loss of Eos can promote conversion from Treg cell to effector-like T cell was proposed. Later, Eos was indeed implicated in the reprogramming of a subset of Treg cells under inflammatory conditions as its down-regulation led to IL-6 mediated conversion of "labile" $CD38^+$ Treg cells into helper like cells (Fig.I.26) (Sharma et al., 2013). Consistent with these observations, also $CD4^+$ T cells from Eos deficient mice appear to be prone for differentiation into effector T cell subsets under inflammatory conditions. In an EAE model $CD4^+$ T cells from $Eos^{-/-}$ cells presented a bias toward Th17 differentiation, and Eos deficient mice developed a more severe disease than their WT controls (Rieder et al., 2015). Conversely, in another study increased expression of Eos was correlated with less severe EAE in mice, due to decreased IL-17 production, all together suggesting that down-regulation of Eos is accompanied by T cell polarization into effector cells (Liu et al., 2014). Taken together, literature data suggest that Eos is important for the maintenance of Treg lineage stability, and loss of this transcription factor in specific conditions leads to an enhanced Treg plasticity.

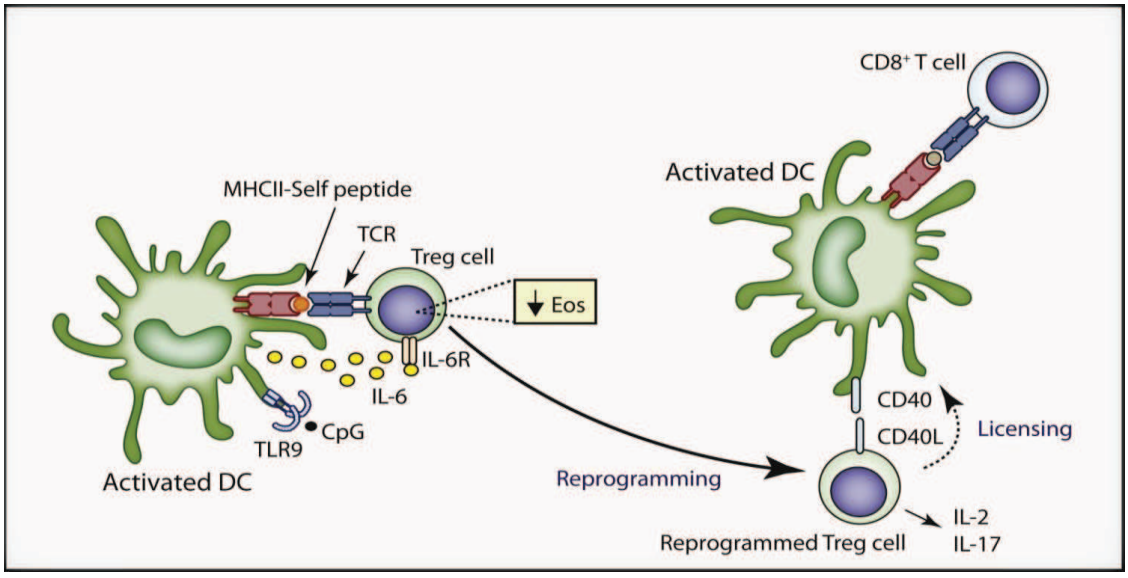

Figure I.26. Role of Eos in Treg cell reprogramming. Under inflammatory conditions a subpopulation of Treg cells, characterized by differential expression of CD38 and CD103, can down-regulate Eos and convert to Th-like cells. Down-regulation of Eos requires IL-6 produced by dendritic cells (DC), in response to TLR9 stimulation by its agonist CpG, vaccination with ovalbumin and recognition of MHC-II - self-peptide complexes. Reprogrammed "Eos-labile" Treg cells secrete proinflammatory cytokines including IL-2 and IL-17, upregulate CD40L and modulate DCs for antigen presentation and $CD8^+$ T cell priming.

I.6.2.2 Helios

Early studies concerning Helios showed its expression in immature thymocytes, but only a small fraction of peripheral mature T cells was described to express Helios (Kelley et al., 1998). It took some years before the role of Helios in mature T cells was brought to interest again. Microarray studies, validated by RT-qPCR, revealed Helios as one of the factors up-regulated in Treg cells, both in the thymus and in the periphery (Fontenot et al., 2005b; Sugimoto et al., 2006). It is known today that Helios is highly expressed in $CD4^+$ Treg cells in mouse and human, with around 90% and 70% of $CD4^+Foxp3^+$ cells expressing Helios in the thymus and in the periphery, respectively (Thornton et al., 2010; Gottschalk et al., 2012). Helios was also reported to be expressed in a population of $CD8^+CD25^+Foxp3^+$ Treg induced *in vivo* under allogeneic conditions (Beres et al., 2012)

Initially, Helios was proposed to act as a specific Treg lineage marker, distinguishing natural from peripheral Treg cells, based on its expression levels and experiments showing that Treg cells induced *in vitro* or *in vivo* can express Foxp3 but fail to express Helios (Thornton et al., 2010; Singh et al., 2015). However, other published data argue against that. $CD4^+$ and $CD8^+$ T cells can induce Helios upon stimulation without Foxp3 expression (Akimova et al., 2011; Serre et al., 2011). Finally, it became clear that Helios can be expressed in iTreg cell *in vivo* and *in vitro*, but this absolutely requires stimulation from APCs which was not provided in previous studies (Akimova et al., 2011; Gottschalk et al., 2012; Verhagen and Wraith, 2010).

A more precise description of the role of Helios came from a study on human Treg cells. Helios was reported to bind to the promoter of *Foxp3* gene, in an experiment that used Myc-tagged Helios ectopically expressed in a cell line that can also induce Foxp3 upon stimulation, suggesting that expression of Foxp3 can be partially controlled by Helios (Getnet et al., 2010). Down-regulation of Helios by siRNA knock-down in purified human $CD4^+CD24^+$ Treg cells led to impaired suppressive activity *in vitro* and a down-regulation of Foxp3 expression (Getnet et al., 2010). These results suggested that Helios may be required for Treg cell suppressive function. Consistent with that, $Helios^+$ cells were enriched in the $CD4^+CD25^+$ Treg population expressing also GITR and CD103. Treg cells purified according to the expression of CD4, CD25, GITR and CD103 were enriched in Helios positive cells, had elevated TGF-β transcript levels, were more suppressive *in vitro* and found to be a major Treg population infiltrating a tumor mass in mice inoculated with mammary tumors (Zabransky et al., 2012). Baine et al. showed that Helios directly suppress IL-2 production in Treg cells, by binding to *Il2* promoter and initiating epigenetic modifications that included

histone deacetylation. This could indicate that Helios may be responsible for maintaining the anergic state of Treg cells. This was supported by the observation that that shRNA mediated knock-down of Helios, specifically in $CD4^+Foxp3^+$ Treg cells from transgenic Foxp3-RFP mice decreased Treg cell functionality *in vitro* and promoted their proliferation as well as IL-2 production (Baine et al., 2013).

All together, available data show that Helios is certainly highly expressed in Treg cells and appears to maintain their suppressive activity. However, two independent studies in including one from our group, showed that Helios deficient mice do not have any defect in Treg development and function, indicating that *in vivo* during steady state hematopoiesis Helios is dispensable for $CD4^+$ Treg cells (Cai et al., 2009; Thornton et al., 2010). Likewise, Eos appeared to be crucial for Treg cell function when knocked-down *in vitro*, but not when it was completely lost in mice (Pan et al., 2009; Fu et al., 2012). So far no experimental explanations for those discrepancies were presented. It is possible that at least *in vivo* a compensatory mechanism exists that protects Treg cell lineage stability, when one of its crucial regulators is lost.

1.7 Summary and aims of study

Below, I briefly summarize some of the major points in the literature that prompted us to study further the role of Eos, and when available Helios, in the Treg cell biology:

1. Eos and Helios share high protein sequence similarity, they can homo- and heterodimerize, they potentially have common target genes because of a similar consensus DNA motif, and they may share mechanisms of gene regulation (sections I.4.2, I.4.5).

2. Eos and Helios have a similar pattern of expression in the hematopoietic system: both are expressed in LT-HSCs and this expression decreases during commitment to ST-HSCs, MPPs and progenitor cells. In mature cells both are most highly expressed in the T cell lineage, particularly in Treg cells (section I.4.4).

3. Helios was shown to play a role in Treg cell compartment. In many studies it was implicated as a specification marker of the Treg cell lineage. It was also proposed that Helios is required for Treg cell suppressive potential and the expression of Foxp3 (section I.6.2.2).

4. Studies from our group and others have revealed that Helios null mice have no defects in the T cell lineage and most importantly, have functional Treg cells, arguing with findings proposing the requirement for Helios in Treg lineage stability (section I.6.2.2).

5. When my project started, Eos was also already implicated to be important for Treg cells. The knock-down of Eos (with siRNA in a cell line) showed a requirement for Eos in Treg cell functionality, although no data were provided showing Eos function in physiological conditions or *in vivo* (section I.6.2.2).

6. In the $CD4^+$ Treg cell lineage, Foxp3 is not sufficient to confer the Treg cell transcriptional signature and functionality, and Treg populations can exist without Foxp3. Other subsets, including $CD8^+$ Treg cells, do express Foxp3, but its role and mechanisms of gene regulation are poorly characterized. Altogether, other factors must play a role in the development and functional regulation of Treg cell lineage (section I.5.3, I.3.2).

In this context, I decided to further study the role of both Eos and Helios in Treg cell populations. My main objective was to obtain a clean experimental system to study the role of Eos in Treg cells using Eos null mice. Further, I studied functions of Eos and Helios in Treg cells by generating double null mice lacking both Eos and Helios. Following the expression pattern of Eos I have also decided to analyze its role in the HSC compartment.

CHAPTER II MATERIALS AND METHODS

In this chapter I will present Materials and Methods used to obtain results presented in sections III.1 and III.2 with the exception of III.1.1.1 where Materials and Methods are part of the paper manuscript. For the latter one I will only add more detailed information concerning mice and flow cytometry procedures which were extensively used during my thesis and overlapping between projects. Experimental procedures from section III.1.3 are also explained in the manuscript presented in the Appendix.

II.1 Mice

$Ezh2^{Tg}$ mice

These mice bear a transgenic *Ezh2* allele, with reporter lacZ cassette inserted upstream of the critical exon 5, disrupting gene function. Homozygous mutation is embryonic lethal. Mice were obtained from EUCOMM collection on a C57BL/6N background. They were kept in the specific pathogen free (SPF) area of the animal facility. The construct used to generate this line as well as mouse characterization is described in detail in section III.2.

$IK^{+/L}$ $Ezh2^{Tg/+}$ mice

These mice, obtained from crossing $Ik^{L/L}$ and $Ezh2^{Tg/+}$ animals, are double heterozygous for Ikaros and Ezh2 deficiency. $Ik^{L/L}$ mice have a hypomorphic mutation generated by insertion of LacZ reporter into exon 2 of the *Ikzf1* gene. They were generated and characterized previously in the lab (Kirstetter et al., 2002). $Ik^{L/L}$ mice have a C57BL/6N background (backcrossed > 10 generations) and are kept in SPF conditions.

$Eos^{mCherry}$ reporter mice

This model was generated in collaboration with Institut Clinique de la Souris (ICS, Illkirch). $Eos^{mCherry}$ reporter mice bear a knock-in of T2A-mCherry cDNA in the C-terminus of *Ikzf4* followed by a STOP cassette. Production of the protein from the knock-in allele should lead to a truncated and non-functional Eos protein and mCherry expression at the same time. Mice had a C57BL/6N background and were kept in a conventional area of the animal facility. The construct used to generate the line turned out to be non-functional as no mCherry expression was detected, and mice were not used for any further analysis.

$Eos^{-/-}$ mice

Eos knock-out mice were generated after CMV-Cre driven germline deletion of exon 8 of *Ikzf4* flanked by loxP sites. The mice were obtained from ICS. Mice were generated and maintained on a C57BL/6 background in SPF conditions and conventional animal facility. The construct used to obtain the null mice is described in section III.1.1.1.

Helios$^{-/-}$ mice

Helios deficient mice were obtained by replacing the C-terminal part of exon 7 of *Ikzf2* by PGK-neo cassette via homologous recombination in embryonic stem cells. Mice have a mixed C57BL/6 and 129/Sv background and are kept in SPF conditions. Described by (Cai et al., 2009).

Eos$^{-/-}$Helios$^{-/-}$ mice

Mice were obtained from crossing Eos$^{-/-}$ and Helios$^{-/-}$ mice and were available on a mixed C57BL/6 and 129/Sv background. Mice were never backcrossed. They are kept in special sterile conditions ("ultra-clean bioBUBBLE) in the ICS.

Recipient and competitor mice in transplantation assays

CD45.1^{+}CD45.2^{-} mice - C57BL/6 congenic mice with differential *Ptprc*^{a} pan leukocyte marker (named CD45.1 or Ly5.1), were used as donors of competitor cells in transplantation assays. CD45.1^{+}CD45.2^{+} mice - C57BL/6 mice obtained from crossing congenic C57BL/6-CD45.1^{+} mice with C57BL/6-CD45.2^{+} inbred mice, were used as recipient mice in transplantation assays. All mice were kept in SPF conditions. Rag1$^{-/-}$ mice - Rag1 deficient mice lacking mature T and B cells, were used as recipients in T cell transfer model of colitis. Rag1$^{-/-}$ tm1Mom strains were used. Balb/c mice - WT Balb/c mice used as recipients in cell transfer experiments and were donors of bone marrow for *in vitro* BMDC (Bone Marrow-derived Dendritic Cell) production.

II.2 DNA and RNA preparation

II.2.1 Genomic DNA extraction

Genomic DNA was extracted from mouse tails cut for genotyping (between 7-14 days of age). First, tails were digested in 500 µl of buffer containing proteinase K in a concentration 0,1 mg/ml (5 µl of 10 mg/ml stock solution in H_2O, Sigma Aldrich, Cat.No: P6556) for 4-5 hours or overnight in an oven in 55°C. Tail digestion buffer was composed of 100 mM Tris (stock pH=8), 200 mM Nacl, 5 mM EDTA (stock pH=8) and 0,2% SDS.

To prepare DNA from digested tails samples were spun down for 5 min in 13,000 g and the supernatant was transferred to new eppendorf tubes. Then, one volume of isopropanol was added to precipitate DNA, samples were mixed by inverting the tubes, spun down for 5 min in 13,000 g and the supernatant was discarded. DNA was then washed by adding and mixing with 70% ethanol and spun for 5 min in 13,000 g. The supernatant was removed and the DNA pellet was dried. Finally, samples were resuspended in 200 µl of TE buffer (10 mM Tris-HCl, 0,1 mM EDTA).

II.2.2 RNA extraction

To prepare RNA samples from mouse lymphoid organs (BM, spleen and thymus) cells were collected and the pellet was resuspended in RLT buffer provided with RNeasy Kit (Qiagen). RNA was then directly extracted or samples were frozen in liquid nitrogen and transferred to -80°C. Isolation of RNA was performed with RNeasy Mini or Micro Kit (Qiagen) depending on the number of cells available and always according to the provided protocol. RLT buffer used for cell lysis was supplemented with β-mercaptoethanol (10 µl for 1 ml of RLT). During RNA isolation an additional step of "on-column DNase digestion" was performed. Concentration of RNA was measured with NanoDrop2000.

Samples for RNA extraction from large intestines were prepared immediately after dissection. Large intestines were removed entirely and kept in Petri dishes with PBS on ice during the whole procedure. First, the feces were flushed out with a syringe (with PBS) and cut open longitudinally with scissors. The tissue was then transferred to a 15 ml falcon with PBS in order to wash remaining feces and then put on a fresh Petri dish. Next, cells from the intestine wall were mechanically scraped using a common microscope glass slide. The content of the plate was then transferred to 50 ml falcons and spun down during 20 minutes at 1500 rpm in 4°C. After removing the supernatant cells were transferred to 1,5 ml eppendorf tubes and spun again for 2 minutes at 13,000 g. The supernatant was then removed and the pellet was directly re-suspended in TRI Reagent (Molecular Research Center, Cat. No: TR-118). RNA was extracted according to the protocol provided. Briefly, 200 µl of chloroform was added to the samples, mixed by vortexing until obtaining a homogenous color and put to rest for 15 min in RT. This was followed by centrifugation 15 min/4°C/12,000 g and transfer of the formed aqueous phase into fresh tubes. Next, 500 µl of isopropanol was added and samples were put to rest for 10 min in RT. This was followed by centrifugation 8 min/4°C/12,000 g and careful removal of the supernatant (with a pipet). Then, 1 ml of 70% ethanol was added, samples were mixed by vortexing and spun 5 min/4°C/7500 g. The supernatant was next removed, pellet left to dry (~5 min in RT) and finally resuspended in 40 µl of water. Concentration of RNA was measured with NanoDrop2000.

II.3 PCR

II.3.1 Genotyping

Genotyping was performed using undiluted genomic DNA (extracted as in II.2.1) and a Polymerase Chain Reaction (PCR) was set up in a total volume of 25 µl according to the following general protocol:

Reagent	µl for 1 PCR sample
DNA	2
PCR 10x buffer with $MgCl_2$ (Roche)	2,5
dNTP mix (10 mM each, Thermo Scientific)	0,5
1 to 3 Primers (100µM, Sigma Aldrich)	0,1 each
Taq Polymerase (in-house made)	0,5
H_2O	QS

All genotyping PCRs were performed in following conditions:

Step	Temperature	Time	Number of cycles
Initial denaturation	94°C	5 min	1
Denaturation Amplification Elongation	94°C 60°C 72°C	30 s 30 s 30 s	40
Final elongation	72°C	7 min	1

To genotype Ezh2 transgenic mice, 2 pairs of primers were used: CasR1+F2 to detect the lacZ cassette, and F4-R4 to confirm genotyping and to distinguish in one reaction between WT and Tg allele.

Primer	Sequence 5'→3'
CasR1	TCGTGGTATCGTTATGCGCC
Ezh2F2	AAGCCTATAGAGGGTGTTTCTCATT
Ezh2F4	TTAGTCCAGCCGGGCGGTGTT
Ezh2R4	AAATGGCTGGGTTTATGACTGGGC

To genotype $Ik^{L/L}$ mice, 3 primers were used to distinguish between the WT and transgenic allele (lacZ insertion).

Primer	Sequence 5'→3'
ABG209	GAAGCCCAGGCAGTGAGGTTTTCC
ABG301	GGCAAAGCGCCATTCGCCATTCAG
ABG304	CATGCCTCGATCACTCTTGGAGTCC

To genotype $Eos^{-/-}$ mice, 4 primers were used to distinguish between the WT and mutant allele. Amplification with PM4 + PM13 shows mutant allele and PM9 + PM12 shows WT allele. In another way PM4, PM13 and PM9 could be used alone to show both mutant and WT allele in one PCR reaction.

Primer	Sequence 5'→3'
PM4	GAACAAGGACTTCAGTCTACATGGGC
PM9	GGACCCAACCCTGGGCTTTACATG
PM12	CAAGGACTTCAGTCTACATGGGCTGAT
PM13	AGAAGGGAGCCATGGGCAGAAGAA

To genotype Helios$^{-/-}$ mice, 3 primers were used to distinguish between the WT and mutant allele. ACB286 + AHF 12 distinguish the WT allele and ACB286 + AHE49 the mutant one. For Helios mouse genotyping different volumes of primers per sample were used: ACB286 0,2 µl, AHF 12 0,1 µl and AHE49 0,07 µl (for all other 0,1 µl/sample was used).

Primer	Sequence 5'→3'
ACB286	CATTAGCAGGGAAACATCTGATAG
AHE49	ATCTGCACGAGACTAGTGAGACG
AHF12	AGCATCCAAAGCCTTGACATC

To genotype Rag$^{-/-}$ mice, 3 primers were used to distinguish between the WT and mutant allele. ADA213 + AAB243 distinguish the WT allele and ADA213 + SH23 the mutant one.

Primer	Sequence 5'→3'
ADA213	TTCTGACTCAACGAGCACTGA
AAB243	CTCCAACAGTCATGGCAGAA
SH23	GGTTCTAAGTACTGTGGTTTCCAAATG

II.3.2 RT-PCR

Reverse transcription-PCR (RT-PCR) was performed using SuperScript II Reverse Transcriptase (Invitrogen, Cat.No: 18064-014). RT-PCR reaction was performed in a final volume of 20 µl. Two separate mixes of reagents were prepared as followed:

1st Mix	µl per 1 sample	2nd Mix	µl per 1 sample
Oligo dT (0,5 µg/µl)	0,1	DTT	0,6
H_2O	0,9	RNasine	0,2
dNTPs (10 mM each)	1	5xbuffer	4
		Reverse transcriptase	0,5
		H_2O	QS 20 µl

2 µl of the first mix was added to a maximum of 500 ng of RNA (and maximum volume of 12,7 µl) and incubated 5 min in 65°C and put on ice. Then, a second mix was added and samples incubated 1h in 42°C followed by 50 s in 95°C.

II.3.3 RT-qPCR

cDNA for real-time quantitative PCR (RT-qPCR) was prepared as described in II.3.2. Reactions were performed using SybrGreen I Master (Roche, Cat.No: 04707516001) and Light Cycler 480 instrument (Roche). Reactions were set up in a total volume of 12 µl and contained: 6 µl of SybrGreen, 2,4 µl of primer mix (10 µl of forward and 10 µl of reverse

primers from 100 µM stock solutions were mixed with 980 µl of water), 1,6 µl of water and 2 µl of cDNA. Primers and conditions for RT-qPCR experiments were as followed:

Target	Primer IDs	Sequence 5'→3'	Cycling conditions
Ezh2	Ezh2_2F Ezh2_3R	ATCTGAGAAGGGACCGGTTT GCTGCTTCCACTCTTGGTTT	95°C 15s, 63°C 30s, 72°C 30s
	Ezh2_10F Ezh2_11F	GAAGCAGGGACTGAAACTGG AGCACCACTCCACTCCACAT	95°C 15s, 63°C 30s 72°C 30s
Ikzf4	Eos_F3 Eos_R4	CCCAAACAGCCAACACTCTT TTATCCAGGAGCCGTTCATC	95°C 15s, 64°C 30s 72°C 30s
IFN-γ	ACY102 ACY103	AACGCTACACACTGCATCTTGG GACTTCAAAGAGTCTGAGG	95°C 15s, 63°C 20s 72°C 15s
TNF-α	TNFαF TNFαR	CATCTTCTCAAAATTCGAGTGACAA TGGGAGTAGACAAGGTACAACCC	95°C 15s, 63°C 20s 72°C 15s
β-actin	AGN34 AGN33	CCATCACAATGCCTGTGGTA TGTTACCAACTGGGACGACA	95°C 15s, 64°C 30s 72°C 30s
HPRT	KP170 KP169	GCTGGTGAAAAGGACCTCT CACAGGACTAGAACACCTGC	95°C 15s, 62°C 30s 72°C 30s

II.4 Western blot

II.4.1 Antibodies

Ezh2: mouse mAb (AC22), Cell Signalling Cat.No: 3147, MW = 98 kDa, isotype mouse IgG1κ, dilution for hybridization 1:1000 in PBST (0,1% Tween-20, 5% non-fat milk in PBS). β-actin: mouse mAb (AC15), Sigma Aldrich, Cat.No: A1978, MW = 42 kDa, isotype mouse IgG1, dilution for hybridization 1:1000 in PBST (0,1% Tween-20, 5% non-fat milk in PBS). HRP conjugated goat anti-mouse: mouse polyclonal Ab, Jackson ImmuneResearch, Cat.No: 115-035-003, isotype mouse IgG, dilution for hybridization 1:1000 in PBST (0,1% Tween-20, 5% non-fat milk in PBS).

II.5 Flow cytometry

II.5.1 Materials and reagents

FDG - Fluorescein Digalactopyranoside – Sigma-Aldrich, Cat.No: F2756, 100 mM stock solution in H_2O/DMSO/ethanol (vol 1:1:1), used at 7,5 mM

Topro3 - TO-PRO(R)-3 IODIDE (642/661) - 1 mM solution in DMSO, Invitrogen, Cat.No: T-3605, diluted 1:1000 in PBS before use

CFSE - 5-CarboxyFluorescein N-Succinimidyl Ester - Sigma-Aldrich, Cat.No: 21888-25MG-F, stock solution at 10 mg/ml, used at 40 µg/ml

DAPI - 4'6-diamidino-2-phenylindole - Invitrogen, Cat.No: D-1306, stock solution at 5 mg/ml, diluted 1:500 in water to 10 µg/ml and used as 10 µl in 1 ml of cell suspension.

Foxp3 staining Kit - eBioscience, Cat.No: 71-5775-40

PBE staining buffer - PBS, 0,5% BSA, 2 mM EDTA

PB buffer - PBS, 0,5% BSA

II.5.2 Single cell suspension preparation

Flow cytometry analysis was performed on samples from mouse bone marrow, thymus, spleen or lymph nodes after preparing single cell suspensions. Briefly, organs were ground with a piston in a small Petri dish or with a mortar (BM) in a PBE buffer. Cells after grinding were filtered with 70 µm cell strainers and washed followed by centrifugation at 1200 rpm for 5 minutes in 4°C. Bone marrow and spleen cells were additionally treated with NH_4Cl to lyse the red blood cells. For that purpose after initial spinning of the suspension cells were resuspended in 1 ml of 0,83% NH_4Cl and incubated 4 minutes in RT, followed by washing in a total volume of 10 ml. Finally cells were counted by Trypan Blue exclusion.

II.5.3 Antibodies

Antibodies for all flow cytometry analyses and sorting were used as directly conjugated with fluorochromes, purified or conjugated with biotin. Concerning the latter ones, secondary anti-rat fluorochrome conjugated or straptavidin fluorochrome conjugated antibodies were used for detection, respectively. All primary antibodies were obtained from BioLegend, eBioscience or BDPharmingen. Secondary antibodies were purchased mainly from Jackson Immunoresearch and Invitrogen. In-house made antibodies were also used and were targeting: CD4 (GK1.5), CD8 (YTS169.4), CD3 (KT3), B220 (RA3.6B2), Mac-1 (M1/70), Gr1 (H30b), NK1.1 (PK136). Commercial antibodies and their clones are listed in the table below:

Antibody against:	Clone	Antibody against:	Clone
BP-1	6C3	**CD38**	90
CD103	2E7	**CD4**	RM 4-5, GK1.5
CD117 (c-Kit)	2B8	**CD43**	S7
CD127	A7-R34	**CD44**	IM7 8.1
CD11b	M1/70.15	**CD45.1**	A20
CD11c	N418, HL3	**CD45.2**	104, 104.2
CD122	TM-b1	**CD45R**	RA3-6B2
CD135 (Flt3)	A2F10.1	**CD48**	HM48-1
CD150	TC15-12F12.2	**CD49b**	DX5

CD16/CD32	93	**CD62L**	MEL-14
CD19	1D3	**CD8**	53-7.3
CD194 (Ccr4)	2G12	**CD90.2**	53-2.1
CD195 (Ccr5)	C34-3488	**Gr1**	RB6-8C5
CD24	M1/69	**Klrg1**	2F1
CD25	PC61	**Ly49**	14B11
CD279 (PD-1)	RMP1-30	**MHC K^b**	AF6-88.5
CD3	145-2C11, KT3	**NK1.1**	PK136
CD304 (Nrp1)	3E12	**Sca-1**	D7
CD34	RAM34	**Ter119**	TER-119
Eos	ESB7C2	**F4/80**	F4/80
Helios	22F6	**Foxp3**	FJK-16S

II.5.4 Cell surface and intracellular staining

Cell surface staining for flow cytometry analysis was performed in round-bottomed 96-well plates and PBE buffer was used for all the steps of incubation and washing. After preparing single cell suspensions, cells (up to 10^7) were transferred into 96-well plates and spun down for 3 minutes at 1200 rpm. Mixes of antibodies were prepared to stain cells in a volume of 50 µl or 25 µl. For samples from spleen and bone marrow cells were then incubated with "Fc block" – CD16/CD32 antibody for 15 min on ice to block Fc receptors. Cells were always washed two times by filling up the wells with wash buffer and spun for 3 minutes at 1200 rpm. Supernatants were removed by fast flipping over the plate to remove liquid and pressing against a paper towel briefly. Incubations with primary antibodies were performed for 10-15 minutes on ice (in darkness) and followed by washing 2 times like previously. Similarly, incubations with secondary antibodies were performed for 10-15 minutes on ice and followed by washing 2 times. Finally, directly before analyzing with the BD LSR II flow cytometer all samples were filtered again. Some stainings required special conditions and incubation times. This includes staining of the DN cells in the thymus, where a cocktail of antibody supernatants (against CD4, CD8, CD3, B220, Mac-1 and Gr1) was used for the Lineage staining. In this case, 100 µl of the cocktail was used and incubated with cells for 30 minutes. After washing 2 times, cells were incubated for 15 minutes with secondary anti-rat antibody, washed 2 times and incubated for 2 minutes with 5% rat serum. After this step, primary antibodies were added without washing and incubated as previously. Then, staining continued like usually. Example of this and conventional stainings are presented in tables below. Common incubation time indicates that antibodies were together in one staining mix.

Antibody against:	Conjugate	µl of Ab/ mix	Incubation time
Lin-supernatant mix	-	100	30 min
Wash 2 times			
anti-rat	FITC	1/50	15 min
Wash 2 times			
RS 5%		15	2 min
CD44	biotin	1/35	15 min
Wash 2 times			
Streptavidin	Cy5/Alexa Fluor405	0,5/50	15 min
CD25	PE/APC	0,3/50	
Wash 2 times			

Antibody against:	Conjugate	µl of Ab/ mix	Incubation time
CD3	biotin	1/50	15 min
CD11c			
DX5			
Gr1			
Ter199			
B220			
Wash 2 times			
c-Kit	APC	0,5/50	10 min
Sca1	PE-Cy7	0,5/50	
Flt3	PE	1/50	
CD34	FITC	1/50	
Streptavidin	eFluor-710	0,5/50	
Wash 2 times			

Antibody:	Conjugate	µl of Ab/ mix	Incubation time
CD4	AF 700	0,5/50	10 min
CD8	PerCP-Cy5.5	0,5/50	
CD25	PE	0,5/50	
CD62L	FITC	0,5/50	
CD44	PE-Cy7	0,5/50	
Wash 2 times			

All intracellular stainings were carried out with Foxp3 Staining Kit (eBioscience) and the provided protocol was modified to stain cells in 96-well plates. First, surface staining was performed like described before. Next, cells were fixed and permeabilized with provided Fixation/Permeabilization buffer in 100 µl for 30 min on ice (always in darkness – plate covered with aluminum or non-transparent cover). Then, samples were washed 2 times (3-5 min/1200 rpm/4°C) with 1x Permeabilization Buffer and incubated with antibody of interest. For antibodies against Helios and Foxp3 it was 30 min in 4°C and for anti-Eos antibody 1h in RT, followed by washing 2 times as before.

II.5.6 β-galactosidase activity assay

To perform FDG staining $5x10^6$ cells were stained with cell surface markers like described previously. Next, cells were re-suspended in 120 µl of PBS. Stock solution of FDG (100 mM) in H_2O/DMSO/ethanol (vol 1:1:1) was diluted to 7,5 mM with H_2O. Both, the diluted FDG and cells were pre-warmed in 37°C in water bath for 5 min. While gently vortexing, 80 µl of FDG was added to cells and incubated for next 5 min in 37°C in the water bath. FDG reaction was stopped by adding 2 ml of ice cold PBS and kept on ice for 5 min. Next, cells were transferred for 30 min to a 15°C water bath to enhance β-galactosidase activity. Cells were then ready to analyze by cytometry (acquisition in FITC channel).

II.5.7 Sorting

For all sorts BD FACSAria II SORP Instrument was used. Cells were stained as described, but in 5 ml round-bottom tubes (BD Falcon, thereafter referred to as FACS tubes) due to their higher number. Stained cells were resuspended at a maximum concentration of $30x10^6$/ml and sorted into FACS tubes containing staining buffer or medium if they would be maintained in cell culture. FACS tubes were coated overnight before sorting with PB buffer, and directly before the sort DAPI was added to samples to distinguish between dead and live cells (stock of 5 mg/ml was diluted 1:500 to 10 µg/ml in water for longer storage in 4°C and each time 10 µl was used to add to 1 ml of cell suspension). Examples of markers used to sort populations of BM, spleen and thymus (Figure III.1, sorts for measuring Eos expression in hematopoietic populations) are listed as follows. LT-HSC ($Lin^-c\text{-}Kit^+Sca\text{-}1^+CD34^-Flt3^-$), ST-HSC ($Lin^-c\text{-}Kit^+Sca1^+CD34^+Flt3^-$), MPP ($Lin^-C\text{-}kit^+Sca1^-CD34^+Flt3^+$), MEP ($Lin^-C\text{-}kit^+Sca1^-CD34^-CD16/32^-$), CMP ($Lin^-C\text{-}kit^+Sca1^-CD34^+CD16/32^{lo}$), GMP ($Lin^-C\text{-}kit^+Sca1^-CD34^+CD16/32^{hi}$), pre-pro-B ($B220^+CD43^+CD24^-BP1^-$), pro-B ($B220^+CD43^+CD24^+BP1^-$), large pro-B ($B220^+CD43^+CD24^+BP1^+$), DN1 ($Lin^-$, $CD44^+CD25^-$), DN2 (Lin^-, $CD44^+CD25^+$), DN3 (Lin^-, $CD44^-CD25^+$), DN4 (Lin^-, $CD44^-CD25^-$), DP ($CD4^+CD8^+$), $CD4^+$ ($CD4^+CD3^{hi}$), $CD8^+$ ($CD8^+CD3^{hi}$), Treg ($CD4^+CD25^+CD3^{hi}$). Lin^-: $CD4^-$, $CD8^-$, $CD3^-$, $B220^-$, $Gr1^-$, $CD11b^-$, $Nk1.1^-$.

II.6 Cell depletion and enrichment

II.6.1 Reagents

MACS MicroBeads – Streptavidin magnetic beads, Miltenyi Biotec, Cat.No: 130-048-101

Dynabeads – Dynabeads sheep anti-rat IgG, Life Technologies, Cat.No: 11035-5ML

Columns for MACS bead separation - LS columns, Miltenyi Biotec, Cat.No: 130-042-401

II.6.2 Cell depletion with Dynabeads

Depletion with Dynabeads was performed before sorting or positive selection to enrich for the final populations, according to provided guidelines. Purified rat anti-mouse antibodies were used to stain cells for depletion and usually included antibodies against: B220, CD4, Gr1, CD11b, Ter119, and Dx5 for T cell sorts and additionally CD4/CD8 if different population was then used. Cells were stained with antibodies diluted 1:200 in PBE buffer in 5 ml (15 ml falcon) for 30 min with gentle rotation in 4°C. After the staining cells were washed 2 times and then incubated with magnetic sheep anti-rat magnetic beads for 30 min with gentle rotation in 4°C. Beads were washed 3 times in PBS before using and calculated to have around $4x10^8$ beads per $6x10^8$ total cells. After incubation, tubes were put on ice for around 5 minutes to let the beads fall down and then depletion was performed using a magnetic stand.

II.6.3 Cell depletion and enrichment with MACS Streptavidin Microbeads

Streptavidin coated beads were used both for depletion and cell enrichment/positive selection. To deplete BM cells of lineage positive cells, cells were stained with biotinylated antibodies against B220, Gr1, CD11b and Ter119, diluted 1:100 in 500 µl of staining buffer (PB) for 15 min on ice. Then, cells were washed 2 times and incubated with MicroBeads (10 µl of beads plus 90 µl of staining buffer per 10^7 cells) for 15 min with gentle rotation in 4°C. Next, cells were washed again once and resuspended in 1 ml of PB. In parallel, separation columns were put on magnetic separators and prepared by passing 3 ml of staining buffer. Finally, cells were put on columns and after passing through, washed by applying 3 times 3 ml of PB. Total volume of 10 ml of lineage negative cells was collected.

For cell enrichment (e.g. *in vitro* iCD8$^+$ Treg experiments) cells were stained with biotinylated anti-CD8 antibody diluted 1:100 in 500 µl of staining buffer (PB) for 15 min on ice. Then, cells were treated exactly like before until obtaining the final 10 ml flow-through. In the case of positive selection cells of interest (here CD8$^+$) remained on the columns together with beads. To release the cells, columns were removed from magnetic stand and placed in new 15 ml collection tubes. Then, additional 5 ml of a staining buffer was applied 2 times on the columns and flushed out by pressing with a provided plunger. Obtained flow-through fraction contained cells highly enriched in CD8 positive cells.

II.7 Cell culture

II.7.1 Media and reagents

IMDM medium – supplemented with 10% heat-inactivated FCS (#3396), 1% penicillin and streptomycin, 40 µg/ml gentamycin and L-glutamine.
NCS – Sigma Aldrich, Cat.No: N9162
MethoCult Kit - Stem Cell Technologies, Cat.No: GF M3434
rmIL-3 - Peprotech, Cat.No: 213-13-B, stock concentration 12,5 µg/ml
rmIL-6 - Peprotech, Cat.No: 216-16, stock concentration 5 µg/ml
rmTpo - Peprotech, Cat.No: 315-14, stock concentration 10 µg/ml
rmSCF - Peprotech, Cat.No: 250-03, stock concentration 10 µg/ml

II.7.2 LSK proliferation assay

LSK cells were sorted from the BM of WT and $Eos^{-/-}$ mice as $Lineage^{-}cKit^{+}sca1^{+}$ cells and cultured for 5 days in a complete IMDM medium supplemented with 10% FCS (#3396), BSA (20%), IL-3 (12,5 ng/ml), IL-6 (10 ng/ml), TPO (50 ng/ml) and SCF (50 ng/ml). At day 0, 600 of freshly sorted LSK cells were plated into 96-well cell culture dishes and counted daily by Trypan Blue exclusion.

II.7.3 NCS treatment

LSK cells were sorted from the BM of WT and $Eos^{-/-}$ mice as $Lineage^{-}cKit^{+}sca1^{+}$ cells, treated for 30 minutes with NCS (500 ng/ml) in 37°C, washed once and cultured for 14 hours in a complete IMDM medium supplemented with 10% FCS (#3396), BSA (20%), IL-3 (12,5 ng/ml), IL-6 (10 ng/ml), TPO (50 ng/ml) and SCF (50 ng/ml). Viability of cells after treatment was verified by Topro3 staining.

II.7.4 CFC assay

CFC assays were performed with total bone marrow cells. Single cell suspensions were prepared as described previously, but in sterile conditions. Experiments were performed according to the protocol provided with MethoCult Kit. MethoCult medium was ready to use and supplemented with cytokines and nutrients including: Methylcellulose, FBS, BSA, rhInsulin, human transferrin, 2-mercaptoethanol, rmSCF, rmIL-3, rhIL-6, rhEpo, IMDM and supplements. First, 10x concentrated cell suspension (500,000 cells/ml) was prepared in IMDM medium with 2% FBS. 300 µl of this suspension was next added to a 3 ml aliquot of MethoCult medium (to obtain plating concentration of 50,000 cells/ml). Prepared suspension in MethoCult was mixed well by vortexing and then let to stand in RT for 5 min to allow bubbles to disappear. Next 1,1 ml of cells in MethoCult was dispensed using a syringe with 16 gauge needle to each of the prepared plates. Each plate was rotated gently to distribute

evenly the medium. All plates were then placed in a big covered (for example 10 cm) plate with one extra uncovered small plate filled with sterile water to maintain proper humidity. Cells were incubated for 8 days, after which the experiment was analyzed. First, the colonies were counted and then cell suspensions were prepared. Next, either flow cytometry analysis or May-Grünwald-Giemsa staining was performed to evaluate the phenotype of colonies. For the latter, 10^5 cells collected from the MethoCult cultures and resuspended in 100 µl of PBS were put on SuperFrost Plus slides by Cytospin (600 rpm for 5 min).

II.8 *In vivo* experiments

II.8.1 Competitive reconstitution assay and serial transplantations

In all transplantation assays recipient mice were lethally irradiated one day before the experiment. Irradiation was performed in two doses of 4,5 Gy, with an interval of around 4h, to obtain a total dose of 9 Gy. In primary competitive transplantations with total bone marrow cells, mice were injected with either $1x10^5$ or $5x10^5$ total BM cells from WT or $Eos^{-/-}$ donors, together with $2x10^5$ competitor cells ($CD45.1^+$). Peripheral blood (PB) of recipient mice after transplantation was collected monthly and percentage of chimerism (donor contribution) in the PB was calculated (% of donor cells/% donor cells + % of competitor cells x 100). Blood cells were also stained each time against CD3, B220, Gr1 and CD11b to calculate how donor cells contribute to the production of each cell population type. In secondary transplantations with BM, cells primary recipients with the highest chimerism from the group injected with $5x10^5$ cells were sacrificed and BM cells were sorted to obtain $CD45.2^+$ donor cells that were then injected into new lethally irradiated recipients ($2x10^5$ cells plus $2x10^5$ competitor cells). In secondary transplantations with LSK cells, primary recipients with the highest chimerism from the group injected with 500 cells were sacrificed and BM cells were sorted to obtain $CD45.2^+$ donor LSK cells. Donor cells were then injected into new lethally irradiated recipients (500 LSK donor cells plus $2x10^5$ competitor cells).

II.8.2 PB collection and preparation for flow cytometry analysis

Blood samples were collected through the tail vain into eppendorf tubes containing 500 µl of PBS and EDTA (2 mM). Next, 500 µl of 2% Dextran (in PBS) was added to each tube, mixed by vortexing and incubated for 30 minutes in water bath in 37°C to enable separation of the red blood cells. After the incubation the formed supernatant was collected to fresh tubes and washed with PBE buffer (PBS, BSA 0,5%, EDTA 2 mM) by filling up the tube and mixing, then spun down at 13,000 rpm (until the maximum speed is reached). The supernatant was next aspirated and the cell pellet was treated with 0,83% NH_4Cl for

4 minutes (mixed well with the cells by pipetting) in RT to lyse the remaining red blood cells. After the treatment cells were washed like previously with PBE buffer (tube was filled up, spun up to 13,000 rpm) and the final cell pellet was re-suspended in 200 µl of the staining buffer (PBE) and cells were ready to stain for flow cytometry analysis.

II.8.2 T cell transfer model of colitis

To induce colitis in mice, naïve $CD4^+$ T cells from WT spleens were injected into Rag1 null mice, alone or together with Treg cells from KO mice or their WT controls. Splenocytes were enriched in T cells by depletion of cells expressing B220, CD8, CD11b, Gr1 and Ter119 (Dynabeads separation according to a protocol described in II.7) and then sorted as $CD4^+CD44^{lo}CD62L^{hi}$ to obtain $CD4^+$ naïve T cells from WT mice and as $CD4^+CD25^+$ to obtain Treg cells from WT and KO mice. After sorting $4x10^5$ $CD4^+CD44^{lo}CD62L^{hi}$ cells alone or together with $1x10^5$ $CD4^+CD25^+$ Treg cells were i.p. injected into $Rag1^{-/-}$ mice (resuspended in 100 µl of IMDM). In the experiment a group of un-manipulated mice was included. Each experimental group contained both females and males between 7-10 weeks old.

II.9 Histology

II.9.1 Colon sample preparation for HE staining

Samples for histological analysis of the intestines were prepared immediately after dissection. Large intestines were removed entirely and kept in Petri dishes with PBS on ice during the whole procedure, similarly as for RNA preparation. First, the feces were flushed out with a syringe (with PBS) and cut open longitudinally with scissors. The tissue was then transferred to a 15 ml falcon with PBS in order to wash remaining feces and then put on a fresh Petri dish. The tissue was arranged lengthwise and rolled using forceps. The prepared “swiss roll” was pinned with a needle to maintain the shape and transferred to a 50 ml falcon with 10% formalin (enough to cover the roll) and kept overnight in 4°C. After that, samples were washed 2 times in PBS and transferred to histological plastic cassettes and kept in 70% ethanol in 4°C. The samples were then dehydrated automatically (at IGBMC histopathology platform) and paraffin-embedded. Next, histological sections were cut at 5 µm, collected on glass slides covered with gelatin water and dried in an oven to remove any remaining water (37°C maximum overnight). The next steps including HE staining were performed with automatic stainer at the histopathology platform of IGBMC.

CHAPTER III RESULTS

When I joined the lab my main objective was to study the role of Eos transcription factor in the hematopoietic system. I have focused on understanding the role of Eos in regulatory T cell biology, and when applicable, the combined role of Eos and Helios in the Treg cell lineage. I have also looked into the function of Eos in hematopoietic stem cell compartment. During the first year of my thesis, I also participated in a project concerning the Ikaros transcription factor and its regulation of Polycomb function.

In this thesis manuscript I will describe three projects. First, my focus will be on the role of Eos and Helios in regulatory T cells, the main subject of my thesis. This part I will present as a paper manuscript. Second, I will write about the role of Eos in the HSC compartment and third, I will present the project concerning Ikaros and Polycomb.

III.1 Role of the Eos transcription factor in the hematopoietic system

With this project we have tried to elucidate the redundant as well as specific functions of Eos that would distinguish it from other Ikaros family proteins. In the laboratory, we have become interested in studying the role of Eos using mouse models, particularly knock-out mice, and see *in vivo* implications of Eos deficiency. We have started from analyzing the expression pattern of Eos within hematopoietic system during homeostasis. Firstly, we generated Eos reporter mice bearing 2A-mCherry insertion at the C-terminus of Eos protein. This model would allow us to track Eos protein levels in detail and distinguish various sub-populations of hematopoietic system that express Eos. Unfortunately, analysis showed that the knock-in mice were not functional and no mCherry expression was detected (data not shown). We have then decided to analyze Eos expression at the mRNA level in major populations of hematopoietic system. For this purpose, cells were sorted from bone marrow, spleen and thymus of wild-type mice and Eos expression was analyzed by RT-qPCR. Cells were FACS sorted according to markers listed precisely in chapter II.5.7. Its highest level was observed in regulatory T cells both in the spleen and thymus, and it is expressed relatively high in DN2-DN3 immature thymocytes and $CD4^+$ single positive cells. A very marginal level of expression was observed in bone marrow immature B cells. Interestingly, Eos was also expressed in HSCs with the highest level in LT-HSCs (Figure III.1). These results corresponded to published data showing expression of Eos in the hematopoietic system (ImmGen Database, Papathanasiou et al., 2009).

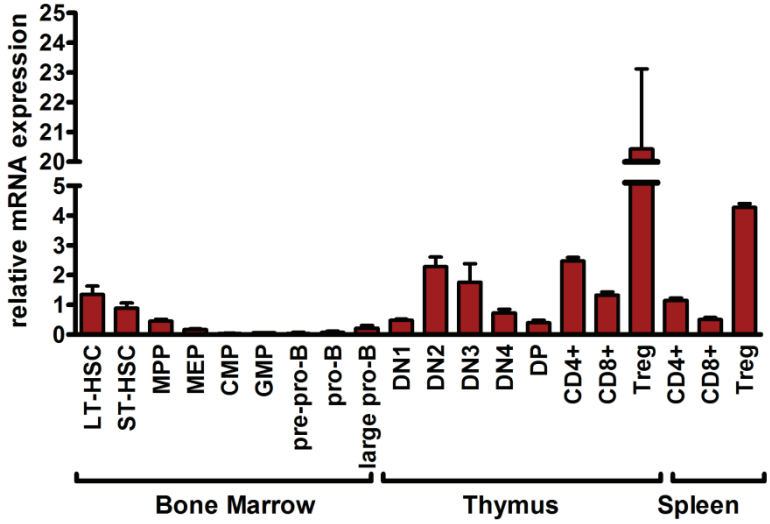

Figure III.1. Eos is differentially expressed during hematopoiesis. Expression of Eos measured by RT-qPCR and normalized to β-actin. Indicated populations were sorted from bone marrow, thymus and spleen of 8-15 wks old WT C57BL/6 mice. Each population was sorted 2-3 times and RT-qPCR was performed in triplicates.

III.1.1 Role of the Eos and Helios transcription factors in the differentiation and function of regulatory T cells

In the manuscript presented in section III.1.1.1 we study the role of Eos and Helios in regulatory T cell biology. To do so we:

- Introduce and characterize Eos knock-out mice.
- Study the $CD4^+$ Treg compartment in KO mice during homeostasis and in functional assays.
- Study induced $CD8^+$ Treg cells *in vitro* and *in vivo* using Eos and Helios deficient mice.
- Assess if Eos and Helios cooperate to regulate Treg cell function using double knock-out $Eos^{-/-}Helios^{-/-}$ mice.
- Analyze the transcriptional profile of Treg cells deficient in Eos and/or Helios.

In Chapter III.1.1.2 complementary results concerning Treg cells are described. In particular I present T cell transfer model of colitis experiment that was set up during the last year of my thesis to study the natural Treg cells *in vivo.*

III.1.1.1 Manuscript in preparation

III.1.1.1 Manuscript in preparation

Eos and Helios are not required for the essential functions of natural CD4$^+$ Treg cells and induced CD8$^+$ Treg cells.

Katarzyna Polak[1], Susan Chan[1] and Philippe Kastner[1,2]

[1]Institut de Génétique et de Biologie Moléculaire et Cellulaire (IGBMC), INSERM U964, CNRS UMR 7104, Université de Strasbourg, 67404 Illkirch, France.
[2]Faculté de Médecine, Université de Strasbourg, 67000 Strasbourg, France.

Correspondence: Susan Chan and Philippe Kastner
IGBMC
BP 10142
67404 Illkirch cedex, France
Tel: 33-3-88-65-34-61
Fax: 33-3-88-65-32-01
Email: scpk@igbmc.fr

SUMMARY

Regulatory T cells (Treg cells) are responsible for the maintenance of immune homeostasis. Foxp3 has been identified as a key marker and functional factor for $CD4^+$ Treg cells. However, other populations of Treg cells also express Foxp3 and this includes alloantigen induced $CD8^+$ Treg cells. The transcription factors Eos and Helios have been implicated as modulators of Treg cell functions, involved also in the regulation of Foxp3. Nonetheless, their potential roles in Treg cell biology remain controversial as conflicting data has been published depending on the system used. To clarify if Eos and Helios can regulate Treg cell functions *in vivo*, we studied mice deficient for one or the other of these factors. We show that Eos and Helios are differentially expressed in natural Treg cells but are not necessary for their essential functions. Transcriptome analysis in knock-out $CD4^+$ Treg cells supports the functional data showing that Eos has a minimal impact on the expression of genes related to Treg cell biology. On the contrary Helios deficient Treg cells show an up-regulation of genes characteristic of activated Treg cells and present a superior suppressive activity. We also show that the expression of Eos and Helios is induced in $CD8^+$ Treg cells but loss of either one of them has a minimal effect on their differentiation and no effect on their function. Moreover, loss of both Eos and Helios has no effect on $CD4^+$ Treg cell biology during homeostasis, but can affect $CD8^+$ Treg cell differentiation *in vitro* and *in vivo*. Finally, gene expression profiling in the double null mice shows that Eos and Helios do not cooperate to regulate Treg cell transcriptional signature. Our results indicate that Eos and Helios are not required and do not cooperate to regulate essential $CD4^+$ Treg cell functions, but absence of Helios may have an impact on their level of activation. Finally, we show that loss of Helios, or both Helios and Eos, negatively affects the differentiation of induced $CD8^+$ Treg cell.

INTRODUCTION

Regulatory T cells (Treg cells) are responsible for the maintenance of immune self-tolerance by executing suppressive functions, controlling inflammation and autoimmunity. Initially Treg cells were identified as $CD4^+CD25^+$ cells capable of dampening ongoing autoimmune reactions (Sakaguchi et al., 1995). Suppressive potential of Treg cells was then considered as their major functional characteristic. Later, the Foxp3 transcription factor (Forkhead box P3) has been identified as key regulatory factor and a phenotypic marker delineating Treg cells from other T cells (Fontenot et al., 2003; Hori et al., 2003; Khattri et al., 2003).

It is known today that much more Treg subsets exist and that a more complex mechanism of regulation is responsible for Treg cell lineage specification. Treg cells can be broadly categorized into thymus-derived natural Treg (nTreg) and peripherally induced Treg (iTreg). They can be both of $CD4^+$ or $CD8^+$ origin. $CD4^+$ Treg cells are characterized by expression of several other markers than CD25 e.g. CTLA-4, GITR, OX-40 or Lag3 (Wing et al., 2008; Petrillo et al., 2015; Josefowicz et al., 2012). Recently also Nrp1 and PD-1 emerged as important markers and factors for Treg cell functions (Delgoffe et al., 2013; Polanczyk et al., 2007; Chen et al., 2014). Their expression was shown to be correlated with Foxp3, and Nrp1 was found to be expressed in $CD4^+$ Treg cells in the context of allograft rejection (Bruder et al., 2004; Campos-Mora et al., 2015a). Nrp1 was also proposed to distinguish between thymus derived and peripheral $CD4^+CD25^+Foxp3^+$ Treg cells (Yadav et al., 2012; Singh et al., 2015).

$CD8^+$ Treg cells are less well characterized and phenotypically diverse. Naturally occurring $CD8^+$ Treg cells were described to express e.g. CD122 and Ly49, possess high suppressive potential and develop independently of Foxp3 (Dai et al., 2014; Endharti et al., 2005; Kim et al., 2011; Rifa'i et al., 2004). Induced $CD8^+$ Treg cells can be generated after stimulation with autoantigen or alloantigen and can express NKG2A, CD103 or Foxp3 (Koch et al., 2008). The $CD8^+$ iTreg cells that can express Foxp3 have been shown to occur in mice in the context of alloantigen stimulation and GvHD (Graft versus Host Disease) (Beres et al., 2012; Lerret et al., 2012; Robb et al., 2012). Interestingly, human natural $CD8^+CD25^+Foxp3^+$ cells can be identified and isolated (Jebbawi et al., 2014). The signaling pathways that regulate nTreg and iTreg cell development are different, but they all appear to require at least TCR stimulation and IL-2 signaling (both $CD4^+$ and $CD8^+$ Treg cells can express IL-2R components – CD25 and CD122) together with co-stimulatory pathways (e.g. CD28) and

additional factors like RA (retinoic acid) or TGF-β1 (Hsieh and Rudensky, 2005; Furtado et al., 2002; Tai et al., 2005; Hill et al., 2008; Marie et al., 2005).

As mentioned above, Foxp3 transcription factor was shown to be crucial and initially also thought to be driving alone the development and suppressive functions of $CD4^+$ Treg cells (Fontenot et al., 2005; Hori et al., 2003). However, Foxp3 is not expressed by all Treg populations and its expression alone does not define a Treg cell. It has been shown that Treg specific genes are controlled not only by Foxp3 and that the Treg cell transcriptional signature requires other molecular regulators (Sugimoto et al., 2006; Hill et al., 2007; Fu et al., 2012).

In this regard, the Helios and Eos transcription factors of the Ikaros family have been implicated as modulators of Treg cell function. Helios (*Ikzf2*) is highly expressed in $CD4^+$ Treg cells and has been proposed to act as a marker distinguishing natural from peripheral Treg cells like Nrp1 (Thornton et al., 2010; Singh et al., 2015). Helios was also reported to regulate Foxp3 expression by binding to its promoter, and down-regulation of Helios led to decreased Foxp3 expression and suppressive activity of $CD4^+$ Treg cells *in vitro* (Getnet et al., 2010). At the same time two independent studies, including one from our group, concluded from experiments using Helios knock-out (KO) mice that this transcription factor is dispensable for $CD4^+$ Treg cells during homeostasis and that loss of Helios do not decrease their suppressive potential (Cai et al., 2009; Thornton et al., 2010). Eos (*Ikzf4*) is also highly expressed in $CD4^+$ Treg cells at the mRNA level. It has been also shown to interact with Foxp3 enabling gene silencing in Treg cells and *in vitro* silencing of Eos with siRNA abrogated Treg cell suppressive activity (Pan et al., 2009). Moreover, Eos has been implicated in the reprogramming of a subset of Treg cells as its down-regulation led to IL-6 mediated conversion of "labile" $CD38^+$ Treg cells into helper like cells (Sharma et al., 2013). Interestingly, down-regulation of Eos was observed in Treg cells from peripheral blood of patients with ongoing GvHD after stem cell transplantation (Ukena et al., 2012). In another study Eos together with Nrp1 were implicated in T cell function stability during allograft rejection, linking loss of Treg activity with decreased Eos expression (Campos-Mora et al., 2015b). Similarly to Helios, knock-out mouse studies showed different results concerning the role of Eos in $CD4^+$ Treg cells. Eos null mice have normal Treg compartment and its loss does not lead to an inhibition of Treg suppressive potential both *in vitro* and *in vivo* (Fu et al., 2012; Rieder et al., 2015). All these observations still leave the roles of Eos and Helios unclear as controversial results were obtained with different systems.

In this manuscript we revisit the roles of Eos and Helios in Treg cells using KO mice. To assess if Eos and Helios cooperate to regulate Treg cell functions we introduce a novel mouse model, double knock-out $Eos^{-/-}Helios^{-/-}$ mice. We analyze the natural Treg cell compartment and show that both transcriptions factors are not necessary for the differentiation of the studied $CD4^+$ and $CD8^+$ Treg subsets and for the function of $CD4^+$ nTreg cells. We also study the alloinduced $CD8^+Foxp3^+$ Treg cells and show, that despite their up-regulation in those cells, only loss of Helios or both Eos and Helios affect $CD8^+Foxp3^+$ Treg cell differentiation. Finally, we study the transcriptional profile of Treg cells deficient in Eos and/or Helios. For the first time, we demonstrate that loss of Helios in $CD4^+$ nTreg cells induces an activated Treg phenotype. All together, our results give a considerable insight into the requirement for Eos and Helios in the regulation of the essential Treg cell functions.

RESULTS

Eos and Helios are differentially expressed in Treg cells.

To evaluate the expression of Eos and Helios in natural $CD4^+$ and $CD8^+$ Treg cells we performed intracellular staining for these proteins in WT mice. In thymic $CD4^+$ nTreg cells, both Eos and Helios were found to be highly expressed. In the spleen, however, only about 70% of $CD4^+$ Treg cells expressed Helios and Eos expression was reduced, confirming results from other studies (Rieder et al., 2015; Singh et al., 2015; Thornton et al., 2010). Moreover, in both spleen and thymus majority of $CD4^+CD25^+Foxp3^+$ cells co-expressed both Eos and Helios (Fig. 1A). We have also analyzed expression of both transcription factors in a population of $CD8^+$ nTreg cells, namely $CD8^+CD44^+CD122^+Ly49^+$ cells, and detected Helios, but not Eos protein (Fig. S1A). These results indicate that Eos and Helios are differentially expressed in natural Treg cells, but at least in the population of $CD4^+CD25^+Foxp3^+$ Treg cells high expression levels of both can be found.

Loss of Eos or Helios has no effect on Treg cells during homeostasis.

To study further the role of Eos and Helios in regulatory T cell compartment we used mice deficient for one or the other transcription factor. Helios KO mice ($Helios^{-/-}$ or $He^{-/-}$) were previously generated in the laboratory and characterized including the T cell compartment (Cai et al., 2009). We have then generated Eos KO mice ($Eos^{-/-}$) by removing the last exon of *Ikzf4* gene (germline deletion of the exon flanked by loxP sites), which is present in all splicing variants and encodes the functionally important dimerization domain (Fig. 1B). We have verified the deletion at the transcript and protein level (Fig. 1C, D). $Eos^{-/-}$

mice remained healthy, were born with Mendelian frequency and had normal body weights (Fig. 1E-G). During homeostasis $Eos^{-/-}$ mice showed normal hematopoiesis with correct proportions of all major populations including frequencies and numbers of $CD4^+CD25^+Foxp3^+$ Treg cells (data not shown, Fig. 2A, B). We have also analyzed Eos conditional and inducible KO mice, namely $Eos^{f/f}$ CD4-Cre and $Eos^{f/f}$ Rosa26-CreERT2 respectively, and found no phenotypic abnormalities and normal frequencies of $CD4^+CD25^+Foxp3^+$ Treg cells (data not shown). Eos has been described to play a role in functional reprogramming of a subset of thymic regulatory T cells characterized by the expression of CD38 and lack of CD103 expression (Sharma et al., 2013). However, this population was not affected in Eos null mice (Fig. S1B). As previously mentioned Eos and Helios are differentially expressed also in the subset of $CD8^+CD122^+$ natural Treg cells. We have then verified if the frequencies of these cells could be affected in the absence of one or the other transcription factor. We found a similar percentage of $CD8^+CD44^+CD122^+Ly49^+$ cells in the spleens of $Eos^{-/-}$ and $He^{-/-}$ mice when compared to their WT littermates (Fig. S1C). As mentioned before $CD4^+$ nTreg cells are characterized by expression of not only CD25 and Foxp3 but also PD-1 and Nrp1. We have analyzed the frequencies of cells expressing PD-1 or Nrp-1 in $CD4^+CD25^+Foxp3^+$ and $CD4^+CD25^+Foxp3^-$ cells of $Eos^{-/-}$ and $He^{-/-}$ mice and WT controls.

However, similarly to other populations analyzed we found no detectable differences between the genotypes (Fig. S1D, E). These results suggest that during steady state loss of Eos or Helios has no effect on the studied natural Treg cell populations of both $CD4^+$ and $CD8^+$ phenotype.

Eos and Helios are not required for the essential functions of $CD4^+$ Treg cells.

We have then focused on the population of $CD4^+CD25^+Foxp3^+$ Treg cells where Eos and Helios were most highly expressed and implicated in modulation of their function (Getnet et al., 2010; Pan et al., 2009). We first studied the functionality of Eos deficient cells with an *in vitro* suppression assay (Fig. 2C). In this experiment Treg cell activity of a given genotype is measured as an ability to inhibit the proliferation of stimulated responder T cells. We used purified $CD4^+CD25^+$ cells as Treg cells in the assay knowing that majority of them express also Foxp3 transcription factor (~90%). We found that Treg cells from $Eos^{-/-}$ mice had similar suppressive capacity as WT cells (Fig. 2D, E). Interestingly $He^{-/-}$ Treg cells presented a slightly superior suppressive activity when compared to WT cells (Fig. 2F). Given that both Eos and Helios are present in the majority of $CD4^+CD25^+Foxp3^+$ one could

hypothesize that they might compensate for each other in the absence of the other one. Following that concept we have verified by intracellular staining the expression of Eos in $He^{-/-}$ $CD4^+CD25^+$, $CD4^+CD25^+Foxp3^-$ and $CD4^+CD25^+Foxp3^+$ populations and the expression of Helios in $Eos^{-/-}$ $CD4^+CD25^+$, $CD4^+CD25^+Foxp3^-$ and $CD4^+CD25^+Foxp3^+$ cells. However, we have found similar frequencies of Eos and Helios in the indicated populations of WT and KO mice (Fig. 2G).

Eos and Helios are induced but dispensable for alloantigen mediated $CD8^+$ Treg cell differentiation and function *in vitro.*

We were then interested in studying the potential roles of Eos and Helios in induced $CD8^+Foxp3^+$ Treg cells. These cells occur naturally in non-manipulated mice in very low frequencies but can be found in mice undergoing Graft versus Host Disease (GvHD) and can be induced both *in vitro* and *in vivo* in specific allogeneic conditions (Beres et al., 2012; Lerret et al., 2012). We therefore used a differentiation system for alloantigen stimulation of $CD8^+$ T cells to induce $CD8^+Foxp3^+$ Treg cells. Bone marrow (BM) cells from WT mice were cultured for 7 days in a medium containing granulocyte-macrophage colony-stimulating factor (GM-CSF) to obtain $CD11c^+$ BM derived dendritic cells (BMDCs). BMDCs were then pre-conditioned with rapamycin and after positive selection or sorting for $CD11c^+$ cells they were co-cultured with $CD8^+$ splenic T cells in the presence of TGF-β1, IL-2 and RA (retinoic acid) for next 7 days. After that cells were stained and analyzed by flow cytometry for the expression of CD8, Foxp3 and other markers or tested in a functional assay (Fig. 3A). First, we have established that BMDCs from Balb/c mice provide best conditions to induce differentiation of $CD8^+$ T cells (with C57BL/6 or mixed C57BL/6 x 129/Sv background) and give the highest percentage of $Foxp3^+$ cells, indicating the role of MHC-mismatch disparity in the induction of these cells (Fig. S2A, B). We then analyzed the differentiation potential of $CD8^+$ T cells from $Eos^{-/-}$, $Helios^{-/-}$ and WT mice in allogeneic conditions using BMCDs from Balb/c mice. After 7 days of culture $CD8^+$ T cells acquired the expression of CD25 marker (up to around 80% of cells) and Foxp3 (20-40% of $CD25^+$ cells). They also expressed CD103, identified to be a marker of alloantigen induced T cells (Uss et al., 2006). However, cells from all genotypes could similarly differentiate into $CD8^+CD25^+Foxp3^+$ cells, with the exception of $Helios^{-/-}$ cells which showed a slightly decreased potential over independent experiments (Fig. 3B). Interestingly, when analyzed in WT cells, expression of both Eos and Helios was induced in differentiated $CD8^+CD25^+$ and $CD8^+CD25^+Foxp3^+$ cells as measured by RT-qPCR and intracellular staining, respectively. (Fig. 3C, D). Finally, we have tested the

functionality of *in vitro* induced cells in a suppression assay like previously. Instead of using freshly isolated and purified Treg cells we have sorted $CD8^+CD25^+$ cells after 7 days of co-culture. We could observe that obtained cells can suppress proliferation of stimulated T cells in Treg to T cell ratios even lower than $CD4^+CD25^+$ cells, but there was no difference in the activity of $Eos^{-/-}$ or $Helios^{-/-}$ cells when compared to WT controls (Fig. 3E). In conclusion, expression of Eos and Helios is induced in the discussed population of $CD8^+$ Treg cells *in vitro*, but Eos or Helios deficiency has only a minimal impact on their differentiation and no apparent effect on their function.

Eos and Helios are induced but dispensable for alloantigen mediated $CD8^+$ Treg cell differentiation *in vivo*.

In addition, we analyzed the role of Eos and Helios in the induction of $CD8^+$ iTreg cells *in vivo*. Splenic $CD3^+CD25^-$ T cells together with bone marrow cells from $Helios^{-/-}$ or $Eos^{-/-}$ and WT control mice (all $CD45.2^+$/MHC K^{b+}) were transplanted into lethally irradiated syngeneic (B6 $CD45.1^+/CD45.2^+$) or allogeneic recipients (Balb/c MHC-K^{b-}). In syngeneic conditions donor cells could be identified as $CD45.2^+$ and in allogeneic as MHC-K^{b+} (Fig. 4A and Fig. S3A). Transplanted mice were sacrificed after 8 days and spleens were analyzed for the expression of indicated markers by flow cytometry. These experiments showed that $CD8^+CD25^+Foxp3^+$ iTreg cells develop only from allogeneic, but not syngeneic grafts. We have also observed different levels of iTreg induction between the two mouse lines used, which could be explained by the different genetic background. However, both $Eos^{-/-}$ and $Helios^{-/-}$ grafts differentiated as efficiently as their WT controls (Fig. 4B-E). Interestingly, similarly to cells induced *in vitro,* expression of Helios and to a lesser extent expression of Eos, was induced in WT differentiated $CD8^+CD25^+Foxp3^+$ as measured by intracellular staining in donor cells (Fig. S3B). These results indicate that despite their expression in $CD8^+CD25^+Foxp3^+$ iTreg cells, Eos and Helios are not required for their differentiation.

Loss of both Eos and Helios does not affect $CD4^+$ Treg cells during homeostasis and does not perturb their essential functions.

As Eos and Helios are closely related in terms of protein sequence and expression patterns the apparent lack of phenotype in the systems used could be due to a redundancy in their function. We have shown that in single KO mice the expression of Eos or Helios is not up-regulated as one might expect (Fig. 2G). To further verify whether Eos and Helios cooperate to regulate Treg cell functions we have crossed $Eos^{-/-}$ and $Helios^{-/-}$ mice to obtain double knock-out $Eos^{-/-}Helios^{-/-}$ mice (dKO). $Eos^{-/-}Helios^{-/-}$ mice were born with low

frequencies and in some cases had decreased body weight (especially females at early age) (Fig. 5A, B). Similar observations were made for Helios$^{-/-}$ mice after establishing the line (Cai et al., 2009). As Eos$^{-/-}$ mice were healthy and born with correct frequencies the observed anomalies were probably not due a cumulative effect of Eos and Helios loss, but dominant effect of Helios deletion and the genetic background of the established line.

Nevertheless, dKO mice were healthy and showed normal hematopoiesis (data not shown). When analyzing Eos$^{-/-}$Helios$^{-/-}$ mice we have then focused on populations where both transcription factors are expressed. First, dKO mice had normal frequencies of CD4^{+} and CD8^{+} T cells as well as CD4^{+}CD25^{+}Foxp3^{+} Treg cells (Fig. 5C). Finally, Eos$^{-/-}$Helios$^{-/-}$ natural CD4^{+}CD25^{+} Treg cells performed equally to WT cells in the *in vitro* suppression assay (Fig. 5D). We have also studied induced CD4^{+} Treg cells in dKO mice as well single mutants. For that we sort purified CD4^{+}CD25^{-} T cells from mice of different genotypes and cultured *in vitro* in the presence of anti-CD3 and anti-CD28 antibody, IL-2, TGF-β1 and some cases also rapamycin. Cells from different origin presented comparable capacity to differentiate into CD4^{+}CD25^{+}Foxp3^{+} Treg cells (He$^{-/-}$ to compare with He$^{+/+}$; Eos$^{-/-}$Helios$^{-/-}$ and Eos$^{-/-}$ to compare with Eos$^{+/+}$) (Fig. S4). In conclusion, loss of both Eos and Helios does not affect CD4^{+} Treg cells during homeostasis, have no effect on their suppressive functions and does not influence iTreg cell generation.

Loss of both Eos and Helios has a minimal impact on the differentiation of alloantigen induces CD8^{+} Treg cells.

We have also studied the CD8^{+} iTreg differentiation using cells from Eos$^{-/-}$Helios$^{-/-}$ mice. *In vitro,* with the same protocol as previously, we obtained different level of Treg cell activation, as explained before probably due to introduction of a different genetic background to the experimental system. However, Eos$^{-/-}$Helios$^{-/-}$ CD8^{+} T cells had a slightly lower efficiency to differentiate into Foxp3^{+} cells when compared to WT cells, presenting a similar phenotype to Helios$^{-/-}$ CD8^{+} T cells (Fig. 6A and Fig. 3B). Obtained CD8^{+}CD25^{+} iTreg cells from both Eos$^{-/-}$Helios$^{-/-}$ and WT mice were functional and could efficiently suppress the proliferation of responder T cells (Fig. 6B). Interestingly, we could also see an inferior differentiation of dKO cells *in vivo* with allogeneic bone marrow transplantation. The frequencies (but not total numbers) of generated CD8^{+}CD25^{+}Foxp3^{+} donor derived Treg cells were significantly lower in mice that received Eos$^{-/-}$Helios$^{-/-}$ grafts when compared to mice transplanted with WT grafts (Fig. 6C, D). With these results we showed that loss of Eos and Helios has a negative impact on allogeneic CD8^{+} Treg cell differentiation both *in vitro* and *in*

vivo. This phenotype could be attributed to the prevailing effect of Helios deficiency, as we observed a diminished differentiation potential in the single mutant Helios$^{-/-}$ cells *in vitro* (Fig. 3B).

Gene expression profile of KO nTreg cells reflects their functional properties.

To have a global view on changes in Treg cells deficient for Eos and/or Helios we have performed a transcriptomic analysis in mutant CD4^{+}CD25^{+} Treg cells. We compared Eos$^{-/-}$Helios$^{-/-}$ and Eos$^{-/-}$ cells with WT ones and Helios$^{-/-}$ cells with their WT controls (Fig. 7). Clustering analysis of differentially expressed genes in dKO, Eos$^{-/-}$ and WT Treg cells showed two main groups of genes. First, clusters with probe sets up- or down-regulated in both Eos$^{-/-}$ and dKO Treg cells. Second, clusters with probe sets up- or down-regulated only in dKO samples. This already indicated that there is no clear interplay and regulation between Eos and Helios on a global gene expression level and the first mentioned group could be attributed mainly to Eos deficiency and the second one to Helios deficiency. This could be also supported by the lack of group of genes differentially expressed only in Eos$^{-/-}$ Treg cells (Fig. 7B).

Moreover, results showed that loss of Eos alone has a small impact on the gene expression profile in CD4^{+} Treg cells (clusters with genes up- or down-regulated in both Eos$^{-/-}$ and dKO samples) and among the genes differentially expressed in Eos$^{-/-}$ samples we found only one (*Gpr15*) related to Treg cell biology and few related to immune responses whatsoever (e.g. *Cxcr2*, *Oasl2*, *Islr*). We found more genes related to immune responses and in particular to Treg cell functions in dKO samples. Among genes up-regulated we found e.g. *Il10*, *Id2*, *Ccr2*, *Ccr3*, *Ccr4*, *Ccr5*, *Lag3*, *Klrg1*, *Gzmb*, *Fgl2* and *Ifng*, all known to be implicated in immune responses and specifically in Treg cells. Among genes down-regulated we found *Hdac9*, shown previously to regulate Treg cell activity (decreased HDAC9 function caused increased Treg activity) (de Zoeten et al., 2010) (Fig. 7B and Supplementary table 1). Concerning the transcriptome analysis in Helios$^{-/-}$ cells, many more genes came up as differentially regulated (> 700), with most of them being up-regulated (Fig. 7A). Enrichment analysis showed that the vast majority of up-regulated genes were related to cell cycle, division, chromosome segregation or DNA packaging (data not shown). Between those genes we found also ones related to immune responses and Treg cell biology overlapping with genes found in dKO Treg cells (*Il10*, *Ccr2*, *Ccr5*, *Fgl2*, *Id2*, *Lag3,* etc.) (Fig. 7A and Supplementary table 1). Next step was to validate the expression of few selected genes on a protein level in mutant Treg cells. Lacking the appropriate number of dKO mice we first

analyzed the expression of selected genes (e.g. *Klrg1*, *Ccr4* and *Ccr5;* all up-regulated in dKO or Helios$^{-/-}$ cells) in Helios mutant mice. We found Klrg1 particularly interesting as it was shown to characterize terminally differentiated Treg cells with superior suppressive activity (Beyersdorf et al., 2007; Cheng et al., 2012). Flow cytometry analysis showed that both in terms of frequency and numbers CD4^{+}CD25^{+} population from Helios$^{-/-}$ was enriched in Klrg1 positive cells. It was not the case for Ccr4, and surprisingly we found a decreased percentage of CD4^{+}CD25^{+}Ccr5^{+} cells in KO samples (Fig. S5A). We could confirm those results also in dKO Treg cells and interestingly observed elevated frequency of CD4^{+}CD25^{+}Klrg1^{+} cells in Eos$^{-/-}$ samples (Fig. S5B).

Gene up- or down-regulated in Helios$^{-/-}$ and dKO cells are found in activated Treg cells.

We have next thought to compare our microarray results with available data, in particular transcriptional profiling of resting and activated Treg cells (aTreg) and effector T cells from Arvey et al., 2014. We found that dKO Treg cells as well as He$^{-/-}$ Treg cells, but not Eos$^{-/-}$, had a transcriptional profile of activated Treg cells (Fig. 8). GSEA analysis showed enrichment of genes up-regulated in dKO or Helios KO in the pool of genes up-regulated in aTreg cells and to a lesser extent enrichment of genes down-regulated in dKO or Helios KO in the pool of genes down-regulated in aTreg cells, suggesting a big similarity between KO Treg cells and activated Treg cells in terms of their overall gene expression profile (Fig. 8, top and bottom). In Eos KO cells, up-regulated genes were not enriched in the group of up-regulated aTreg cell genes, but some of the down-regulated genes were positively enriched within genes down-regulated in activated Treg cells (Fig. 8, middle), all together indicating that the observed changes in dKO Treg cells are rather an effect of Helios deficiency and not a cumulative effect of Eos and Helios absence.

To support the latter hypothesis, a majority of genes (168) up-regulated in both He$^{-/-}$ and activated Treg cells (274) overlapped with genes up-regulated in both dKO and activated Treg cells (240) (Fig. S6A). As shown also by the GSEA, each KO had common down-regulated genes with aTreg cells (86 for He$^{-/-}$, 91 for Eos$^{-/-}$ and 124 for Eos$^{-/-}$Helios$^{-/-}$) with overlapping genes between all groups (Fig. S6B). We also found genes up-regulated in aTreg and down-regulated in Eos$^{-/-}$ (91) and genes up-regulated in aTreg and down-regulated in dKO (124), but none of these genes overlapped with genes up-regulated in both aTreg and He$^{-/-}$ (where the aTreg vs. KO overlap was highest), suggesting that they are regulated specifically by Eos (Fig. S6C). Finally, the transcriptional profile of KO CD4^{+} Treg cells resembling activated Treg cells, could explain their superior suppressive activity observed in

the *in vitro* suppression assay (Fig. 2F) and on the cellular level could result from the enrichment in Klrg1$^+$ cells (Fig. S5A).

Collectively, our results show that despite the fact that Eos and Helios are highly expressed in CD4$^+$ Treg cells, they do not play roles in the maintenance of their essential functions in mice. Transcriptomic analysis of Treg cells from single or double KO mice show that Eos has a minimal impact on the expression of Treg related genes and that Helios and Eos do not cooperate to regulate Treg cell compartment, supporting functional data. Interestingly, Helios$^{-/-}$ and dKO Treg cells acquire an activated transcriptional profile, reflected by higher suppressive activity of Helios$^{-/-}$ cells. Finally, we show that both transcription factors are induced in alloantigen specific CD8$^+$ Treg cells *in vitro* and *in vivo* but only loss of Helios or both has an impact on their differentiation.

DISCUSSION

In this study we investigated the roles of Eos and Helios in the differentiation and function of Treg cells using mice deficient for one or both of the transcription factors. We show that Eos deficiency has no impact on the steady state hematopoiesis and natural Treg cell development and function in mice, similarly to recently published data (Fu et al., 2012; Rieder et al., 2015). Interestingly, previous studies showed that Eos is necessary for Foxp3 mediated gene regulation in CD4$^+$ Treg cells and that siRNA knockdown of Eos abrogates their suppressive potential (Pan et al., 2009). These results are contradictive, but it is noteworthy that they come from different experimental systems, namely germline gene deletion in mice and siRNA mediated knockdown in purified Treg cells. The first system is more physiological, but gives a possibility for compensatory mechanisms to occur. Thus, we have also analyzed conditional (Eos$^{f/f}$ Rosa26-CreERT2) and inducible (Eos$^{f/f}$ CD4-Cre) Eos KO mice, hypothesizing that it may result in a phenotype where Treg cells have an impaired function. However, we did not find any defects in those mice as well (data not shown). Our gene expression data from Eos KO CD4$^+$ Treg cells confirm the functional studies showing that Eos alone has a minimal impact on Treg cell transcriptomic signature (Fig.7). We also demonstrate that loss of Eos has no effect on CD4$^+$ and CD8$^+$ iTreg cells. Taken together, our results show that Eos is certainly dispensable for Treg cell development and function in steady state conditions, despite playing a role in specific Treg cell subsets under inflammatory conditions (Sharma et al., 2013; Ukena et al., 2012).

We also show that Helios deficiency does not impair the suppressive potential of CD4$^+$ Treg cells. Helios has been first described to be an important marker and factor for Treg cells

after a series of microarray studies (Fontenot et al., 2005; Sugimoto et al., 2006). Together with Eos it has been shown to be expressed in human Treg cells (Birzele et al., 2011). Others demonstrated that Helios directly interacts with Foxp3 and that loss of Helios (siRNA) attenuates Treg cell functionality (Getnet et al., 2010). At the same time, Helios deficiency in mice does not impair Treg cell functions (Cai et al., 2009; Thornton et al., 2010). Our study adds to the latter findings in mice and shows that Helios$^{-/-}$ Treg cells are actually more suppressive, both in a functional assay and in terms of their transcriptional signature (Fig.8). This novel observation can be supported by an up-regulation of certain genes in Helios$^{-/-}$ cells, which are known to be associated with highly suppressive and active Treg cells e.g. *Klrg1*, *Id2*, *Fgl2* or *Lag3* or *Il10* (Beyersdorf et al., 2007; Tauro et al., 2013; Miyazaki et al., 2014; Shalev et al., 2009; Do et al., 2015; Sun et al., 2010; Heo et al., 2010). It will be now important to test if Helios$^{-/-}$ Treg cells are also more suppressive *in vivo* and under inflammatory conditions in colitis or autoimmune encephalomyelitis model. Interestingly, we also observed a defect in Helios$^{-/-}$ and dKO CD8$^+$ T cells to differentiate into cells expressing Foxp3 transcription factor. Alloinduced CD8$^+$ Treg cells share characteristics with CD4$^+$ Treg cells. This includes expression of CD25, CD103, CTLA4 or IL-10 together with dependency on IL-2 and TGF-β signaling (Mahic et al., 2008; Mayer et al., 2011; Muthu Raja et al., 2012). However, little is known about their regulation on a transcriptional level and whether Foxp3 shares its protein partners from CD4$^+$ Treg regulatory network. We propose that Eos and Helios are involved in the regulation of this Treg subset. A better understanding of their roles in CD8$^+$ iTreg cells will require an insight into the molecular mechanisms of CD8$^+$ Treg cell differentiation. First, a comparison of gene expression profiles in WT and KO cells could reveal genes or pathways potentially regulated by Ikaros family proteins. Second, it will be crucial to know if Eos or Helios can bind to the *Foxp3* locus and directly regulate its function.

In this study we also verified if Eos, Helios or other genes implicated in Treg cell lineage regulation may have compensatory functions. However, on the expression level, Eos and Helios do not compensate for each other and other “key” Treg transcriptional regulators such as Satb1, Lef1, Irf4, Gata1, or Foxp3 itself, are also normally expressed in Eos or Helios deficient cells (transcriptome data and Fig.2). Possible cooperation between Eos and Helios in regulating Treg cell functions was also assessed with double null Eos$^{-/-}$Helios$^{-/-}$ mice. Transcriptome data from CD4$^+$ Treg cells demonstrated lack of apparent co-regulation between Eos and Helios and observed differentially regulated genes are mainly related to Helios deficiency. Similarly to Helios, dKO Treg cells also have a transcriptional signature of

activated Treg cells (Fig.8; Fig.S6). Concerning $CD8^+$ Treg cells, we demonstrate an inferior potential of dKO $CD8^+$ T cells to differentiate into cells expressing Foxp3 transcription factor *in vitro* and *in vivo*. However, we hypothesize that again, the observed phenotype is related more to the absence of Helios as it could be detected in the single mutant $Helios^{-/-}$ cells.

Treg cells possess a distinct gene-expression signature and this comprises not only cell surface markers, but also a wide array of transcription factors. Foxp3 does not act alone to establish Treg cell transcriptional signature, but in cooperation with other factors including Eos and Helios next to Satb1, Lef1, Irf4 or Gata1 (Fu et al., 2012). In this regard, our results bring more knowledge to the understanding of the complex regulatory network within studied Treg subsets. We show that knocking out Eos and Helios does not result in a drastic impairment of Treg lineage stability in mice. Finally, with these results we also show that Eos and Helios, despite being closest relatives within Ikaros family and sharing similar expression pattern, appear to have distinct roles in Treg cell biology.

MATERIALS AND METHODS

Mice

Eos knock-out mice were generated after CMV-Cre driven germline deletion of exon 8 of *Ikzf4* flanked by loxP sites. Construct and mice were generated by Institut Clinique de la Souris: ICS (Illkirch). Mice were generated and maintained on a C57BL/6 background in SPF conditions and conventional animal facility. Construct to obtain the null mice is described in Figure 1. Helios deficient mice were described previously (Cai et al., 2009). Mice have a mixed C57BL/6 and 129/Sv background and are kept in SPF conditions. $Eos^{-/-}Helios^{-/-}$ mice were obtained from crossing $Eos^{-/-}$ and $Helios^{-/-}$ mice. They are kept in special sterile conditions ("ultra-clean bioBUBBLE) in the ICS. WT Balb/c mice used as recipients in cell transfer experiments as well as WT mice with C57BL/6, CD1 or 129/Pas backgrounds used as BM donors for in vitro BMDC production were obtained from IGBMC conventional animal facility stock. Recipient C57BL/6 $CD45.1^+CD45.2^+$ mice were obtained from crossing congenic C57BL/6 $CD45.1^+$ mice with wild-type C57BL/6 inbred mice that express CD45.2 allele and were kept in SPF conditions. All animal procedures were carried out in strict accordance with local Ethical Committee rules (IGBMC) and approved by Ministère de l'Enseignement Supérieur et de la Recherche (protocol #2014-028).

RT-PCR and quantitative real-time PCR

RNA was extracted using RNeasy Mini Kit (Qiagen). Reverse transcription was performed using SuperScript II Reverse Transcriptase (Invitrogen, Cat.No: 18064-014). RT-qPCRs were

performed using SybrGreen I Master (Roche, Cat.No: 04707516001) and Light Cycler 480 instrument (Roche). Primers used for RT-PCR and RT-qPCR were as followed:

Eos, forward 5'- ACTGAACGGCCAACTTTCAT, reverse 5'- GGAAGGTCT GAGAGGCTGAA; Helios, forward 5'- ACACCTCAGGACCCATTCTG, reverse 5'- TCCATGCTGACATTCTGGAG; HPRT, forward 5'- GCTGGTGAAAAGGACCTCT, reverse 5'- CACAGGACTAGAACACCTGC; β-actin, forward 5'- CCATCACAATGCCTGTGGTA, reverse 5'- TGTTACCAACTGGGACGACA; A, 5'- GGTGTGCTCCGGATTTCTT, B, 5'- GGGTGAAGAGTGTTGGCTGT, C, 5'- ACTGAACGGCCAACTTTCAT, D 5'- GGTGTAACAGGAATTGGGCTAGACC.

Microarray

RNA for the transcriptome was obtained from sorted $CD4^+CD25^+$ Treg cells and extracted with RNeasy Mini Kit (Qiagen). Transcriptome comparison of mutant Treg cells was performed with GeneChip Mouse Gene 1.0 ST array (Affymetrix), covering 28 853 genes and represented by around 27 probes spread across the full length of the gene. cDNA was prepared from 4-15ng of total RNA. Raw data were processed with Affymetrix Expression Console software version 1.3.1 to calculate probe set signal intensities. Clustering analysis was performed with Cluster 3.0. Only the most differentially expressed genes were considered in the analysis according to the following criteria. For up-regulated genes: mean KO1:KO3 ($He^{-/-}$ or $Eos^{-/-}$ or dKO) – mean WT1:WT3 ≥ 0,4 and MIN (KO1:KO3) – MAX (WT1:WT3) > 0.4. For down-regulated genes: mean KO1:KO3 ($He^{-/-}$ or $Eos^{-/-}$ or dKO) – mean WT1:WT3 ≤ -0,4 and MIN (WT1:WT3) – MAX (KO1:KO3) > 0. For the comparison with activated Treg cells microarray data were analyzed with GSEA (Gene Set Enrichment Analysis) software to identify functionally related gene sets.

Antibodies, flow cytometry analysis and cell sorting

Cells from mouse lymphoid organs were analyzed using BD LSR II or sorted with BD FACSAria II SORP. All primary antibodies were purchased from eBioscience, BioLegend or BDPharmingen. Secondary antibodies were obtained from Jackson Immunoresearch and Invitrogen. Antigens and clones of the primary antibodies were as followed: CD3 (145-2C11, KT3), CD4 (RM 4-5, GK1.5), CD8 (53-7.3), CD25 (PC61), CD103 (2E7), CD44 (IM7 8.1), CD62L (MEL-14), Foxp3 (FJK-16S), Eos (ESB7C2), Helios (22F6), CD90.2 (53-2.1), CD38 (90), CD122 (TM-b1), Klrg1 (2F1), Ccr4 (2G12), Ccr5 (C34-3488), Ly49 (14B11), PD-1 (RMP1-30), Nrp1 (3E12), CD11b (M1/70.15), CD11c (N418, HL3), CD45.1 (A20), CD45.2

(104, 104.2), CD45R (RA3-6B2), CD16/CD32 (93), Gr1 (RB6-8C5), MHC Kb (AF6-88.5), Ter119 (TER-119). Intracellular staining was performed according to the Foxp3 staining protocol (eBioscience, Cat.No: 71-5775-40), with the exception of anti-Eos antibody which was incubated 1h in RT in a high concentration (8 µg/ml). Data were analyzed with FlowJo software (Tree Star). Before cell sorting cells were depleted using Dynabeads (Life Technologies, Cat.No: 11035). For T cell sorting cells were depleted from cells expressing CD11b, B220, Gr1, Ter119 and additionally CD4/CD8 if another population was sorted. For $CD8^+$ iTreg experiments, cells ($CD8^+$ T cells, $CD11c^+$ BMDCs) were also obtained by positive selection with MACS Streptavidin MicroBeads (Miltenyi Biotec, Cat.No: 130-048-101). Purity of sorted or purified populations was >95%.

Induction of allogeneic $CD8^+$ Treg cells *in vitro*

Splenic $CD8^+$ T cells ($60x10^3$) were cultured with allogeneic (Balb/c throughout the paper or from test strains as presented in Fig. S2) $CD11c^+$ BM-derived dendritic cells ($20x10^3$, preconditioned with 10 nM rapamycin overnight before the co-culture) in the presence of IL-2 (10 ng/ml), TGF-β1 (2 ng/ml) and retinoic acid (100 nM) for 7 days in 96-well plates. All experiments were carried out with complete RPMI medium with 10% FCS 25 mM HEPES, 1% penicilin and streptomycin, 40 µg/ml gentamycin, 2 mM L-Glutamine, 1x Non-essential Amino Acid Solution, 1 mM Sodium Pyruvate and 50 µM β-mercaptethanol. Fresh medium supplemented with cytokines was added every 2 days. To perform bigger scale experiments cells were cultured in 24-well plates while always keeping the ratio between T cells and BM-derived dendritic cells at 3:1, respectively. $CD8^+$ T cells for *in vitro* experiments were either sort purified or obtained by positive selection as described above. BM-derived dendritic cells were obtained by culturing total BM cells from Balb/c mice with mouse GM-CSF for 7 days. After pre-conditioning with rapamycin and before the co-culture cells were sorted or enriched to obtain $CD11c^+$ cells. GM-CSF was used as a supernatant (4-5%) from a J558L mouse macrophage cell line producing GM-CSF. The J558L cell line was kindly provided by Dr. Philippe Pierre from the Centre d'Immunologie de Marseille-Luminy. Reagents used for $CD8^+$ iTreg experiments: rapamycin (Calbiochem, Cat.No: 553210-100), rhIL-2 (Peprotech, Cat.No: 200-02), rmTGF-β1 (Peprotech, Cat.No: 200-02) and retinoic acid (ATRA, MP-Biomedicals, Cat.No: 02190269.6).

$CD4^+$ iTreg differentiation *in vitro*

$CD4^+CD25^-$ T cells were sort purified from mice of indicated genotypes and 10^5 cells were plated in 96-well cell culture dishes pre-coated with anti-CD3 antibody (overnight in 4°C,

10 µg/ml antibody in PBS) and in the presence of soluble anti-CD28 antibody (2 µg/ml), TGF-β1 (5 ng/ml) and IL-2 (10 ng/ml) for 4 days. Cells were then analyzed by flow cytometry for the expression of CD25 and Foxp3. All experiments were carried out with complete RPMI medium with 10% FCS 25 mM HEPES, 1% penicilin and streptomycin, 40 µg/ml gentamycin, 2 mM L-Glutamine, 1x Non-essential Amino Acid Solution, 1 mM Sodium Pyruvate and 50 µM β-mercaptethanol. Reagents used for $CD4^+$ iTreg experiments: rhIL-2 (Peprotech, Cat.No: 200-02), rmTGF-β1 (Peprotech, Cat.No: 200-02), anti-mouse CD3 Ab (functional grade purified, eBioscience, Cat.No: 16-0031), anti-mouse CD28 Ab (functional grade purified, eBioscience, Cat.No: 16-0281).

Treg suppression assays

Cells from lymph nodes and spleens of WT and KO mice were sorted according to the expression of cell surface markers: WT $Thy1.1^-$ antigen presenting cells – APCs; WT $CD4^+CD25^-$ responder T cells; WT or KO $CD4^+CD25^+$ Treg cells. For $CD8^+$ iTreg suppression assays Treg cells were sorted 7 days after *in vitro* differentiation experiment (described above) as $CD8^+CD25^+$ cells. APCs were sorted as $Thy1.1^-$ cells from WT Balb/c mice. Other parts of suppression assays were common. APCs were treated with mitomycin C (50 µg/ml) and responder T cells labeled with CFSE (40 µg/ml) directly after sorting. T cells were labeled with CFSE for 10 min in 37°C water bath and APCs were treated with Mitomycin C for 20 min in 37°C water bath. In both cases cells were washed 3 times after treatment. Obtained cells were co-cultured in 96-well plates (with triplicate of each condition) as followed: $25x10^3$ WT APCs and $25x10^3$ WT responder T cells with WT or KO Treg cells (6,25 $x10^3$, 12,5$x10^3$, 25$x10^3$, 50$x10^3$ for Treg to responder T cell ratios 0,25:1, 0,5:1, 1:1, 2:1 respectively). Cells were co-cultured in the indicated ratios in the presence of soluble anti-CD3 antibody (5 µg/ml). Experiments were carried out with complete RPMI medium with 10% FCS 25 mM HEPES, 1% penicilin and streptomycin, 40 µg/ml gentamycin, 2 mM L-Glutamine, 1x Non-essential Amino Acid Solution, 1 mM Sodium Pyruvate and 50 µM β-mercaptethanol. Reagents used for suppression assays: CFSE (Sigma-Aldrich, Cat.No: 21888), Mitomycin C (from Streptomyces caespitosus, Sigma-Aldrich, Cat.No: M4287, prepared in PBS and kept in non-transparent tubes in 4°C, used within 2 weeks), anti-mouse CD3 Ab (functional grade purified, eBioscience, Cat.No: 16-0031).

Syngeneic and allogeneic bone marrow transplantations

One day before transplantation recipient mice were lethally irradiated (9 Gy). C57Bl/6 $CD45.1^+CD45.2^+$ (syngeneic) and MHC-K^{b+} Balb/c (allogeneic) recipient mice were

intravenously injected (into tail vein) with BM cells (10^7) and $CD3^+CD25^-$ T cells ($0.6x10^6$) from $CD45.2^+$/ MHC-K^{b-} KO mice and their WT littermates. BM cells and T cells came from mice of the same genotype. After 8 days, spleen cells were analyzed by flow cytometry. In allogeneic conditions donor versus recipient cells could be distinguished by MHC K^b expression and in syngeneic conditions by the expression of CD45.1 and CD45.2. To control the T cell depletion from BM control Balb/c recipients are also injected with BM cells alone. To obtain a sufficient number of cells splenocytes of 2-3 mice were pooled and depleted (Dynabeads, Life Technologies, Cat.No: 11035) from cells expressing B220, Gr1, CD11b and Ter119 before sorting. BM cells were depleted with Dynabeads from cells expressing CD4 and CD8 before injections and the efficiency was verified by flow cytometry (>95%).

Statistical analysis

Data were analyzed with unpaired Student's t-test, two-tailed Student's t test and Chi-squared test. In all cases, $P < 0,05$ was considered as statistically significant. GraphPad Prism software version 5.0 was used to analyze part of the data.

REFERENCES

Arvey, A., van der Veeken, J., Samstein, R.M., Feng, Y., Stamatoyannopoulos, J.A., and Rudensky, A.Y. (2014). Inflammation-induced repression of chromatin bound by the transcription factor Foxp3 in regulatory T cells. Nat. Immunol. *15*, 580–587.

Beres, A.J., Haribhai, D., Chadwick, A.C., Gonyo, P.J., Williams, C.B., and Drobyski, W.R. (2012). CD8+ Foxp3+ regulatory T cells are induced during graft-versus-host disease and mitigate disease severity. J. Immunol. *189*, 464–474.

Beyersdorf, N., Ding, X., Tietze, J.K., and Hanke, T. (2007). Characterization of mouse CD4 T cell subsets defined by expression of KLRG1. Eur. J. Immunol. *37*, 3445–3454.

Birzele, F., Fauti, T., Stahl, H., Lenter, M.C., Simon, E., Knebel, D., Weith, A., Hildebrandt, T., and Mennerich, D. (2011). Next-generation insights into regulatory T cells: expression profiling and FoxP3 occupancy in Human. Nucleic Acids Res. *39*, 7946–7960.

Bruder, D., Probst-Kepper, M., Westendorf, A.M., Geffers, R., Beissert, S., Loser, K., von Boehmer, H., Buer, J., and Hansen, W. (2004). Neuropilin-1: a surface marker of regulatory T cells. Eur. J. Immunol. *34*, 623–630.

Cai, Q., Dierich, A., Oulad-Abdelghani, M., Chan, S., and Kastner, P. (2009). Helios deficiency has minimal impact on T cell development and function. J. Immunol. *183*, 2303–2311.

Campos-Mora, M., Morales, R.A., Pérez, F., Gajardo, T., Campos, J., Catalan, D., Aguillón, J.C., and Pino-Lagos, K. (2015a). Neuropilin-1+ regulatory T cells promote skin allograft survival and modulate effector CD4+ T cells phenotypic signature. Immunol. Cell Biol. *93*, 113–119.

Chen, X., Fosco, D., Kline, D.E., Meng, L., Nishi, S., Savage, P.A., and Kline, J. (2014). PD-1 regulates extrathymic regulatory T-cell differentiation. Eur. J. Immunol. *44*, 2603–2616.

Cheng, G., Yuan, X., Tsai, M.S., Podack, E.R., Yu, A., and Malek, T.R. (2012). IL-2 receptor signaling is essential for the development of Klrg1+ terminally differentiated T regulatory cells. J. Immunol. *189*, 1780–1791.

Dai, Z., Zhang, S., Xie, Q., Wu, S., Su, J., Li, S., Xu, Y., and Li, X.C. (2014). Natural CD8+CD122+ T cells are more potent in suppression of allograft rejection than CD4+CD25+ regulatory T cells. Am. J. Transplant. Off. J. Am. Soc. Transplant. Am. Soc. Transpl. Surg. *14*, 39–48.

Delgoffe, G.M., Woo, S.-R., Turnis, M.E., Gravano, D.M., Guy, C., Overacre, A.E., Bettini, M.L., Vogel, P., Finkelstein, D., Bonnevier, J., et al. (2013). Stability and function of regulatory T cells is maintained by a neuropilin-1-semaphorin-4a axis. Nature *501*, 252–256.

Do, J.-S., Visperas, A., Sanogo, Y.O., Bechtel, J.J., Dvorina, N., Kim, S., Jang, E., Stohlman, S.A., Shen, B., Fairchild, R.L., et al. (2015). An IL-27/Lag3 axis enhances Foxp3(+) regulatory T cell-suppressive function and therapeutic efficacy. Mucosal Immunol.

Endharti, A.T., Rifa'I, M., Shi, Z., Fukuoka, Y., Nakahara, Y., Kawamoto, Y., Takeda, K., Isobe, K.-I., and Suzuki, H. (2005). Cutting edge: CD8+CD122+ regulatory T cells produce IL-10 to suppress IFN-gamma production and proliferation of CD8+ T cells. J. Immunol. *175*, 7093–7097.

Fontenot, J.D., Gavin, M.A., and Rudensky, A.Y. (2003). Foxp3 programs the development and function of CD4+CD25+ regulatory T cells. Nat. Immunol. *4*, 330–336.

Fontenot, J.D., Rasmussen, J.P., Williams, L.M., Dooley, J.L., Farr, A.G., and Rudensky, A.Y. (2005). Regulatory T cell lineage specification by the forkhead transcription factor foxp3. Immunity *22*, 329–341.

Fu, W., Ergun, A., Lu, T., Hill, J.A., Haxhinasto, S., Fassett, M.S., Gazit, R., Adoro, S., Glimcher, L., Chan, S., et al. (2012). A multiply redundant genetic switch "locks in" the transcriptional signature of regulatory T cells. Nat. Immunol. *13*, 972–980.

Furtado, G.C., Curotto de Lafaille, M.A., Kutchukhidze, N., and Lafaille, J.J. (2002). Interleukin 2 signaling is required for CD4(+) regulatory T cell function. J. Exp. Med. *196*, 851–857.

Getnet, D., Grosso, J.F., Goldberg, M.V., Harris, T.J., Yen, H.-R., Bruno, T.C., Durham, N.M., Hipkiss, E.L., Pyle, K.J., Wada, S., et al. (2010). A role for the transcription factor Helios in human CD4(+)CD25(+) regulatory T cells. Mol. Immunol. *47*, 1595–1600.

Heo, Y.-J., Joo, Y.-B., Oh, H.-J., Park, M.-K., Heo, Y.-M., Cho, M.-L., Kwok, S.-K., Ju, J.-H., Park, K.-S., Cho, S.G., et al. (2010). IL-10 suppresses Th17 cells and promotes regulatory T cells in the CD4+ T cell population of rheumatoid arthritis patients. Immunol. Lett. *127*, 150–156.

Hill, J.A., Feuerer, M., Tash, K., Haxhinasto, S., Perez, J., Melamed, R., Mathis, D., and Benoist, C. (2007). Foxp3 transcription-factor-dependent and -independent regulation of the regulatory T cell transcriptional signature. Immunity *27*, 786–800.

Hill, J.A., Hall, J.A., Sun, C.-M., Cai, Q., Ghyselinck, N., Chambon, P., Belkaid, Y., Mathis, D., and Benoist, C. (2008). Retinoic acid enhances Foxp3 induction indirectly by relieving inhibition from CD4+CD44hi Cells. Immunity *29*, 758–770.

Hori, S., Nomura, T., and Sakaguchi, S. (2003). Control of regulatory T cell development by the transcription factor Foxp3. Science *299*, 1057–1061.

Hsieh, C.S., and Rudensky, A.Y. (2005). The role of TCR specificity in naturally arising CD25+ CD4+ regulatory T cell biology. Curr. Top. Microbiol. Immunol. *293*, 25–42.

Jebbawi, F., Fayyad-Kazan, H., Merimi, M., Lewalle, P., Verougstraete, J.-C., Leo, O., Romero, P., Burny, A., Badran, B., Martiat, P., et al. (2014). A microRNA profile of human CD8(+) regulatory T cells and characterization of the effects of microRNAs on Treg cell-associated genes. J. Transl. Med. *12*, 218.

Josefowicz, S.Z., Lu, L.-F., and Rudensky, A.Y. (2012). Regulatory T cells: mechanisms of differentiation and function. Annu. Rev. Immunol. *30*, 531–564.

Khattri, R., Cox, T., Yasayko, S.-A., and Ramsdell, F. (2003). An essential role for Scurfin in CD4+CD25+ T regulatory cells. Nat. Immunol. *4*, 337–342.

Kim, H.-J., Wang, X., Radfar, S., Sproule, T.J., Roopenian, D.C., and Cantor, H. (2011). CD8+ T regulatory cells express the Ly49 Class I MHC receptor and are defective in autoimmune prone B6-Yaa mice. Proc. Natl. Acad. Sci. U. S. A. *108*, 2010–2015.

Koch, S.D., Uss, E., van Lier, R.A.W., and ten Berge, I.J.M. (2008). Alloantigen-induced regulatory CD8+CD103+ T cells. Hum. Immunol. *69*, 737–744.

Lerret, N.M., Houlihan, J.L., Kheradmand, T., Pothoven, K.L., Zhang, Z.J., and Luo, X. (2012). Donor-specific CD8+ Foxp3+ T cells protect skin allografts and facilitate induction of conventional CD4+ Foxp3+ regulatory T cells. Am. J. Transplant. Off. J. Am. Soc. Transplant. Am. Soc. Transpl. Surg. *12*, 2335–2347.

Mahic, M., Henjum, K., Yaqub, S., Bjørnbeth, B.A., Torgersen, K.M., Taskén, K., and Aandahl, E.M. (2008). Generation of highly suppressive adaptive CD8(+)CD25(+)FOXP3(+) regulatory T cells by continuous antigen stimulation. Eur. J. Immunol. *38*, 640–646.

Marie, J.C., Letterio, J.J., Gavin, M., and Rudensky, A.Y. (2005). TGF-beta1 maintains suppressor function and Foxp3 expression in CD4+CD25+ regulatory T cells. J. Exp. Med. *201*, 1061–1067.

Mayer, C.T., Floess, S., Baru, A.M., Lahl, K., Huehn, J., and Sparwasser, T. (2011). CD8+ Foxp3+ T cells share developmental and phenotypic features with classical CD4+ Foxp3+ regulatory T cells but lack potent suppressive activity. Eur. J. Immunol. *41*, 716–725.

Miyazaki, M., Miyazaki, K., Chen, S., Itoi, M., Miller, M., Lu, L.-F., Varki, N., Chang, A.N., Broide, D.H., and Murre, C. (2014). Id2 and Id3 maintain the regulatory T cell pool to suppress inflammatory disease. Nat. Immunol. *15*, 767–776.

Muthu Raja, K.R., Kubiczkova, L., Rihova, L., Piskacek, M., Vsianska, P., Hezova, R., Pour, L., and Hajek, R. (2012). Functionally Suppressive CD8 T Regulatory Cells Are Increased in Patients with Multiple Myeloma: A Cause for Immune Impairment. PLoS ONE *7*, e49446.

Pan, F., Yu, H., Dang, E.V., Barbi, J., Pan, X., Grosso, J.F., Jinasena, D., Sharma, S.M., McCadden, E.M., Getnet, D., et al. (2009). Eos mediates Foxp3-dependent gene silencing in CD4+ regulatory T cells. Science *325*, 1142–1146.

Petrillo, M.G., Ronchetti, S., Ricci, E., Alunno, A., Gerli, R., Nocentini, G., and Riccardi, C. (2015). GITR+ regulatory T cells in the treatment of autoimmune diseases. Autoimmun. Rev. *14*, 117–126.

Polanczyk, M.J., Hopke, C., Vandenbark, A.A., and Offner, H. (2007). Treg suppressive activity involves estrogen-dependent expression of programmed death-1 (PD-1). Int. Immunol. *19*, 337–343.

Rieder, S.A., Metidji, A., Glass, D.D., Thornton, A.M., Ikeda, T., Morgan, B.A., and Shevach, E.M. (2015). Eos Is Redundant for Regulatory T Cell Function but Plays an Important Role in IL-2 and Th17 Production by CD4+ Conventional T Cells. J. Immunol. *195*, 553–563.

Rifa'i, M., Kawamoto, Y., Nakashima, I., and Suzuki, H. (2004). Essential roles of CD8+CD122+ regulatory T cells in the maintenance of T cell homeostasis. J. Exp. Med. *200*, 1123–1134.

Robb, R.J., Lineburg, K.E., Kuns, R.D., Wilson, Y.A., Raffelt, N.C., Olver, S.D., Varelias, A., Alexander, K.A., Teal, B.E., Sparwasser, T., et al. (2012). Identification and expansion of highly suppressive CD8(+)FoxP3(+) regulatory T cells after experimental allogeneic bone marrow transplantation. Blood *119*, 5898–5908.

Sakaguchi, S., Sakaguchi, N., Asano, M., Itoh, M., and Toda, M. (1995). Immunologic self-tolerance maintained by activated T cells expressing IL-2 receptor alpha-chains (CD25). Breakdown of a single mechanism of self-tolerance causes various autoimmune diseases. J. Immunol. *155*, 1151–1164.

Shalev, I., Wong, K.M., Foerster, K., Zhu, Y., Chan, C., Maknojia, A., Zhang, J., Ma, X.-Z., Yang, X.C., Gao, J.F., et al. (2009). The novel CD4+CD25+ regulatory T cell effector molecule fibrinogen-like protein 2 contributes to the outcome of murine fulminant viral hepatitis. Hepatol. *49*, 387–397.

Sharma, M.D., Huang, L., Choi, J.-H., Lee, E.-J., Wilson, J.M., Lemos, H., Pan, F., Blazar, B.R., Pardoll, D.M., Mellor, A.L., et al. (2013). An inherently bifunctional subset of Foxp3+ T helper cells is controlled by the transcription factor eos. Immunity *38*, 998–1012.

Singh, K., Hjort, M., Thorvaldson, L., and Sandler, S. (2015). Concomitant analysis of Helios and Neuropilin-1 as a marker to detect thymic derived regulatory T cells in naïve mice. Sci. Rep. *5*, 7767.

Sugimoto, N., Oida, T., Hirota, K., Nakamura, K., Nomura, T., Uchiyama, T., and Sakaguchi, S. (2006). Foxp3-dependent and -independent molecules specific for CD25+CD4+ natural regulatory T cells revealed by DNA microarray analysis. Int. Immunol. *18*, 1197–1209.

Sun, L., Yi, S., and O'Connell, P.J. (2010). IL-10 is required for human CD4(+)CD25(+) regulatory T cell-mediated suppression of xenogeneic proliferation. Immunol. Cell Biol. *88*, 477–485.

Tai, X., Cowan, M., Feigenbaum, L., and Singer, A. (2005). CD28 costimulation of developing thymocytes induces Foxp3 expression and regulatory T cell differentiation independently of interleukin 2. Nat. Immunol. *6*, 152–162.

Tauro, S., Nguyen, P., Li, B., and Geiger, T.L. (2013). Diversification and senescence of Foxp3+ regulatory T cells during experimental autoimmune encephalomyelitis. Eur. J. Immunol. *43*, 1195–1207.

Thornton, A.M., Korty, P.E., Tran, D.Q., Wohlfert, E.A., Murray, P.E., Belkaid, Y., and Shevach, E.M. (2010). Expression of Helios, an Ikaros transcription factor family member, differentiates thymic-derived from peripherally induced Foxp3+ T regulatory cells. J. Immunol. *184*, 3433–3441.

Ukena, S.N., Geffers, R., Buchholz, S., Stadler, M., and Franzke, A. (2012). Biomarkers for acute and chronic graft-versus-host disease in regulatory T cells. Transpl. Immunol. *27*, 179–183.

Uss, E., Rowshani, A.T., Hooibrink, B., Lardy, N.M., van Lier, R.A.W., and ten Berge, I.J.M. (2006). CD103 is a marker for alloantigen-induced regulatory CD8+ T cells. J. Immunol. *177*, 2775–2783.

Wing, K., Onishi, Y., Prieto-Martin, P., Yamaguchi, T., Miyara, M., Fehervari, Z., Nomura, T., and Sakaguchi, S. (2008). CTLA-4 control over Foxp3+ regulatory T cell function. Science *322*, 271–275.

Yadav, M., Louvet, C., Davini, D., Gardner, J.M., Martinez-Llordella, M., Bailey-Bucktrout, S., Anthony, B.A., Sverdrup, F.M., Head, R., Kuster, D.J., et al. (2012). Neuropilin-1 distinguishes natural and inducible regulatory T cells among regulatory T cell subsets in vivo. J. Exp. Med. *209*, 1713–1722, S1–S19.

De Zoeten, E.F., Wang, L., Sai, H., Dillmann, W.H., and Hancock, W.W. (2010). Inhibition of HDAC9 increases T regulatory cell function and prevents colitis in mice. Gastroenterology *138*, 583–594.

FIGURE LEGENDS

Figure 1. Generation of Eos$^{-/-}$ mice.

A. Eos and Helios are co-expressed in CD4^{+}CD25^{+}Foxp3^{+} natural Treg cells. Measured by flow cytometry in the spleen and thymus of WT mice. Gated on CD4^{+}CD25^{+}Foxp3^{+} cells. **B.** Targeting strategy to generate Eos$^{-/-}$ mice. Schematic representation of Eos protein, where exons are depicted as grey bars and zinc fingers as white rectangles; N-ter Ab - N terminal antibody used to confirm the deletion at the protein level. Targeting vector with fragments of Eos locus (5' homology arm, floxed fragment and 3'homology arm respectively) and neomycin selection cassette. **C.** RT-PCR of Eos and β-actin in WT and Eos$^{-/-}$ thymocytes with primers up-stream of the deletion (AB) and covering the deletion (CD). Position of the primers indicated in B. **D.** Eos protein in WT and Eos$^{-/-}$ thymocytes. Flow cytometry results with N-terminal anti-Eos antibody, gated on CD4^{+}CD25^{+}Foxp3^{+} cells (Treg) and CD4^{+}CD25^{-} Foxp3^{-} (non – Treg). **E.** Representative WT and Eos$^{-/-}$ male littermates at 7 wks of age. **F.** Frequencies of WT, Eos$^{+/-}$ and Eos$^{-/-}$ mice generated from Eos$^{+/-}$ crosses (152 mice in total). **G.** Body weights of adult WT and Eos$^{-/-}$ female and male littermates. Females were between 6-10 wks old (WT n=10, Eos$^{-/-}$ n=7) and males 6-11 wks old (WT n=11, Eos$^{-/-}$ n=6). Bars represent mean with standard deviation.

Figure 2. Development and function of natural CD4^{+} Treg cell in Eos$^{-/-}$ and He$^{-/-}$ mice.

A. Representative flow cytometry results and gating strategy to analyze CD4^{+} Treg cells in Eos$^{-/-}$ mice. **B.** Numbers of CD4^{+}CD25^{+}Foxp3^{+} Treg cells in the spleen (9 independent experiments) and thymus (8 independent experiments) of WT and Eos$^{-/-}$ mice. Bars represent mean with standard deviation. **C.** *In vitro* suppression assay. Cells from lymph nodes and spleens of WT and Eos$^{-/-}$ mice were sorted according to the expression of indicated surface markers. APCs were treated with mitomycin C and responder T cells labeled with CFSE. Cells were co-cultured in the indicated ratios in triplicates in the presence of soluble anti-CD3 antibody in 96-well plates. The percentage of proliferating cells was measured after 72 hours. **D.** Representative flow cytometry results of *in vitro* suppression assay. Proliferating cells are marked on histograms as cells diluting CFSE marker. **E.** Percentage of proliferating cells (gated on live Topro3^{-} and CFSE^{+} cells) with the increasing ratios of Treg cells from WT or Eos$^{-/-}$ mice. CT+, cells stimulated with anti-CD3 antibody and without Treg cells. CT-, cells without stimulation and without Treg cells. Data from 3 independent experiments. Bars represent mean with standard deviation. **F**. Percentage of proliferating cells with the increasing ratios of Treg cells from WT or Helios$^{-/-}$ mice. Controls like in panel E. Data from

one representative experiment. Bars represent mean with standard deviation of a triplicate of one Treg:Responder ratio (left). Each square represent the He/WT ratio in one condition of the suppression assay (like in the left panel). Data from 6 independant experiments. Ratios below 1 indicate condition where $He^{-/-}$ cells presented better suppression than WT controls. Statistical analysis with Chi-Square Test. **G.** Representative flow cytometry analysis of Eos and Helios expression in KO Treg cells in the spleen (left) and percentage of Eos/Helios positive cells in indicated populations (right). Bars represent mean with standard deviation. Helios KO line: WT n=3, $Helios^{-/-}$ n=3. Eos KO line: WT n=2, $Eos^{-/-}$ n=2.

Figure 3. Differentiation and function of *in vitro* induced $Eos^{-/-}$ and $He^{-/-}$ $CD8^+$ Treg cells.
A. *In vitro* $CD8^+$ Treg cell differentiation from $Eos^{-/-}$ and $Helios^{-/-}$ cells. Splenic $CD8^+$ T cells were cultured with allogeneic (Balb/c) BM-derived dendritic cells (preconditioned with rapamycin) in the presence of IL-2, TGF-β1 and retinoic acid for 7 days. **B.** Representative flow cytometry analysis of *in vitro* differentiated $CD8^+$ Treg cells (left) and percentage of $Foxp3^+$ cells in $CD8^+CD25^+$ differentiated cells (right) after 7 days of culture. Bars represent mean with standard deviation. Statistical analysis with paired t-test. Data from 4-6 experiments. **C.** Expression of Helios and Eos in induced CD8 Treg cells, measured by RT-qPCR and normalized to HPRT. CD8 Treg – $CD8^+CD25^+$ cells sorted from *in vitro* differentiation experiment, WT non-Treg - $CD8^+CD25^-$ cells sorted from *in vitro* differentiation experiment, primary CD8 – primary splenic $CD8^+$ T cells. Bars represent mean with standard deviation from 2 independent experiments. **D.** Expression of Eos and Helios in differentiated *in vitro* $CD8^+CD25^+Foxp3^+$ Treg cells. Analyzed by intracellular staining. **E.** Quantification of *in vitro* suppression assay with $Helios^{-/-}$ or $Eos^{-/-}$ and WT induced $CD8^+$ Treg cells. Shown as a percentage of proliferating cells with an increasing ratios of Treg cells. CT+, stimulated with anti-CD3 antibody and without Treg cells. CT-, without stimulation and without Treg cells. Data from 3 independent experiments (WT vs $Eos^{-/-}$) and 2 independent experiments (WT vs $Helios^{-/-}$). WT, $Eos^{-/-}$ or $Helios^{-/-}$ $CD8^+CD25^+$ Treg cells were sorted from *in vitro* differentiation cultures at day 8. The percentage of proliferating cells was measured after 72 hours.

Figure 4. *In vivo* induced $Eos^{-/-}$ and $He^{-/-}$ $CD8^+$ Treg cells.
A. Allogeneic bone marrow transplantation. Lethally irradiated (9 Gy) C57Bl/6 $CD45.1^+CD45.2^+$ (syngeneic) and MHC-K^{b+} Balb/c (allogeneic) recipient mice were transplanted i.v. with T cell depleted BM cells (10^7) and $CD3^+CD25^-$ T cells ($0.6x10^6$) from $CD45.2^+$/ MHC-K^{b-} $Helios^{-/-}$ or $Eos^{-/-}$ mice and their WT littermates. After 8d, spleen cells

were analyzed by flow cytometry. **B.** Flow cytometry analysis of *in vivo* differentiated $CD8^+$ Treg cells from WT and $Eos^{-/-}$ grafts. Gated on $CD8^+$ donor cells. **C.** Percentage of $CD8^+CD25^+Foxp3^+$ cells from WT or $Eos^{-/-}$ grafts (right). Bars represent mean with standard deviation. Data from 2 experiments. Balb/c recipients (WT n=6, $Eos^{-/-}$ n=6) and syngeneic B6 recipients (WT n=6, $Eos^{-/-}$ n=6). **D.** Flow cytometry analysis of *in vivo* differentiated $CD8^+$ Treg cells from WT and $Helios^{-/-}$ grafts. Gated on $CD8^+$ donor cells. **E.** Percentage of $CD8^+CD25^+Foxp3^+$ cells from WT or $He^{-/-}$ grafts (right). Bars represent mean with standard deviation. Data from 3 experiments. Balb/c recipients (WT n=10, $Helios^{-/-}$ n=9) and syngeneic B6 recipients (WT n=9, $Helios^{-/-}$ n=9).

Figure 5. T cell and $CD4^+$ nTreg cell development and function in $Eos^{-/-}Helios^{-/-}$ mice.
A. Frequencies of $Eos^{-/-}He^{+/+}$, $Eos^{-/-}$ $He^{+/-}$ and $Eos^{-/-}$ $He^{-/-}$ mice generated from $Eos^{-/-}$ $He^{+/-}$ crosses (289 mice in total). **B.** Body weights of adult $Eos^{+/+}$ $He^{+/+}$, $Eos^{-/-}$ $He^{+/+}$ and $Eos^{-/-}$ $He^{-/-}$ female and male littermates. Females were between 6-9 wks old ($Eos^{+/+}$ $He^{+/+}$ n=8, $Eos^{-/-}$ $He^{+/+}$ n= 10 and $Eos^{-/-}$ $He^{-/-}$ n=5) and males 6-9 wks old ($Eos^{+/+}$ $He^{+/+}$ n=4, $Eos^{-/-}$ $He^{+/+}$ n=6 and $Eos^{-/-}$ $He^{-/-}$ n=4). Bars represent mean with standard deviation. **C.** Gating strategy to analyze T cells and natural $CD4^+$ Treg cells in $Eos^{-/-}Helios^{-/-}$ mice by flow cytometry (left). Cell number of indicated population in the spleen (3 independent experiments) and thymus (3 independent experiments) of WT, $Eos^{-/-}$ and $Eos^{-/-}Helios^{-/-}$ mice right). Bars represent mean with standard deviation. **D.** *In vitro* suppression assay with WT and $Eos^{-/-}He^{-/-}$ Treg cells. Graph shows percentage of proliferating cells with the increasing ratios of Treg cells. CT+, stimulated with anti-CD3 antibody and without Treg cells. CT-, without stimulation and without Treg cells. Bars represent mean with standard deviation. Data from 2 independent experiments.

Figure 6. *In vitro* and *in vivo* induced $Eos^{-/-}Helios^{-/-}$ $CD8^+$ Treg cells.
A. Representative flow cytometry analysis of *in vitro* differentiated $CD8^+$ Treg cells that express CD25 and Foxp3 (left) and percentage of $Foxp3^+$ cells in $CD8^+CD25^+$ differentiated cells (left) after 7 days of culture from WT and $Eos^{-/-}He^{-/-}$ mice (right). Bars represent mean with standard deviation. Statistical analysis with paired t-test. Data from 5 experiments. **B.** Quantification of *in vitro* suppression assay with $Eos^{-/-}He^{-/-}$ and WT induced $CD8^+$ Treg cells. Shown as percentage of proliferating cells with the increasing ratios of Treg cells. CT+, stimulated with anti-CD3 antibody and without Treg cells. CT-, without stimulation and without Treg cells. Data from 3 independent experiments. **C.** Flow cytometry analysis of *in vivo* differentiated $CD8^+$ Treg cells from WT and $Eos^{-/-}Helios^{-/-}$ grafts. Gated on $CD8^+$ donor

cells. **D.** Percentage of $CD8^+CD25^+Foxp3^+$ cells from WT or $He^{-/-}$ grafts (right). Bars represent mean with standard deviation. Statistical analysis with Student's t-test. Data from 2 experiments. Balb/c recipients (WT n=5, $Eos^{-/-}He^{-/-}$ n=6) and syngeneic B6 recipients (WT n=8, $Eos^{-/-}He^{-/-}$ n=7).

Figure 7. Gene expression profile of $He^{-/-}$, $Eos^{-/-}$ and dKO Treg cells.

Gene expression profile comparison between **A.** WT and $Helios^{-/-}$ Treg cells and **B.** WT, $Eos^{-/-}$ and $Eos^{-/-}Helios^{-/-}$ (dKO) Treg cells. Each genotype is represented by 3 independent samples. Transcriptome was performed with GeneChip Mouse Gene 1.0 ST array (Affymetrix). The most differentially expressed genes were analyzed with Cluster 3.0. Examples of genes up-regulated in KO Treg cells are indicated in red next to a corresponding cluster and genes down-regulated in KO Treg cells are indicated in green, next to a corresponding cluster. Selected up-regulated genes were also found to be up-regulated in activated Treg cells from (Arvey et al., 2014).

Figure 8. Gene expression profile of $He^{-/-}$, $Eos^{-/-}$ and dKO Treg cells and activated Treg cells.

Differentially regulated genes in $He^{-/-}$, $Eos^{-/-}$ and dKO Treg cells were compared with genes up- and down-regulated in activated Treg cells from Arvey et al., 2014. Microarray data were analyzed with GSEA (Gene Set Enrichment Analysis) software to identify functionally related gene sets. Left panel compares genes up-regulated in activated Treg cells and right panel genes down-regulated in activated Treg cells. The green curve shows the enrichment score and reflects the degree to which each probe set (represented by the vertical lines) is represented at the top or bottom of the ranked gene list (from up-regulated in KO to down-regulated in KO). KO: $He^{-/-}$, $Eos^{-/-}$ or dKO: $Eos^{-/-}Helios^{-/-}$, as indicated on the right of each panel.

Figure 1. Generation of Eos$^{-/-}$ mice.

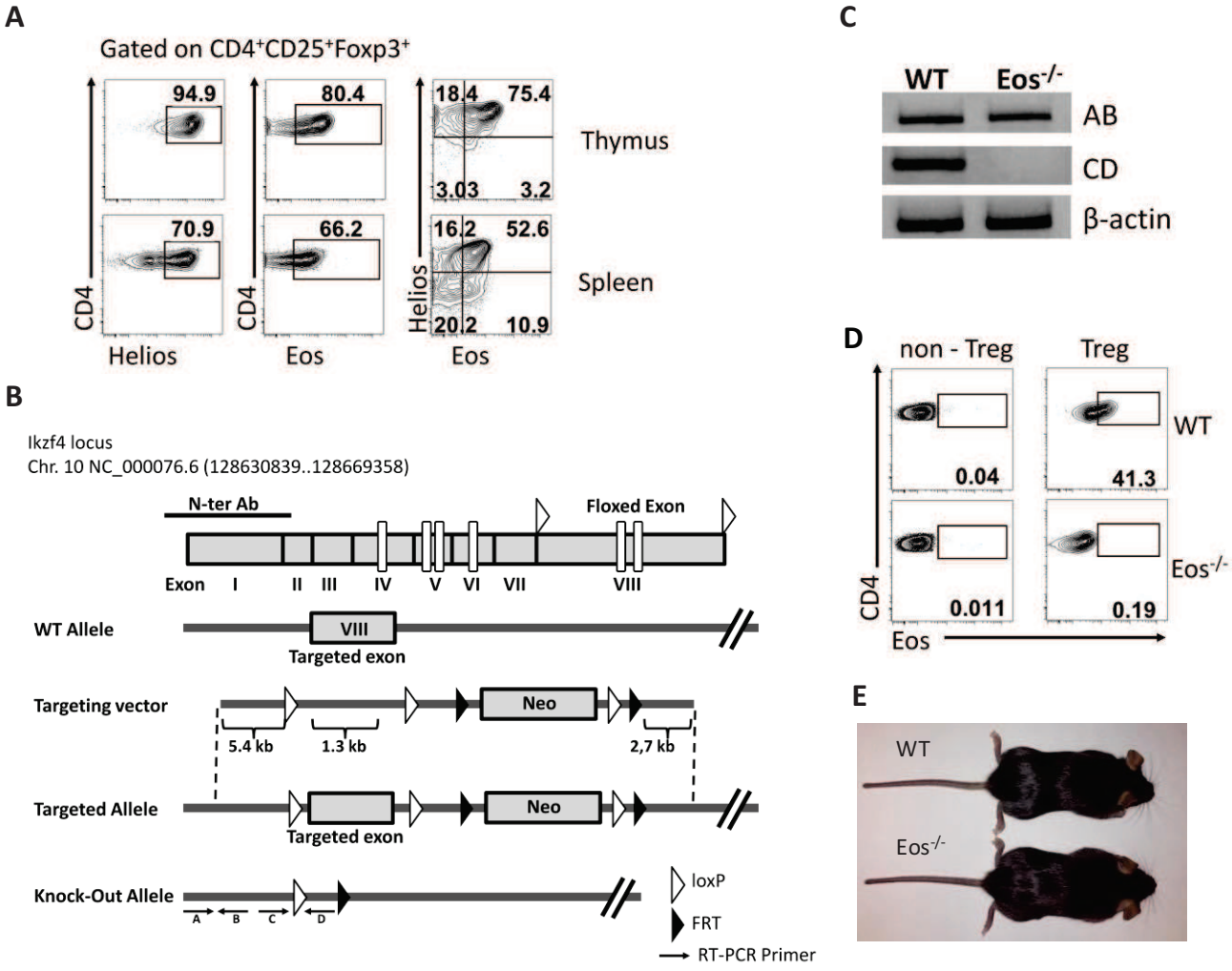

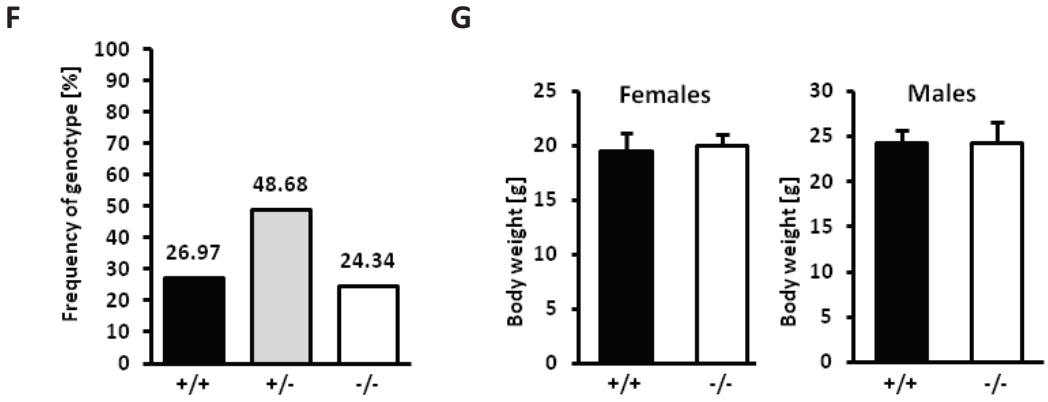

Figure 2. Development and function of natural CD4$^+$ Treg cell in Eos$^{-/-}$ and He$^{-/-}$ mice.

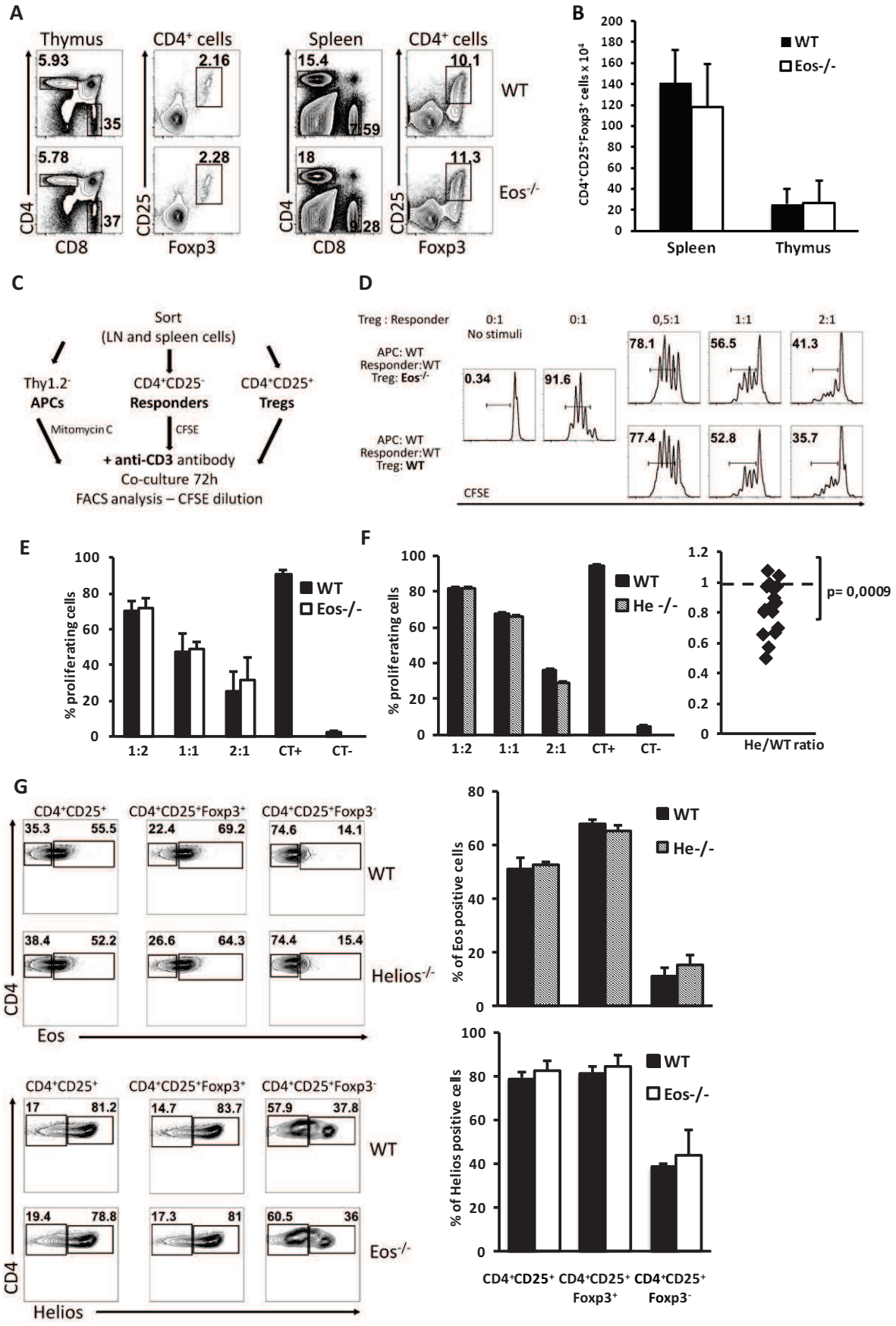

Figure 3. Differentiation and function of *in vitro* induced Eos$^{-/-}$ and He$^{-/-}$ CD8^{+} Treg cells.

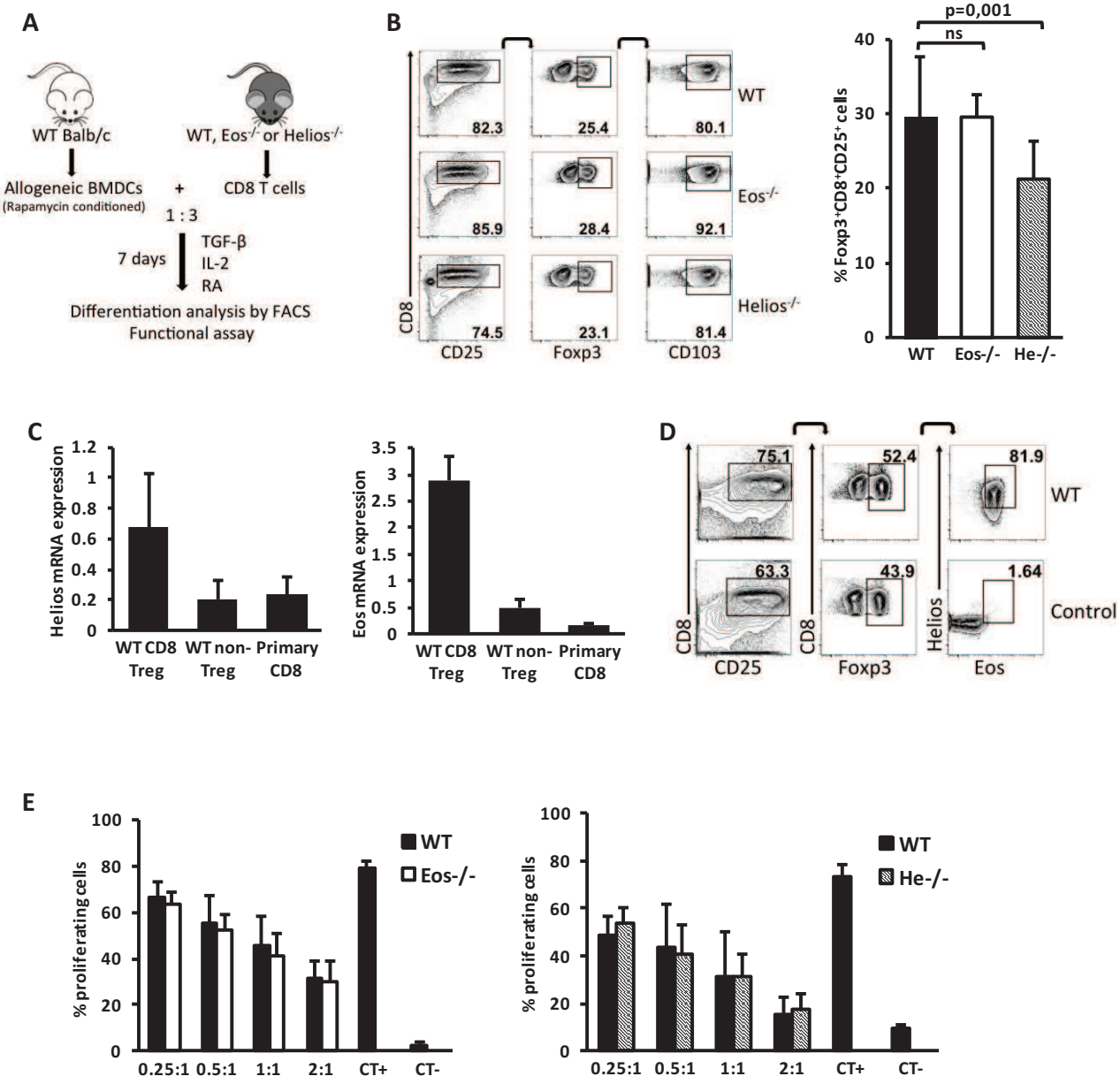

Figure 4. *In vivo* induced Eos$^{-/-}$ and He$^{-/-}$ CD8^{+} Treg cells.

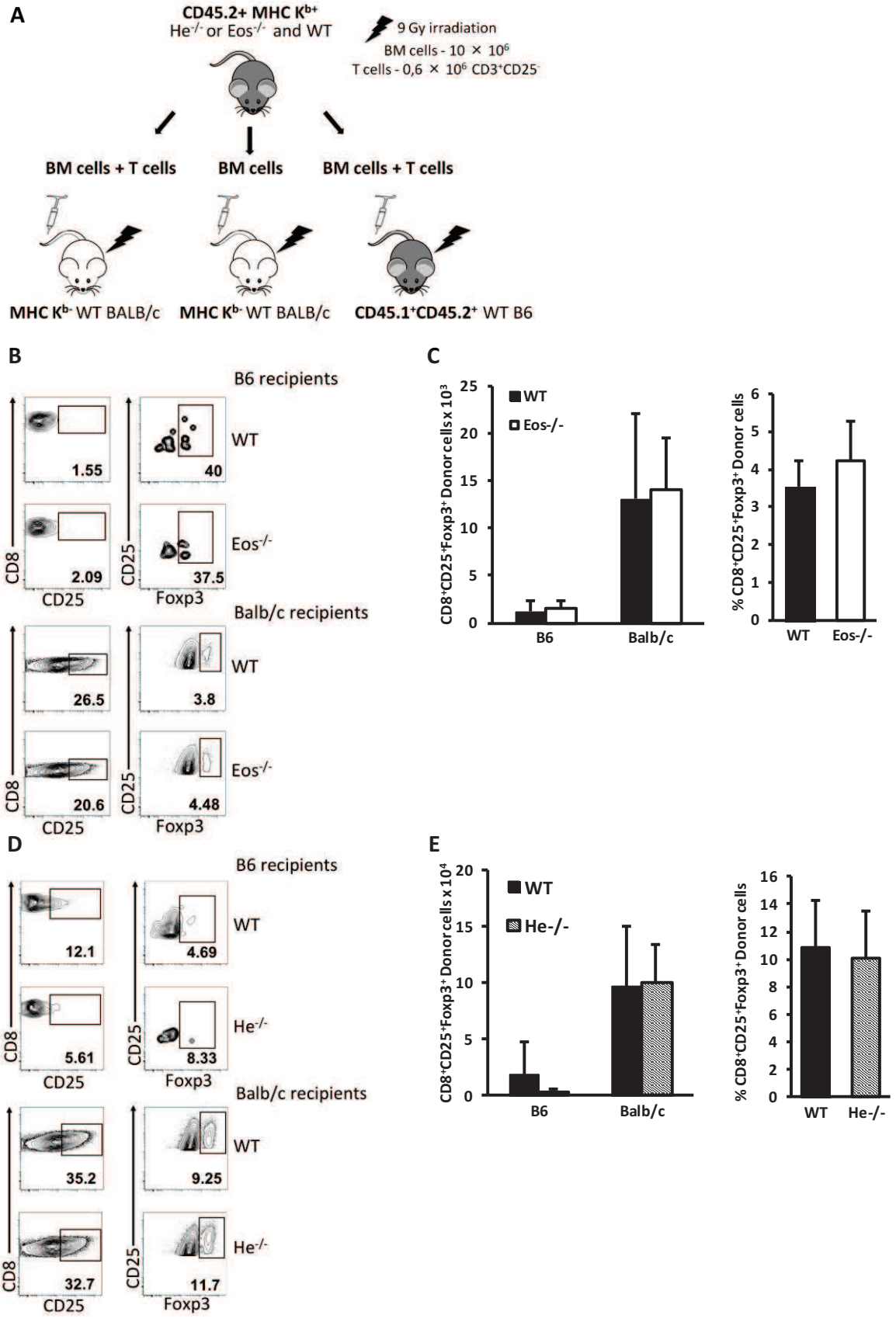

Figure 5. T cell and CD4$^+$ nTreg cell development and function in Eos$^{-/-}$Helios$^{-/-}$ mice.

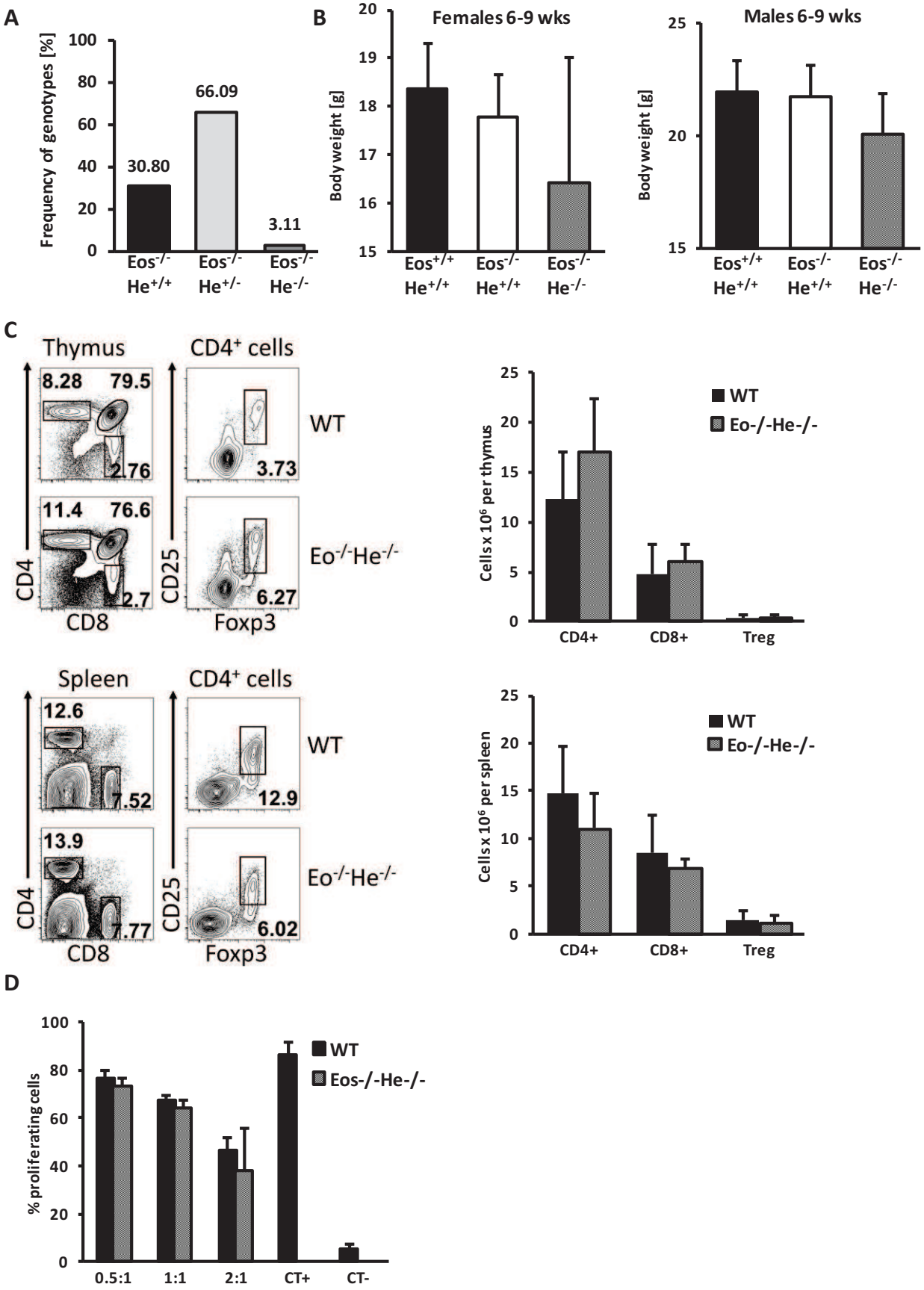

Figure 6. ***In vitro*** **and** ***in vivo*** **induced Eos$^{-/-}$Helios$^{-/-}$ CD8^{+} Treg cells.**

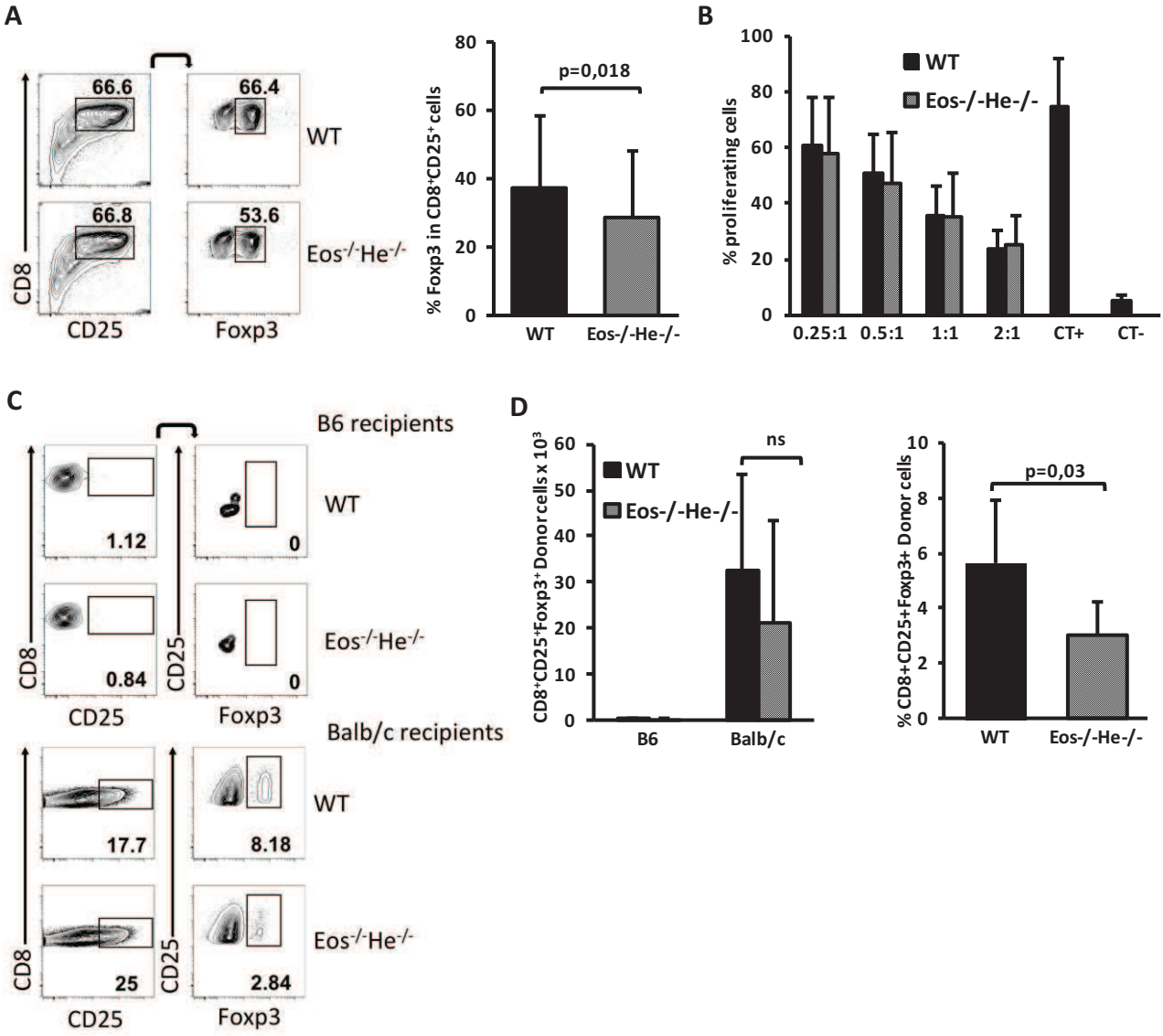

Figure 7. Gene expression profile of $He^{-/-}$, $Eos^{-/-}$ and dKO Treg cells.

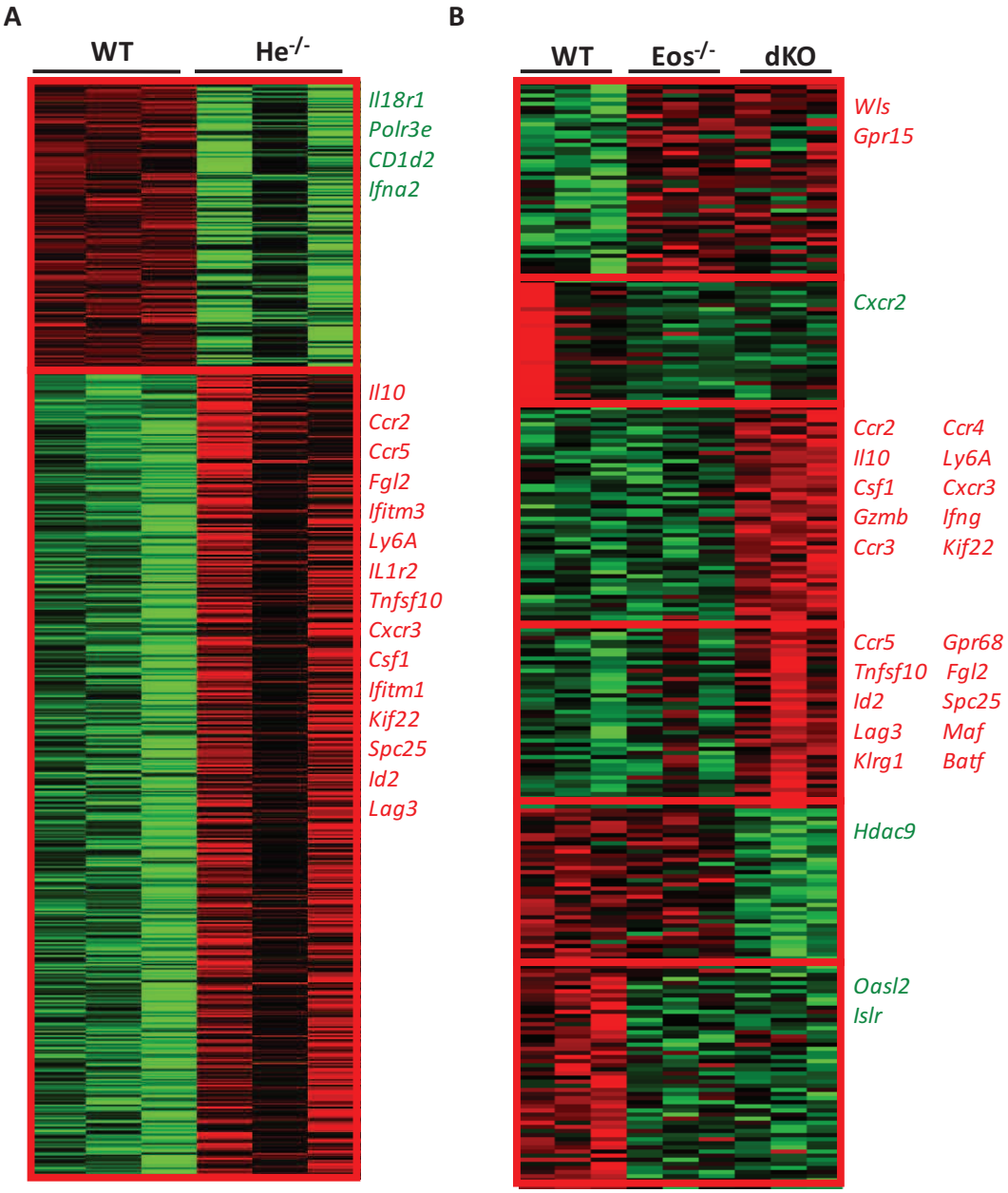

Figure 8. Gene expression profile of $He^{-/-}$, $Eos^{-/-}$ and dKO Treg cells and activated Treg cells.

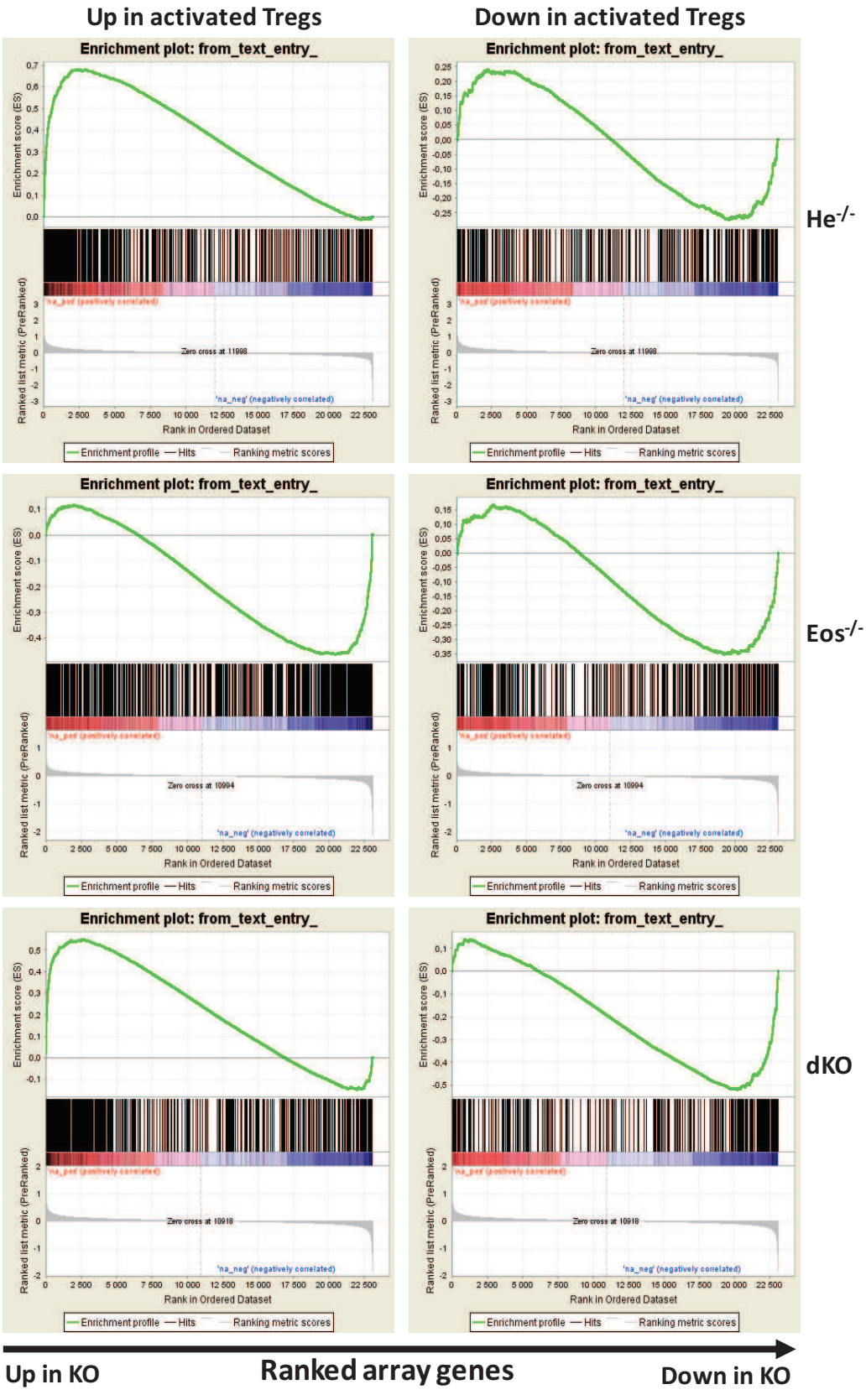

SUPPLEMENTARY FIGURE LEGENDS:

Supplementary Figure 1. nTreg populations in KO mice. (Related to figure 2)
A. Eos and Helios are differentially expressed in peripheral $CD8^+$ nTreg cells. Representative result showing the expression of Eos and Helios by intracellular staining in the $CD8^+CD44^{high}CD122^+Ly49^+$ and $CD8^+CD44^{high}CD122^+Ly49^+$ cells in the spleen. Gated on $CD8^+CD3^{high}$ cells. **B.** $CD4^+$ nTreg cells in the thymus of WT and $Eos^{-/-}$ mice. Representative staining showing the expression of CD103 and CD38, identifying mature and active/highly suppressive Treg cell populations, respectively. **C.** $CD8^+$ nTreg cells in the spleen of WT; $Eos^{+/+}$ and $He^{+/+}$ and $Eos^{-/-}$ or $He^{-/-}$ mice. Representative staining showing the expression of CD122, CD44 and Ly49, identifying natural $CD8^+$ Treg cell populations in the periphery. Gated on $CD8^+CD3^{high}$ cells. **D.** Expression of $CD4^+$ Treg cell markers Nrp1 and PD-1 in $Eos^{-/-}$ and $Helios^{-/-}$ mice. Representative staining of Nrp1 and PD-1 in the thymus (top) and spleen (bottom) of WT ($Eos^{+/+}$) vs. $Eos^{-/-}$ mice and WT ($He^{+/+}$) vs. $He^{-/-}$ mice. Gated on $CD4^+CD25^+$ cells. **E.** Frequencies of indicated populations in $CD4^+CD25^+$ cells in the thymus and spleen of WT ($Eos^{+/+}$) vs. $Eos^{-/-}$ mice and WT ($He^{+/+}$) vs. $He^{-/-}$ mice. Bars represent mean with SD. $Eos^{+/+}$ n=4 mice, $Eos^{-/-}$ n=4 mice, $He^{+/+}$ n=3 mice, $He^{-/-}$ n=3 mice for analysis both in the thymus and spleen.

Supplementary Figure 2. MHC-mismatch dependent induction of $CD8^+$ Treg cell differentiation *in vitro*. (Related to figure 3 and 6) **A.** Efficiency of bone marrow (BM) cells from different strains of mice (C57BL/6N, 129/Pas, CD1, Balb/c) to differentiate into BM-derived dendritic cells (BMDCs). BM cells were cultured for 7 days with GM-CSF and differentiation into $CD11c^+$ cells was measured by flow cytometry. **B.** BMDCs from indicated strains ($20x10^3$, preconditioned with rapamycin) were used for co-culture with $CD8^+$ T cells from C57BL/6N mice (splenic $CD8^+$ T cells, $60x10^3$) in the presence of IL-2, TGF-β1 and retinoic acid for 7 days to induce differentiation into $CD8^+CD25^+Foxp3^+$ cells. Representative flow cytometry analysis shows different potential to induce $CD8^+$ Treg cells depending on the MHC-mismatch disparity.

Supplementary Figure 3. Induction of $CD8^+$ Treg differentiation *in vivo*. (Related to figure 4 and 6) **A.** Gating strategy to analyze donor derived $CD8^+$ Treg cells. In allogeneic conditions (top panel) gates are set up using control cells from the spleens of un-manipulated WT Balb/c recipients (MHC K^{b+}) and WT B6 donors (MHC K^{b-}). To control the T cell depletion from BM control Balb/c recipients are also injected with BM cells alone (indicated

on the example as Balb/c recipient + BM alone) to compare with normal experimental conditions where T cell depleted BM cells are injected together with $CD3^+CD25^-$ T cells (indicated on the example as Balb/c recipient + BM & T cells). In syngeneic conditions (bottom panel) gates are set up using control cells from the spleens of un-manipulated $CD45.2^+$ control mice (as Balb/c recipient) and WT B6 recipients ($CD45.1^+/CD45.2^+$). Example of normal experimental conditions where T cell depleted BM cells are injected together with $CD3^+CD25^-$ T cells into WT B6 $CD45.1^+/CD45.2^+$ recipients is presented on the bottom (indicated as B6 recipient + BM & T cells). **B.** Expression of Eos and Helios is induced in the *in vivo* differentiated $CD8^+$ Treg cells. Expression of Eos and Helios was measured by intracellular staining in splenic cells 8 days after BM transplantation. Gated on donor derived $CD8^+$ Treg cells. Representative of at least 2 experiments.

Supplementary Figure 4. Development of iTreg populations from $He^{-/-}$, $Eos^{-/-}$ and dKO cells.

Flow cytometry analysis of *in vitro* assay to obtain induced Treg cells (iTreg cells). $CD4^+CD25^-$ T cells were sorted from mice of indicated genotypes and 10^5 cells were plated in 96-well dishes pre-coated with anti-CD3 antibody and in the presence of soluble anti-CD28 antibody, TGF-β1 and IL-2 for 4 days. Cells were analyzed by flow cytometry for the expression of CD25 and Foxp3. $He^{-/-}$ cells should be compared with $He^{+/+}$; $Eos^{-/-}$ and $Eos^{-/-}$ $He^{-/-}$ with $Eos^{+/+}$ (mice used for these experiments come from different lines). Control cells: no cytokines.

Supplementary Figure 5. Protein expression of genes up-regulated in $He^{-/-}$ and dKO Treg cells. (Related to figure 7) Expression of genes up-regulated in $He^{-/-}$ and dKO Treg cells in the microarray analysis was verified at the protein level by flow cytometry. Three examples are shown. **A.** Representative results of Klrg1, Ccr4 and Ccr5 staining in the spleen of WT and $He^{-/-}$ mice. Gated on $CD4^+CD25^+$ cells (top). Number and frequencies of $CD4^+CD25^+$ cells expressing Klrg1, Ccr4 and Ccr5 in the spleen of WT and $He^{-/-}$ mice. Bars represent mean with SD of the analyzed mice from one experiment. Statistical analysis with Student's t-test. WT n = 3 mice, $He^{-/-}$ n = 3 mice (bottom). **B.** Representative results of Klrg1, Ccr4 and Ccr5 staining in the spleen of WT, $Eos^{-/-}$ and $Eos^{-/-}He^{-/-}$ mice. Gated on $CD4^+CD25^+$ cells (top).

Supplementary Figure 6. Gene expression profile in $Eos^{-/-}$, $He^{-/-}$, and dKO Treg cells and activated Treg cells. (Related to figure 8) Differentially regulated genes in $He^{-/-}$, $Eos^{-/-}$ and dKO Treg cells were compared with genes up- or down-regulated in activated $CD4^+CD25^+$

Treg cells from (Arvey et al., 2014) and depicted as Venn diagrams on two or three indicated data sets. **A,B and C.** ↑-up-regulated, ↓-down-regulated, dKO - $Eos^{-/-}Helios^{-/-}$, aTreg – activated Treg.

Supplementary Table 1. Differentially regulated genes in $He^{-/-}$, $Eos^{-/-}$ and dKO Treg cells.

Table comprises up-regulated and down-regulated genes (probe sets) from the two microarrays performed: WT vs. $He^{-/-}$ and WT vs $Eos^{-/-}$ and dKO. Only the most differentially expressed genes are presented and were selected according to the following criteria. For up-regulated genes: mean KO1:KO3 ($He^{-/-}$ or $Eos^{-/-}$ or dKO) – mean WT1:WT3 ≥ 0,4 (0,6 for $He^{-/-}$) and MIN (KO1:KO3) – MAX (WT1:WT3) > 0.4. For down-regulated genes: mean KO1:KO3 ($He^{-/-}$ or $Eos^{-/-}$ or dKO) – mean WT1:WT3 ≤ -0,4 and MIN (WT1:WT3) – MAX (KO1:KO3) > 0.

Supplementary Figure 1. nTreg populations in KO mice. (Related to figure 2)

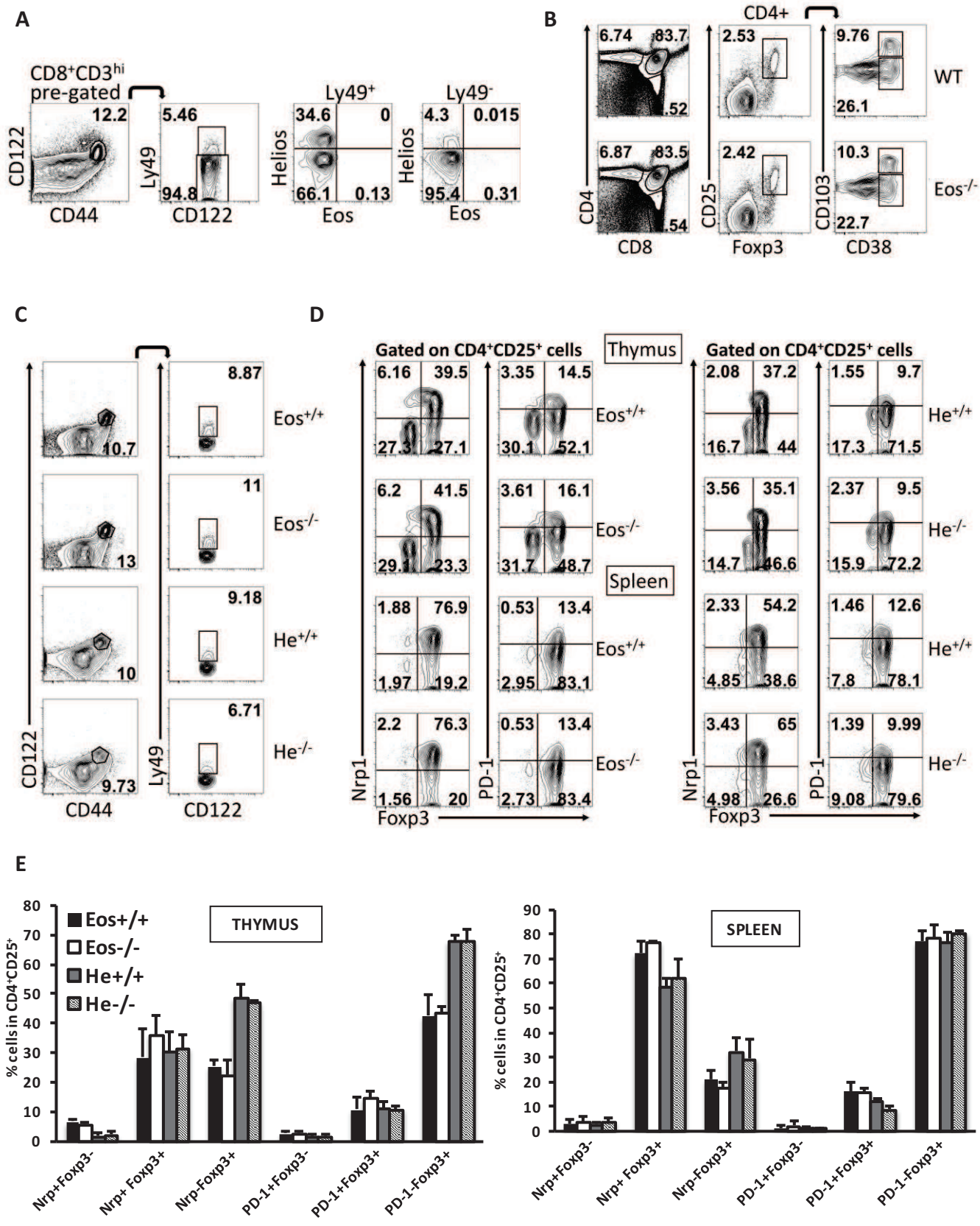

Supplementary Figure 2. MHC-mismatch dependent induction of CD8$^+$ Treg cell differentiation *in vitro*. (Related to figure 3 and 6)

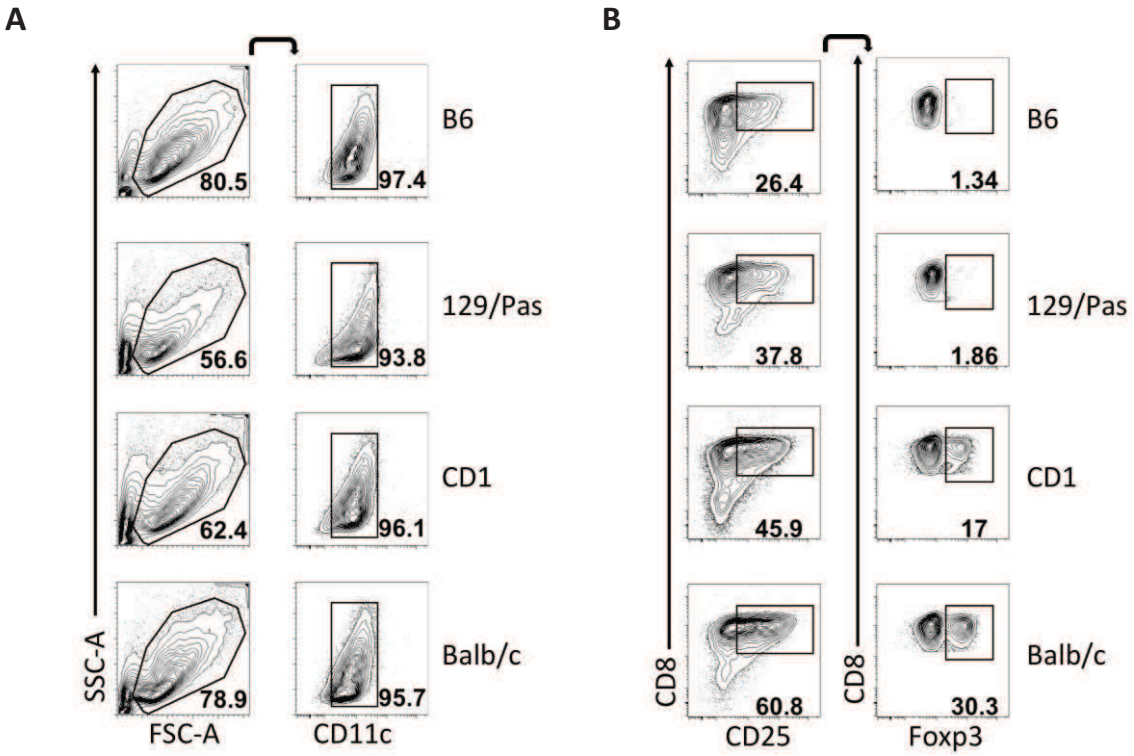

Supplementary Figure 3. Induction of CD8$^+$ Treg differentiation *in vivo*.

(Related to figure 4 and 6)

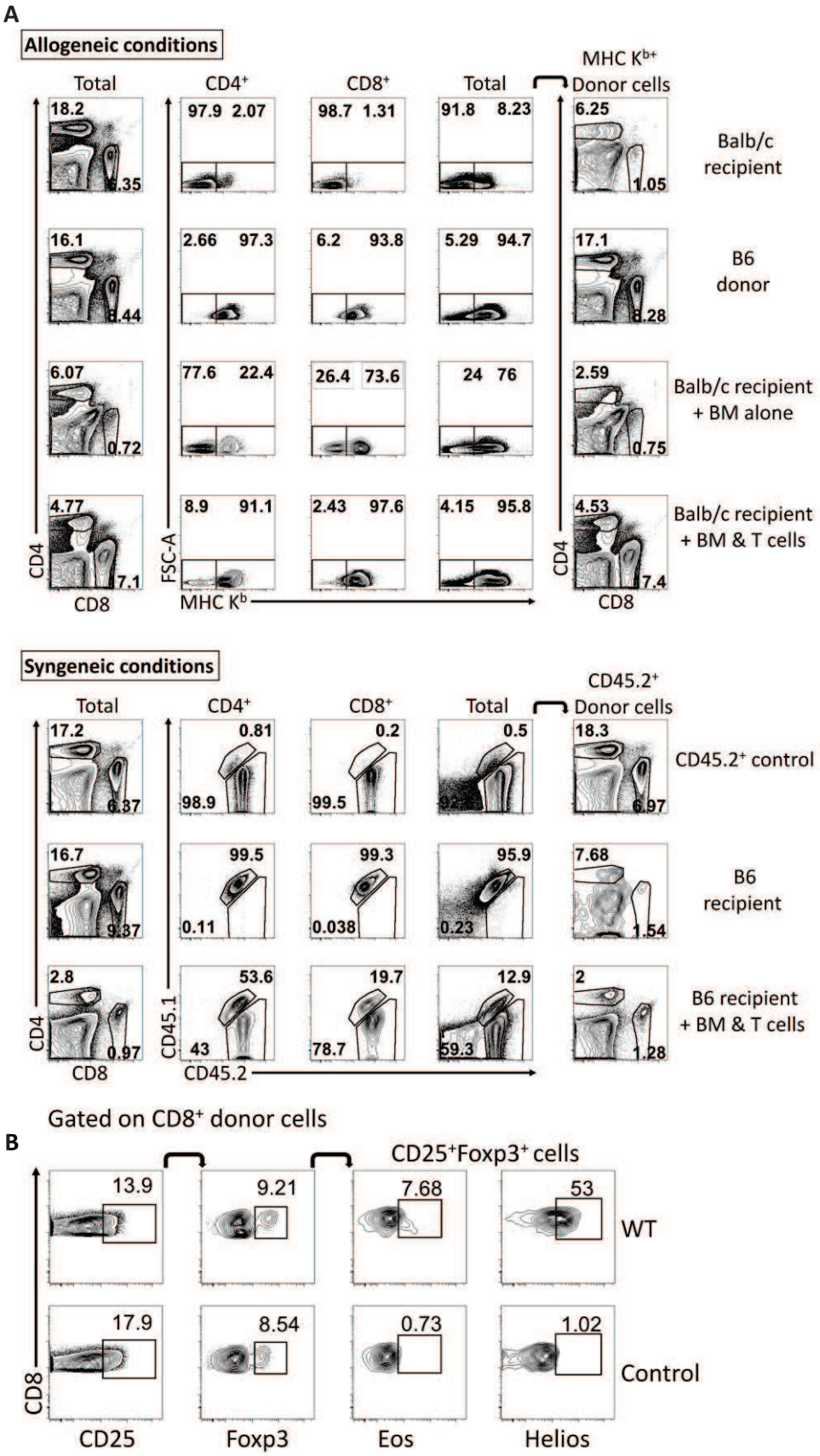

Supplementary Figure 4. Development of iTreg populations from $He^{-/-}$, $Eos^{-/-}$ and dKO cells.

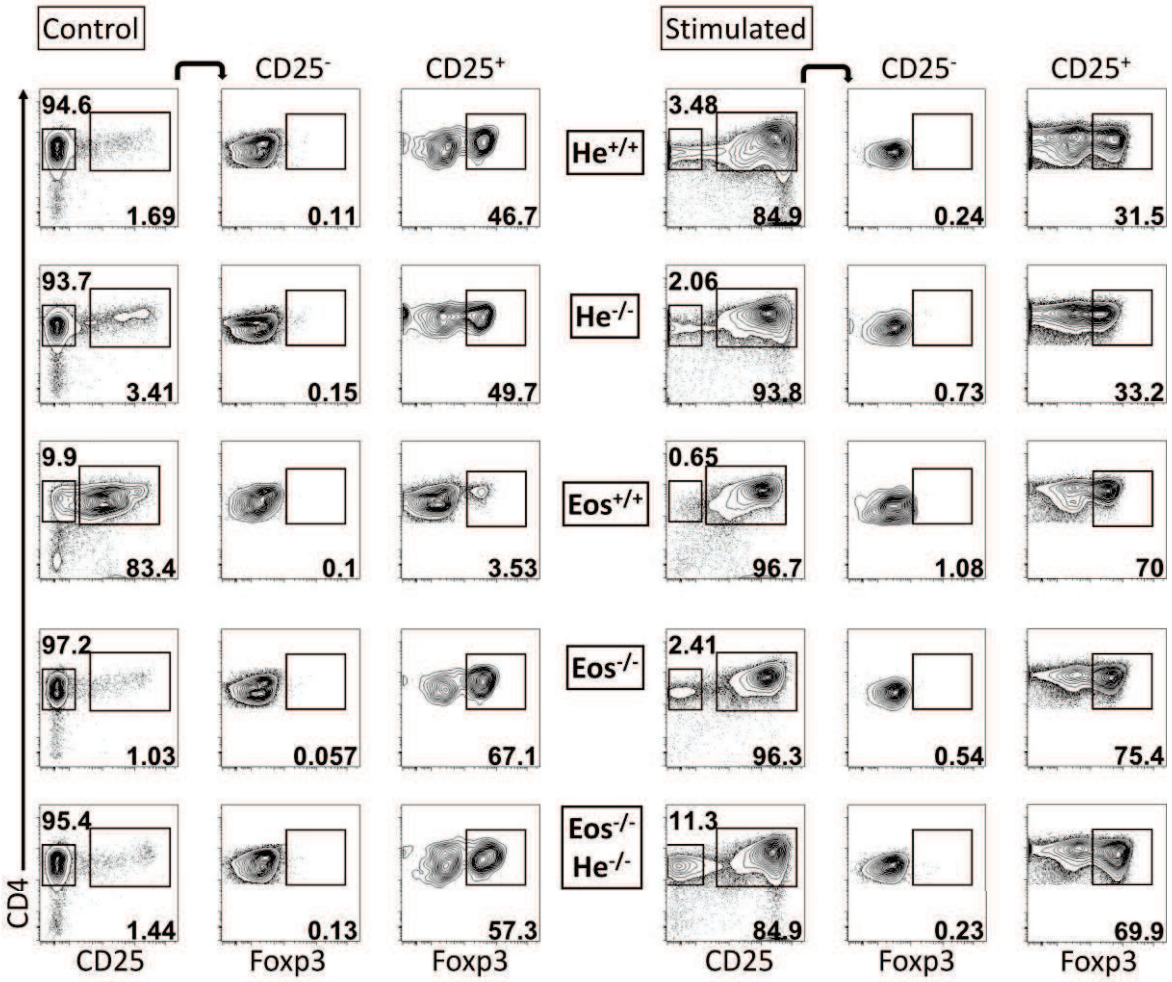

Supplementary Figure 5. Protein expression of genes up-regulated in $He^{-/-}$ and dKO Treg cells. (Related to figure 7)

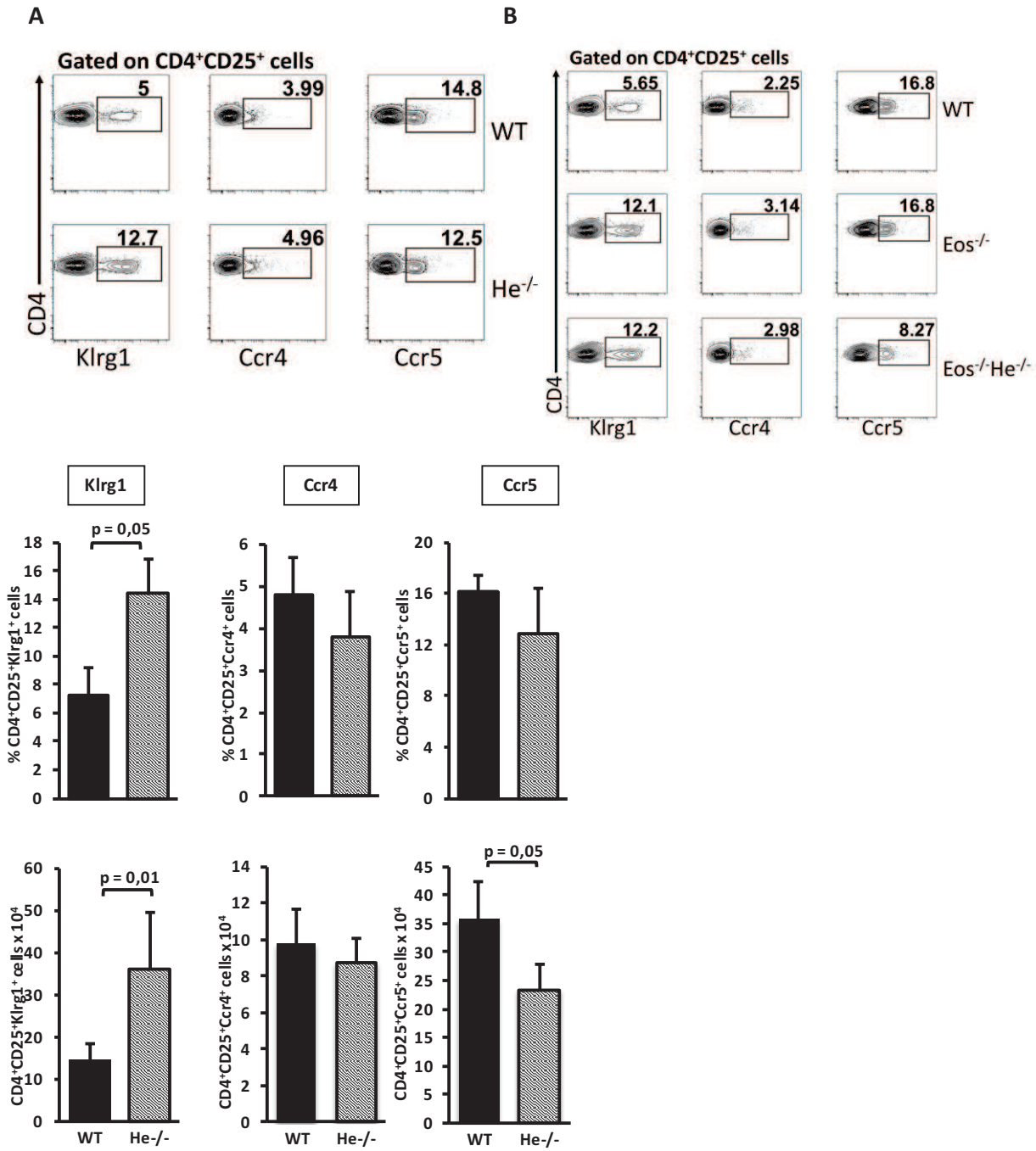

Supplementary Figure 6. Gene expression profile in $He^{-/-}$, $Eos^{-/-}$ and dKO Treg cells and activated Treg cells. (Related to figure 8)

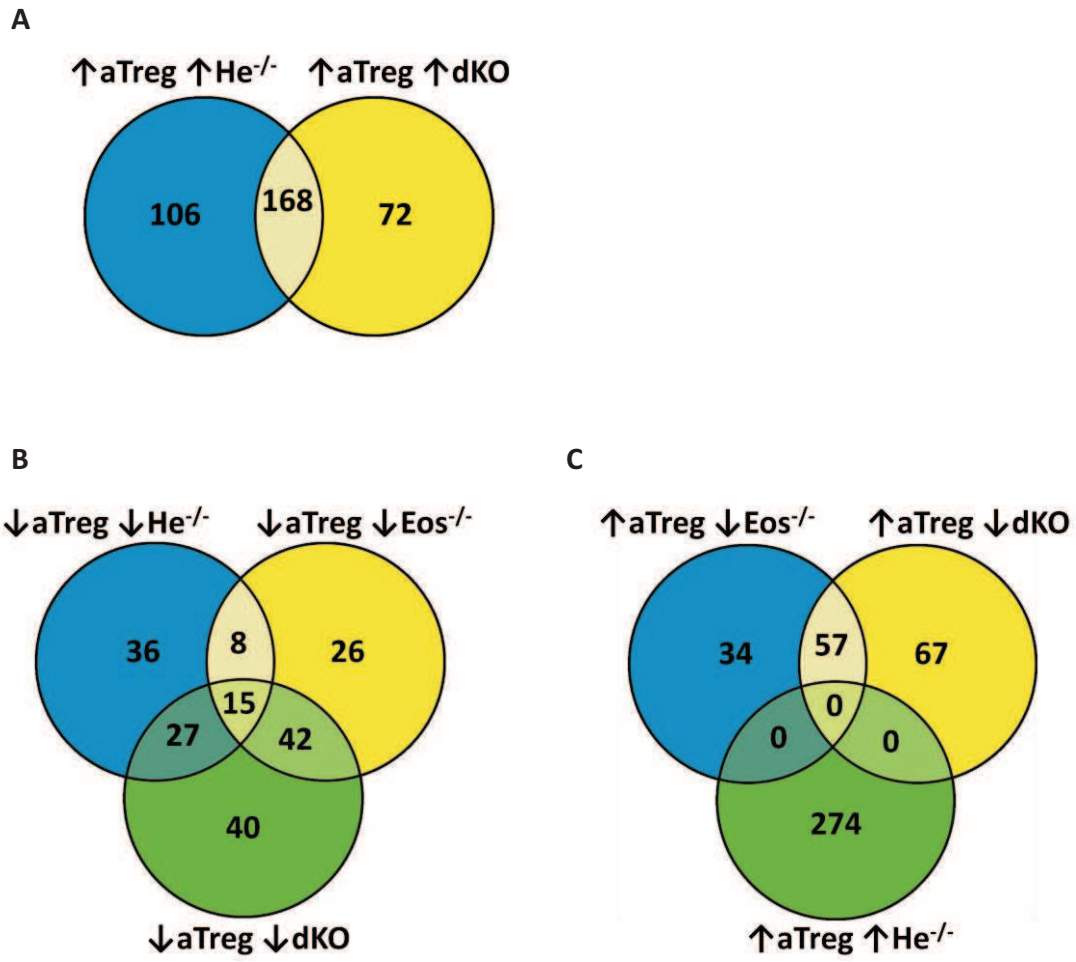

Supplementary Table 1. Differentially regulated genes in Eos$^{-/-}$, He$^{-/-}$, and dKO Treg cells.

	Genes up-regulated in Eos$^{-/-}$ (Eos-WT > 0.4)		
#	Symbol	Gene description	Fold change
1	mt-Ta	mitochondrially encoded tRNA alanine	1.07
2	Wls	wntless homolog (Drosophila)	0.91
3	Snora69	small nucleolar RNA, H/ACA box 69	0.85
4	Gpx8	glutathione peroxidase 8 (putative)	0.84
5	Akr1e1	aldo-keto reductase family 1, member E1	0.75
6	Gm17535	predicted gene, 17535	0.73
7	Mir92-1	microRNA 92-1	0.67
8	Acer2	alkaline ceramidase 2	0.67
9	mt-Tt	mitochondrially encoded tRNA threonine	0.67
10	Prrg4	proline rich Gla (G-carboxyglutamic acid) 4 (transmembrane)	0.66
11	Hddc3	HD domain containing 3	0.63
12	mt-Tn	mitochondrially encoded tRNA asparagine	0.61
13	Rpa3	replication protein A3	0.59
14	Kcnq5	potassium voltage-gated channel, subfamily Q, member 5	0.57
15	Mir15b	microRNA 15b	0.57
16	Lta4h	leukotriene A4 hydrolase	0.54
17	4930520O04Rik	RIKEN cDNA 4930520O04 gene	0.53
18	Gpr15	G protein-coupled receptor 15	0.51
19	Zfp459	zinc finger protein 459	0.50
20	Trps1	trichorhinophalangeal syndrome I (human)	0.50
21	Fut11	fucosyltransferase 11	0.50
22	Nynrin	NYN domain and retroviral integrase containing	0.47
23	Gm14305	predicted gene 14305	0.47
24	Camk2b	calcium/calmodulin-dependent protein kinase II, beta	0.46
25	Tlcd2	TLC domain containing 2	0.45
26	2810408A11Rik	RIKEN cDNA 2810408A11 gene	0.45
27	Mtx3	metaxin 3	0.44
28	Rif1	Rap1 interacting factor 1 homolog (yeast)	0.44
29	Gpatch8	G patch domain containing 8	0.44
30	Gm14335	predicted gene 14335	0.43
31	Macrod2	MACRO domain containing 2	0.43
32	Yod1	YOD1 OTU deubiquitinating enzyme 1 homologue (S. cerevisiae)	0.43
33	Gm14420	predicted gene 14420	0.42
34	Ifnab	interferon alpha B	0.42
35	Eid2b	EP300 interacting inhibitor of differentiation 2B	0.42
36	Mpp7	membrane protein, palmitoylated 7 (MAGUK p55 subfamily member 7)	0.41
37	Zfp758	zinc finger protein 758	0.41
38	Ldlr	low density lipoprotein receptor	0.41
39	Rnaseh1	ribonuclease H1	0.41
40	Qser1	glutamine and serine rich 1	0.40
	Genes down-regulated in Eos$^{-/-}$ (Eos-WT < -0.4)		
#	Symbol	Gene description	Fold change
1	Cxcr2	chemokine (C-X-C motif) receptor 2	-1.26
2	H2-Ob	histocompatibility 2, O region beta locus	-1.21
3	Ntn4	netrin 4	-1.21
4	Cd79a	CD79A antigen (immunoglobulin-associated alpha)	-1.20
5	Casp4	caspase 4, apoptosis-related cysteine peptidase	-1.06
6	Rnu3a	U3A small nuclear RNA	-0.89
7	Ifitm2	interferon induced transmembrane protein 2	-0.88
8	Oasl2	2'-5' oligoadenylate synthetase-like 2	-0.85
9	Rasgrp3	RAS, guanyl releasing protein 3	-0.74
10	Apoe	apolipoprotein E	-0.69
11	Rnu3b4	U3B small nuclear RNA 4	-0.68
12	Rnu3b4	U3B small nuclear RNA 4	-0.68

13	Rnu3b4	U3B small nuclear RNA 4	-0.68
14	Rnu3b4	U3B small nuclear RNA 4	-0.68
15	Set	SET nuclear oncogene	-0.66
16	B430306N03Rik	RIKEN cDNA B430306N03 gene	-0.63
17	Chi3l7	chitinase 3-like 7	-0.63
18	Sord	sorbitol dehydrogenase	-0.62
19	Snora7a	small nucleolar RNA, H/ACA box 7A	-0.61
20	Carhsp1	calcium regulated heat stable protein 1	-0.59
21	Siglecg	sialic acid binding Ig-like lectin G	-0.58
22	Acp1	acid phosphatase 1, soluble	-0.57
23	Igkv5-43	immunoglobulin kappa chain variable 5-43	-0.56
24	Apoc2	apolipoprotein C-II	-0.56
25	Myadm	myeloid-associated differentiation marker	-0.55
26	Tdgf1	teratocarcinoma-derived growth factor 1	-0.55
27	Islr	immunoglobulin superfamily containing leucine-rich repeat	-0.54
28	Csf1r	colony stimulating factor 1 receptor	-0.53
29	Myo1d	myosin ID	-0.52
30	Hhex	hematopoietically expressed homeobox	-0.52
31	Il1f9	interleukin 1 family, member 9	-0.51
32	Sord	sorbitol dehydrogenase	-0.51
33	Cers4	ceramide synthase 4	-0.51
34	Gsta4	glutathione S-transferase, alpha 4	-0.50
35	Hist1h2bg	histone cluster 1, H2bg	-0.50
36	Bcl11a	B cell CLL/lymphoma 11A (zinc finger protein)	-0.50
37	Chd1	chromodomain helicase DNA binding protein 1	-0.49
38	Chd7	chromodomain helicase DNA binding protein 7	-0.48
39	Lpar5	lysophosphatidic acid receptor 5	-0.48
40	Alyref2	Aly/REF export factor 2	-0.47
41	Rassf4	Ras association (RalGDS/AF-6) domain family member 4	-0.47
42	Adcy6	adenylate cyclase 6	-0.47
43	Rnf213	ring finger protein 213	-0.46
44	Cnr2	cannabinoid receptor 2 (macrophage)	-0.46
45	Lysmd2	LysM, putative peptidoglycan-binding, domain containing 2	-0.46
46	H2-T24	histocompatibility 2, T region locus 24	-0.46
47	1700047G07Rik	RIKEN cDNA 1700047G07 gene	-0.46
48	Slc22a13b-ps	solute carrier family 22 (organic cation transporter), member 13b, pseudogene	-0.45
49	Slx1b	SLX1 structure-specific endonuclease subunit homolog B (S. cerevisiae)	-0.45
50	Snord49a	small nucleolar RNA, C/D box 49A	-0.45
51	As3mt	arsenic (+3 oxidation state) methyltransferase	-0.44
52	Ear1	eosinophil-associated, ribonuclease A family, member 1	-0.43
53	Cyp4f16	cytochrome P450, family 4, subfamily f, polypeptide 16	-0.43
54	Rpl10l	ribosomal protein L10-like	-0.43
55	Bmp2k	BMP2 inducible kinase	-0.42
56	Gm10693	predicted pseudogene 10693	-0.41
57	Igkv6-20	immunoglobulin kappa variable 6-20	-0.41
58	Prune2	prune homolog 2 (Drosophila)	-0.41
59	Myl4	myosin, light polypeptide 4	-0.41
60	AB124611	cDNA sequence AB124611	-0.40
61	Trim34a	tripartite motif-containing 34A	-0.40
	Genes up-regulated in $He^{-/-}$ (He-WT > 0.6)		
#	**Symbol**	**Gene description**	**Fold change**
1	S100a8	S100 calcium binding protein A8 (calgranulin A)	3.20
2	Ear1	eosinophil-associated, ribonuclease A family, member 1	3.04
3	S100a9	S100 calcium binding protein A9 (calgranulin B)	2.93
4	Stfa3	stefin A3	2.79
5	Ear2	eosinophil-associated, ribonuclease A family, member 2	1.96
6	Cd24a	CD24a antigen	1.94
7	Hba-a2	hemoglobin alpha, adult chain 2	1.90

8	Camp	cathelicidin antimicrobial peptide	1.88
9	Hba-a2	hemoglobin alpha, adult chain 2	1.86
10	Ifitm6	interferon induced transmembrane protein 6	1.76
11	Prg2	proteoglycan 2, bone marrow	1.75
12	Hist1h2bc	histone cluster 1, H2bc	1.57
13	Il10	interleukin 10	1.54
14	Ang5	angiogenin, ribonuclease A family, member 5	1.49
15	Fcer2a	Fc receptor, IgE, low affinity II, alpha polypeptide	1.47
16	Vpreb3	pre-B lymphocyte gene 3	1.41
17	Cd63	CD63 antigen	1.41
18	Ccnb2	cyclin B2	1.38
19	Klk1b22	kallikrein 1-related peptidase b22	1.36
20	Ear12	eosinophil-associated, ribonuclease A family, member 12	1.30
21	Ly6d	lymphocyte antigen 6 complex, locus D	1.27
22	Prr11	proline rich 11	1.24
23	Slc43a1	solute carrier family 43, member 1	1.22
24	Hp	haptoglobin	1.20
25	5730408K05Rik	RIKEN cDNA 5730408K05 gene	1.16
26	Sdr39u1	short chain dehydrogenase	1.15
27	Car5b	carbonic anhydrase 5b, mitochondrial	1.15
28	Gm12891	predicted gene 12891	1.14
29	Hist2h3c2	histone cluster 2, H3c2	1.13
30	Serpinb1a	serine (or cysteine) peptidase inhibitor, clade B, member 1a	1.12
31	Alox5ap	arachidonate 5-lipoxygenase activating protein	1.11
32	Ly96	lymphocyte antigen 96	1.11
33	Cks2	CDC28 protein kinase regulatory subunit 2	1.11
34	Ear12	eosinophil-associated, ribonuclease A family, member 12	1.10
35	Mki67	antigen identified by monoclonal antibody Ki 67	1.08
36	Retnlg	resistin like gamma	1.08
37	Ccr2	chemokine (C-C motif) receptor 2	1.07
38	H2afx	H2A histone family, member X	1.06
39	Ifi30	interferon gamma inducible protein 30	1.06
40	Ccr5	chemokine (C-C motif) receptor 5	1.05
41	Ccr5	chemokine (C-C motif) receptor 5	1.05
42	Nusap1	nucleolar and spindle associated protein 1	1.04
43	Fgl2	fibrinogen-like protein 2	1.04
44	Faim3	Fas apoptotic inhibitory molecule 3	1.04
45	Ccr3	chemokine (C-C motif) receptor 3	1.03
46	Ifitm3	interferon induced transmembrane protein 3	1.02
47	Rplp0	ribosomal protein, large, P0	1.01
48	Mpo	myeloperoxidase	1.01
49	Ccna2	cyclin A2	0.99
50	Tnfrsf13c	tumor necrosis factor receptor superfamily, member 13c	0.98
51	Spib	Spi-B transcription factor (Spi-1	0.94
52	Klk1b21	kallikrein 1-related peptidase b21	0.94
53	2810417H13Rik	RIKEN cDNA 2810417H13 gene	0.93
54	Ube2c	ubiquitin-conjugating enzyme E2C	0.93
55	Cks2	CDC28 protein kinase regulatory subunit 2	0.93
56	Ceacam1	carcinoembryonic antigen-related cell adhesion molecule 1	0.91
57	Sf3b4	splicing factor 3b, subunit 4	0.90
58	Cdca5	cell division cycle associated 5	0.90
59	Tpx2	TPX2, microtubule-associated protein homolog (Xenopus laevis)	0.88
60	Trappc2	trafficking protein particle complex 2	0.87
61	Cks1b	CDC28 protein kinase 1b	0.86
62	Wfdc17	WAP four-disulfide core domain 17	0.86
63	Sgol2	shugoshin-like 2 (S. pombe)	0.85
64	Plbd1	phospholipase B domain containing 1	0.85
65	Mmp8	matrix metallopeptidase 8	0.85
66	Snord35a	small nucleolar RNA, C	0.84

67	Ddx28	DEAD (Asp-Glu-Ala-Asp) box polypeptide 28	0.83
68	Unc93b1	unc-93 homolog B1 (C. elegans)	0.83
69	Marcks	myristoylated alanine rich protein kinase C substrate	0.82
70	Ncaph	non-SMC condensin I complex, subunit H	0.82
71	Cenpe	centromere protein E	0.81
72	Ly6a	lymphocyte antigen 6 complex, locus A	0.81
73	Il1r2	interleukin 1 receptor, type II	0.81
74	Top2a	topoisomerase (DNA) II alpha	0.81
75	Serpinb6a	serine (or cysteine) peptidase inhibitor, clade B, member 6a	0.81
76	mt-Tm	mitochondrially encoded tRNA methionine	0.81
77	Napsa	napsin A aspartic peptidase	0.81
78	Cisd1	CDGSH iron sulfur domain 1	0.81
79	Higd1a	HIG1 domain family, member 1A	0.81
80	D17H6S56E-5	DNA segment, Chr 17, human D6S56E 5	0.80
81	C1galt1c1	C1GALT1-specific chaperone 1	0.80
82	Fcrla	Fc receptor-like A	0.80
83	H1f0	H1 histone family, member 0	0.79
84	Igkv4-70	immunoglobulin kappa chain variable 4-70	0.79
85	Kif23	kinesin family member 23	0.78
86	Depdc1a	DEP domain containing 1a	0.78
87	Klrd1	killer cell lectin-like receptor, subfamily D, member 1	0.78
88	Gm561	predicted gene 561	0.78
89	Cd9	CD9 antigen	0.78
90	Gm5593	predicted gene 5593	0.78
91	Prorsd1	prolyl-tRNA synthetase domain containing 1	0.78
92	Rrs1	RRS1 ribosome biogenesis regulator homolog (S. cerevisiae)	0.77
93	Mcpt8	mast cell protease 8	0.77
94	Mis18a	MIS18 kinetochore protein homolog A (S. pombe)	0.77
95	Spred2	sprouty-related, EVH1 domain containing 2	0.77
96	F2rl1	coagulation factor II (thrombin) receptor-like 1	0.77
97	Kmo	kynurenine 3-monooxygenase (kynurenine 3-hydroxylase)	0.76
98	Ticrr	TOPBP1-interacting checkpoint and replication regulator	0.76
99	Racgap1	Rac GTPase-activating protein 1	0.76
100	C330027C09Rik	RIKEN cDNA C330027C09 gene	0.75
101	Themis2	thymocyte selection associated family member 2	0.75
102	Depdc1a	DEP domain containing 1a	0.74
103	Ctsh	cathepsin H	0.74
104	Myadm	myeloid-associated differentiation marker	0.74
105	Fbxo5	F-box protein 5	0.74
106	Fignl1	fidgetin-like 1	0.73
107	Tnfsf10	tumor necrosis factor (ligand) superfamily, member 10	0.73
108	Dusp4	dual specificity phosphatase 4	0.73
109	Rmi1	RMI1, RecQ mediated genome instability 1, homolog (S. cerevisiae)	0.73
110	Rpl13	ribosomal protein L13	0.73
111	Dnajb9	DnaJ (Hsp40) homolog, subfamily B, member 9	0.72
112	Cxcr3	chemokine (C-X-C motif) receptor 3	0.72
113	mt-Tf	mitochondrially encoded tRNA phenylalanine	0.72
114	Csf1	colony stimulating factor 1 (macrophage)	0.71
115	4930412O13Rik	RIKEN cDNA 4930412O13 gene	0.70
116	Ufm1	ubiquitin-fold modifier 1	0.70
117	Tacc3	transforming, acidic coiled-coil containing protein 3	0.70
118	Bard1	BRCA1 associated RING domain 1	0.70
119	Kif15	kinesin family member 15	0.69
120	Imp3	IMP3, U3 small nucleolar ribonucleoprotein, homolog (yeast)	0.69
121	Mnf1	mitochondrial nucleoid factor 1	0.69
122	Emc6	ER membrane protein complex subunit 6	0.68
123	Slirp	SRA stem-loop interacting RNA binding protein	0.68
124	Aurka	aurora kinase A	0.68
125	Milr1	mast cell immunoglobulin like receptor 1	0.68

126	Stmn1	stathmin 1	0.68
127	2410016O06Rik	RIKEN cDNA 2410016O06 gene	0.68
128	Slc15a2	solute carrier family 15 (H+	0.67
129	9430016H08Rik	RIKEN cDNA 9430016H08 gene	0.67
130	Stmn1	stathmin 1	0.67
131	Ccdc28b	coiled coil domain containing 28B	0.67
132	Cd55	CD55 antigen	0.67
133	Prim1	DNA primase, p49 subunit	0.67
134	Lmo2	LIM domain only 2	0.67
135	Igkv4-55	immunoglobulin kappa variable 4-55	0.67
136	Uxt	ubiquitously expressed transcript	0.67
137	Lztfl1	leucine zipper transcription factor-like 1	0.66
138	Rdm1	RAD52 motif 1	0.66
139	Ndufa6	NADH dehydrogenase (ubiquinone) 1 alpha subcomplex, 6 (B14)	0.66
140	Ly6c1	lymphocyte antigen 6 complex, locus C1	0.66
141	Gm9847	predicted pseudogene 9847	0.66
142	H2afv	H2A histone family, member V	0.66
143	Ggct	gamma-glutamyl cyclotransferase	0.66
144	Ell2	elongation factor RNA polymerase II 2	0.66
145	Ifitm1	interferon induced transmembrane protein 1	0.66
146	Scp2	sterol carrier protein 2, liver	0.65
147	Mrpl22	mitochondrial ribosomal protein L22	0.65
148	Snrpc	U1 small nuclear ribonucleoprotein C	0.65
149	BC028528	cDNA sequence BC028528	0.65
150	Ahsp	alpha hemoglobin stabilizing protein	0.65
151	Map6	microtubule-associated protein 6	0.65
152	Siva1	SIVA1, apoptosis-inducing factor	0.65
153	Slc19a2	solute carrier family 19 (thiamine transporter), member 2	0.64
154	Kif22	kinesin family member 22	0.64
155	Mad2l1bp	MAD2L1 binding protein	0.64
156	Prg4	proteoglycan 4 (megakaryocyte stimulating factor, articular superficial zone protein)	0.64
157	Oasl2	2'-5' oligoadenylate synthetase-like 2	0.63
158	Gm6611	predicted gene 6611	0.63
159	Hist2h2be	histone cluster 2, H2be	0.63
160	Cenpk	centromere protein K	0.63
161	Klk1	kallikrein 1	0.63
162	Gm10693	predicted pseudogene 10693	0.63
163	Pebp1	phosphatidylethanolamine binding protein 1	0.62
164	Ear7	eosinophil-associated, ribonuclease A family, member 7	0.62
165	Osgep	O-sialoglycoprotein endopeptidase	0.62
166	Ndc80	NDC80 homolog, kinetochore complex component (S. cerevisiae)	0.62
167	Spc25	SPC25, NDC80 kinetochore complex component, homolog (S. cerevisiae)	0.62
168	Rdm1	RAD52 motif 1	0.62
169	mt-Tn	mitochondrially encoded tRNA asparagine	0.61
170	2310039H08Rik	RIKEN cDNA 2310039H08 gene	0.61
171	Rbbp8	retinoblastoma binding protein 8	0.61
172	Tssc4	tumor-suppressing subchromosomal transferable fragment 4	0.61
173	Hhex	hematopoietically expressed homeobox	0.61
174	Fcer1g	Fc receptor, IgE, high affinity I, gamma polypeptide	0.61
175	Plekho1	pleckstrin homology domain containing, family O member 1	0.61
176	Apitd1	apoptosis-inducing, TAF9-like domain 1	0.61
177	Ckap2l	cytoskeleton associated protein 2-like	0.61
178	Leprot	leptin receptor overlapping transcript	0.61
179	Gins1	GINS complex subunit 1 (Psf1 homolog)	0.60
180	Spc24	SPC24, NDC80 kinetochore complex component,	0.60
181	Crtap	cartilage associated protein	0.60

	Genes down-regulated in $He^{-/-}$ (He-WT < -0.4)		
#	Symbol	Gene description	Fold change
1	Gm10462	predicted gene 10462	-1.84
2	C530030P08Rik	RIKEN cDNA C530030P08 gene	-1.57
3	Dnah8	dynein, axonemal, heavy chain 8	-1.17
4	D630008O14Rik	RIKEN cDNA D630008O14 gene	-1.10
5	Myo9a	myosin IXa	-1.10
6	Myo9a	myosin IXa	-1.09
7	Tbrg3	transforming growth factor beta regulated gene 3	-1.06
8	Traj41	T cell receptor alpha joining 41	-1.05
9	Myo9a	myosin IXa	-1.00
10	Airn	antisense Igf2r RNA	-0.97
11	Gm12266	predicted gene 12266	-0.95
12	Gpr52	G protein-coupled receptor 52	-0.93
13	Gm7030	predicted gene 7030	-0.92
14	Fam196b	family with sequence similarity 196, member B	-0.92
15	Gm3696	predicted gene 3696	-0.90
16	Gm3269	predicted gene 3269	-0.89
17	Gm3242	predicted gene 3242	-0.88
18	Nlrc5	NLR family, CARD domain containing 5	-0.88
19	Mcoln3	mucolipin 3	-0.86
20	Ikzf2	IKAROS family zinc finger 2	-0.86
21	2610042L04Rik	RIKEN cDNA 2610042L04 gene	-0.85
22	A330023F24Rik	RIKEN cDNA A330023F24 gene	-0.84
23	Gm2888	predicted gene 2888	-0.83
24	Gm10413	predicted gene 10413	-0.83
25	Gm3727	predicted gene 3727	-0.82
26	Gm3696	predicted gene 3696	-0.82
27	LOC100862064	uncharacterized LOC100862064	-0.82
28	Gm3696	predicted gene 3696	-0.81
29	Gm9078	predicted gene 9078	-0.81
30	Hspa8	heat shock protein 8	-0.78
31	Cdc23	CDC23 cell division cycle 23	-0.78
32	Thada	thyroid adenoma associated	-0.77
33	Hspa8	heat shock protein 8	-0.76
34	Gm8237	predicted gene 8237	-0.76
35	Gm10548	ribosomal protein L29 pseudogene	-0.76
36	LOC101056064	uncharacterized LOC101056064	-0.74
37	Gm3317	predicted gene 3317	-0.74
38	Gm3339	predicted gene 3339	-0.74
39	Dennd4a	DENN	-0.73
40	Olfr98	olfactory receptor 98	-0.71
41	4930524L23Rik	RIKEN cDNA 4930524L23 gene	-0.70
42	Gm5458	predicted gene 5458	-0.69
43	Myo9a	myosin IXa	-0.69
44	Myo9a	myosin IXa	-0.69
45	Snord8	small nucleolar RNA, C	-0.68
46	B130006D01Rik	RIKEN cDNA B130006D01 gene	-0.68
47	Gm6034	predicted gene 6034	-0.68
48	Tpk1	thiamine pyrophosphokinase	-0.68
49	Agk	acylglycerol kinase	-0.65
50	Uprt	uracil phosphoribosyltransferase (FUR1)	-0.65
51	D3Ertd751e	DNA segment, Chr 3, ERATO Doi 751, expressed	-0.64
52	Nlrc5	NLR family, CARD domain containing 5	-0.64
53	D130062J21Rik	RIKEN cDNA D130062J21 gene	-0.63
54	Gdap10	ganglioside-induced differentiation-associated-protein 10	-0.63
55	AB041803	cDNA sequence AB041803	-0.62
56	Airn	antisense Igf2r RNA	-0.62
57	4932438A13Rik	RIKEN cDNA 4932438A13 gene	-0.61

58	Mir344-2	microRNA 344-2	-0.61
59	Slc9a9	solute carrier family 9 (sodium	-0.60
60	Chic1	cysteine-rich hydrophobic domain 1	-0.59
61	Trav8d-1	T cell receptor alpha variable 8D-1	-0.59
62	Scaper	S phase cyclin A-associated protein in the ER	-0.59
63	Wwp1	WW domain containing E3 ubiquitin protein ligase 1	-0.58
64	4932438A13Rik	RIKEN cDNA 4932438A13 gene	-0.58
65	1700054O19Rik	RIKEN cDNA 1700054O19 gene	-0.58
66	Gm3173	predicted gene 3173	-0.58
67	Utrn	utrophin	-0.58
68	Szt2	seizure threshold 2	-0.58
69	Arhgap15	Rho GTPase activating protein 15	-0.58
70	Slc5a3	solute carrier family 5 (inositol transporters), member 3	-0.58
71	Sntb1	syntrophin, basic 1	-0.57
72	Arl15	ADP-ribosylation factor-like 15	-0.56
73	Lyrm2	LYR motif containing 2	-0.56
74	Nlrc5	NLR family, CARD domain containing 5	-0.56
75	Gm10858	predicted gene 10858	-0.56
76	Polr3e	polymerase (RNA) III (DNA directed) polypeptide E	-0.56
77	Myo9a	myosin IXa	-0.55
78	Gm15455	predicted gene 15455	-0.55
79	Fryl	furry homolog-like (Drosophila)	-0.55
80	Cd160	CD160 antigen	-0.55
81	Snhg1	small nucleolar RNA host gene (non-protein coding) 1	-0.55
82	B3galt2	UDP-Gal:betaGlcNAc beta 1,3-galactosyltransferase, polypeptide 2	-0.54
83	Pik3r3	phosphatidylinositol 3 kinase, regulatory subunit, polypeptide 3 (p55)	-0.54
84	Ift80	intraflagellar transport 80	-0.54
85	Gm10838	predicted gene 10838	-0.54
86	Mir344	microRNA 344	-0.53
87	Zfp512	zinc finger protein 512	-0.53
88	Gm10552	predicted gene 10552	-0.53
89	Snora43	small nucleolar RNA, H	-0.52
90	LOC100503923	uncharacterized LOC100503923	-0.52
91	Scarna17	small Cajal body-specific RNA 17	-0.52
92	Scarna17	small Cajal body-specific RNA 17	-0.52
93	Gbp9	guanylate-binding protein 9	-0.51
94	Il18r1	interleukin 18 receptor 1	-0.51
95	A530032D15Rik	RIKEN cDNA A530032D15Rik gene	-0.51
96	Vps13c	vacuolar protein sorting 13C (yeast)	-0.51
97	Ptbp2	polypyrimidine tract binding protein 2	-0.51
98	Bzw2	basic leucine zipper and W2 domains 2	-0.51
99	Vps13a	vacuolar protein sorting 13A (yeast)	-0.50
100	Gas5	growth arrest specific 5	-0.50
101	Zbtb20	zinc finger and BTB domain containing 20	-0.50
102	Cd1d2	CD1d2 antigen	-0.49
103	Gm10372	predicted gene 10372	-0.49
104	Lrrc4	leucine rich repeat containing 4	-0.49
105	Fam174b	family with sequence similarity 174, member B	-0.49
106	Daam1	dishevelled associated activator of morphogenesis 1	-0.48
107	Gpr174	G protein-coupled receptor 174	-0.48
108	Ankrd55	ankyrin repeat domain 55	-0.48
109	4932442E05Rik	RIKEN cDNA 4932442E05 gene	-0.48
110	Actn1	actinin, alpha 1	-0.48
111	Szt2	seizure threshold 2	-0.48
112	Btnl5	butyrophilin-like 5	-0.48
113	Trav15d-1-dv6d-1	T cell receptor alpha variable 15D-1-DV6D-1	-0.48
114	Trav15d-1-dv6d-1	T cell receptor alpha variable 15D-1-DV6D-1	-0.48
115	Phxr1	per-hexamer repeat gene 1	-0.48
116	Cep112	centrosomal protein 112	-0.47

117	Lrrtm2	leucine rich repeat transmembrane neuronal 2	-0.47
118	Fam65b	family with sequence similarity 65, member B	-0.47
119	Ifitm5	interferon induced transmembrane protein 5	-0.47
120	Plcb4	phospholipase C, beta 4	-0.47
121	Zfp609	zinc finger protein 609	-0.47
122	Gnb2l1	guanine nucleotide binding protein (G protein), beta polypeptide 2 like 1	-0.47
123	Zfp264	zinc finger protein 264	-0.46
124	Ppp1r12b	protein phosphatase 1, regulatory (inhibitor) subunit 12B	-0.46
125	Ralgapa2	Ral GTPase activating protein, alpha subunit 2 (catalytic)	-0.46
126	Cspp1	centrosome and spindle pole associated protein 1	-0.46
127	Prdm5	PR domain containing 5	-0.46
128	Nlrc5	NLR family, CARD domain containing 5	-0.46
129	Sidt1	SID1 transmembrane family, member 1	-0.46
130	4932438A13Rik	RIKEN cDNA 4932438A13 gene	-0.45
131	Tmem245	transmembrane protein 245	-0.45
132	4932438A13Rik	RIKEN cDNA 4932438A13 gene	-0.45
133	Sfxn4	sideroflexin 4	-0.45
134	Wdr66	WD repeat domain 66	-0.45
135	Fdft1	farnesyl diphosphate farnesyl transferase 1	-0.45
136	Dock6	dedicator of cytokinesis 6	-0.45
137	Tasp1	taspase, threonine aspartase 1	-0.45
138	Fbxl17	F-box and leucine-rich repeat protein 17	-0.45
139	Foxred1	FAD-dependent oxidoreductase domain containing 1	-0.45
140	Gm10688	predicted gene 10688	-0.45
141	Lrmp	lymphoid-restricted membrane protein	-0.45
142	Zfp407	zinc finger protein 407	-0.44
143	Rab37	RAB37, member of RAS oncogene family	-0.44
144	5830416P10Rik	RIKEN cDNA 5830416P10 gene	-0.44
145	Map2k6	mitogen-activated protein kinase kinase 6	-0.44
146	Zfp661	zinc finger protein 661	-0.44
147	Mir667	microRNA 667	-0.43
148	D7Bwg0826e	DNA segment, Chr 7, Brigham & Women's Genetics 0826 expressed	-0.43
149	Abcb1a	ATP-binding cassette, sub-family B (MDR	-0.43
150	Igflr1	IGF-like family receptor 1	-0.43
151	Copg2	coatomer protein complex, subunit gamma 2	-0.43
152	Hal	histidine ammonia lyase	-0.43
153	Exoc6	exocyst complex component 6	-0.43
154	Mdm4	transformed mouse 3T3 cell double minute 4	-0.43
155	Serpind1	serine (or cysteine) peptidase inhibitor, clade D, member 1	-0.43
156	Mettl21c	methyltransferase like 21C	-0.43
157	Tanc2	tetratricopeptide repeat, ankyrin repeat and coiled-coil containing 2	-0.43
158	Tspyl2	TSPY-like 2	-0.43
159	Plcxd2	phosphatidylinositol-specific phospholipase C, X domain containing 2	-0.43
160	Tnip2	TNFAIP3 interacting protein 2	-0.42
161	Tceanc	transcription elongation factor A (SII) N-terminal and central domain containing	-0.42
162	LOC101055847	attractin-like	-0.42
163	Rfx3	regulatory factor X, 3 (influences HLA class II expression)	-0.42
164	Dennd1c	DENN	-0.42
165	Gucy1a3	guanylate cyclase 1, soluble, alpha 3	-0.42
166	Gm3435	predicted gene 3435	-0.41
167	AV039307	expressed sequence AV039307	-0.41
168	Mir15a	microRNA 15a	-0.41
169	Slc14a1	solute carrier family 14 (urea transporter), member 1	-0.41
170	n-R5s168	nuclear encoded rRNA 5S 168	-0.41
171	Cspp1	centrosome and spindle pole associated protein 1	-0.41
172	n-R5s193	nuclear encoded rRNA 5S 193	-0.41
173	Rundc3b	RUN domain containing 3B	-0.41
174	Eml5	echinoderm microtubule associated protein like 5	-0.41
175	Tbc1d23	TBC1 domain family, member 23	-0.41

176	Mbtd1	mbt domain containing 1	-0.41
177	Ubtd1	ubiquitin domain containing 1	-0.40
178	Mir200c	microRNA 200c	-0.40
179	Apol7b	apolipoprotein L 7b	-0.40
180	Asah2	N-acylsphingosine amidohydrolase 2	-0.40
181	Ifna2	interferon alpha 2	-0.40
	Genes up-regulated in dKO (dKO-WT > 0.4)		
#	**Symbol**	**Gene description**	**Fold change**
1	Ccr2	chemokine (C-C motif) receptor 2	1.51
2	Il10	interleukin 10	1.13
3	Csf1	colony stimulating factor 1 (macrophage)	1.12
4	Gm14085	predicted gene 14085	1.07
5	Gzmb	granzyme B	1.05
6	Ccr5	chemokine (C-C motif) receptor 5	1.02
7	Ccr5	chemokine (C-C motif) receptor 5	1.02
8	Wls	wntless homolog (Drosophila)	1.01
9	Gbp5	guanylate binding protein 5	1.01
10	Mir92-1	microRNA 92-1	0.99
11	Tnfsf8	tumor necrosis factor (ligand) superfamily, member 8	0.98
12	Gm4951	predicted gene 4951	0.97
13	4930412O13Rik	RIKEN cDNA 4930412O13 gene	0.97
14	Gm4841	predicted gene 4841	0.97
15	Gpm6b	glycoprotein m6b	0.96
16	Ccl1	chemokine (C-C motif) ligand 1	0.96
17	Lgmn	legumain	0.93
18	Rpa3	replication protein A3	0.91
19	Itga9	integrin alpha 9	0.90
20	Tnfsf10	tumor necrosis factor (ligand) superfamily, member 10	0.88
21	Slc43a1	solute carrier family 43, member 1	0.83
22	Ccr3	chemokine (C-C motif) receptor 3	0.79
23	Hddc3	HD domain containing 3	0.78
24	Akr1e1	aldo-keto reductase family 1, member E1	0.77
25	Id2	inhibitor of DNA binding 2	0.76
26	Gpr15	G protein-coupled receptor 15	0.76
27	Angptl2	angiopoietin-like 2	0.76
28	Ppp1r12b	protein phosphatase 1, regulatory (inhibitor) subunit 12B	0.74
29	Ppic	peptidylprolyl isomerase C	0.74
30	Lag3	lymphocyte-activation gene 3	0.73
31	Il10ra	interleukin 10 receptor, alpha	0.72
32	Podnl1	podocan-like 1	0.71
33	Klrg1	killer cell lectin-like receptor subfamily G, member 1	0.71
34	Scoc	short coiled-coil protein	0.71
35	Trps1	trichorhinophalangeal syndrome I (human)	0.67
36	Gpr68	G protein-coupled receptor 68	0.67
37	Ccr4	chemokine (C-C motif) receptor 4	0.67
38	Scin	scinderin	0.66
39	Iigp1	interferon inducible GTPase 1	0.66
40	Pla2g4b	phospholipase A2, group IVB (cytosolic)	0.66
41	Ifng	interferon gamma	0.64
42	Tcp1	t-complex protein 1	0.64
43	Ces2d-ps	carboxylesterase 2D, pseudogene	0.63
44	Fgl2	fibrinogen-like protein 2	0.63
45	Gm4955	predicted gene 4955	0.62
46	Itgb1	integrin beta 1 (fibronectin receptor beta)	0.61
47	Ly6a	lymphocyte antigen 6 complex, locus A	0.60
48	Sytl2	synaptotagmin-like 2	0.60
49	Tnfsf9	tumor necrosis factor (ligand) superfamily, member 9	0.59
50	Cxcr3	chemokine (C-X-C motif) receptor 3	0.59
51	4932438A13Rik	RIKEN cDNA 4932438A13 gene	0.58

52	Gpatch8	G patch domain containing 8	0.58
53	Gbp2	guanylate binding protein 2	0.57
54	Nrn1	neuritin 1	0.57
55	Matn2	matrilin 2	0.57
56	Eea1	early endosome antigen 1	0.57
57	Spc25	SPC25, NDC80 kinetochore complex component, homolog (S. cerevisiae)	0.56
58	Axl	AXL receptor tyrosine kinase	0.56
59	Adat2	adenosine deaminase, tRNA-specific 2	0.56
60	Rif1	Rap1 interacting factor 1 homolog (yeast)	0.55
61	Tnfaip8	tumor necrosis factor, alpha-induced protein 8	0.55
62	Iigp1b	interferon inducible GTPase 1B	0.55
63	Ptpn13	protein tyrosine phosphatase, non-receptor type 13	0.55
64	Gm9847	predicted pseudogene 9847	0.54
65	Arl5a	ADP-ribosylation factor-like 5A	0.54
66	Hsph1	heat shock 105kDa/110kDa protein 1	0.54
67	Arrdc4	arrestin domain containing 4	0.53
68	E330021D16Rik	RIKEN cDNA E330021D16 gene	0.53
69	Il17rb	interleukin 17 receptor B	0.52
70	Cldn25	claudin 25	0.52
71	Sh3bgrl2	SH3 domain binding glutamic acid-rich protein like 2	0.52
72	Gemin8	gem (nuclear organelle) associated protein 8	0.52
73	Rdh10	retinol dehydrogenase 10 (all-trans)	0.52
74	Gm14335	predicted gene 14335	0.51
75	Atp6v0a1	ATPase, H+ transporting, lysosomal V0 subunit A1	0.51
76	Tmem14a	transmembrane protein 14A	0.51
77	B630019A10Rik	RIKEN cDNA B630019A10 gene	0.51
78	BC005685	cDNA sequence BC005685	0.51
79	Maf	avian musculoaponeurotic fibrosarcoma (v-maf) AS42 oncogene homolog	0.51
80	BC005685	cDNA sequence BC005685	0.50
81	4932438A13Rik	RIKEN cDNA 4932438A13 gene	0.50
82	Gm12026	predicted gene 12026	0.50
83	Cyp11a1	cytochrome P450, family 11, subfamily a, polypeptide 1	0.50
84	Qser1	glutamine and serine rich 1	0.49
85	Ell2	elongation factor RNA polymerase II 2	0.49
86	Hist2h2be	histone cluster 2, H2be	0.48
87	Trav11d	T cell receptor alpha variable 11D	0.48
88	Pip4k2b	phosphatidylinositol-5-phosphate 4-kinase, type II, beta	0.47
89	Tm2d2	TM2 domain containing 2	0.47
90	Tlcd2	TLC domain containing 2	0.47
91	Larp1b	La ribonucleoprotein domain family, member 1B	0.47
92	Tk1	thymidine kinase 1	0.46
93	Fgd6	FYVE, RhoGEF and PH domain containing 6	0.46
94	Rpl39l	ribosomal protein L39-like	0.45
95	BC005685	cDNA sequence BC005685	0.45
96	Ccdc109b	coiled-coil domain containing 109B	0.45
97	Slamf6	SLAM family member 6	0.45
98	Gbp3	guanylate binding protein 3	0.45
99	Kcnf1	potassium voltage-gated channel, subfamily F, member 1	0.44
100	Spdl1	spindle apparatus coiled-coil protein 1	0.44
101	Arhgap19	Rho GTPase activating protein 19	0.44
102	n-R5s180	nuclear encoded rRNA 5S 180	0.43
103	Lta4h	leukotriene A4 hydrolase	0.43
104	Gpatch8	G patch domain containing 8	0.43
105	Cycs	cytochrome c, somatic	0.43
106	Zfp758	zinc finger protein 758	0.43
107	Sh3bgrl	SH3-binding domain glutamic acid-rich protein like	0.43
108	H1f0	H1 histone family, member 0	0.43
109	F730043M19Rik	RIKEN cDNA F730043M19 gene	0.43
110	Cpe	carboxypeptidase E	0.42

111	Isg20	interferon-stimulated protein	0.42
112	BC002059	cDNA sequence BC002059	0.42
113	Gm6253	predicted pseudogene 6253	0.42
114	Sntb2	syntrophin, basic 2	0.42
115	Cenph	centromere protein H	0.42
116	Dnajc15	DnaJ (Hsp40) homolog, subfamily C, member 15	0.42
117	Batf	basic leucine zipper transcription factor, ATF-like	0.42
118	Tada1	transcriptional adaptor 1	0.41
119	4930422G04Rik	RIKEN cDNA 4930422G04 gene	0.41
120	Pyhin1	pyrin and HIN domain family, member 1	0.41
121	Arsb	arylsulfatase B	0.41
122	B930041F14Rik	RIKEN cDNA B930041F14 gene	0.41
123	Gm5486	predicted gene 5486	0.41
124	Kcnq5	potassium voltage-gated channel, subfamily Q, member 5	0.41
125	Glrx	glutaredoxin	0.41
126	Spic	Spi-C transcription factor (Spi-1/PU.1 related)	0.41
127	Rad54l2	RAD54 like 2 (S. cerevisiae)	0.41
128	Zfp287	zinc finger protein 287	0.40
129	Ptprv	protein tyrosine phosphatase, receptor type, V	0.40
130	Kif22	kinesin family member 22	0.40
131	Fam160b1	family with sequence similarity 160, member B1	0.40
	Genes down-regulated in dKO (dKO-WT < -0.4)		
#	**Symbol**	**Gene description**	**Fold change**
1	Fabp2	fatty acid binding protein 2, intestinal	-1.86
2	Acadl	acyl-Coenzyme A dehydrogenase, long-chain	-1.64
3	H2-DMb1	histocompatibility 2, class II, locus Mb1	-1.37
4	H2-Ob	histocompatibility 2, O region beta locus	-1.28
5	Klrb1b	killer cell lectin-like receptor subfamily B member 1B	-1.25
6	Ntn4	netrin 4	-1.25
7	Serpinb1a	serine (or cysteine) peptidase inhibitor, clade B, member 1a	-1.03
8	Eif2ak2	eukaryotic translation initiation factor 2-alpha kinase 2	-1.01
9	Asns	asparagine synthetase	-0.99
10	Hdac9	histone deacetylase 9	-0.93
11	Snord118	small nucleolar RNA, C/D box 118	-0.89
12	Snord118	small nucleolar RNA, C/D box 118	-0.89
13	Islr	immunoglobulin superfamily containing leucine-rich repeat	-0.84
14	6330403K07Rik	RIKEN cDNA 6330403K07 gene	-0.83
15	Sord	sorbitol dehydrogenase	-0.82
16	Oasl2	2'-5' oligoadenylate synthetase-like 2	-0.80
17	Igk-V1	immunoglobulin kappa chain variable 1 (V1)	-0.79
18	Ctsw	cathepsin W	-0.78
19	Cd7	CD7 antigen	-0.78
20	Cnr2	cannabinoid receptor 2 (macrophage)	-0.77
21	Il18r1	interleukin 18 receptor 1	-0.77
22	As3mt	arsenic (+3 oxidation state) methyltransferase	-0.75
23	Tet1	tet methylcytosine dioxygenase 1	-0.74
24	Ampd1	adenosine monophosphate deaminase 1	-0.74
25	Snora7a	small nucleolar RNA, H/ACA box 7A	-0.73
26	Rnu3a	U3A small nuclear RNA	-0.70
27	Sord	sorbitol dehydrogenase	-0.67
28	Cep112	centrosomal protein 112	-0.66
29	Cd160	CD160 antigen	-0.66
30	Pak1	p21 protein (Cdc42/Rac)-activated kinase 1	-0.63
31	Cd83	CD83 antigen	-0.63
32	Atp6v0d2	ATPase, H+ transporting, lysosomal V0 subunit D2	-0.63
33	Ms4a4c	membrane-spanning 4-domains, subfamily A, member 4C	-0.62
34	Prrt2	proline-rich transmembrane protein 2	-0.61
35	Tdgf1	teratocarcinoma-derived growth factor 1	-0.61
36	Slx1b	SLX1 structure-specific endonuclease subunit homolog B (S. cerevisiae)	-0.60

37	Chd7	chromodomain helicase DNA binding protein 7	-0.59
38	Rtn4rl1	reticulon 4 receptor-like 1	-0.58
39	Actg2	actin, gamma 2, smooth muscle, enteric	-0.58
40	9530009G21Rik	RIKEN cDNA 9530009G21 gene	-0.58
41	2010005H15Rik	RIKEN cDNA 2010005H15 gene	-0.57
42	Tmem176a	transmembrane protein 176A	-0.57
43	Siglecg	sialic acid binding Ig-like lectin G	-0.56
44	Rnu3b4	U3B small nuclear RNA 4	-0.56
45	Rnu3b4	U3B small nuclear RNA 4	-0.56
46	Rnu3b4	U3B small nuclear RNA 4	-0.56
47	Rnu3b4	U3B small nuclear RNA 4	-0.56
48	Pxdc1	PX domain containing 1	-0.56
49	Snord49a	small nucleolar RNA, C/D box 49A	-0.55
50	Fsd2	fibronectin type III and SPRY domain containing 2	-0.54
51	Chd7	chromodomain helicase DNA binding protein 7	-0.53
52	Gm9001	predicted gene 9001	-0.53
53	Casp4	caspase 4, apoptosis-related cysteine peptidase	-0.53
54	Prune2	prune homolog 2 (Drosophila)	-0.53
55	Ttbk2	tau tubulin kinase 2	-0.52
56	Yipf2	Yip1 domain family, member 2	-0.52
57	Ndrg2	N-myc downstream regulated gene 2	-0.51
58	AY761184	cDNA sequence AY761184	-0.51
59	Sidt1	SID1 transmembrane family, member 1	-0.51
60	Sv2a	synaptic vesicle glycoprotein 2 a	-0.50
61	Syk	spleen tyrosine kinase	-0.49
62	F630048H11Rik	RIKEN cDNA F630048H11 gene	-0.49
63	Sorl1	sortilin-related receptor, LDLR class A repeats-containing	-0.49
64	Igflr1	IGF-like family receptor 1	-0.49
65	Pon3	paraoxonase 3	-0.49
66	Rpl31-ps23	ribosomal protein L31, pseudogene 23	-0.48
67	Akap12	A kinase (PRKA) anchor protein (gravin) 12	-0.48
68	Syt17	synaptotagmin XVII	-0.48
69	Acaa2	acetyl-Coenzyme A acyltransferase 2 (mitochondrial 3-oxoacyl-Coenzyme A thiolase)	-0.48
70	Scamp1	secretory carrier membrane protein 1	-0.47
71	Stard4	StAR-related lipid transfer (START) domain containing 4	-0.47
72	Tpst1	protein-tyrosine sulfotransferase 1	-0.47
73	Tet1	tet methylcytosine dioxygenase 1	-0.47
74	Sacm1l	SAC1 (suppressor of actin mutations 1, homolog)-like (S. cerevisiae)	-0.47
75	Chi3l7	chitinase 3-like 7	-0.47
76	Cerk	ceramide kinase	-0.47
77	1700047G07Rik	RIKEN cDNA 1700047G07 gene	-0.46
78	Mex3a	mex3 homolog A (C. elegans)	-0.45
79	Pgpep1l	pyroglutamyl-peptidase I-like	-0.45
80	Coro2a	coronin, actin binding protein 2A	-0.45
81	Cd300lf	CD300 antigen like family member F	-0.44
82	Plcg2	phospholipase C, gamma 2	-0.44
83	Gm15293	predicted gene 15293	-0.43
84	Usp11	ubiquitin specific peptidase 11	-0.43
85	Gm15401	predicted gene 15401	-0.43
86	Ldhal6b	lactate dehydrogenase A-like 6B	-0.42
87	Ephx1	epoxide hydrolase 1, microsomal	-0.42
88	Rhoq	ras homolog gene family, member Q	-0.42
89	Pik3ap1	phosphoinositide-3-kinase adaptor protein 1	-0.42
90	Atrnl1	attractin like 1	-0.42
91	Clnk	cytokine-dependent hematopoietic cell linker	-0.41
92	Arfgef2	ADP-ribosylation factor guanine nucleotide-exchange factor 2 (brefeldin A-inhibited)	-0.41
93	Strbp	spermatid perinuclear RNA binding protein	-0.41
94	Cd68	CD68 antigen	-0.41

III.1.1.2 Complementary results

III.1.1.2.1 T cell transfer model of colitis

To study the role of Eos and Helios transcription factors in the natural Treg cells *in vivo* we have set up a T cell transfer of inflammatory bowel disease (IBD), known also as colitis. IBD is a chronic inflammation of gastrointestinal tract mediated by exposing mucosal surface antigens (from diet or commensal bacteria) and causing aberrant immune responses. In man it has a diverse etiopathology and can be accompanied by genetic predisposition, but also environmental influences. It is characterized by infiltration of colon by T cells (Th1/Th2/Th17) and production of large amounts of inflammatory cytokines (e.g. TNF-α, IFN-γ), that ultimately leads to lesions and tissue damage (Geremia et al., 2014). Colitis model has been extensively used to study Treg cells as it has been demonstrated that they can prevent or suppress the intestinal inflammation (Asseman et al., 2000; Singh et al., 2001; Xu et al., 2003; Mottet et al., 2003). Thus, we wanted to use this model in order to verify if Treg cells deficient for Eos and/or Helios are fully functional in *vivo*.

We carried out the experimental procedure with Rag1 deficient mice ($Rag1^{-/-}$ lacking mature B and T cells) as recipients of naive T cells adapting available protocols (Ostanin et al., 2009; Workman et al., 2011). The IBD model involved transferring naive $CD4^+$ T cells from WT spleens ($CD4^+CD44^{lo}CD62L^{hi}$) into $Rag1^{-/-}$ mice, alone or together with $CD4^+CD25^+$ Treg cells from the mutant mice or their WT littermate controls. Here, colitis would develop in the absence, but not presence, of functional Treg cells. The recipient mice were followed weekly and sacrificed when they lost 15-20% of their body weight (or 8 weeks later). The colon was analyzed by histopathology to evaluate for lymphocyte infiltration and damage. Spleen and mesenteric lymph node cell populations were analyzed by flow cytometry and cytokine production was evaluated. We have performed the first experiment with naïve T cells from WT mice and Treg cells from WT and $Eos^{-/-}$ mice. Naïve $CD4^+$ T cells ($4x10^5$) were injected alone or co- injected (intraperitoneally) together with Treg cells ($1x10^5$) into $Rag1^{-/-}$ mice. A group of $Rag1^{-/-}$ were left as un-manipulated controls. First, we could observe that during the period of 8 weeks when the mice where monitored, only the ones that received T cells alone were losing body weight (loss in a range between 6-18% of initial weight), whereas recipients of T cells and Treg cells were protected from body weight loss (they gained weight ranging from 3-16% of the initial measurement) (Fig.III.2). Each experimental group comprised both females and males between 7-10 weeks old and we observed similar pattern of body weight loss/gain for all mice in a given group.

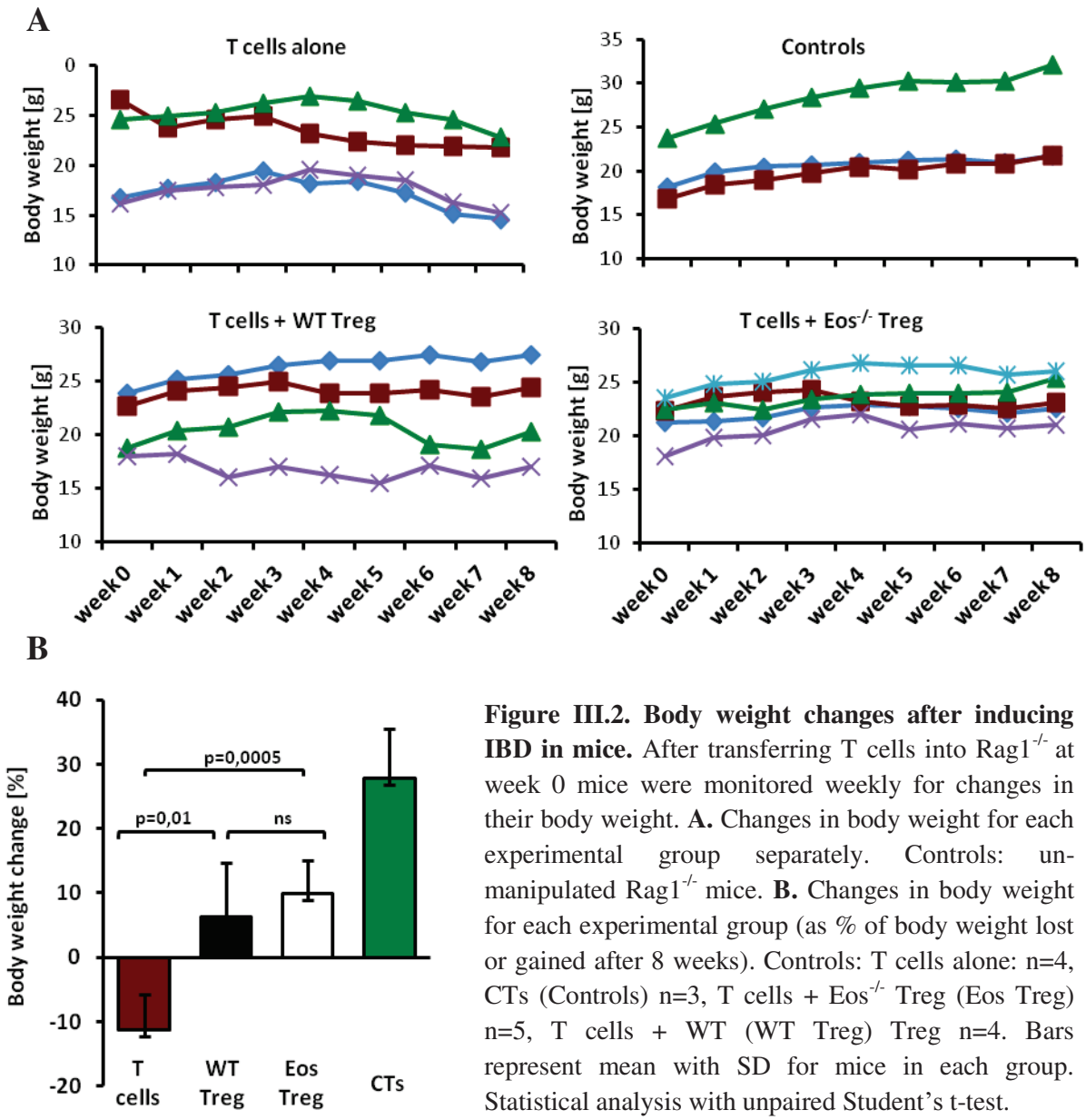

Figure III.2. Body weight changes after inducing IBD in mice. After transferring T cells into Rag1$^{-/-}$ at week 0 mice were monitored weekly for changes in their body weight. **A.** Changes in body weight for each experimental group separately. Controls: un-manipulated Rag1$^{-/-}$ mice. **B.** Changes in body weight for each experimental group (as % of body weight lost or gained after 8 weeks). Controls: T cells alone: n=4, CTs (Controls) n=3, T cells + Eos$^{-/-}$ Treg (Eos Treg) n=5, T cells + WT (WT Treg) Treg n=4. Bars represent mean with SD for mice in each group. Statistical analysis with unpaired Student's t-test.

The large intestine of recipient mice was also prepared for histological analysis to access if the observed changes in body weight are indeed due to the ongoing inflammation. In mice that received T cells alone we could observe large lymphocyte infiltrates in the mucosal and sub-mucosal space and between the crypt cells. The crypt cells themselves also appeared deformed and elongated. In all experimental groups we could also see thickening of the intestine wall. Mice that received Treg cells together with naïve T cells were rescued at least partially from those severe changes and showed less infiltrates and tissue damage, both when WT and Eos deficient cells were used (Fig.III.3).

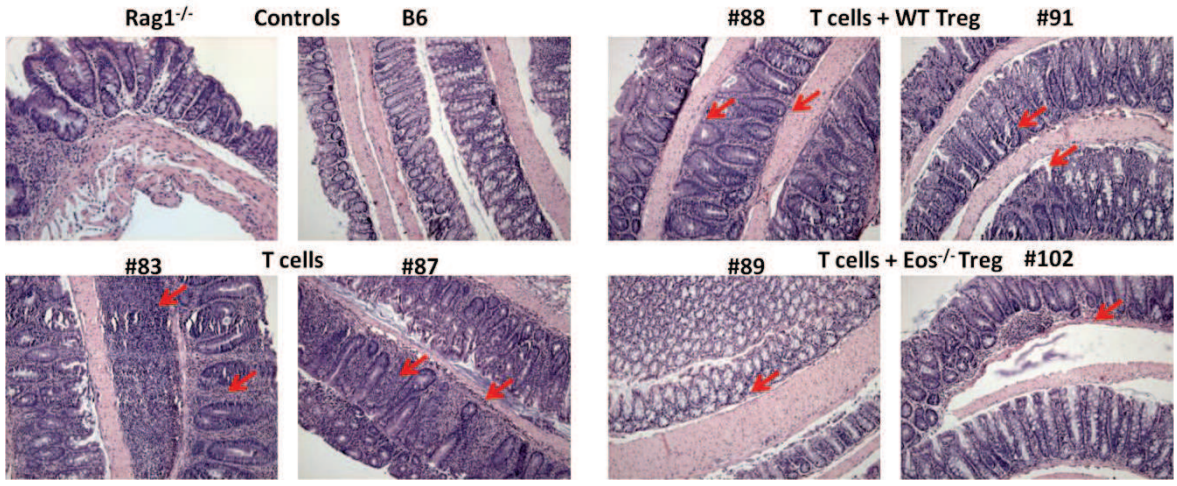

Figure III.3. Histological analysis of mice with colon inflammation. 8 weeks after T cell transfer, mice were sacrificed and large intestines prepared for histological analysis. Hematoxylin and eosin staining (HE) was performed on 5 µm sections of colon "swiss rolls". Representative mice from each group are presented. Arrows point at lymphocyte infiltrates or "improved" phenotype in mice that received Treg cells. All presented pictures were taken with 10x magnification.

In parallel, production of inflammatory cytokines was analyzed in the large intestine of mice after T cell transfer. Results showed that transfer of T cells alone cause a higher production of inflammatory cytokines (TNF-α, IFN-γ) when compared to mice that received T cells together with WT or Eos$^{-/-}$ Treg cells (Fig.III.4).

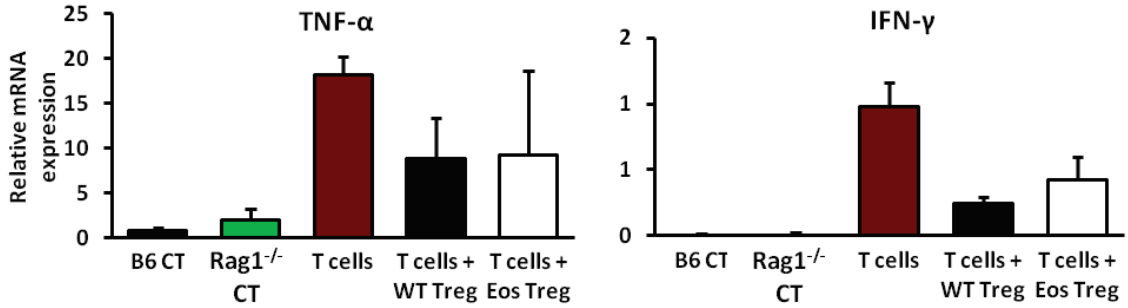

Figure III.4. Production of inflammatory cytokines in the large intestine of mice after IBD induction. 8 weeks after T cell transfer, mice were sacrificed and RNA was prepared from whole tissues of large intestines of 2 mice from each group. Expression normalized to HPRT. Bars represent mean with SD.

Lastly, we have analyzed by flow cytometry cells from spleens and mesenteric lymph nodes (mLNs) of all mice in each group for the presence of injected T cells and Treg cells (Fig.III.5). As expected we found higher frequencies of Treg cells ($CD4^+CD25^+Foxp3^+$) in the spleens and mLNs of mice that received naïve T cells together with Treg cells of both genotypes. Concerning naïve $CD4^+$ T cells, lower numbers were observed in the spleens of mice injected with T cells and Treg cells, but those cells appeared to accumulate in mLNs,

where we found similar frequencies of T cells in mice that received both T cells alone or together with Treg cells (Fig.III.6). These results indicate a successful transfer of T cells and Treg cells that accumulate not only in the large intestine as shown by HE staining but also in peripheral lymphoid organs of recipient mice.

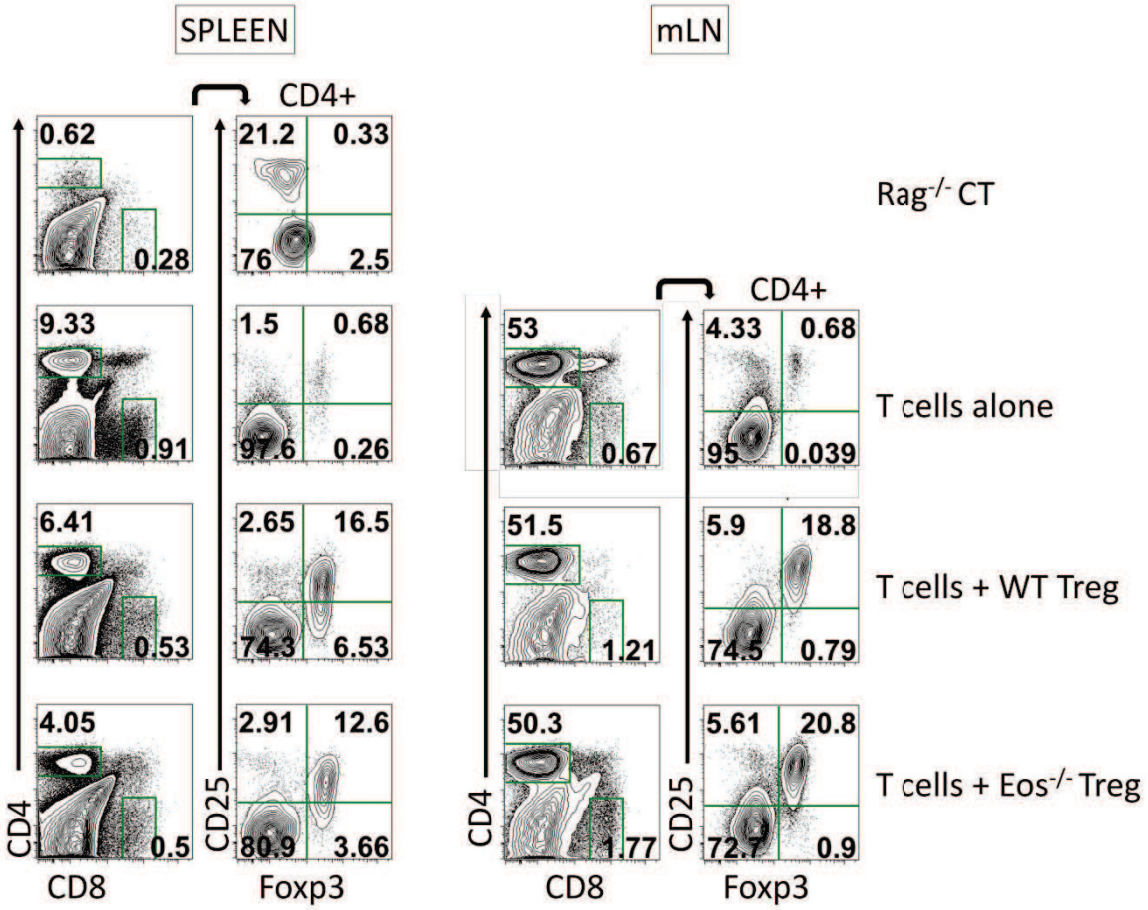

Figure III.5. Flow cytometry analysis shows presence of injected T cells and Treg cells in the peripheral lymphoid organs of recipient mice. 8 weeks after T cell transfer, mice were sacrificed and peripheral lymphoid organs were prepared for flow cytometry analysis. Representative staining for indicated markers with one mouse per each group is presented. Staining of mLNs only in mice after T cell transfer is shown, as no mesenteric lymph nodes could be recovered from Rag1$^{-/-}$ mice.

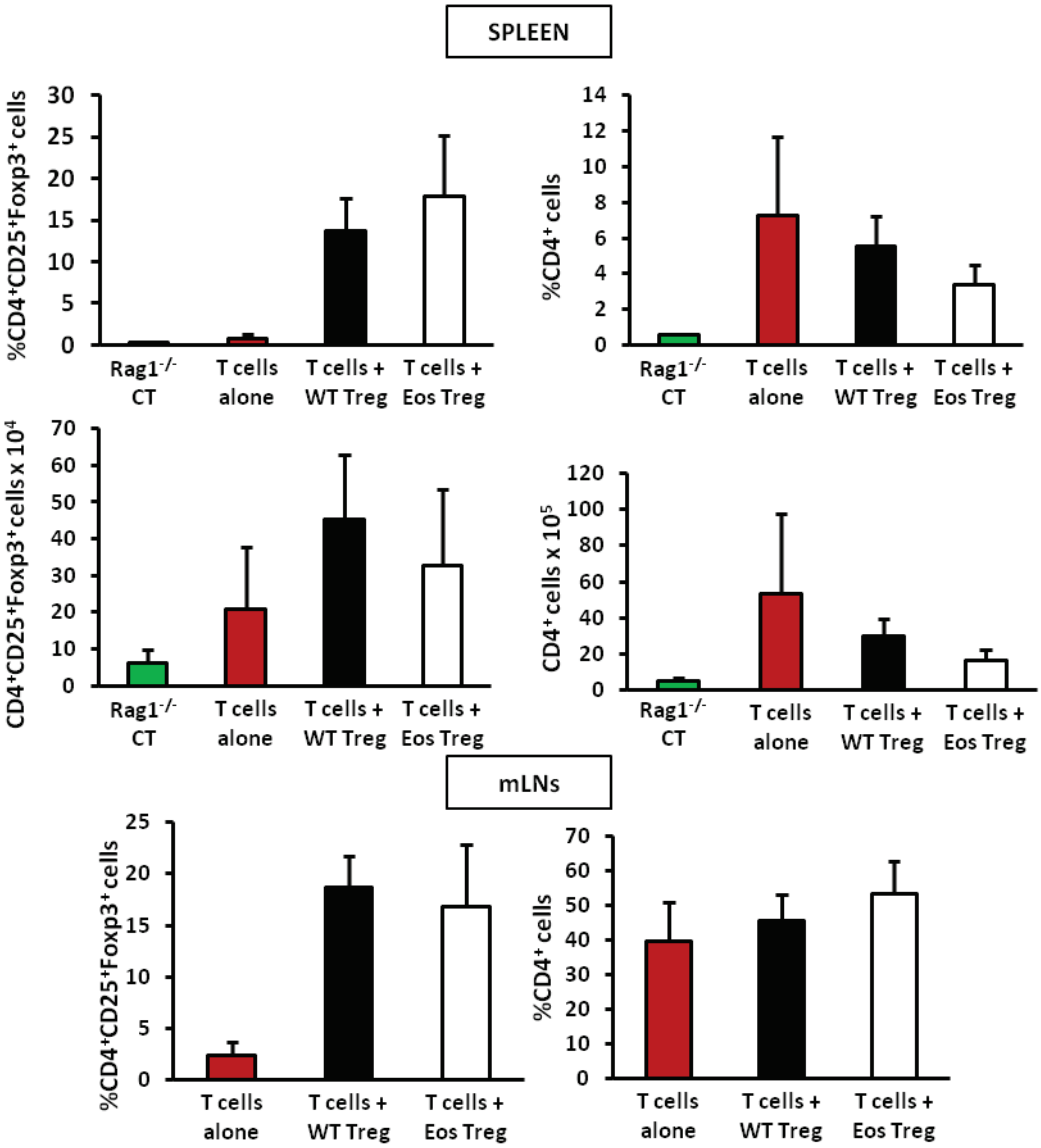

Figure III.6. Frequencies and number of injected T cells and Treg cells in the peripheral lymphoid organs of recipient mice. Flow cytometry results showing frequencies [%] and cell numbers of $CD4^+$ T cells and $CD4^+CD25^+Foxp3^+$ Treg cells in spleens and mLNs of recipient mice 8 weeks after T cell transfer. Bars represent mean with SD of each group. T cells alone: n=4 mice, $Rag1^{-/-}$ CT n=2, T cells + Eos Treg n=5, T cells + WT Treg n=4.

Collectively, I have tested a murine experimental system that allows studying the functionality of Treg cells *in vivo* and give various phenotypic read-outs. In the experiment described before we compared WT Treg cells with $Eos^{-/-}$ cells and did not observe any apparent differences in their suppressive efficiency similarly to results obtained *in vitro* (presented in the paper manuscript). It is important to mention here that the results of the colitis model come from one experiment only (preceded by pilot experiments) and could not be repeated so far because of insufficient number of available $Rag1^{-/-}$ recipient mice.

III.1.2 Eos in hematopoietic stem cells

Eos shows high sequence similarity to Helios, as well as similar expression patterns (see chapter I). Both are expressed in ES and HSC cells with the highest level in LT-HSCs (Fig.III.1 and Papathanasiou et al., 2009). Work from our lab shows that Helios has a specific role in this compartment, particularly in regulating HSC functions under stress conditions (DNA damage and aging) and maintaining the genome integrity of HSCs (Vesin RM et al., in preparation). The founding member of the family, Ikaros, is critical for hematopoietic stem cell functions. In particular, Ikaros deficient mice have dramatically decreased activity of HSC as measured both *in vivo* and in *vitro* (Nichogiannopoulou et al., 1999). Thus, we hypothesized a potential role for Eos in the HSC compartment and verified if this role could be specific or redundant with Helios or Ikaros.

To do so, we have studied the main functions of HSCs during homeostasis as well during stress conditions in $Eos^{-/-}$ mice by:

- Analyzing HSCs from KO mice in steady state by flow cytometry
- Performing competitive reconstitution assays
- Performing serial competitive reconstitution assays
- Analyzing proliferation and response to DNA damage of KO HSCs
- Assessing the functionality of hematopoietic progenitors from KO mice

III.1.2.1 HSCs in $Eos^{-/-}$ mice during steady state and in transplantation assays

First, in steady state, Eos deficient mice showed normal frequencies of progenitor cells and LT-HSCs. Only in some cases we observed a decreased number of LSK (Lin^- $Sca1^+c\text{-}Kit^+$) cells, which comprise hematopoietic stem and progenitor cells, but these results were not reproducible between mice and experiments (Fig.III.7). We have then analyzed the functionality of HSCs from Eos null mice during serial engraftments. In particular, we have assessed the ability of these cells to reconstitute hematopoietic system in competitive transplantation assays. These assays allow evaluating the contribution of hematopoietic stem cells of given origin to the reconstitution of hematopoietic compartment. In our experimental system, total bone marrow cells (BM) or LSK cells from donor WT or $Eos^{-/-}$ mice were injected into lethally irradiated recipient mice together with competitor WT cells. During secondary transplantations, sorted donor total bone marrow or LSK cells were injected into new lethally irradiated recipient mice together with competitor WT cells, similarly to primary experiments. In this experimental set-up donor cells are $CD45.2^+$, recipient cells are

$CD45.1^+CD45.2^+$ and competitors are $CD45.1^+$ which distinguishes those populations and allows analyzing the reconstitution of hematopoietic system in the blood of transplanted mice using flow cytometry (Fig.III.8).

Those experiments showed that Eos deficient cells reconstitute similarly to wild type cells in primary transplantations with total bone marrow cells, but $Eos^{-/-}$ cells show inferior reconstitution than WT cells in secondary transplantations (Fig.III.9A).

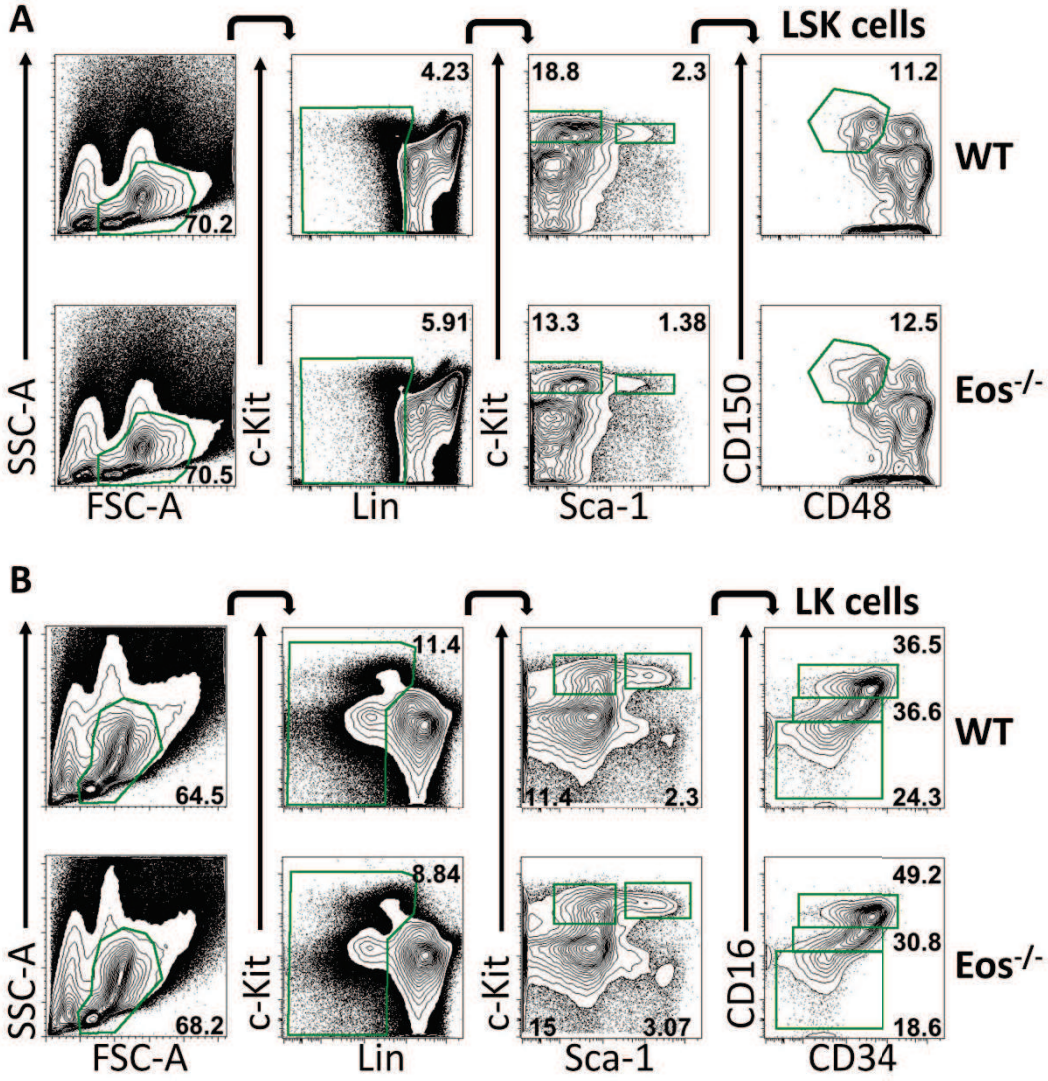

Figure III.7. $Eos^{-/-}$ mice have normal HSC compartment. Representative flow cytometry results showing hematopoietic stem and progenitor cells in the bone marrow. **A.** LT-HSC - $Lin^-Sca1^+c\text{-}Kit^+CD48^-CD15^+$ (comprised within LSK cells); **B.** MEP - Megakaryocyte Erythroid Progenitors - $Lin^-C\text{-}Kit^+Sca1^-CD34^-CD16/32^-$, CMP - Common Myeloid Progenitors - $Lin^-C\text{-}Kit^+Sca1^-CD34^+CD16/32^{lo}$, GMP - Granulocyte Macrophage Progenitor ($Lin^-C\text{-}Kit^+Sca1^-CD34^+CD16/32^{hi}$ (comprised within LK cells).

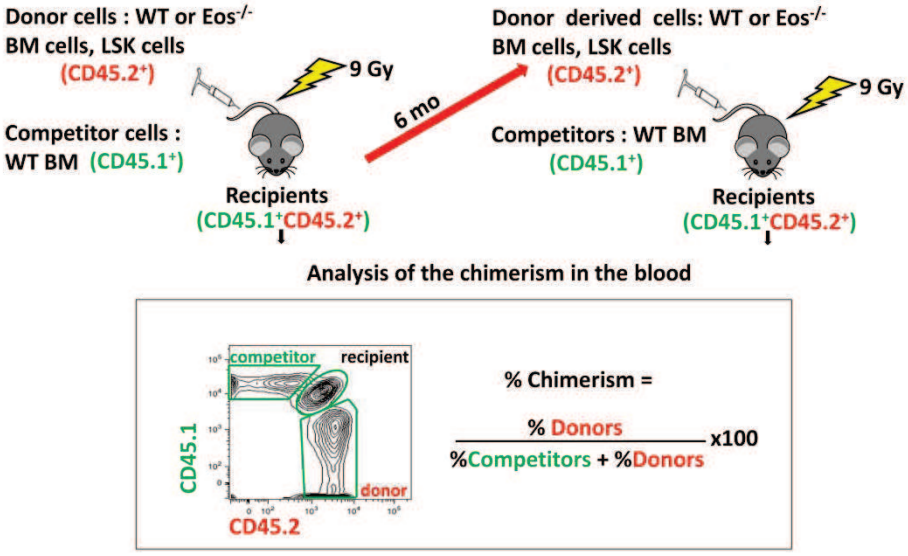

Figure III.8. Serial competitive reconstitution assay. In primary transplantations, total bone marrow cells or purified LSK cells from donor mice (WT or Eos$^{-/-}$) are injected into lethally irradiated recipient mice together with competitor WT cells. Donor cells are CD45.2^{+}, recipient cells are CD45.1^{+}CD45.2^{+} and competitor cells are CD45.1^{+} which distinguishes those populations by flow cytometry. In secondary assays, mice from primary experiments are sacrificed and donor derived cells (BM or LSK cells sorted as CD45.2^{+} cells) are injected into new lethally irradiated recipient mice together with competitor WT cells. Throughout the experiment peripheral blood is collected to calculate the chimerism as depicted on the scheme.

During the analysis of peripheral blood from transplanted mice, cells were also stained for different lineage markers to evaluate the ability to fully reconstitute the hematopoietic system. Donor bone marrow cells from WT and Eos$^{-/-}$ mice could efficiently produce cells from lymphoid and myeloid lineages. Even in the secondary transplantations, where Eos$^{-/-}$ cells had less activity, we did not observe significant differences in the capacity of donor cells to produce myeloid (monocyte and granulocyte populations expressing CD11b or Gr1) or lymphoid (T cell and B cell populations expressing CD3 and B220, respectively) cell populations (Fig.III.9B).

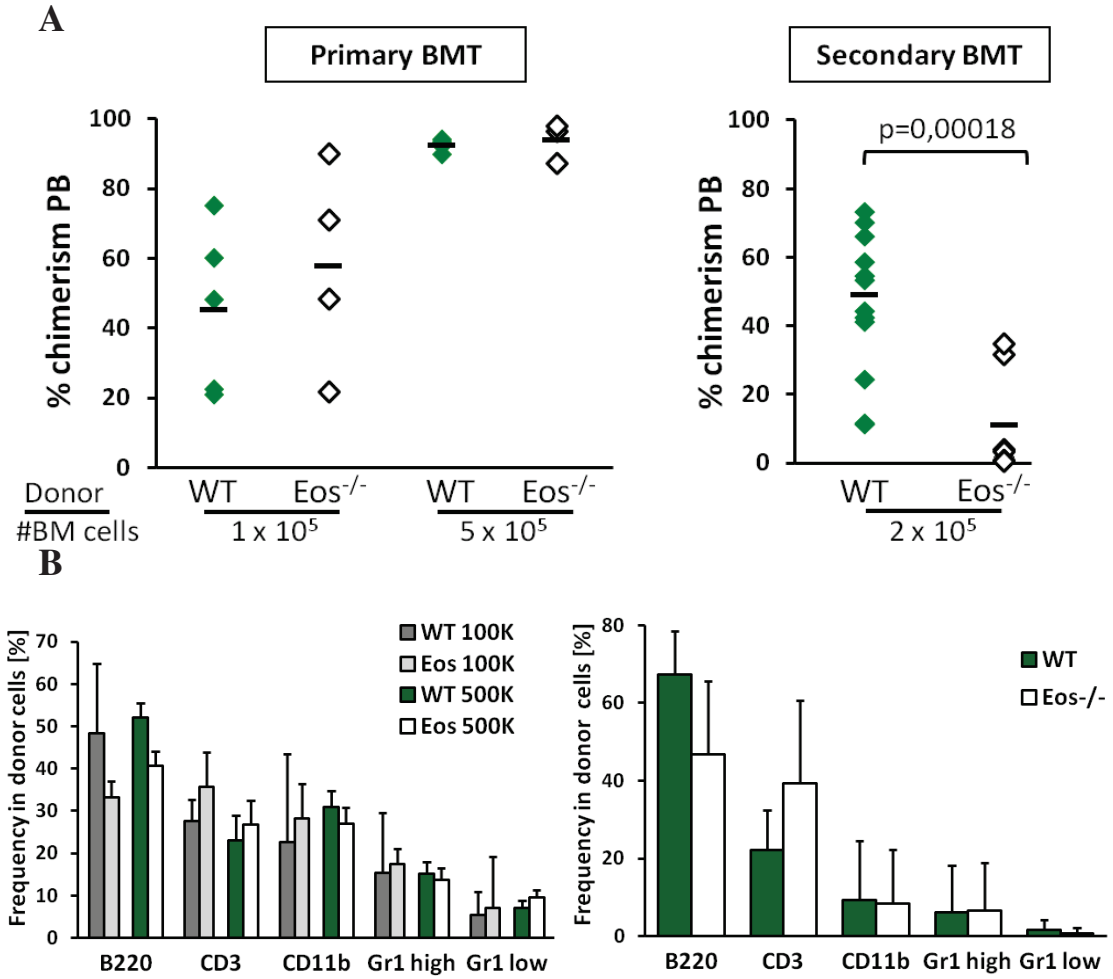

Figure III.9. Eos$^{-/-}$ BM cells reconstitute hematopoietic system similarly to WT cells in primary but not secondary bone marrow transplantations. A. In primary BMT mice were injected with either 1x10^5 or 5x10^5 total BM cells from WT or Eos$^{-/-}$ donors as indicated, together with 2x10^5 competitor cells. Percentage of chimerism (donor contribution) in the peripheral blood (PB) was assessed 6 months after transplantation. Each point on the graph represents one recipient mouse and line indicates mean of each group. Representative of 2 experiments (1x10^5: WT n=5 mice, Eos$^{-/-}$ n=4, 5x10^5: WT n=4 mice, Eos$^{-/-}$ n=3) (left). In secondary transplantations primary recipients with the highest chimerism from the group injected with 5x10^5 cells were sacrificed and BM cells were sorted to obtain CD45.2$^+$ donor cells that were then injected into new lethally irradiated recipients (2x10^5 cells plus 2x10^5 competitor cells). Percentage of chimerism in the peripheral blood was calculated 6 month after transplantation. Representative of 4 experiments (WT n=11 mice, Eos$^{-/-}$ n=8) (right). **B.** Peripheral blood of mice after primary (left) and secondary (right) transplantation was stained to evaluate the frequency of different lineages, as indicated by the markers on the graph, in the donor CD45.2$^+$ cells. Each graph corresponds to the experiment in the top panel. Bars represent mean with SD. 500K - 5x10^5, 100K - 1x10^5. BMT – bone marrow transplantation.

To complement the analysis in the peripheral blood, bone marrow of recipient mice was also analyzed. HSC staining was performed on bone marrow cells from primary recipients sacrificed to become BM donors for secondary transplantations, and at the end of the assays (after 6 months). This analysis didn't reveal why Eos$^{-/-}$ cells would be less efficient

in competitive reconstitution assays, as the HSC frequencies, including LT-HSCs, were usually similar to WT controls (Fig.III.10).

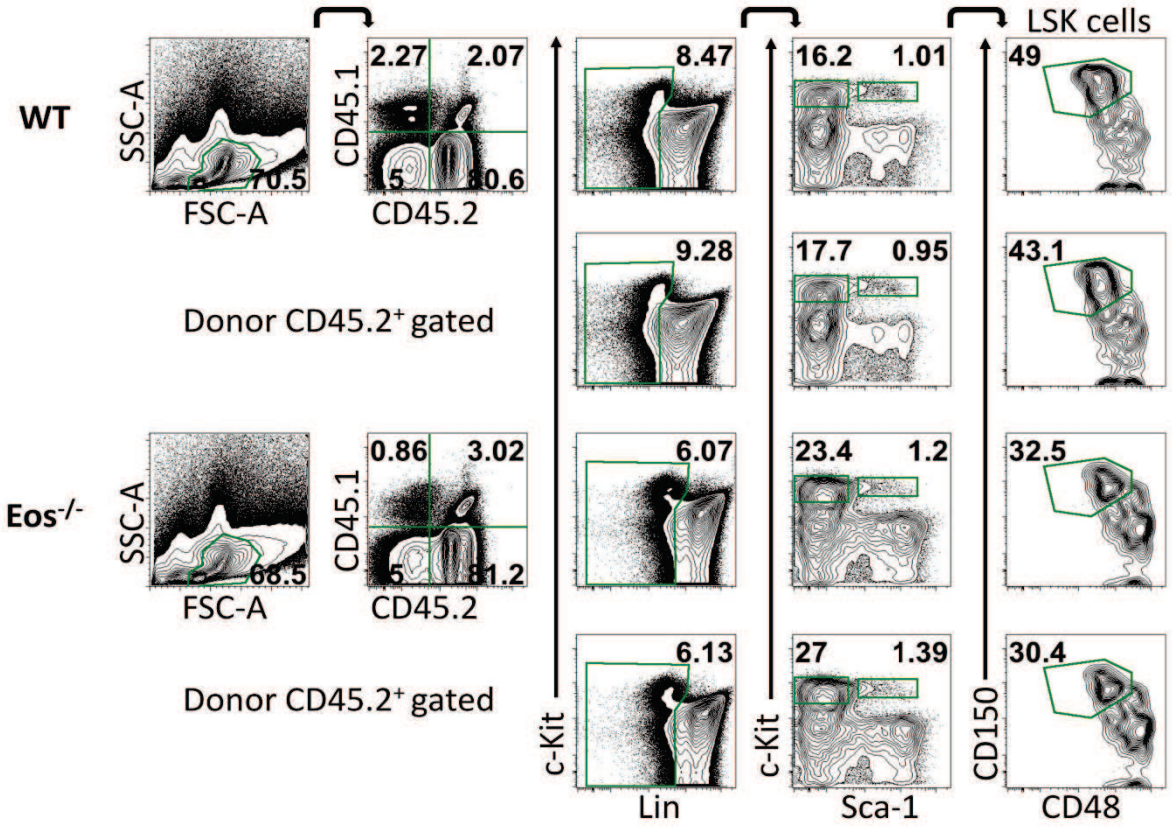

Figure III.10. Primary recipients of Eos$^{-/-}$ BM cells show similar HSC frequency to WT controls. Representative flow cytometry result and gating strategy to analyze hematopoietic stem cells in the bone marrow of transplanted mice. Gating on CD45.2^{+} cells allow to distinguish donor cells and analyze LT-HSCs (Lin^{-}Sca1^{+}c-Kit^{+}CD48^{-}CD150^{+}, comprised within LSK cells). BM comes from representative primary recipients used as donors for secondary transplantation.

To avoid a bias that could be caused by possibly different frequencies of HSCs in WT and KO mice, in parallel we used a more homogenous population in the transplantation assays and injected mice like previously, but with sorted LSK cells from WT and Eos$^{-/-}$ mice. Interestingly, Eos$^{-/-}$ cells showed less efficient reconstitution than WT cells but only up to two months following the primary experiment, after this time differences became less pronounced and mutant cells presented normal long-term repopulation potential (Fig.III.11A).

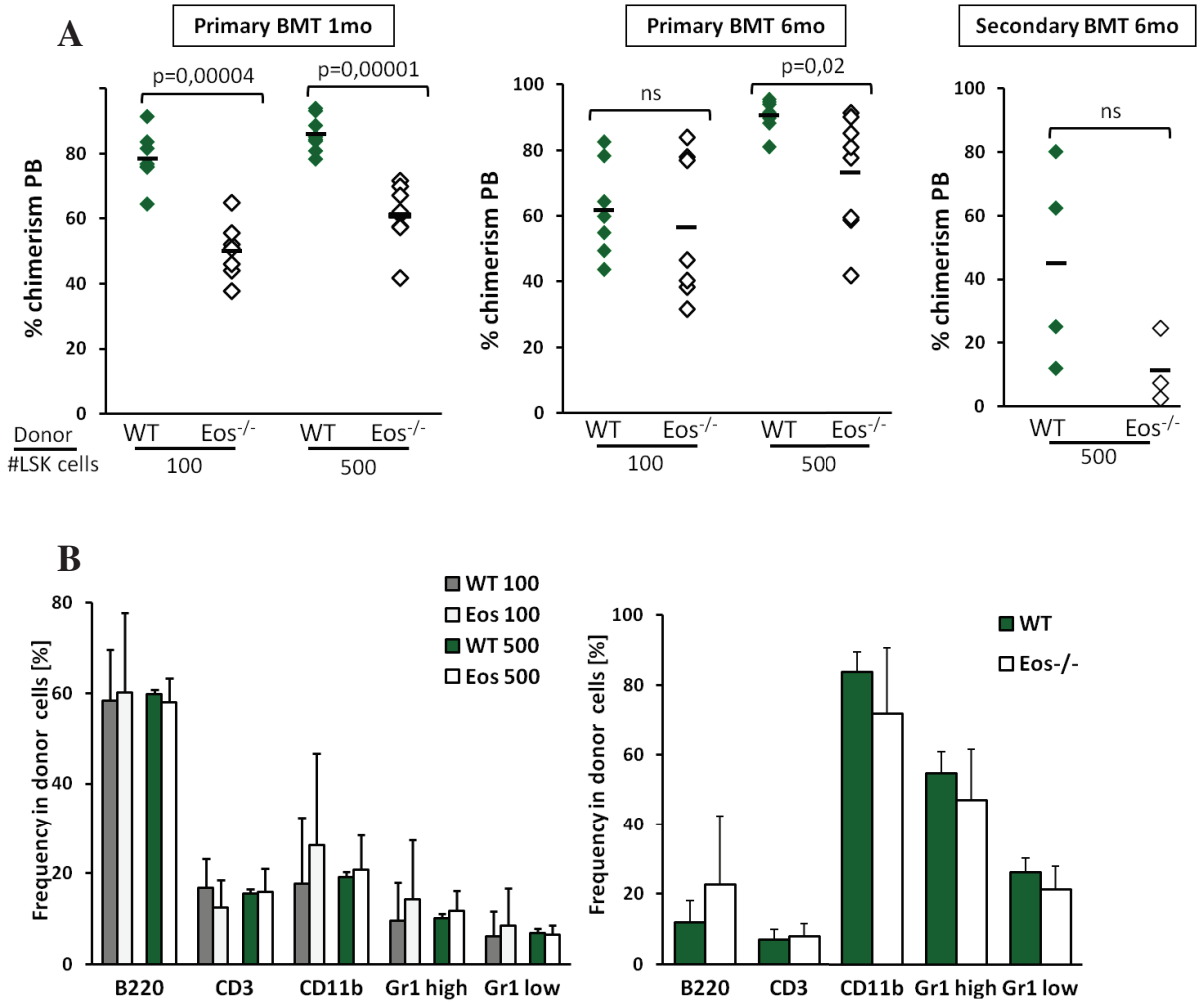

Figure III.11. Eos$^{-/-}$ LSK have inferior activity early during primary transplantation. A. In primary transplantation mice were injected with either 100 or 500 LSK cells from WT or Eos$^{-/-}$ donors as indicated, together with 2x10^5 competitor cells. Percentage of chimerism (donor contribution) in the peripheral blood (PB) was assessed 6 months after transplantation. Each point on the graph represents one recipient mouse and line indicates mean of each group. Representative of 2 experiments (100: WT n=7 mice, Eos$^{-/-}$ n=7, 500: WT n=8 mice, Eos$^{-/-}$ n=8) (left). In secondary transplantations primary recipients with highest chimerism from the group injected with 500 cells were sacrificed and donor LSK cells that were then injected into new lethally irradiated recipients (500 LSK cells plus 2x10^5 competitor cells). Percentage of chimerism in the peripheral blood was calculated 6 months after transplantation. Representative of 3 experiments (WT n=4 mice, Eos$^{-/-}$ n=3) (right). **B.** Peripheral blood of mice after primary (left) and secondary (right) transplantation was stained to evaluate the frequency of different lineages, as indicated by the markers on the graph, in the donor CD45.2$^+$ cells. Each graph corresponds to the experiment in the top panel.

In secondary transplantations with LSK cells, results showed more variability between transplanted mice and some animals were lost throughout the experiment. However Eos$^{-/-}$ cells appeared to have less ability for reconstitution. Finally, in both primary and secondary transplantations donor LSK cells from both genotypes similarly produced cells of different lineages that could be identified in the peripheral blood (Fig.III.11B). In conclusion,

serial competitive transplantation assays suggested that Eos$^{-/-}$ HSCs have less biological activity and particularly the phenotype observed in secondary transplantations indicated a decrease in their self-renewal potential.

III.1.2.2 *In vitro* proliferation and the DNA damage response of Eos$^{-/-}$ LSK cells

The early phenotype in primary transplantation with LSK cells could on the other hand suggest a proliferation problem of the mutant HSCs or aberrant response to stress conditions. Thus, we have measured the proliferation of LSK cell *in vitro* but observed no differences between WT and Eos null cells (Fig.III.12).

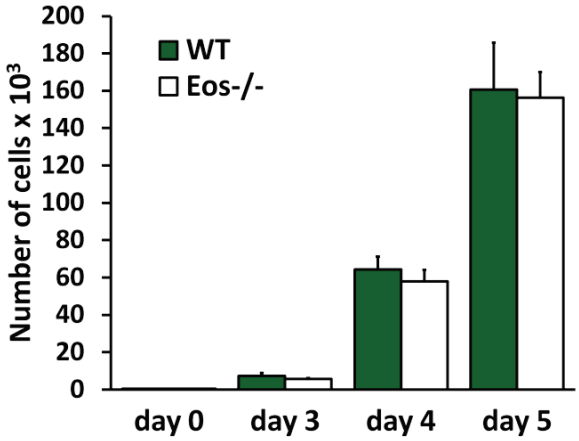

Figure III.12. Eos$^{-/-}$ LSK cells proliferate similarly to WT controls. LSK cells were sorted from the BM of WT and Eos$^{-/-}$ mice and cultured for 5 days in supplemented medium (IL-3 12,5 ng/ml, IL-6 10 ng/ml, TPO 50 ng/ml and SCF 50 ng/ml) starting with 600 cells. Bars represent mean with SD of a condition triplicate in one experiment.

As mentioned in the introduction Helios transcription factor plays a crucial role in maintaining genome stability of HSC cells. Namely, it regulates HSC response to stress, including DNA damage. Following this clue, we have analyzed DNA damage response of Eos$^{-/-}$ LSK cells by treatment with Neocarzinostatin (NCS), an agent that induces both single-strand and double-strand DNA breaks. However, Eos$^{-/-}$ LSK had a similar survival to WT cells after the NCS treatment (Fig.III.13).

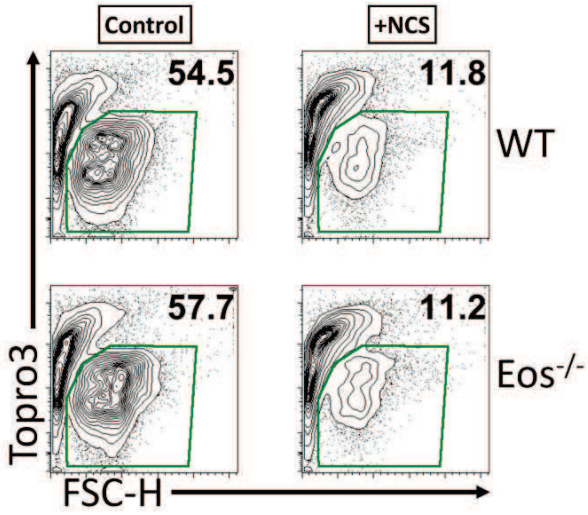

Figure III.13. Eos$^{-/-}$ LSKs have a normal response to DNA damage after NCS treatment. LSK cells were sorted from the BM of WT and Eos$^{-/-}$ mice, treated for 30 minutes with NCS (500 ng/ml) and cultured for 14 hours in supplemented medium (IL-3 12,5 ng/ml, IL-6 10 ng/ml, TPO 50 ng/ml and SCF 50 ng/ml). Viability of cells after treatment was verified by Topro3 staining.

III.1.2.2 Production of hematopoietic progenitors by Eos$^{-/-}$ cells

We have then decided to analyze the ability of Eos$^{-/-}$ BM cells to produce hematopoietic progenitors and performed colony-forming cell assays (CFC). We have used total BM cells and studied only myeloid lineage in the CFC assay. Firstly, results showed that Eos$^{-/-}$ BM cells can produce significantly less colonies in the methylcellulose medium (Fig.III.14A/B).

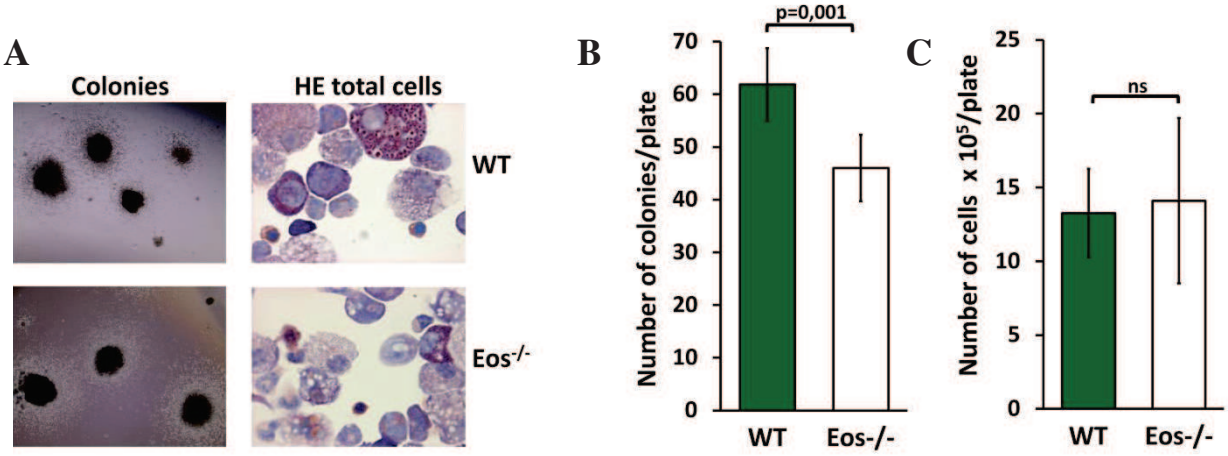

Figure III.14. Eos$^{-/-}$ BM cells produce less hematopoietic progenitors in CFC assay. Total bone marrow cells (50,000) were cultured for 8 days after placing into semi-solid methylcellulose medium, supplemented with nutrients and cytokines (rmSCF, rmIl-3, rmIL-6, rhEpo). In this matrix, individual progenitors (colony-forming cells) proliferate to form cell clusters or colonies from myeloid lineages. **A.** Examples of colonies obtained after 8 days of culture (left) and profile of pooled colonies after Hematoxylin and Eosin stainining (HE)**. B.** Number of colonies from one cell culture dish. Bars represent mean with SD from 2 experiments (with 2 mice per genotype, duplicates of each condition).**C.** Number of cells from one cell culture dish. Bars represent mean with SD from 2 experiments.

At the same time there was no difference in the total cell number recovered from a single plate suggesting a defect in colony forming by Eos null cells (Fig.III.14C). We also tried to study the phenotype of obtained colonies, by looking at their morphology and by analyzing total cells and single colonies by HE staining (Fig.III.14A). However, we could not observe any differences in the formation of particular colony forming units. We have then used flow cytometry to evaluate the formation of myeloid cells in a more quantitative manner using flow cytometry. Staining showed that there is no difference in the frequency of analyzed populations (erythroid, granulocytic or progenitor cells) between genotypes indicating that probably the observed phenotype is only quantitative but not qualitative (Fig.III.15A/B).

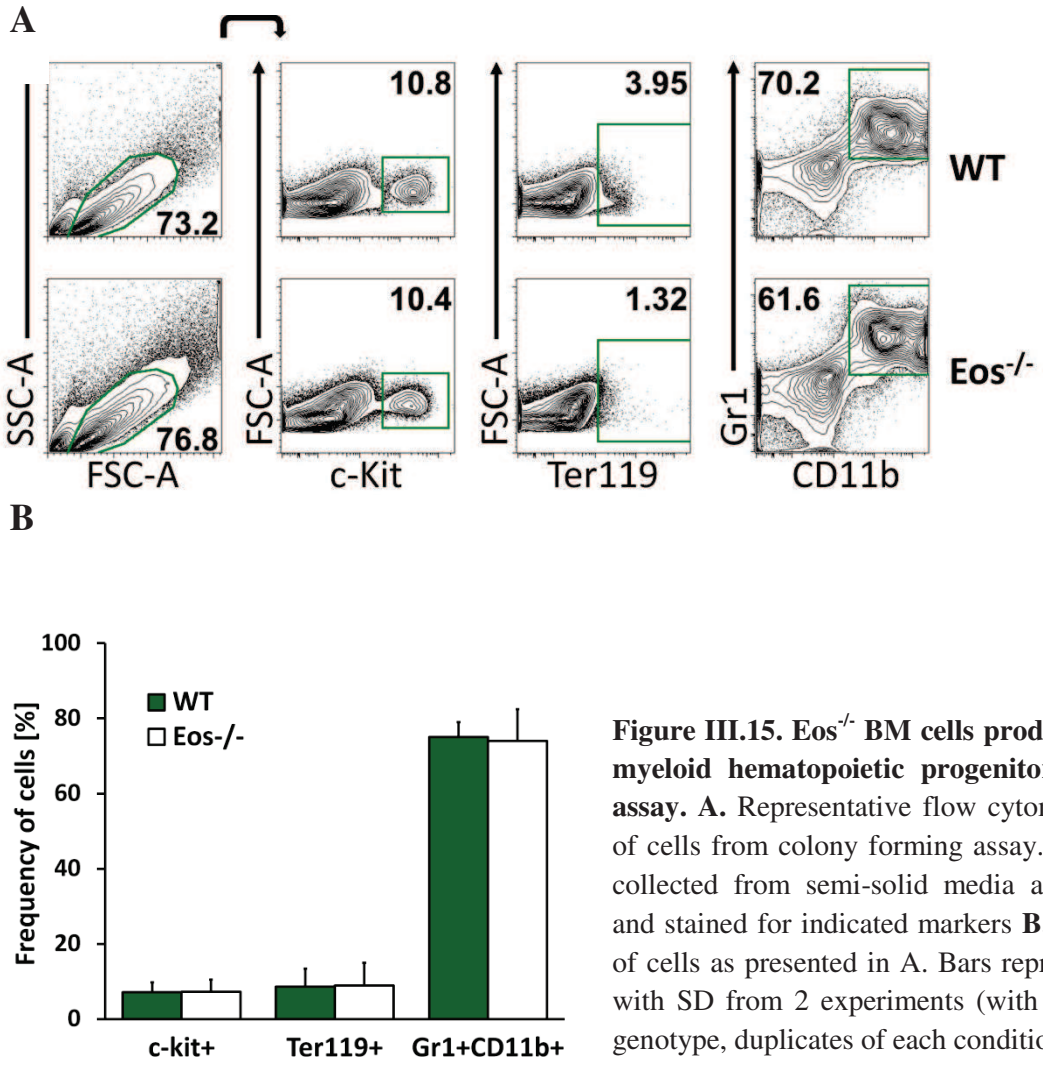

Figure III.15. Eos$^{-/-}$ BM cells produce similar myeloid hematopoietic progenitors in CFC assay. A. Representative flow cytometry result of cells from colony forming assay. Cells were collected from semi-solid media after 8 days and stained for indicated markers **B.** Frequency of cells as presented in A. Bars represent mean with SD from 2 experiments (with 2 mice per genotype, duplicates of each condition).

In conclusion, performed experiments indicate that Eos deficient cells have normal HSC compartment during homeostasis. At the same time, during proliferative stress induced in serial transplantations, they have less biological activity and appear to have defective self-renewal properties (primary and secondary bone marrow transplantations). However, they proliferate normally and have response to DNA damage similar to WT cells. In colony formation assay Eos null bone marrow cells produce slightly less hematopoietic progenitors (colonies), but of the same phenotype, giving inconclusive observations. All these results indicate that Eos may regulate a different HSC function, or the observed phenotype is specific to the system used.

III.2 Ikaros regulation of Polycomb function

During the first year of my thesis, while setting up and characterizing the Eos null mouse model, I participated in a project concerning the role of Ikaros in modeling the chromatin landscape within the hematopoietic compartment. A manuscript describing this project is presented in the appendix (Oravecz et al., 2015).

In the next sections I present results concerning the new mouse strain, which I characterized. As this project is not related to my main PhD subject, I also give a brief background to the subject.

III.1.1 Studying the role of Ikaros and Polycomb function in T cells

Ikaros is well known as a tumor suppressor in the hematopoietic system. Mutations leading to a decreased Ikaros function or expression were found to be major characteristics of B-ALL (B-cell acute lymphoblastic leukemia) (Mullighan et al., 2008). In mice, Ikaros acts as a tumor suppressor also in the T cell lineage and Ikaros deficient mice develop aggressive T cell lymphomas at early age (Dumortier et al., 2006; Winandy et al., 1995). It has been shown that Ikaros is expressed in T cells, can bind to and directly repress expression of many target genes in the T cell lineage (Geimer Le Lay et al., 2014; Zhang et al., 2012). Interestingly, ChIP sequencing analysis of epigenetic marks in Ikaros deficient T cells showed a widespread decrease or loss of the PRC2 dependent H3K27me3 repressive mark (Kleinmann et al., 2008). This indicates that Ikaros may repress the expression of its target genes by epigenetic mechanisms. Recent results from our group indicate that Ikaros is required to establish the H3K27me3 mark during T cell differentiation, as this epigenetic modification is lost in Ikaros deficient cells for several genes expressed in hematopoietic stem cells but repressed during T cell development (Fig.III.16). Moreover, it has been shown that Ikaros interacts with components of PRC2 complex, suggesting that H3K27me3 modification is a direct effect of Ikaros binding (Oravecz et al., 2015).

H3K27me3 modification is deposited by PRC2 complex, a member of Polycomb group, with Ezh2 as its catalytic subunit (Rea S et al., 2000). Ezh2 also plays a role in T cell differentiation and function (Zhang et al., 2014) and similarly to Ikaros inactivating mutations correlate with appearance of hematological malignancies, particularly leukemias, including T-ALL (T-cell lymphoblastic leukemia) (Ntziachristos et al., 2012). We wanted to elucidate how Ikaros regulates Polycomb function and H3K27 tri-methylation and build a project to address this question using an *in vivo* model. To do so, we generated transgenic (Tg) mice

deficient in the methyltransferase Ezh2 and crossed them with Ikaros deficient mice in order to obtain double heterozygous mice. We thought that this model would help us to determine the level of "cross-talk" between Ikaros and Polycomb and if Polycomb is required for Ikaros function *in vivo*.

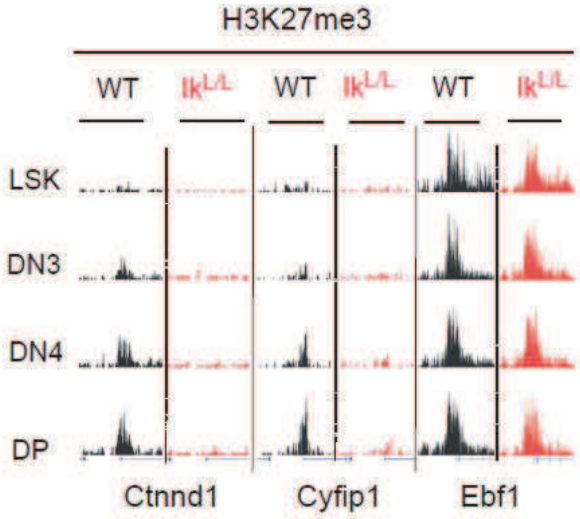

Figure III.16. Ikaros is required to establish H3K27me3 mark in developing T cells. (Reproduced from Oravecz et al., submitted manuscript). ChIP-seq profiles in bone marrow LSK cells and DN3, DN4 and DP stages of T cell differentiation for genes affected (Ctnnd2, Cyfip1) and not affected (Ebf1) in Ikaros deficient mice ($Ik^{L/L}$) mice.

We hypothesized that a resulting phenotype would be observed in developing T cells, and that a change in the H3K27me3 modification and a change in the expression of Ikaros target genes could be detected in T cells. During this project I collaborated with Attila Oravecz a post-doctoral fellow of our laboratory, who performed the gene expression analysis and ChIP experiments, while I developed my knowledge and new competences for maintaining and characterizing a novel mouse model.

The characterization of the mouse model included:

- Analyzing T cell differentiation in Ezh2 transgenic mice during steady-state by flow cytometry
- Verifying the presence of the reporter transgenic construct in Ezh2 Tg mice
- Verifying the Ezh2 haploinsufficiency at the protein level and mRNA level in Ikaros/Ezh2 double heterozygous mice
- Studying hematopoiesis and T cell differentiation in Ikaros/Ezh2 double heterozygous mice during steady-state by flow cytometry
- Studying the T cell compartment of Ikaros/Ezh2 double heterozygous mice at a molecular level by measuring H3K27me3 and expression of Ikaros target gene in T cells.

III.1.2 Generation and characterization of mice deficient in Ikaros and Ezh2

To obtain mice with Ikaros and Ezh2 deficiency we crossed two mouse lines. First, we used Ikaros deficient mice, designated as $Ik^{L/L}$. These mice were generated and characterized previously in the lab (Kirstetter et al., 2002; Dumortier et al., 2006). This model was obtained by the insertion of β-galactosidase reporter (lacZ) cassette into the second protein coding exon of *Ikzf1* gene and resulted in a hypomorphic mutation, as 10% of WT Ikaros protein could be still expressed. We obtained Ezh2 deficient mice as knock-out first allele strain, with a reporter lacZ cassette inserted upstream of the exon 5, present in all splicing variants of Ezh2 transcript. Insertion of this cassette results in a disruption of the gene and expression of lacZ reporter (Fig.III.17). We designated the Ezh2 transgenic line as $Ezh2^{Tg}$.

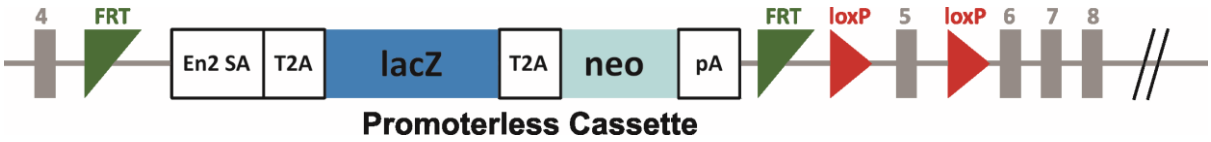

Figure III.17. Map of the *Ezh2* transgenic allele. The inserted cassette is composed of an FRT flanked lacZ/neomycin sequence followed by a loxP site. An additional loxP site is inserted downstream of the targeted exon. A "conditional ready" (floxed) allele can be created by flp recombinase expression and Cre expression can result in a knock-out mouse. If Cre expression occurs without flp expression, a reporter knock-out mouse can be created. The En2 SA sequence (splice acceptor) within the intron of an expressed gene together with the polyA signal interrupts endogenous splicing. T2A self-cleaving peptides replace classical IRES sequence and provide the excision of lacZ reporter cassette.

PRC2 was previously shown as essential during development as deletion of Ezh2 in mice results in early embryonic lethality and Ezh2 null mice die early during gastrulation (O'Carroll et al., 2001). In our Ezh2 transgenic line in a cross between heterozygous mice no $Ezh2^{Tg/Tg}$ mice were born. This confirmed that our construct was fully functional and disrupted efficiently Ezh2 protein causing early lethality in homozygous mice. Thus, in the following experiments we always used mice with only one transgenic allele designated as $Ezh2^{Tg/+}$. First, the steady state hematopoiesis of $Ezh2^{Tg/+}$ mice was analyzed by flow cytometry. No changes were observed in the various subpopulations of hematopoietic system, including hematopoietic stem and progenitor cell compartment and both myeloid and lymphoid lineages (data not shown). The T cell development was also not affected. Thymic T cell populations including DN1-DN4, (DN1: $Lin^-CD44^+CD25^-$, DN2: $Lin^-CD44^+CD25^+$, DN3: $Lin^-CD44^-CD25^+$, DN4: $Lin^-CD44^-CD25^-$), DP ($CD4^+CD8^+$), $CD4^+$, $CD8^+$ and Treg ($CD4^+CD25^+$) were similar between WT and $Ezh2^{Tg/+}$ mice (Fig.III.18). In the spleen, $CD4^+$

and $CD8^+$ T cells were normal with similar proportions of naïve ($CD44^{lo}CD62L^{hi}$) and memory/effector cells ($CD44^{hi}CD62L^{lo}$) and Treg cells.

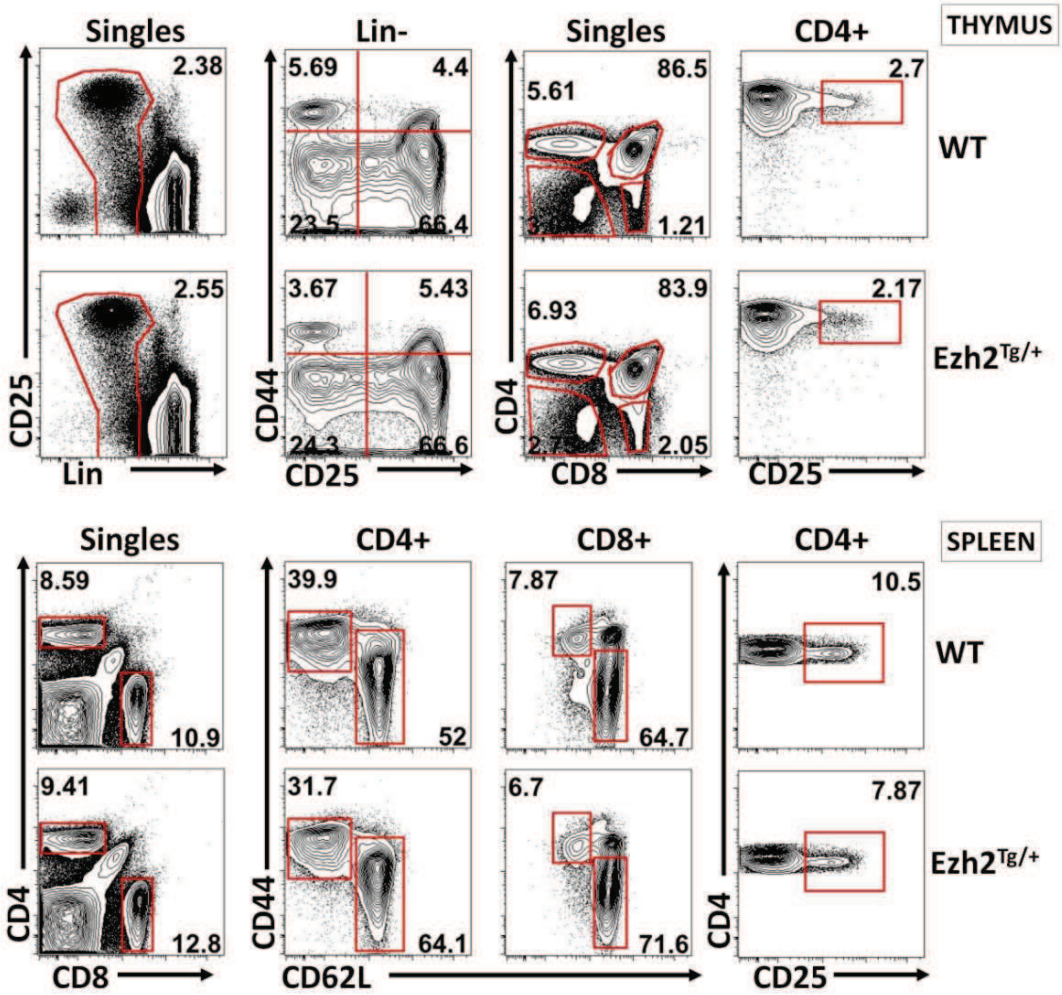

Figure III.18. Ezh2$^{Tg/+}$ mice have normal T cell development. Representative flow cytometry results in thymic (top) and splenic (bottom) T cells analyzed for expression of indicated markers in Ezh2$^{Tg/+}$ and WT mice. Lin- (Lineage negative: $CD4^-$, $CD8^-$, $CD3^-$, $B220^-$, $Gr1^-$, $CD11b^-$, $Nk1.1^-$) Gated population is indicated on the top of each panel.

To validate the developed reporter strain the activity of lacZ (β-galactosidase) was assessed by flow cytometry using FDG (Fluorescein β-D-Galactopyranoside) substrate. Firstly, total thymocytes from Ezh2$^{Tg/+}$ mice showed expression of fluorescein after the FDG treatment (Fig.III.19A). As the aim of this project was to see the possible cross-talk between Ikaros and Ezh2 in developing thymocytes it was also interesting to verify through the reporter how Ezh2 is expressed in the T cell lineage. Expression was analyzed in immature thymocytes from DN1 to DN4 stages, DP cells as well as $CD4^+$ and $CD8^+$ SP thymocytes. Its highest expression was detected in DN cells, particularly in DN3, DN4 and DN2

(Fig.III.19B). This correlated with Ikaros expression in thymocytes which peaks at DN4 stage (Kleinmann et al., 2008).

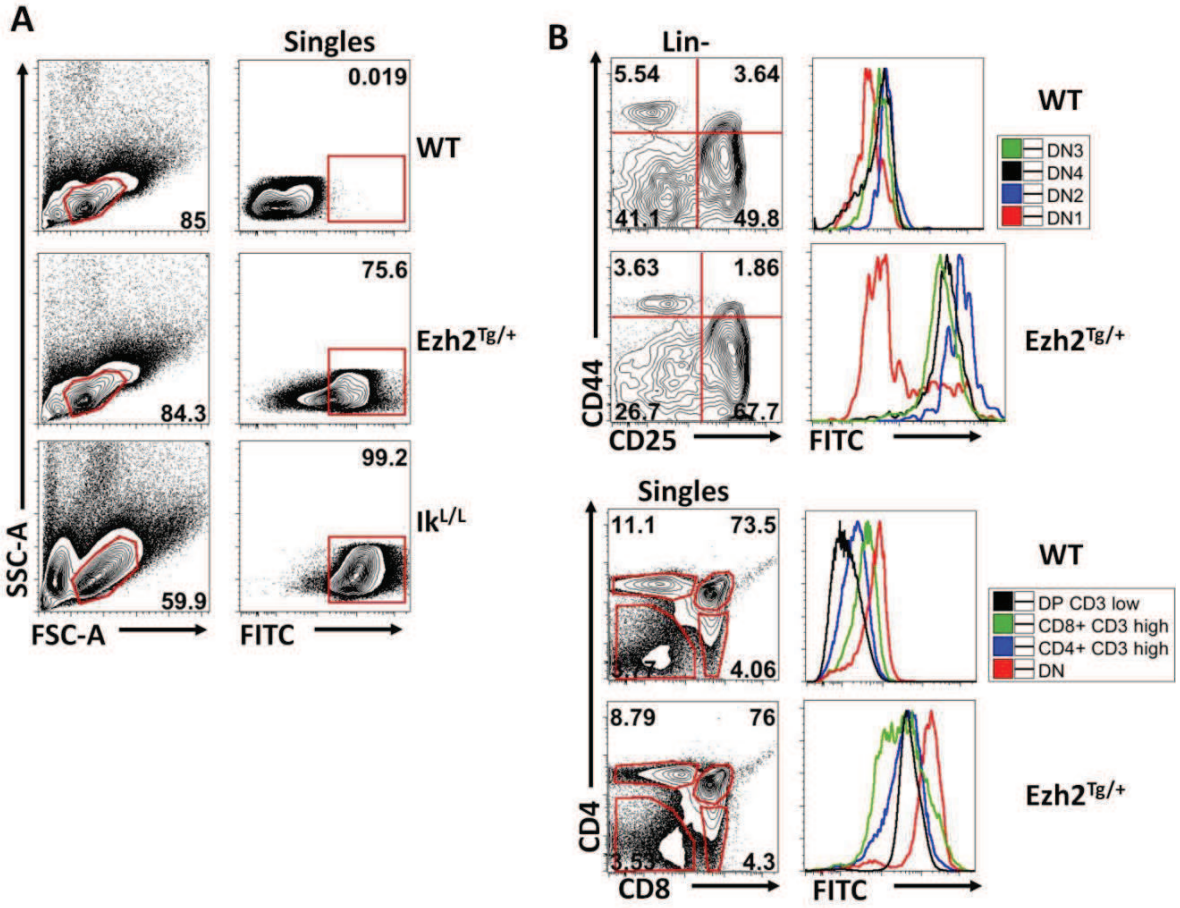

Figure III.19. LacZ reporter shows Ezh2 expression in developing T cells. LacZ cassette detection by flow cytometry measured as β-galactosidase activity. Treatment of cells expressing lacZ with FDG substrate will result in hydrolysis of the FDG and production of fluorescein that can be detected by flow cytometry in FITC channel. A) Total thymocytes from $Ezh2^{+/+}$, $Ezh2^{Tg/+}$ and $Ik^{L/L}$ (positive control) analyzed to detect lacZ expression. B) Analysis of lacZ expression (Ezh2) in different stages of T cell differentiation; DN1-DN4 (left); DN, DP ($CD3^{lo}$), $CD4^{+}$ ($CD3^{hi}$), $CD8^{+}$ ($CD3^{hi}$) in $Ezh2^{+/+}$ and $Ezh2^{Tg/+}$ cells (right). Gated population is indicated on the top of each panel.

Simultaneously, western blot experiments showed that there is no decrease in the expression of Ezh2 at the protein level in transgenic thymocytes and splenocytes (Fig.III.20). Results presented above show that Ezh2 is expressed during T cell differentiation and that $Ezh2^{Tg/+}$ have no phenotypic abnormalities and have normal T cell development. Lack of any phenotype could be partially explained by the fact that loss of one functional allele of Ezh2 was not sufficient to decrease significantly Ezh2 protein levels (Fig.III.20).

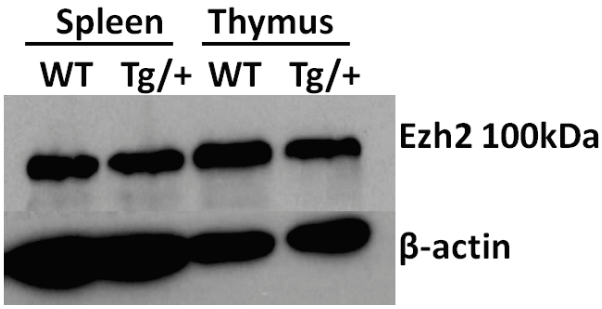

Figure III.20. Ezh2 protein level in transgenic mice. Western blot analysis of Ezh2 protein in total splenocytes and thymocytes of WT and Ezh2 transgenic mice (Tg/+).

After establishing the $Ezh2^{Tg/+}$ line in the SPF animal facility mice were crossed with previously mentioned $Ik^{L/L}$ mice. These mice develop T cell-acute lymphoblastic lymphomas/leukemias (T-ALL) with 100% penetrance and die at 4 to 6 months of age. For that reason, in all analyses young mice between 4-6 weeks of age were used, before the disease could manifest. We have also analyzed only mice heterozygous for both Ikaros and Ezh2 deficiency ($Ik^{+/L}Ezh2^{Tg/+}$), as full Ikaros deficiency could mask the anticipated result. First, the thymocytes of $Ik^{+/L}Ezh2^{Tg/+}$ mice and controls were analyzed for Ezh2 expression. Despite a non-altered Ezh2 protein in $Ezh2^{Tg/+}$ mice, as expected we observed a decrease of mRNA expression (Fig.III.21). Interestingly Ezh2 had a higher expression in $Ik^{+/L}$ mice than in WT, but in double heterozygous $Ik^{+/L}$ $Ezh2^{Tg/+}$ it had an expression comparable to $Ezh2^{Tg/+}$ mice.

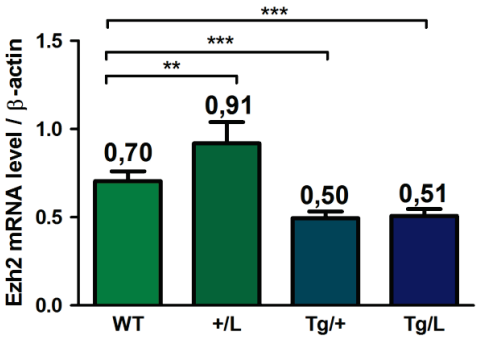

Figure III.21. Ezh2 expression in $Ik^{+/L}$ $Ezh2^{Tg/+}$ mice. Ezh2 mRNA levels in total thymocytes from WT, $Ik^{+/L}$ (+/L), $Ezh2^{Tg/+}$ (Tg/+) and $Ik^{+/L}$ $Ezh2^{Tg/+}$ (Tg/L) mice analyzed by RT-qPCR and normalized to β-actin. Mean expression levels with SD from 3 independent experiments.

The following step in the analysis of the new line was to look at hematopoiesis during homeostasis. Major populations of hematopoietic system were analyzed by flow cytometry in the thymus spleen and bone marrow of $Ik^{+/L}Ezh2^{Tg/+}$ mice and control littermates. The analysis included all steps of hematopoiesis starting from hematopoietic stem cells (including LT-HSC and ST-HSC), progenitor cells (MPP, MEP, GMP) and mature populations of both lymphoid (subtypes of B cells, T cells, dendritic cells) and myeloid lineage (monocytes, granulocytes, dendritic cells). The most immature cells had normal proportions in $Ik^{+/L}Ezh2^{Tg/+}$ when compared to controls. In some cases we have observed changes in

dendritic cell populations, but only in $Ik^{+/L}Ezh2^{Tg/+}$ and $Ik^{+/L}$ samples, confirming an already described defect related to Ikaros deficiency (Allman et al., 2006). However, most mature cells from both lymphoid and myeloid lineage had correct and similar frequencies as analyzed in the bone marrow and spleen (Fig.III.22).

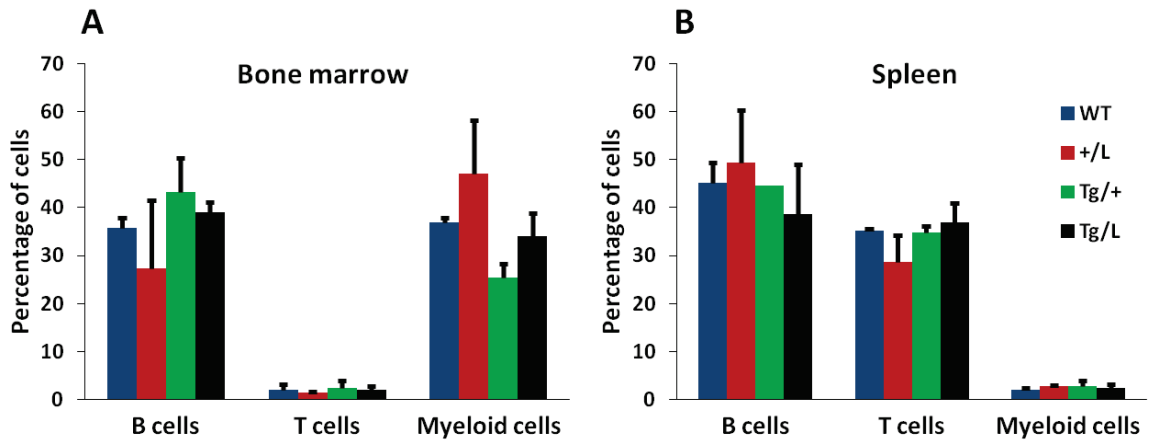

Figure III.22. Lymphoid and myeloid cells in $Ik^{+/L}Ezh2^{Tg/+}$ mice. Percentage of populations representing lymphoid lineage: B cells ($B220^+$), T cells ($CD3^+$) and myeloid lineage ($CD11b^+Gr1^+$) from flow cytometry analysis in WT, $Ik^{+/L}$ (+/L), $Ezh2^{Tg/+}$ (Tg/+) and $Ik^{+/L}$ $Ezh2^{Tg/+}$ (Tg/L) in A) bone marrow and B) spleen. Percentage of cells gated on live cells and singles. Error bars represent SD. Data from 2 independent experiments with 2 mice of each genotype per experiment.

We also analyzed in detail populations of the T cell lineage. As previously mentioned only young mice were analyzed, though even in a 5 week old $Ik^{+/L}$ mouse we could find disease symptoms, including cystic kidneys and thymus changes. Thus, only healthy mice were analyzed and we looked at general proportions of cell populations. Frequencies of thymic and splenic populations were analyzed like previously for $Ezh2^{Tg/+}$ mice by flow cytometry. Results showed that T cells in the thymus of $Ik^{+/L}Ezh2^{Tg/+}$ undergo normal differentiation from double negative stages to single positive $CD4^+$ and $CD8^+$ mature cells. In the periphery (spleen) T cells also appear with normal proportions and no major differences between analyzed genotypes (Fig.III.23A/B). These results suggest that during homeostasis the loss of one allele of Ezh2 complemented by Ikaros haploinsufficiency do not impair more the hematopoiesis and in particular T cell development.

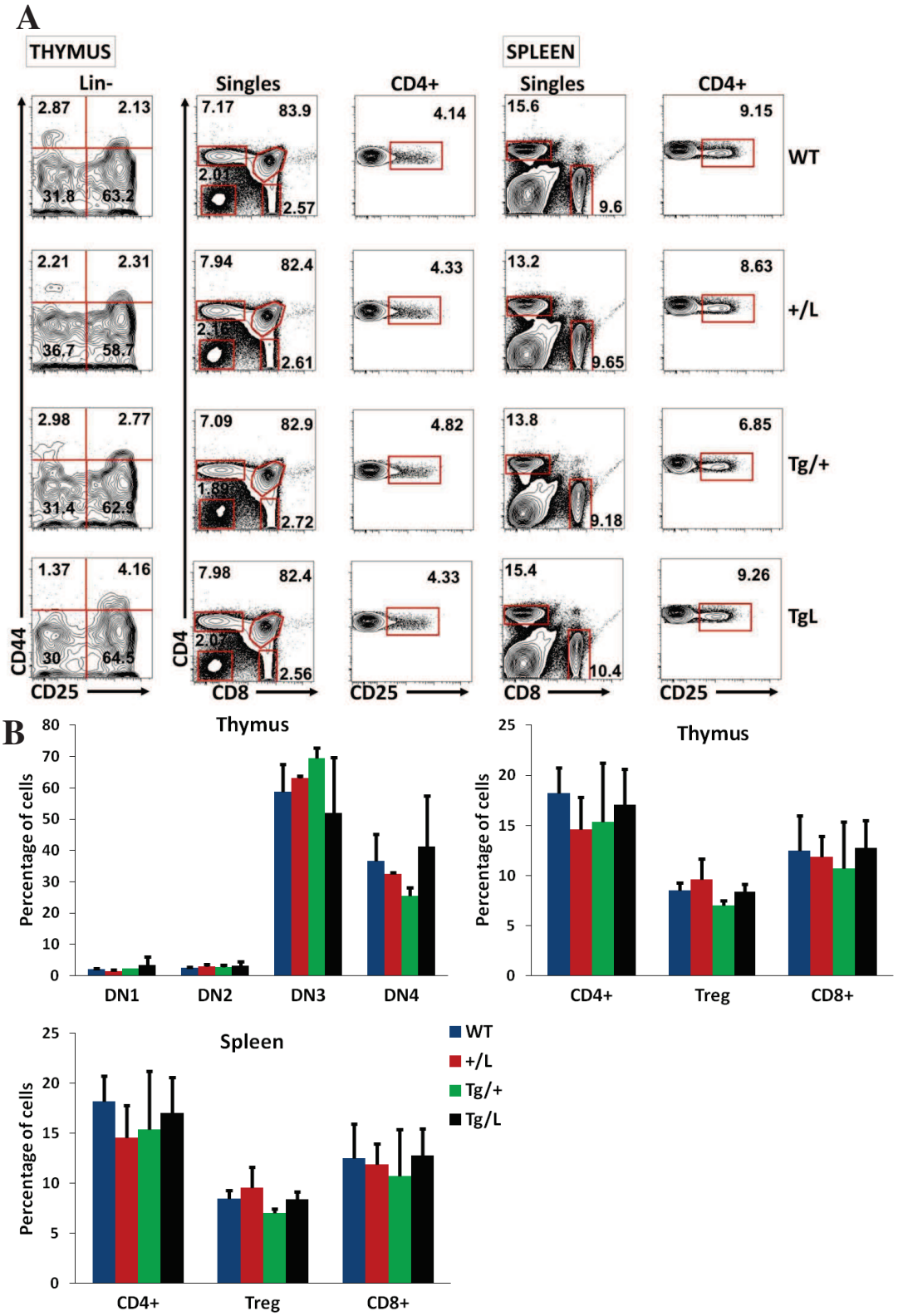

Figure III.23. T cells in Ik$^{+/L}$Ezh2$^{Tg/+}$ mice. A) Representative flow cytometry plots from T cells analyzed in the thymus (left) and spleen (right) of WT, Ik$^{+/L}$ (+/L), Ezh2$^{Tg/+}$ (Tg/+) and Ik$^{+/L}$ Ezh2$^{Tg/+}$ (Tg/L) mice, gated population is indicated on the top of each panel. B) Percentage of T cell populations analyzed by flow cytometry in the thymus for expression of indicated cell surface markers identifying DN1-DN4 populations, CD4^{+}, CD8^{+} and Treg cells; and spleen: CD4^{+}, CD8^{+} and Treg. Lin- (Lineage negative: CD4^{-}, CD8^{-}, CD3^{-}, B220^{-}, Gr1^{-}, CD11b^{-}, Nk1.1^{-}), DN (double negative). Error bars represent SD. Data from 2 independent experiments with 2 mice of each genotype per experiment.

These results suggested that during homeostasis loss of one allele of Ezh2 on the top of Ikaros haploinsufficiency do not impair the hematopoiesis and in particular T cell development.

III.1.3 H3K27me3 and expression of Ikaros target gene in $Ik^{+/L}Ezh2^{Tg/+}$ mice

H3K27me3 mark can be lost or decreased in the absence of Ikaros, thus we hypothesized that the removal of Ezh2 could result in a stronger loss of H3K27me3 and at the same time increase in the expression of genes identified as regulated by Ikaros in T cells. To confirm this, we proceeded in two steps. First, we sorted cells from the thymus to perform H3K27me3 ChIP-qPCR on chromatin from DP cells. As expected, when compared to WT sample we observed a reduction in H3K27me3 levels in the $Ik^{+/L}$ sample in selected genes (*Mpzl2* and *Ctnnd*). However, we observed no change in H3K27me3 in $Ezh2^{Tg/+}$ and the $Ezh2^{Tg/+}Ik^{+/L}$ sample had a H3K27 methylation level similar to the $Ik^{+/L}$ sample, indicating that only Ikaros dependent changes were detected (Fig.III.24A). Second, we studied the expression of the same genes in DN3, DN4 and DP cells. We emphasize here that these results were obtained from analyzing samples from only two or in some cases one mouse. However, the decrease of H3K27me3 observed in $Ik^{+/L}$ samples on selected genes correlated with their increased expression levels. Nevertheless, no stronger up-regulation of these genes was detected in $Ik^{+/L}Ezh2^{Tg/+}$ samples, when compared to $Ik^{+/L}$ controls. Moreover, there was also no gene expression change in the $Ezh2^{Tg/+}$ sample (Fig.III.24B).

To conclude, our experiments performed on this mouse model could not demonstrate the synergy between Ikaros and Polycomb to impair hematopoiesis and in particular gene repression. The expected increase in the loss of H3K27me3 mark did not occur, as well as significant changes in the expression of Ikaros target genes in T cells.

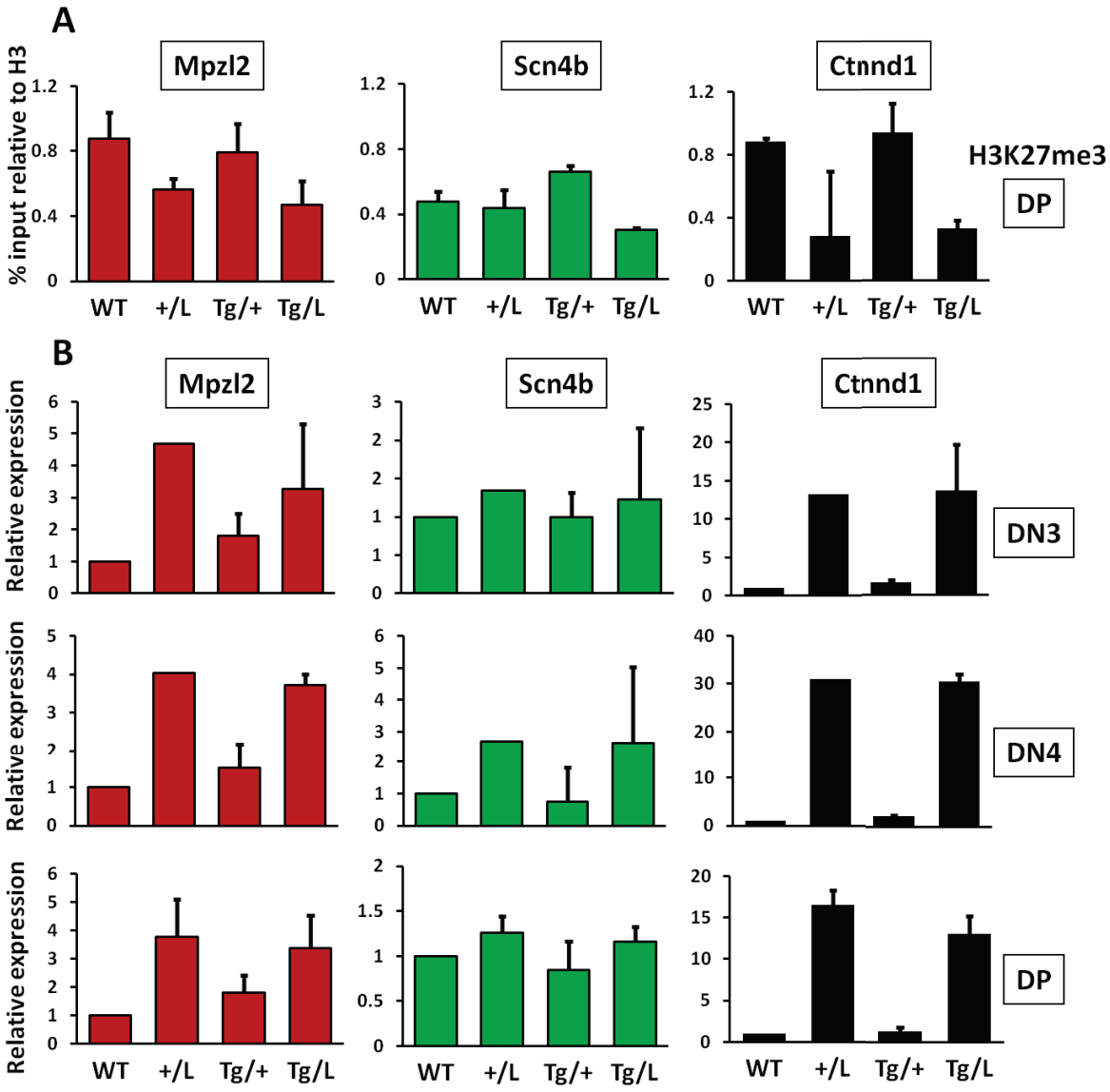

Figure III.24. H3K27me3 and expression of Ikaros target genes in $Ik^{+/L}Ezh2^{Tg/+}$ T cells. A) H3K27me3 ChIP-qPCR on chromatin from DP cells for three selected genes (*Mpzl2*, *Scn4b*, *Ctnnd1*). Results obtained from 2 samples per genotype. Error bars represent SD. B) mRNA expression levels of Mpzl2, Scn4b, Ctnnd1 in DN3, DN4 and DP cells. Normalized to 28S RNA (DP cells, Ctnnd1 in DN3 cells) and β-actin (remaining samples). Results obtained from 2 samples per genotype in DP cells, only one for +/L in DN3 and DN4. Error bars represent SD. +/L ($Ik^{+/L}$), Tg/+ ($Ezh2^{Tg/+}$) and Tg/L ($Ik^{+/L}$ $Ezh2^{Tg/+}$).

CHAPTER IV DISCUSSION

IV.1 What are the roles of Eos and Helios in Treg cell biology?

In the manuscript presented in chapter III.1.1.1 we show that, despite its high expression levels, Eos deficiency does not impair the differentiation and function of natural $CD4^+CD25^+$ Treg cells in mice, as studied *in vitro* in a suppression assay and suggested *in vivo* from preliminary results of the colitis experiment (III.1.1.2). Moreover, $Eos^{-/-}$ mice do not show any abnormalities during steady state hematopoiesis and remain healthy up to 2 years of age. Lack of an apparent phenotype was unexpected as we hypothesized that Eos null mice may present a specific phenotype, reflecting its expression and similarities to other Ikaros proteins.

Why do Eos deficient mice not show any apparent phenotype?

Eos expression can be detected outside of the hematopoietic system, in tissues of several organs including the developing nervous system, testis and unspecialized cell lines (ES cells). Interestingly, high levels of Eos can be also found in the amnion sac protecting the developing embryo, all together pointing at the importance of Eos during development and in unspecialized cells (chapter I.4.4, EMBL-EBI Expression Atlas). However, $Eos^{-/-}$ mice did not show any developmental defects either early during postnatal life or later in adulthood.

At the same time, within the hematopoietic system, Eos has a very distinct expression pattern, suggesting that its high levels may be important in HSCs and Treg cells (chapter I.4.4, Fig.III.1). Indeed, Eos appears to play a role in the HSC compartment, which is discussed in section IV.2, but not in Treg cells. From these observations we could hypothesize that Eos is either dispensable during homeostasis or its function can be compensated by another factor, possibly Helios, considering their high homology and the recent evolutionary emergence of the Ikaros family (chapter I.4; John et al., 2009) .

In regards to the first hypothesis, the absence of any phenotype related to Treg cells in $Eos^{-/-}$ mice was intriguing, especially in the light of the study by Pan et al., who showed that Eos is required for Treg cell function, and particularly for Foxp3 mediated gene regulation in $CD4^+$ Treg cells and their suppression activity (Pan et al., 2009). These discrepancies may result from different experimental systems. Pan et al. used siRNA to knock-down Eos in a T

cell line in experiments showing Eos interaction with Foxp3, and in primary Treg cells in suppression assays and *in vivo* experiments. Although the efficiency of the knock-down was high and the observed loss of suppressive activity could be rescued by the expression of functional Eos, these conditions were far from physiological. For the suppression assays and *in vivo* experiments these authors used freshly purified $CD4^+CD25^+$ Treg cells, which were transduced with anti-Eos siRNA. Cells were cultured for 40h after infection prior to sorting for positively transduced cells, and additionally during the last 24h they were supported by the presence of rhIL-2. Their results do not indicate whether, during this time, the cells were analyzed for Treg markers, including Foxp3, or how much they proliferated, leaving the chance that phenotypically distinct cells were used at the end of the experiments and not nTreg cells (Pan et al., 2009). This possibility is particularly plausible in regards to other observations from the same study and others, which suggested that loss of Eos promotes the conversion of a Treg cell to an effector-like T cell, perhaps because these cells are less stable and prone to further differentiate under certain conditions (discussed in chapter I.6.2.1, Sharma et al., 2013). The study by Sharma et al. showed that it is the $CD4^+CD38^+CD103^-$ population of Treg cells which is "labile" and susceptible to the loss of Eos and phenotypical conversion. We have also analyzed this population by flow cytometry and found that it is present in normal proportions in $Eos^{-/-}$ Treg cells, suggesting that Eos itself does not participate in the development of this "labile" population (Fig.S1 of the manuscript).

Our findings concerning Treg cell compartment in $Eos^{-/-}$ mice have been supported by other groups. First, Fu et al. showed that Eos deficient mice are healthy and have normal $CD4^+CD25^+$ Treg cell compartment during homeostasis (Fu et al., 2012). Another study, published very recently, generated Eos deficient mice (deletion of the last three coding exons of *Ikzf4*) and studied $CD4^+$ Treg cells phenotypically and functionally (Rieder et al., 2015). These authors showed that Eos deficient mice have normal numbers of $CD4^+CD25^+Foxp3^+$ Treg cells and that $CD4^+CD25^+$ Treg cells are suppressive *in vitro*. Interestingly, Eos deficient Treg cells had significantly higher suppressive potential in two Treg to T cell ratios using a [^{3}H] thymidine incorporation assay. However, in a classical assay where the effector T cells were labeled with CFSE throughout the co-culture with Treg cells and APCs, $Eos^{-/-}$ Treg cells suppressed the proliferation of T cells as efficiently as WT cells. The difference in those two *in vitro* essays may stem from the fact that, in the first assay, the cells were pulsed with [^{3}H] thymidine only during the last 6 hours of a 72h co-culture, and the proliferation was measured as global thymidine uptake. Thus, it is possible that the proliferation of other cells

(Treg cells) was measured in this assay, or again, the $Eos^{-/-}$ Treg cells had acquired distinct properties and indeed become more potent suppressors at the end of the co-culture (Rieder et al., 2015). In our case, the latter possibility could not be measured in our experimental system, thus we did not observe any difference in the suppressive activity between Eos deficient and WT Treg cells.

In addition, in the study by Rieder et al., $Eos^{-/-}$ $CD4^+Foxp3^+$ Treg cells (sorted from $Eos^{-/-}$ Foxp3-GFP mice) were analyzed *in vivo* in an IBD model, and could efficiently protect mice from disease progression, and inhibit the production of proinflammatory cytokines, confirming our preliminary results with this experimental system. These authors also used another model to test the suppressive potential of Treg cells. Rag2 deficient mice were irradiated and injected with fetal liver cells from scurfy mice (lacking Treg cells), which resulted in the development of systemic inflammation characterized by the presence of highly activated $CD4^+$ and $CD8^+$ Treg cells. The co-transfer of total BM cells from WT or $Eos^{-/-}$ mice could reduce T cell activation and IFN-γ production, suggesting the development of fully suppressive Treg cells. The Treg cells that were generated in the BM chimeras were phenotypically similar between WT and $Eos^{-/-}$ donors, and expressed Foxp3. Since the normal BM contains rather low number of T cells, including Treg populations, the Treg cells generated in the chimeras were either expanded from the existing cells and/or induced from conventional T cells present in the bone marrow. Thus, this experiment also confirmed another observation from our experiments, namely that Eos is not required for the development of both nTreg and iTreg cells (Fig.S4 of the manuscript, Rieder et al., 2015).

It is also noteworthy that, during homeostasis, Eos may have a role in Treg subsets, which we did not study here (e.g. other naturally occurring $CD8^+$ Treg cells, small $CD4^+$ Treg subsets like $Lag3^+$ cells or $CD103^+$ cells). Additionally, even though Eos is highly expressed in $CD4^+CD25^+Foxp3^+$ Treg cells not all cells are Eos^+ (more than 60% of $CD4^+CD25^+Foxp3^+$ cells are Eos^+ both in the thymus and periphery). Thus, with appropriate tools (reporter mice) it could be also interesting to analyze only the population of Treg cells that express Eos in suppression assays *in vitro* or *in vivo*. The lack of phenotype that we observed in $Eos^{-/-}$ mice did not prompt us to study further the Treg cells under specific conditions or to access more in detail the functionality of Eos deficient Treg cells. However, as discussed in chapter I.3.3 Treg cells utilize diverse mechanisms to suppress effector T cells, hence it is possible that Eos may play a role in a specific mechanism, which can be easy

to miss as Treg cells use more than one mechanism at a time (for example cytokine secretion and DC modulation).

Nevertheless, my observation that Eos is not required for Treg cell development and function do not exclude the possibility that absence of Eos can be compensated by a different factor, for example, another Ikaros family member. It is certainly a possibility in the case where Eos is globally deleted in mice, but not necessarily when its expression is only transiently knocked down and the functionality of the Treg cells lacking Eos is measured soon after (study by Pan et al., 2009).

We have hypothesized then that the potential defect in Treg cells can be revealed when we delete Eos in a conditional or inducible manner. Thus, we also generated and analyzed Eos conditional ($Eos^{f/f}$ CD4-Cre) and tamoxifen inducible-Cre ($Eos^{f/f}$ Rosa26-Cre^{ERT2}) knock-out mice, but preliminary results also showed no phenotype in the hematopoietic system or specifically in the Treg cell compartment. In addition, this hypothesis was also not supported by the fact that global deletion of Eos in mice can give a clear phenotype, as shown in experiments with $CD4^+$ T cells from Eos deficient mice, which have an anergic phenotype and defect in IL-2 production (Rieder et al., 2015).

Finally, our gene expression data from Eos KO $CD4^+$ Treg cells confirm the functional studies showing that Eos alone has a minimal impact on the Treg cell transcriptome (Fig.7 of the manuscript). This observation is interesting, especially in regards to the study by Fu et al., who showed that Treg cells possess a distinct gene-expression signature which comprises not only cell surface markers, but also a wide array of transcription factors (Fu et al., 2012). These authors defined transcription factors which, together with Foxp3, can facilitate the transcriptional signature of Treg cells. Eos (and to a lesser extent Helios) was identified as one of them, along with Irf4, Satb1, Lef1 and Gata1, in experiments where conventional T cells were transduced with Foxp3 and one of the listed transcription factors. However, mice deficient for Eos, Gata1 or Xbp1 had a normal Treg cell compartment (studied only in steady state and not in functional assays) and their predicted target genes were minimally affected, which was in line with our results (Fu et al., 2012). Altogether, our combined results indicate that the deletion of one major gene is not sufficient to impair Treg cell development and function.

Is Helios redundant for CD4$^+$ Treg cells?

Helios can directly interact with Foxp3 and the knock-down of Helios with siRNA impairs Treg cell functionality (Getnet et al., 2010). However, studies from our group and others showed that loss of Helios *in vivo* does not impair Treg cell functions, including their potential to suppress T cell proliferation (Cai et al., 2009; Thornton et al., 2010). These contradictory results suggested that Helios is redundant in CD4$^+$ Treg cells during steady state hematopoiesis in mice, and that its function is compensated by another factor or that it plays a distinct role under specific conditions.

My results show that Helios deficiency does not impair the suppressive potential of CD4$^+$ Treg cells. On the contrary, Helios$^{-/-}$ Treg cells are more suppressive than WT cells, both in a functional assay *in vitro* and in terms of their transcriptional signature, which is reminiscent of activated Treg cells (Fig.8 of the manuscript). This conclusion came after comparing our transcriptome data obtained from WT and Helios deficient CD4$^+$CD25$^+$ Treg cells with data from the study by Arvey et al. (Arvey et al., 2014). These authors used an *in vivo* system to obtain activated Treg cells. They depleted transiently mice from Treg cells through administration of diphtheria toxin (DT) to Foxp3^{DTR} mice (endogenous *Foxp3* locus controls the expression of human DT receptor). This led to the emergence of highly activated effector CD4$^+$ and CD8$^+$ T cells and systemic inflammation, which could be attenuated after the withdrawal of DT, and as a result of Treg cell re-appearance. Those highly active and "busy" Treg cells were analyzed and displayed higher expression of activation markers (Arvey et al., 2014). Thus it was interesting to find out that Helios deficient Treg cells from un-manipulated and healthy mice share the transcriptional profile with those *in vivo* activated Treg cells (Fig.7, Fig.8, Fig.S6 of the manuscript).

In the transcriptomic analysis we found a group of up-regulated genes that particularly support our observations. Helios$^{-/-}$ cells up-regulate genes encoding molecules associated with highly suppressive and active Treg cells e.g. Klrg1, Id2, Fgl2 or Lag3 or IL-10 (Beyersdorf et al., 2007; Tauro et al., 2013; Miyazaki et al., 2014; Shalev et al., 2009; Do et al., 2015; Sun et al., 2010; Heo et al., 2010). Experimentally, we have validated only the higher levels of Klrg1 in Helios$^{-/-}$ Treg cells (Fig.S5 of the manuscript). However, this already provided an interesting insight into the phenotype of Helios deficient Treg cells. As discussed in section I.3.2.1, Klrg1 marks activated and terminally differentiated Treg cells, with higher suppressive potential, when compared to their Klrg1$^-$ counterparts. Enrichment

for Klrg1^{+} cells within the CD4^{+}CD25^{+} population could partially explain the higher suppressive potential of Helios$^{-/-}$ Treg cells. It would be interesting to compare now the suppressive activity of equal numbers of CD4^{+}CD25^{+}Klrg1^{-} and CD4^{+}CD25^{+}Klrg1^{+} Treg cells from WT mice with these populations from Helios$^{-/-}$ mice. This way we could observe whether the activated phenotype of Helios$^{-/-}$ Treg cells is only due to the enrichment in Klrg1^{+} cells (which are highly functional and have enhanced proliferative and migratory abilities) or other mechanisms, for example enhanced release of IL-10 or expression of co-inhibitory receptor Lag3 (in the case when Helios$^{-/-}$ CD4^{+}CD25^{+}Klrg1^{+} Treg cells will be still more suppressive than the same number of WT CD4^{+}CD25^{+}Klrg1 cells). Thus, it is crucial to validate the expression of remaining genes, which are possibly responsible for the activated phenotype. It will be also very interesting to verify if Helios$^{-/-}$ Treg cells are also more potent to suppress inflammatory responses *in vivo* in a colitis or autoimmune encephalomyelitis model.

Can Eos and Helios compensate for each other?

Transient knock-down of Eos or Helios results in a defect of CD4^{+} Treg cell suppressive activity, but a complete loss of one of these transcription factors in mice has no effect on the development and function of Treg cells (Cai et al., 2009; Getnet et al., 2010; Pan et al., 2009; Rieder et al., 2015). Hence, the hypothesis that the function of Eos and Helios can be compensated by another factor in their absence is plausible. Taking into consideration the fact that Eos and Helios share many characteristics and functional properties, these two factors could compensate for each other in Treg cells. As discussed in sections I.4.2 and I.4.5, Eos and Helios have high protein sequence similarity, and can potentially form heterodimers together and may have similar target genes. However, the expression level of Eos and Helios do not indicate such a mechanism, as Helios$^{-/-}$ Treg cells have similar levels of Eos protein as WT cells, and Eos$^{-/-}$ Treg cells have normal expression of Helios (Fig.2 of the manuscript).

To assess if Eos and Helios cooperate together to regulate Treg cell functions and to address the possibility concerning compensatory mechanisms, we generated and analyzed double knock-out Eos$^{-/-}$Helios$^{-/-}$ mice. From the first dKO Eos$^{-/-}$Helios$^{-/-}$ mice, it became clear that these mice are born with very low frequency and in some cases have decreased body weights (Fig.5 of the manuscript). At the same time, these mice that were born were healthy and caught up with WT mice in terms of body weight few weeks after birth. Due to the low number of dKO mice that we obtained, we have not managed to assess for example their

fertility. Nevertheless, the phenotype and frequency of birth in the dKO line resembled the one observed for Helios deficient mice generated in our lab. Helios$^{-/-}$ mice were born with normal frequencies but many of them died early during postnatal life in a conventional facility (Cai et al., 2009). However, on a mixed 129/Sv-B6 genetic background in SPF conditions, the survival of Helios deficient mice is markedly improved and more than 80% of mutant mice survive. At the same time Eos$^{-/-}$ mice are born with normal frequencies, and are healthy and fertile. Thus, it is clear that the survival of the dKO Eos$^{-/-}$Helios$^{-/-}$ mice is worse than that of the single KO strains (Fig.1 and Fig.5 of the manuscript).

One possible explanation for the observed phenotype can be the dominant effect of the Helios deletion combined with the genetic background of the mice. Crossing Helios null mice, which have a mixed background, with Eos deficient mice with B6 background, could accelerate the mortality of mice, was in the case when Helios mice were backcrossed onto the B6 background. Another possibility is that the loss of both Eos and Helios has a dramatic effect on mouse development. This could be related to the expression of both Eos and Helios outside of the hematopoietic system. Eos and Helios may have roles during the embryogenesis in the cell types derived from the endoderm (liver) ectoderm (developing nervous system) and mesoderm (reproductive system) where they are independently expressed (EMBL-EBI Expression Atlas; Kelley et al., 1998; Honma et al., 1999). From an evolutionary point of view, that would also be a possibility, considering that these embryologic complexity emerged with the vertebrates, and Ikaros gene family expanded and became complex at the same time (John et al., 2009). Thus, this hypothesis is certainly worth addressing, for example by analyzing the developing embryos in dKO mice.

The defect could also stem from the hematopoietic system, which could be impaired early during embryogenesis. However, there are arguments that rather exclude this possibility. Eos$^{-/-}$Helios$^{-/-}$ mice that are born, have normal hematopoietic populations and are healthy (though we did not follow the mice for longer than 3-4 months). In addition, the mortality of Helios$^{-/-}$ mice which was observed after establishing the line, was also rather not attributed to defects in the hematopoietic system, as fetal liver cells from Helios deficient mice could reconstitute the hematopoietic system of irradiated mice (un-published observation). It could be interesting to perform a similar experiment with dKO cells and analyze the sites of hematopoiesis in mutant embryos in more detail. We have also tried to improve the housing conditions of mice, and transferred them from the SPF to an “ultra clean BioBubble” area of the animal facility, hypothesizing that these mice die more due to a

possible hematopoietic defect and susceptibility to infections. However, we did not observe any improvements in the frequency of born Eos$^{-/-}$Helios$^{-/-}$ mice. At the same time there is a possibility that dKO mice die more due to an intrinsic defect (other than infection) in the hematopoietic system. Thus, the survival problem of dKO mice still needs to be addressed in the ways proposed above.

In regards to the Eos$^{-/-}$Helios$^{-/-}$ mice, we have not observed any of the expected phenotypes in the Treg cell compartment. When compared to WT controls, dKO mice had normal numbers of Treg cells, which were functional and expressed normal levels of Foxp3 (Fig.5 and Fig.S4 of the manuscript). In addition, CD4^{+} T cells from dKO mice could efficiently convert into iTreg cells and express CD25 and Foxp3, all together suggesting that Eos and Helios are redundant for CD4^{+} Treg cells during homeostasis.

In addition, the transcriptome data from the CD4^{+} Treg cells presented a lack of apparent co-regulation between Eos and Helios, and the observed differentially regulated genes were mainly related to Helios deficiency and (Fig.7 of the manuscript). Moreover, the dKO Treg cells had a transcriptional signature reminiscent of activated Treg cells, which concerned both the up-regulated and down-regulated genes, similarly to Helios$^{-/-}$ Treg cells (Fig.8; Fig.S6 of the manuscript). Another level of complexity is added by the *in vitro* suppression assay, where dKO Treg cells did not show a superior suppressive activity, although they also contained more Klrg1 positive cells (Fig.5 and Fig.S5 of the manuscript). However, the levels of suppression in the tested ratios, of Treg to responder T cells, were lower than in previous experiments (and no difference in suppression was observed between the first two conditions). Thus, these experiments should be repeated when Helios$^{-/-}$ mutant controls will be available in the dKO line. Combining all these observations we hypothesize that, the observed phenotype in dKO cells is related more to the absence of Helios.

While discussing the possible functional compensation between Eos and Helios in Treg cells, it is interesting to cite again the study of Fu et al., where a group of transcription factors combined with Foxp3 can confer the Treg cell transcriptional signature (Fu et al., 2012). However, these “key” transcriptional regulators were normally expressed in dKO Treg cells (transcriptome data), indicating that even knocking out two of important components does not result in a drastic impairment of Treg lineage stability in mice.

Our transcriptome data indicated that Eos has a minimal impact on the transcriptional signature of Treg cells, contrary to Helios, and that Eos and Helios do not cooperate to

regulate gene expression in Treg cells. Simultaneously, we have not made an attempt to identify the potential target genes of Eos and Helios in Treg cells by more direct methods, including ChIP or ChIP-sequencing. Such study would be extremely informative for both $CD4^+$ and $CD8^+$ Treg cells, and could clarify the direct requirement for Eos and Helios in Treg cell function maintenance.

Are Eos and Helios important for $CD8^+$ Treg cells?

We have also studied the potential roles of Eos and Helios in $CD8^+$ Treg cells. First, we found that Eos and Helios are differentially expressed in a population of naturally occurring $CD8^+CD122^+$ Treg cells, with a high number of Helios positive cells within this population that expressed low levels of Eos. Moreover, no differences were observed in the percentage of these cells in the periphery of $Eos^{-/-}$ or $Helios^{-/-}$ mice, indicating that Eos and Helios are also not required for the development of $CD8^+CD122^+$ Treg cells (Fig.S1 of the manuscript). This provided an example similar to the $CD4^+CD25^+Foxp3^+$ Treg cells, where Eos and Helios are expressed, but their loss doesn't affect the population during homeostasis. This may suggest that Eos and Helios play a role in this population, but only under specific conditions, for example during inflammation.

Another population of Treg cells, namely alloinduced $CD8^+$ Treg cells, share characteristics with $CD4^+$ Treg cells, including the expression of CD25, CD103, CTLA4 or IL-10 together with dependency on IL-2 and TGF-β signaling (Mahic et al., 2008; Mayer et al., 2011; Muthu Raja et al., 2012). However, little is known about their regulation on a transcriptional level and whether Foxp3 shares its protein partners from $CD4^+$ Treg regulatory network, or whether Foxp3 is required at all for the differentiation and function of alloinduced $CD8^+$ Treg cells.

Interestingly, the expression of Helios was observed in a population of Foxp3 positive $CD8^+$ iTreg cells induced in allogeneic conditions (Beres et al., 2012). This prompted us to study the potential roles of Helios and Eos in this subset. We have found high expression levels of both Helios and Eos in WT $CD8^+CD25^+Foxp3^+$ Treg cells after differentiation *in vitro*. However, in Treg cells after allogeneic BM transplantation only a small percentage of cells expressed Eos while having high expression of Helios (Fig.3 and Fig.S3 of the manuscript). This could indicate that Eos is only a marker of differentiated and/or activated cells, and that its expression can be induced *in vitro* through the TGF-β1, IL-2 or TCR signals. Consistently, Eos expression is up-regulated in naïve $CD4^+$ T cells after stimulation

in vitro with anti-CD3 and anti-CD28 antibodies, and at the mRNA level in activated conventional T cells 48h after stimulation expression of Eos, is similar to Treg cells (Rieder et al., 2015). Interestingly, Eos protein levels are also up-regulated in conventional $CD8^+$ T cells after stimulation (Rieder et al., 2015). In addition, when looking at the $CD4^+$ Treg compartment, Eos is induced on iTreg cells generated with TGF-β1, IL-2 and anti-CD3 and anti-CD28 antibodies, which together provide similar stimulation as needed for $CD8^+$ iTreg cells, but loss of Eos has no effect on the generation of these cells. This could suggest that Eos is indeed a marker of activated T cells, and is redundant for their function, similar to Helios (Akimova et al., 2011; Cai et al., 2009; Daley et al., 2013).

Simultaneously, we observed a defect in the ability of $Helios^{-/-}$ $CD8^+$ T cells to differentiate into cells expressing Foxp3 *in vitro*, but Eos deficient cells were not affected, consistent with the suggestion that Eos may function as a marker of activated Treg cells, but its presence is redundant for their function. In addition, *in vivo* we did not observe differentiation defects, for both $Eos^{-/-}$ and $Helios^{-/-}$ $CD8^+$ Treg cells. However, when we analyzed the dKO mice we could see a phenotype and a slightly decreased potential of $CD8^+$ T cells to differentiate into $CD8^+CD25^+Foxp3^+$ Treg cells. At the same time, the Treg cells obtained *in vitro* from all mutant strains were functional in a suppression assay. Thus, it appears that it is Helios that might play a role in the development of $CD8^+$ Treg cells and that most probably the small defect observed in dKO cells is due the loss of Helios and not the cumulative effect of the double knock-out.

It also noteworthy that the differences in the generation of $CD8^+CD25^+Foxp3^+$ cells from $Helios^{-/-}$ and dKO cells were observed both *in vivo* and *in vitro*, but the pool of $CD8^+CD25^+$ cells was usually comparable between the genotypes. As we did not observe any defects in the functionality of $CD8^+$ Treg cells, sorted after co-culture only according to the expression of CD8 and CD25, it could suggest that maybe Foxp3 itself is not contributing to the suppressive function of these cells to the extent observed in $CD4^+$ Treg cells.

In addition, we cannot exclude the possibility that there is some level of co-regulation between Eos and Helios, as we can observe a decreased potential for the differentiation of $CD8^+$ T cells from dKO mice, but not single KO animals. As these experiments were performed using mice with slightly different genetic backgrounds a more uniform experimental system would be necessary for a more definitive answer.

Finally, it appears that Eos and Helios are involved in the regulation of this Treg subset, but both play distinct roles. Thus, it may be conclusive to compare gene expression profiles in differentiated WT and KO $CD8^+$ iTreg cells, preferentially from both *in vivo* and *in vitro* experiments. A simultaneous analysis of Eos and Helios expression kinetics, throughout the *in vitro* co-culture and *in vivo* differentiation, could also give interesting insight into the relationship with Foxp3 $CD8^+$ Treg cells in these cells. In the performed experiments we have looked at the expression of Eos and Helios at the end time points of the experiments (after day 7). Hence we do not know which one is induced first, or if possibly they precede the expression of Foxp3. Concerning the functionality of the alloinduced $CD8^+$ Treg cells, it is crucial to verify their suppressive potential *in vivo*. Sorted cells from WT or KO mice could be evaluated in the established colitis model. This could possibly reveal their other properties and functions.

At the end of the discussion I go back to the main question: **what are the roles of Eos and Helios in Treg cell biology?**

Our results show that during homeostasis, Eos and Helios do not cooperate to regulate Treg cell functions and are dispensable for $CD4^+$ Treg cell development and function, although Helios appears to regulate the overall "activation program" of these cells. We demonstrate also a potential role for Eos and Helios in the differentiation of alloinduced $CD8^+$ iTreg cells.

In conclusion, our data support the developmental and functional stability of Treg cells, which is governed by a regulatory network composed of extrinsic and intrinsic signals, with the latter one including a plethora of transcription factors. Our data add to this knowledge by clarifying the potential roles of Eos and Helios in Treg cell biology.

IV.2. Does Eos have a role in hematopoietic stem cells?

Here we show that Eos, similarly to Helios transcription factor, is expressed in hematopoietic stem cells and that this expression measured at mRNA level peaks in LT-HSCs (Fig.III.1 and Papathanasiou et al., 2009). Knowing that Helios as well as Ikaros play a particular role in the maintenance of HSC cells we investigated if Eos may also have a redundant or specific function in this compartment.

Are Eos$^{-/-}$ HSCs functional?

We started by analyzing HSCs from Eos$^{-/-}$ mice during homeostasis and in serial competitive transplantation assays. Despite the lack of changes in the frequencies of main progenitor populations and hematopoietic stem cells in Eos null mice (Fig.III.7) the first phenotype concerning HSC in KO mice was observed in transplantation assays (Fig.III.9 and Fig.III.11). Transplanting bone marrow cells into lethally irradiated mice is the best known and well established method to detect and study hematopoietic stem cells. Protection from irradiation mediated hematopoietic failure indicates a successful engraftment of transplanted cells. At the same time, maintenance of the hematopoiesis and production of all blood cell types over time after transplantation shows the function that only hematopoietic stem cells have, namely long-term repopulation potential. Over all our transplantation assays, the most interesting results came from the secondary transplantations, where we observed a reduced reconstitution potential of Eos$^{-/-}$ cells (Fig.III.9 and Fig.III.11). This could indicate that Eos plays a role in the self-renewal of hematopoietic stem cells. In parallel, we were analyzing mice transplanted with purified LSK cells. We hypothesized that if we use cells highly enriched in hematopoietic stem and progenitor cells, which we suspected to be the source of the phenotype observed in secondary transplantations with total BM cells, we will observe a reinforced and clear phenotype probably already in primary transplantations with LSK cells. Interestingly, we saw that Eos null cells have indeed a strongly impaired reconstitution potential in the two conditions used (we have injected either 100 or 500 LSK cells) but only shortly after transplantation (up to 8 weeks). Later on, analysis of the chimerism in PB showed that the differences obliterated, and 6 months after primary transplantations WT and Eos$^{-/-}$ grafts presented similar reconstitution. In secondary transplantations with LSK cells, results were more variable but we could still see in repeated experiments that Eos null LSK cells are inferior to WT cells in the reconstitution potential. It is known that serial transplantation is inducing replicative stress and decreased proliferation potential leading to the exhaustion in the reconstitution capabilities (Harrison et al., 1978; Harrison, 1979). This

could indicate that Eos$^{-/-}$ cells have a cell intrinsic defect in self renewal or a defective response to stress (manifested for example as a decreased proliferation).

Do Eos$^{-/-}$ HSCs have normal proliferation and stress response?

HSCs are considered to be a quiescent population, with very small frequency of 1-3% cycling cells (Goodell et al., 1996). The maintenance of HSC quiescence is important for stem cell activity. Impaired function of HSCs from several KO mice showing an increased cell cycle entry demonstrate that quiescence protects HSCs from functional exhaustion and ensure lifelong hematopoietic cell production (Nakamura-Ishizu et al., 2014; Orford and Scadden, 2008). Thus, while performing HSC assays, it is important to study their proliferation status. We also knew that Helios transcription factor, the closest relative of Eos, is playing a role in HSCs to regulate response to stress and maintain genome stability and that Helios deficient HSCs have differential response to DNA damage and different proliferation properties (Vesin et al., manuscript in preparation). However, the *in vitro* proliferation and DNA damage response properties of Eos$^{-/-}$ HSCs were similar to WT cells (Fig.III.12 and III.13). Interestingly, these experiments do not exclude the proposed hypotheses. It would be interesting to study the proliferation of Eos null HSCs *in vivo*. BrdU labeling of cells before transplantation could allow differentiating the proliferative potential of HSC from progenitor populations and studying HSC cycling after few days post experiment. Concerning the secondary transplantations it could be also informative to perform tertiary (or further) transplantations to see if the decreased reconstitution capacity of Eos$^{-/-}$ cells is persistent over serial engraftments.

Are Eos$^{-/-}$ hematopoietic progenitors functional?

Decreasing difference in the reconstitution between WT and KO LSK cells in the primary transplantation shows (Fig.III.11) that another function can be impaired in KO cells. First, a proliferation defect in Eos$^{-/-}$ LSK cells that would induce a time-shift necessary to“catch up” with WT counterparts is plausible. Alternatively, the difference observed at early time points after transplantation can result not from a defect in HSCs but progenitor cells. At early time points after transplantation (4 weeks) the peripheral blood cells produced from donor cells can be the progeny of short-term HSCs or progenitor cells. On the contrary, the only cells that can self-renew and contribute to blood production for more than 4 months post-transplant are long-term HSCs and all blood cell types found during this time are their direct progeny (Zhong et al., 1996; Purton and Scadden, 2007; Mayle et al., 2013). Indeed,

the LSK population used for our transplantations contains not only hematopoietic stem cells (LT-HSCs and ST-HSCs) but also multipotent progenitor cells. It has been already shown that progenitor cells of both myeloid and lymphoid lineage can provide radioprotection like HSCs but only transiently, probably contributing to short term reconstitution as mentioned above (Na Nakorn et al., 2002). When we addressed this hypothesis *in vitro* (Fig.III.14), we indeed observed that Eos deficient BM cells give rise to slightly less myeloid colonies, but could not find any particular cell population type that would be more affected. However, the defect in the colony formation could at least point in the direction that the observed phenotype may be attributed to progenitor cells. In this regard, it would be interesting to transplant different progenitor populations into lethally irradiated recipients, and follow the reconstitution of hematopoietic system as well as colony formation in the spleen or bone marrow.

Could other properties of HSC and progenitor cells be tested in Eos$^{-/-}$ mice?

To obtain a more global view on the changes in Eos deficient HSC and progenitor cells it could be interesting to perform gene expression profiling in WT and KO sort purified populations. Affected genes could point out a pathway or process responsible for the observed changes. A strong phenotype concerning Eos and HSCs was observed in serial transplantations. Those serial engraftments could be compared with the aging of hematopoietic stem cell compartment. This claim could be supported by two arguments. First, HSC activity declines during normal aging in mice (Rossi et al., 2005; Chambers et al., 2007; Kamminga and de Haan, 2006; Waterstrat and Van Zant, 2009). Second, even though HSCs can maintain their function longer then the lifespan of a recipient in a BM transplantation, they can be engrafted only for a limited number of times and this is accompanied by a functional decline (Harrison, 1979; Kamminga et al., 2005; Kamminga and de Haan, 2006). Thus, studying the aging of HSC compartment also appears to be important in revealing their properties and mechanisms of regulation. In this regard, HSCs in aged Eos$^{-/-}$ mice could be analyzed. First, analysis of HSCs in aged Eos$^{-/-}$ during steady state could be performed. Next, aged KO HSCs could be also studied in functional assays like competitive reconstitution transplantation.

Finally, my results show that Eos$^{-/-}$ HSCs and/or progenitor cells have less biological activity, yet it remains to be clarified with function of the hematopoietic stem cell and progenitor compartment may be regulated by Eos.

IV.3. Why $Ik^{+/L}Ezh2^{Tg/+}$ mice cannot show synergy between Ikaros and PRC2?

We generated and characterized mice with Ikaros and Ezh2 haploinsufficiency. We expected that the $Ik^{+/L}Ezh2^{Tg/+}$ mice will demonstrate an impaired T cell development and/or tumorigenesis. At the molecular level, we hypothesized to see a stronger loss of H3K27me3 on genes affected by Ikaros, and an increase in the expression of these genes. However, we did not observe any additive effect of Ikaros and Ezh2 deficiency.

These negative results could be explained by the fact that Ezh2 haploinsufficiency is not enough to impair the protein function. It is also important to mention here that in the $Ezh2^{Tg/+}$ mice Ezh2 protein was not decreased in T cells (Fig III.20), which is not unusual for monoallelic inactivation but could explain lack of phenotype in our system. Concerning the T cell differentiation and potential leukemogenesis, it should be mentioned that while we were maintaining the $Ik^{+/L}Ezh2^{Tg/+}$ line, we never tried to age the double heterozygous mice. The anticipated results may be masked by the strong effect of Ikaros deficiency but at the molecular level it could be worth analyzing the H3K27me3 and gene expression profiles of genes known to be affected by Ikaros. Another explanation for the observed results could be that Ezh2 function is compensated by another factor for example Ezh1, a gene homolog present in a noncanonical PRC2 complex. In embryonic stem cells, in the absence of Ezh2 it is Ezh1 that preserves H3K27me3 residual repressive mark and complement Ezh2 function (Shen et al., 2008). Thus, it is essential to verify the expression level of Ezh1 in $Ezh2^{Tg/+}$ and $Ik^{+/L}Ezh2^{Tg/+}$ T cells both at the mRNA and protein level, by RT-qPCR and western blot respectively.

Finally, our model could not show the synergy between Ikaros and PRC2. However, it is clear that Ikaros represses its target genes in T cells through PRC2 complex with which it can directly interact (Oravecz et al., 2015). Nevertheless, it could be still interesting to perform a further analysis on a molecular level with our mouse model. For example, the occupancy of particular genomic loci by Ikaros, and Ezh2 is now known and analysis of these particular regions in T cells from $Ik^{+/L}Ezh2^{Tg/+}$ could be performed using H3K27me3 ChIP-sequencing.

In conclusion, the new mouse model that was characterized in the lab did not meet our expectations and obtained results were not published. However, my work contributed to the project that resulted in a manuscript which is enclosed in the appendix.

BIBLIOGRAPHY

Databases:

Ensembl genome browser	http://www.ensembl.org/
Vega genome browser	http://vega.sanger.ac.uk/
ImmGen database	https://www.immgen.org/
EMBL-EBI Expression Atlas	http://www.ebi.ac.uk/gxa/home

References:

Adolfsson, J., Månsson, R., Buza-Vidas, N., Hultquist, A., Liuba, K., Jensen, C.T., Bryder, D., Yang, L., Borge, O.-J., Thoren, L.A.M., et al. (2005). Identification of Flt3+ lympho-myeloid stem cells lacking erythro-megakaryocytic potential a revised road map for adult blood lineage commitment. Cell *121*, 295–306.

Akashi, K., Traver, D., Miyamoto, T., and Weissman, I.L. (2000). A clonogenic common myeloid progenitor that gives rise to all myeloid lineages. Nature *404*, 193–197.

Akimova, T., Beier, U.H., Wang, L., Levine, M.H., and Hancock, W.W. (2011). Helios expression is a marker of T cell activation and proliferation. PloS One *6*, e24226.

Alinikula, J., Kohonen, P., Nera, K.-P., and Lassila, O. (2010). Concerted action of Helios and Ikaros controls the expression of the inositol 5-phosphatase SHIP. Eur. J. Immunol. *40*, 2599–2607.

Allan, S.E., Crome, S.Q., Crellin, N.K., Passerini, L., Steiner, T.S., Bacchetta, R., Roncarolo, M.G., and Levings, M.K. (2007). Activation-induced FOXP3 in human T effector cells does not suppress proliferation or cytokine production. Int. Immunol. *19*, 345–354.

Allman, D., Dalod, M., Asselin-Paturel, C., Delale, T., Robbins, S.H., Trinchieri, G., Biron, C.A., Kastner, P., and Chan, S. (2006). Ikaros is required for plasmacytoid dendritic cell differentiation. Blood *108*, 4025–4034.

Apostolou, I., and von Boehmer, H. (2004). In vivo instruction of suppressor commitment in naive T cells. J. Exp. Med. *199*, 1401–1408.

Arvey, A., van der Veeken, J., Samstein, R.M., Feng, Y., Stamatoyannopoulos, J.A., and Rudensky, A.Y. (2014). Inflammation-induced repression of chromatin bound by the transcription factor Foxp3 in regulatory T cells. Nat. Immunol. *15*, 580–587.

Asano, M., Toda, M., Sakaguchi, N., and Sakaguchi, S. (1996). Autoimmune disease as a consequence of developmental abnormality of a T cell subpopulation. J. Exp. Med. *184*, 387–396.

Aschenbrenner, K., D'Cruz, L.M., Vollmann, E.H., Hinterberger, M., Emmerich, J., Swee, L.K., Rolink, A., and Klein, L. (2007). Selection of Foxp3+ regulatory T cells specific for self antigen expressed and presented by Aire+ medullary thymic epithelial cells. Nat. Immunol. *8*, 351–358.

Asseman, C., Mauze, S., Leach, M.W., Coffman, R.L., and Powrie, F. (1999). An essential role for interleukin 10 in the function of regulatory T cells that inhibit intestinal inflammation. J. Exp. Med. *190*, 995–1004.

Asseman, C., Fowler, S., and Powrie, F. (2000). Control of experimental inflammatory bowel disease by regulatory T cells. Am. J. Respir. Crit. Care Med. *162*, S185–S189.

Aster, J.C., Blacklow, S.C., and Pear, W.S. (2011). Notch signalling in T-cell lymphoblastic leukaemia/lymphoma and other haematological malignancies. J. Pathol. *223*, 262–273.

Atarashi, K., Tanoue, T., Shima, T., Imaoka, A., Kuwahara, T., Momose, Y., Cheng, G., Yamasaki, S., Saito, T., Ohba, Y., et al. (2011). Induction of colonic regulatory T cells by indigenous Clostridium species. Science *331*, 337–341.

Baas, M.C., Kuhn, C., Valette, F., Mangez, C., Duarte, M.S., Hill, M., Besançon, A., Chatenoud, L., Cuturi, M.-C., and You, S. (2014). Combining autologous dendritic cell therapy with CD3 antibodies promotes regulatory T cells and permanent islet allograft acceptance. J. Immunol. *193*, 4696–4703.

Baine, I., Basu, S., Ames, R., Sellers, R.S., and Macian, F. (2013). Helios induces epigenetic silencing of IL2 gene expression in regulatory T cells. J. Immunol. *190*, 1008–1016.

Baldridge, M.T., King, K.Y., Boles, N.C., Weksberg, D.C., and Goodell, M.A. (2010). Quiescent haematopoietic stem cells are activated by IFN-gamma in response to chronic infection. Nature *465*, 793–797.

Bao, J., Lin, H., Ouyang, Y., Lei, D., Osman, A., Kim, T.-W., Mei, L., Dai, P., Ohlemiller, K.K., and Ambron, R.T. (2004). Activity-dependent transcription regulation of PSD-95 by neuregulin-1 and Eos. Nat. Neurosci. *7*, 1250–1258.

Bennett, C.L., Christie, J., Ramsdell, F., Brunkow, M.E., Ferguson, P.J., Whitesell, L., Kelly, T.E., Saulsbury, F.T., Chance, P.F., and Ochs, H.D. (2001). The immune dysregulation, polyendocrinopathy, enteropathy, X-linked syndrome (IPEX) is caused by mutations of FOXP3. Nat. Genet. *27*, 20–21.

Bersenev A., (2011). Congenic mouse model. StemCellAssays. Experimental bone marrow transplantation 101 – part 2: November 6.

Beres, A.J., Haribhai, D., Chadwick, A.C., Gonyo, P.J., Williams, C.B., and Drobyski, W.R. (2012). CD8+ Foxp3+ regulatory T cells are induced during graft-versus-host disease and mitigate disease severity. J. Immunol. *189*, 464–474.

Bettini, M., and Vignali, D.A.A. (2009). Regulatory T cells and inhibitory cytokines in autoimmunity. Curr. Opin. Immunol. *21*, 612–618.

Bettini, M.L., Pan, F., Bettini, M., Finkelstein, D., Rehg, J.E., Floess, S., Bell, B.D., Ziegler, S.F., Huehn, J., Pardoll, D.M., et al. (2012). Loss of epigenetic modification driven by the Foxp3 transcription factor leads to regulatory T cell insufficiency. Immunity *36*, 717–730.

Beyersdorf, N., Ding, X., Tietze, J.K., and Hanke, T. (2007). Characterization of mouse CD4 T cell subsets defined by expression of KLRG1. Eur. J. Immunol. *37*, 3445–3454.

Bhattacharya, D., Rossi, D.J., Bryder, D., and Weissman, I.L. (2006). Purified hematopoietic stem cell engraftment of rare niches corrects severe lymphoid deficiencies without host conditioning. J. Exp. Med. *203*, 73–85.

Blank, U., Karlsson, G., and Karlsson, S. (2008). Signaling pathways governing stem-cell fate. Blood *111*, 492–503.

Von Boehmer, H., and Fehling, H.J. (1997). Structure and function of the pre-T cell receptor. Annu. Rev. Immunol. *15*, 433–452.

Bottardi, S., Zmiri, F.A., Bourgoin, V., Ross, J., Mavoungou, L., and Milot, E. (2011). Ikaros interacts with P-TEFb and cooperates with GATA-1 to enhance transcription elongation. Nucleic Acids Res. *39*, 3505–3519.

Broere, F., Apasov, S.G., Sitkovsky, M.V., and Eden, W. van (2011). A2 T cell subsets and T cell-mediated immunity. In Principles of Immunopharmacology, F.P. Nijkamp, and M.J. Parnham, eds. (Birkhäuser Basel), pp. 15–27.

Brown, K.E., Guest, S.S., Smale, S.T., Hahm, K., Merkenschlager, M., and Fisher, A.G. (1997). Association of transcriptionally silent genes with Ikaros complexes at centromeric heterochromatin. Cell *91*, 845–854.

Brunkow, M.E., Jeffery, E.W., Hjerrild, K.A., Paeper, B., Clark, L.B., Yasayko, S.A., Wilkinson, J.E., Galas, D., Ziegler, S.F., and Ramsdell, F. (2001). Disruption of a new forkhead/winged-helix protein, scurfin, results in the fatal lymphoproliferative disorder of the scurfy mouse. Nat. Genet. *27*, 68–73.

Burchill, M.A., Yang, J., Vogtenhuber, C., Blazar, B.R., and Farrar, M.A. (2007). IL-2 receptor beta-dependent STAT5 activation is required for the development of Foxp3+ regulatory T cells. J. Immunol. *178*, 280–290.

Burchill, M.A., Yang, J., Vang, K.B., Moon, J.J., Chu, H.H., Lio, C.-W.J., Vegoe, A.L., Hsieh, C.-S., Jenkins, M.K., and Farrar, M.A. (2008). Linked T cell receptor and cytokine signaling govern the development of the regulatory T cell repertoire. Immunity *28*, 112–121.

Bushell, A., Morris, P.J., and Wood, K.J. (1995). Transplantation tolerance induced by antigen pretreatment and depleting anti-CD4 antibody depends on CD4+ T cell regulation during the induction phase of the response. Eur. J. Immunol. *25*, 2643–2649.

Cabezas-Wallscheid, N., Klimmeck, D., Hansson, J., Lipka, D.B., Reyes, A., Wang, Q., Weichenhan, D., Lier, A., von Paleske, L., Renders, S., et al. (2014). Identification of regulatory networks in HSCs and their immediate progeny via integrated proteome, transcriptome, and DNA methylome analysis. Cell Stem Cell *15*, 507–522.

Cai, Q., Dierich, A., Oulad-Abdelghani, M., Chan, S., and Kastner, P. (2009). Helios deficiency has minimal impact on T cell development and function. J. Immunol. *183*, 2303–2311.

Campbell, D.J., and Ziegler, S.F. (2007). FOXP3 modifies the phenotypic and functional properties of regulatory T cells. Nat. Rev. Immunol. *7*, 305–310.

Campos-Mora, M., Morales, R.A., Pérez, F., Gajardo, T., Campos, J., Catalan, D., Aguillón, J.C., and Pino-Lagos, K. (2015). Neuropilin-1+ regulatory T cells promote skin allograft survival and modulate effector CD4+ T cells phenotypic signature. Immunol. Cell Biol. *93*, 113–119.

Cantor, H., Hugenberger, J., McVay-Boudreau, L., Eardley, D.D., Kemp, J., Shen, F.W., and Gershon, R.K. (1978). Immunoregulatory circuits among T-cell sets. Identification of a subpopulation of T-helper cells that induces feedback inhibition. J. Exp. Med. *148*, 871–877.

Cantrell, D.A. (2002). Transgenic analysis of thymocyte signal transduction. Nat. Rev. Immunol. *2*, 20–27.

Cao, X., Cai, S.F., Fehniger, T.A., Song, J., Collins, L.I., Piwnica-Worms, D.R., and Ley, T.J. (2007). Granzyme B and perforin are important for regulatory T cell-mediated suppression of tumor clearance. Immunity *27*, 635–646.

Cepek, K.L., Shaw, S.K., Parker, C.M., Russell, G.J., Morrow, J.S., Rimm, D.L., and Brenner, M.B. (1994). Adhesion between epithelial cells and T lymphocytes mediated by E-cadherin and the alpha E beta 7 integrin. Nature *372*, 190–193.

Chambers, S.M., Shaw, C.A., Gatza, C., Fisk, C.J., Donehower, L.A., and Goodell, M.A. (2007). Aging hematopoietic stem cells decline in function and exhibit epigenetic dysregulation. PLoS Biol. *5*, e201.

Chaput, N., Louafi, S., Bardier, A., Charlotte, F., Vaillant, J.-C., Ménégaux, F., Rosenzwajg, M., Lemoine, F., Klatzmann, D., and Taieb, J. (2009). Identification of CD8+CD25+Foxp3+ suppressive T cells in colorectal cancer tissue. Gut *58*, 520–529.

Chaudhry, A., Rudra, D., Treuting, P., Samstein, R.M., Liang, Y., Kas, A., and Rudensky, A.Y. (2009). CD4+ regulatory T cells control TH17 responses in a Stat3-dependent manner. Science *326*, 986–991.

Chen, X., and Oppenheim, J.J. (2011). Resolving the identity myth: key markers of functional CD4+FoxP3+ regulatory T cells. Int. Immunopharmacol. *11*, 1489–1496.

Chen, Q., Kim, Y.C., Laurence, A., Punkosdy, G.A., and Shevach, E.M. (2011). IL-2 controls the stability of Foxp3 expression in TGF-beta-induced Foxp3+ T cells in vivo. J. Immunol. *186*, 6329–6337.

Chen, W., Jin, W., Hardegen, N., Lei, K., Li, L., Marinos, N., McGrady, G., and Wahl, S.M. (2003). Conversion of Peripheral CD4+CD25− Naive T Cells to CD4+CD25+ Regulatory T Cells by TGF-β Induction of Transcription Factor Foxp3. J. Exp. Med. *198*, 1875–1886.

Chen, Z., Laurence, A., and O'Shea, J.J. (2007). Signal transduction pathways and transcriptional regulation in the control of Th17 differentiation. Semin. Immunol. *19*, 400–408.

Cheng, G., Yuan, X., Tsai, M.S., Podack, E.R., Yu, A., and Malek, T.R. (2012). IL-2 receptor signaling is essential for the development of Klrg1+ terminally differentiated T regulatory cells. J. Immunol. *189*, 1780–1791.

Cheng, T., Rodrigues, N., Shen, H., Yang, Y., Dombkowski, D., Sykes, M., and Scadden, D.T. (2000). Hematopoietic stem cell quiescence maintained by p21cip1/waf1. Science *287*, 1804–1808.

Chiffoleau, E., Bériou, G., Dutartre, P., Usal, C., Soulillou, J.-P., and Cuturi, M.C. (2002). Role for thymic and splenic regulatory CD4+ T cells induced by donor dendritic cells in allograft tolerance by LF15-0195 treatment. J. Immunol. *168*, 5058–5069.

Churlaud, G., Pitoiset, F., Jebbawi, F., Lorenzon, R., Bellier, B., Rosenzwajg, M., and Klatzmann, D. (2015). Human and Mouse CD8(+)CD25(+)FOXP3(+) Regulatory T Cells at Steady State and during Interleukin-2 Therapy. Front. Immunol. *6*, 171.

Ciofani, M., and Zúñiga-Pflücker, J.C. (2010). Determining γδ versus αß T cell development. Nat. Rev. Immunol. *10*, 657–663.

Ciofani, M., Knowles, G.C., Wiest, D.L., von Boehmer, H., and Zúñiga-Pflücker, J.C. (2006). Stage-specific and differential notch dependency at the alphabeta and gammadelta T lineage bifurcation. Immunity *25*, 105–116.

Cobb, B.S., Morales-Alcelay, S., Kleiger, G., Brown, K.E., Fisher, A.G., and Smale, S.T. (2000). Targeting of Ikaros to pericentromeric heterochromatin by direct DNA binding. Genes Dev. *14*, 2146–2160.

Cobbold, S.P., Castejon, R., Adams, E., Zelenika, D., Graca, L., Humm, S., and Waldmann, H. (2004). Induction of foxP3+ regulatory T cells in the periphery of T cell receptor transgenic mice tolerized to transplants. J. Immunol. *172*, 6003–6010.

Collison, L.W., Workman, C.J., Kuo, T.T., Boyd, K., Wang, Y., Vignali, K.M., Cross, R., Sehy, D., Blumberg, R.S., and Vignali, D.A.A. (2007). The inhibitory cytokine IL-35 contributes to regulatory T-cell function. Nature *450*, 566–569.

Coombes, J.L., Siddiqui, K.R.R., Arancibia-Cárcamo, C.V., Hall, J., Sun, C.-M., Belkaid, Y., and Powrie, F. (2007). A functionally specialized population of mucosal CD103+ DCs induces Foxp3+ regulatory T cells via a TGF-beta and retinoic acid-dependent mechanism. J. Exp. Med. *204*, 1757–1764.

Cosgun, K.N., Rahmig, S., Mende, N., Reinke, S., Hauber, I., Schäfer, C., Petzold, A., Weisbach, H., Heidkamp, G., Purbojo, A., et al. (2014). Kit regulates HSC engraftment across the human-mouse species barrier. Cell Stem Cell *15*, 227–238.

Cullen, S.M., Mayle, A., Rossi, L., and Goodell, M.A. (2014). Hematopoietic stem cell development: an epigenetic journey. Curr. Top. Dev. Biol. *107*, 39–75.

Daley, S.R., Hu, D.Y., and Goodnow, C.C. (2013). Helios marks strongly autoreactive CD4+ T cells in two major waves of thymic deletion distinguished by induction of PD-1 or NF-κB. J. Exp. Med. *210*, 269–285.

Davidson, T.S., DiPaolo, R.J., Andersson, J., and Shevach, E.M. (2007). Cutting Edge: IL-2 is essential for TGF-beta-mediated induction of Foxp3+ T regulatory cells. J. Immunol. *178*, 4022–4026.

D'Cruz, L.M., and Klein, L. (2005). Development and function of agonist-induced CD25+Foxp3+ regulatory T cells in the absence of interleukin 2 signaling. Nat. Immunol. *6*, 1152–1159.

Desbarats, J., Wade, T., Wade, W.F., and Newell, M.K. (1999). Dichotomy between naïve and memory CD4(+) T cell responses to Fas engagement. Proc. Natl. Acad. Sci. U. S. A. *96*, 8104–8109.

Dick, J.E., Magli, M.C., Huszar, D., Phillips, R.A., and Bernstein, A. (1985). Introduction of a selectable gene into primitive stem cells capable of long-term reconstitution of the hemopoietic system of W/Wv mice. Cell *42*, 71–79.

Dovat, S., Montecino-Rodriguez, E., Schuman, V., Teitell, M.A., Dorshkind, K., and Smale, S.T. (2005). Transgenic expression of Helios in B lineage cells alters B cell properties and promotes lymphomagenesis. J. Immunol. *175*, 3508–3515.

Dumortier, A., Jeannet, R., Kirstetter, P., Kleinmann, E., Sellars, M., dos Santos, N.R., Thibault, C., Barths, J., Ghysdael, J., Punt, J.A., et al. (2006). Notch activation is an early and critical event during T-Cell leukemogenesis in Ikaros-deficient mice. Mol. Cell. Biol. *26*, 209–220.

Duplan, V., Beriou, G., Heslan, J.-M., Bruand, C., Dutartre, P., Mars, L.T., Liblau, R.S., Cuturi, M.-C., and Saoudi, A. (2006). LF 15-0195 treatment protects against central nervous system autoimmunity by favoring the development of Foxp3-expressing regulatory CD4 T cells. J. Immunol. *176*, 839–847.

Ema, H., Sudo, K., Seita, J., Matsubara, A., Morita, Y., Osawa, M., Takatsu, K., Takaki, S., and Nakauchi, H. (2005). Quantification of self-renewal capacity in single hematopoietic stem cells from normal and Lnk-deficient mice. Dev. Cell *8*, 907–914.

Endharti, A.T., Rifa'I, M., Shi, Z., Fukuoka, Y., Nakahara, Y., Kawamoto, Y., Takeda, K., Isobe, K.-I., and Suzuki, H. (2005). Cutting edge: CD8+CD122+ regulatory T cells produce IL-10 to suppress IFN-gamma production and proliferation of CD8+ T cells. J. Immunol. *175*, 7093–7097.

Essers, M.A.G., Offner, S., Blanco-Bose, W.E., Waibler, Z., Kalinke, U., Duchosal, M.A., and Trumpp, A. (2009). IFNalpha activates dormant haematopoietic stem cells in vivo. Nature *458*, 904–908.

Fahlén, L., Read, S., Gorelik, L., Hurst, S.D., Coffman, R.L., Flavell, R.A., and Powrie, F. (2005). T cells that cannot respond to TGF-beta escape control by CD4(+)CD25(+) regulatory T cells. J. Exp. Med. *201*, 737–746.

Fallarino, F., Grohmann, U., Hwang, K.W., Orabona, C., Vacca, C., Bianchi, R., Belladonna, M.L., Fioretti, M.C., Alegre, M.-L., and Puccetti, P. (2003). Modulation of tryptophan catabolism by regulatory T cells. Nat. Immunol. *4*, 1206–1212.

Fantini, M.C., Dominitzki, S., Rizzo, A., Neurath, M.F., and Becker, C. (2007). In vitro generation of CD4+ CD25+ regulatory cells from murine naive T cells. Nat. Protoc. *2*, 1789–1794.

Feng, G., Wood, K.J., and Bushell, A. (2008a). Interferon-gamma conditioning ex vivo generates CD25+CD62L+Foxp3+ regulatory T cells that prevent allograft rejection: potential avenues for cellular therapy. Transplantation *86*, 578–589.

Feng, G., Gao, W., Strom, T.B., Oukka, M., Francis, R.S., Wood, K.J., and Bushell, A. (2008b). Exogenous IFN-gamma ex vivo shapes the alloreactive T-cell repertoire by inhibition of Th17 responses and generation of functional Foxp3+ regulatory T cells. Eur. J. Immunol. *38*, 2512–2527.

Feuerer, M., Hill, J.A., Mathis, D., and Benoist, C. (2009). Foxp3+ regulatory T cells: differentiation, specification, subphenotypes. Nat. Immunol. *10*, 689–695.

Feuerer, M., Hill, J.A., Kretschmer, K., von Boehmer, H., Mathis, D., and Benoist, C. (2010). Genomic definition of multiple ex vivo regulatory T cell subphenotypes. Proc. Natl. Acad. Sci. U. S. A. *107*, 5919–5924.

Fontenot, J.D., Gavin, M.A., and Rudensky, A.Y. (2003). Foxp3 programs the development and function of CD4+CD25+ regulatory T cells. Nat. Immunol. *4*, 330–336.

Fontenot, J.D., Rasmussen, J.P., Gavin, M.A., and Rudensky, A.Y. (2005a). A function for interleukin 2 in Foxp3-expressing regulatory T cells. Nat. Immunol. *6*, 1142–1151.

Fontenot, J.D., Rasmussen, J.P., Williams, L.M., Dooley, J.L., Farr, A.G., and Rudensky, A.Y. (2005b). Regulatory T cell lineage specification by the forkhead transcription factor foxp3. Immunity *22*, 329–341.

Foudi, A., Hochedlinger, K., Van Buren, D., Schindler, J.W., Jaenisch, R., Carey, V., and Hock, H. (2009). Analysis of histone 2B-GFP retention reveals slowly cycling hematopoietic stem cells. Nat. Biotechnol. *27*, 84–90.

Francis, R.S., Feng, G., Tha-In, T., Lyons, I.S., Wood, K.J., and Bushell, A. (2011). Induction of transplantation tolerance converts potential effector T cells into graft-protective regulatory T cells. Eur. J. Immunol. *41*, 726–738.

Freeman, G.J., Long, A.J., Iwai, Y., Bourque, K., Chernova, T., Nishimura, H., Fitz, L.J., Malenkovich, N., Okazaki, T., Byrne, M.C., et al. (2000). Engagement of the PD-1 immunoinhibitory receptor by a novel B7 family member leads to negative regulation of lymphocyte activation. J. Exp. Med. *192*, 1027–1034.

Frisullo, G., Nociti, V., Iorio, R., Plantone, D., Patanella, A.K., Tonali, P.A., and Batocchi, A.P. (2010). CD8(+)Foxp3(+) T cells in peripheral blood of relapsing-remitting multiple sclerosis patients. Hum. Immunol. *71*, 437–441.

Fu, W., Ergun, A., Lu, T., Hill, J.A., Haxhinasto, S., Fassett, M.S., Gazit, R., Adoro, S., Glimcher, L., Chan, S., et al. (2012). A multiply redundant genetic switch "locks in" the transcriptional signature of regulatory T cells. Nat. Immunol. *13*, 972–980.

Fujii, K., Ishimaru, F., Nakase, K., Tabayashi, T., Kozuka, T., Naoki, K., Miyahara, M., Toki, H., Kitajima, K., Harada, M., et al. (2003). Over-expression of short isoforms of Helios in patients with adult T-cell leukaemia/lymphoma. Br. J. Haematol. *120*, 986–989.

Fyhrquist, N., Lehtimäki, S., Lahl, K., Savinko, T., Lappeteläinen, A.-M., Sparwasser, T., Wolff, H., Lauerma, A., and Alenius, H. (2012). Foxp3+ cells control Th2 responses in a murine model of atopic dermatitis. J. Invest. Dermatol. *132*, 1672–1680.

Gavin, M.A., Rasmussen, J.P., Fontenot, J.D., Vasta, V., Manganiello, V.C., Beavo, J.A., and Rudensky, A.Y. (2007). Foxp3-dependent programme of regulatory T-cell differentiation. Nature *445*, 771–775.

Geimer Le Lay, A.-S., Oravecz, A., Mastio, J., Jung, C., Marchal, P., Ebel, C., Dembélé, D., Jost, B., Le Gras, S., Thibault, C., et al. (2014). The tumor suppressor Ikaros shapes the repertoire of notch target genes in T cells. Sci. Signal. *7*, ra28.

Georgopoulos, K., Moore, D.D., and Derfler, B. (1992). Ikaros, an early lymphoid-specific transcription factor and a putative mediator for T cell commitment. Science *258*, 808–812.

Georgopoulos, K., Bigby, M., Wang, J.H., Molnar, A., Wu, P., Winandy, S., and Sharpe, A. (1994). The Ikaros gene is required for the development of all lymphoid lineages. Cell *79*, 143–156.

Geremia, A., Biancheri, P., Allan, P., Corazza, G.R., and Di Sabatino, A. (2014). Innate and adaptive immunity in inflammatory bowel disease. Autoimmun. Rev. *13*, 3–10.

Gershon, R.K., and Kondo, K. (1970). Cell interactions in the induction of tolerance: the role of thymic lymphocytes. Immunology *18*, 723–737.

Gershon, R.K., Cohen, P., Hencin, R., and Liebhaber, S.A. (1972). Suppressor T cells. J. Immunol. *108*, 586–590.

Gershon, R.K., Eardley, D.D., Naidorf, K.F., and Ptak, W. (1977). The hermaphrocyte: a suppressor-helper T cell. Cold Spring Harb. Symp. Quant. Biol. *41 Pt 1*, 85–91.

Getnet, D., Grosso, J.F., Goldberg, M.V., Harris, T.J., Yen, H.-R., Bruno, T.C., Durham, N.M., Hipkiss, E.L., Pyle, K.J., Wada, S., et al. (2010). A role for the transcription factor Helios in human CD4(+)CD25(+) regulatory T cells. Mol. Immunol. *47*, 1595–1600.

Godfrey, V.L., Wilkinson, J.E., and Russell, L.B. (1991). X-linked lymphoreticular disease in the scurfy (sf) mutant mouse. Am. J. Pathol. *138*, 1379–1387.

Gondek, D.C., Lu, L.-F., Quezada, S.A., Sakaguchi, S., and Noelle, R.J. (2005). Cutting edge: contact-mediated suppression by CD4+CD25+ regulatory cells involves a granzyme B-dependent, perforin-independent mechanism. J. Immunol. *174*, 1783–1786.

Goodell, M.A., Brose, K., Paradis, G., Conner, A.S., and Mulligan, R.C. (1996). Isolation and functional properties of murine hematopoietic stem cells that are replicating in vivo. J. Exp. Med. *183*, 1797–1806.

Göttgens, B. (2015). Regulatory network control of blood stem cells. Blood *125*, 2614–2620.

Gottschalk, R.A., Corse, E., and Allison, J.P. (2012). Expression of Helios in peripherally induced Foxp3+ regulatory T cells. J. Immunol. *188*, 976–980.

Green, D.R., Chue, B., and Gershon, R.K. (1983). Discrimination of 2 types of suppressor T cells by cell surface phenotype and by function: the ability to regulate the contrasuppressor circuit. J. Mol. Cell. Immunol. JMCI *1*, 19–30.

Gurel, Z., Ronni, T., Ho, S., Kuchar, J., Payne, K.J., Turk, C.W., and Dovat, S. (2008). Recruitment of ikaros to pericentromeric heterochromatin is regulated by phosphorylation. J. Biol. Chem. *283*, 8291–8300.

Hahm, K., Cobb, B.S., McCarty, A.S., Brown, K.E., Klug, C.A., Lee, R., Akashi, K., Weissman, I.L., Fisher, A.G., and Smale, S.T. (1998). Helios, a T cell-restricted Ikaros family member that quantitatively associates with Ikaros at centromeric heterochromatin. Genes Dev. *12*, 782–796.

Hahn, B.H., Singh, R.P., Cava, A.L., and Ebling, F.M. (2005). Tolerogenic Treatment of Lupus Mice with Consensus Peptide Induces Foxp3-Expressing, Apoptosis-Resistant, TGFβ-Secreting CD8+ T Cell Suppressors. J. Immunol. *175*, 7728–7737.

Hara, M., Kingsley, C.I., Niimi, M., Read, S., Turvey, S.E., Bushell, A.R., Morris, P.J., Powrie, F., and Wood, K.J. (2001). IL-10 is required for regulatory T cells to mediate tolerance to alloantigens in vivo. J. Immunol. *166*, 3789–3796.

Haribhai, D., Lin, W., Edwards, B., Ziegelbauer, J., Salzman, N.H., Carlson, M.R., Li, S.-H., Simpson, P.M., Chatila, T.A., and Williams, C.B. (2009). A central role for induced regulatory T cells in tolerance induction in experimental colitis. J. Immunol. *182*, 3461–3468.

Harrison, D.E. (1979). Mouse erythropoietic stem cell lines function normally 100 months: loss related to number of transplantations. Mech. Ageing Dev. *9*, 427–433.

Harrison, D.E. (1980). Competitive repopulation: a new assay for long-term stem cell functional capacity. Blood *55*, 77–81.

Harrison, D.E., and Astle, C.M. (1982). Loss of stem cell repopulating ability upon transplantation. Effects of donor age, cell number, and transplantation procedure. J. Exp. Med. *156*, 1767–1779.

Harrison, D.E., Astle, C.M., and Delaittre, J.A. (1978). Loss of proliferative capacity in immunohemopoietic stem cells caused by serial transplantation rather than aging. J. Exp. Med. *147*, 1526–1531.

Hayflick, L., and Moorhead, P.S. (1961). The serial cultivation of human diploid cell strains. Exp. Cell Res. *25*, 585–621.

Heinzel, K., Benz, C., Martins, V.C., Haidl, I.D., and Bleul, C.C. (2007). Bone marrow-derived hemopoietic precursors commit to the T cell lineage only after arrival in the thymic microenvironment. J. Immunol. *178*, 858–868.

Hill, J.A., Feuerer, M., Tash, K., Haxhinasto, S., Perez, J., Melamed, R., Mathis, D., and Benoist, C. (2007). Foxp3 transcription-factor-dependent and -independent regulation of the regulatory T cell transcriptional signature. Immunity *27*, 786–800.

Hill, J.A., Hall, J.A., Sun, C.-M., Cai, Q., Ghyselinck, N., Chambon, P., Belkaid, Y., Mathis, D., and Benoist, C. (2008). Retinoic acid enhances Foxp3 induction indirectly by relieving inhibition from CD4+CD44hi Cells. Immunity *29*, 758–770.

Hock, H., Hamblen, M.J., Rooke, H.M., Schindler, J.W., Saleque, S., Fujiwara, Y., and Orkin, S.H. (2004). Gfi-1 restricts proliferation and preserves functional integrity of haematopoietic stem cells. Nature *431*, 1002–1007.

Hogquist, K.A., and Jameson, S.C. (2014). The self-obsession of T cells: how TCR signaling thresholds affect fate “decisions” and effector function. Nat. Immunol. *15*, 815–823.

Holmfeldt, L., Wei, L., Diaz-Flores, E., Walsh, M., Zhang, J., Ding, L., Payne-Turner, D., Churchman, M., Andersson, A., Chen, S.-C., et al. (2013). The genomic landscape of hypodiploid acute lymphoblastic leukemia. Nat. Genet. *45*, 242–252.

Honma, Y., Kiyosawa, H., Mori, T., Oguri, A., Nikaido, T., Kanazawa, K., Tojo, M., Takeda, J., Tanno, Y., Yokoya, S., et al. (1999). Eos: a novel member of the Ikaros gene family expressed predominantly in the developing nervous system. FEBS Lett. *447*, 76–80.

Hori, S., Nomura, T., and Sakaguchi, S. (2003). Control of regulatory T cell development by the transcription factor Foxp3. Science *299*, 1057–1061.

Hsieh, C.-S., Zheng, Y., Liang, Y., Fontenot, J.D., and Rudensky, A.Y. (2006). An intersection between the self-reactive regulatory and nonregulatory T cell receptor repertoires. Nat. Immunol. *7*, 401–410.

Hu, D., Ikizawa, K., Lu, L., Sanchirico, M.E., Shinohara, M.L., and Cantor, H. (2004). Analysis of regulatory CD8 T cells in Qa-1-deficient mice. Nat. Immunol. *5*, 516–523.

Hu, R., Sharma, S.M., Bronisz, A., Srinivasan, R., Sankar, U., and Ostrowski, M.C. (2007). Eos, MITF, and PU.1 recruit corepressors to osteoclast-specific genes in committed myeloid progenitors. Mol. Cell. Biol. *27*, 4018–4027.

Huehn, J., Siegmund, K., Lehmann, J.C.U., Siewert, C., Haubold, U., Feuerer, M., Debes, G.F., Lauber, J., Frey, O., Przybylski, G.K., et al. (2004). Developmental stage, phenotype, and migration distinguish naive- and effector/memory-like CD4+ regulatory T cells. J. Exp. Med. *199*, 303–313.

Ikuta, K., and Weissman, I.L. (1992). Evidence that hematopoietic stem cells express mouse c-kit but do not depend on steel factor for their generation. Proc. Natl. Acad. Sci. U. S. A. *89*, 1502–1506.

Jenkins, M.K., and Schwartz, R.H. (1987). Antigen presentation by chemically modified splenocytes induces antigen-specific T cell unresponsiveness in vitro and in vivo. J. Exp. Med. *165*, 302–319.

Jiang, H., Ware, R., Stall, A., Flaherty, L., Chess, L., and Pernis, B. (1995). Murine CD8+ T cells that specifically delete autologous CD4+ T cells expressing V beta 8 TCR: a role of the Qa-1 molecule. Immunity *2*, 185–194.

John, L.B., Yoong, S., and Ward, A.C. (2009). Evolution of the Ikaros Gene Family: Implications for the Origins of Adaptive Immunity. J. Immunol. *182*, 4792–4799.

Jordan, M.S., Boesteanu, A., Reed, A.J., Petrone, A.L., Holenbeck, A.E., Lerman, M.A., Naji, A., and Caton, A.J. (2001). Thymic selection of CD4+CD25+ regulatory T cells induced by an agonist self-peptide. Nat. Immunol. *2*, 301–306.

Josefowicz, S.Z., Wilson, C.B., and Rudensky, A.Y. (2009). Cutting edge: TCR stimulation is sufficient for induction of Foxp3 expression in the absence of DNA methyltransferase 1. J. Immunol. *182*, 6648–6652.

June, C.H., Ledbetter, J.A., Gillespie, M.M., Lindsten, T., and Thompson, C.B. (1987). T-cell proliferation involving the CD28 pathway is associated with cyclosporine-resistant interleukin 2 gene expression. Mol. Cell. Biol. *7*, 4472–4481.

Kamminga, L.M., and de Haan, G. (2006). Cellular memory and hematopoietic stem cell aging. Stem Cells Dayt. Ohio *24*, 1143–1149.

Kamminga, L.M., van Os, R., Ausema, A., Noach, E.J.K., Weersing, E., Dontje, B., Vellenga, E., and de Haan, G. (2005). Impaired hematopoietic stem cell functioning after serial transplantation and during normal aging. Stem Cells Dayt. Ohio *23*, 82–92.

Kamminga, L.M., Bystrykh, L.V., de Boer, A., Houwer, S., Douma, J., Weersing, E., Dontje, B., and de Haan, G. (2006). The Polycomb group gene Ezh2 prevents hematopoietic stem cell exhaustion. Blood *107*, 2170–2179.

Katayama, N., Shih, J.P., Nishikawa, S., Kina, T., Clark, S.C., and Ogawa, M. (1993). Stage-specific expression of c-kit protein by murine hematopoietic progenitors. Blood *82*, 2353–2360.

Kaufmann, E., and Knöchel, W. (1996). Five years on the wings of fork head. Mech. Dev. *57*, 3–20.

Kelley, C.M., Ikeda, T., Koipally, J., Avitahl, N., Wu, L., Georgopoulos, K., and Morgan, B.A. (1998). Helios, a novel dimerization partner of Ikaros expressed in the earliest hematopoietic progenitors. Curr. Biol. CB *8*, 508–515.

Khattri, R., Cox, T., Yasayko, S.-A., and Ramsdell, F. (2003). An essential role for Scurfin in CD4+CD25+ T regulatory cells. Nat. Immunol. *4*, 337–342.

Kiel, M.J., Yilmaz, O.H., Iwashita, T., Yilmaz, O.H., Terhorst, C., and Morrison, S.J. (2005). SLAM family receptors distinguish hematopoietic stem and progenitor cells and reveal endothelial niches for stem cells. Cell *121*, 1109–1121.

Kikuchi, H., Nakayama, M., Takami, Y., Kuribayashi, F., and Nakayama, T. (2011). Possible involvement of Helios in controlling the immature B cell functions via transcriptional regulation of protein kinase Cs. Results Immunol. *1*, 88–94.

Kim, H.-J., Verbinnen, B., Tang, X., Lu, L., and Cantor, H. (2010). Inhibition of follicular T-helper cells by CD8(+) regulatory T cells is essential for self tolerance. Nature *467*, 328–332.

Kim, H.-J., Wang, X., Radfar, S., Sproule, T.J., Roopenian, D.C., and Cantor, H. (2011). CD8+ T regulatory cells express the Ly49 Class I MHC receptor and are defective in autoimmune prone B6-Yaa mice. Proc. Natl. Acad. Sci. U. S. A. *108*, 2010–2015.

Kim, J., Sif, S., Jones, B., Jackson, A., Koipally, J., Heller, E., Winandy, S., Viel, A., Sawyer, A., Ikeda, T., et al. (1999). Ikaros DNA-binding proteins direct formation of chromatin remodeling complexes in lymphocytes. Immunity *10*, 345–355.

Kiniwa, Y., Miyahara, Y., Wang, H.Y., Peng, W., Peng, G., Wheeler, T.M., Thompson, T.C., Old, L.J., and Wang, R.-F. (2007). CD8+ Foxp3+ regulatory T cells mediate immunosuppression in prostate cancer. Clin. Cancer Res. Off. J. Am. Assoc. Cancer Res. *13*, 6947–6958.

Kirstetter, P., Thomas, M., Dierich, A., Kastner, P., and Chan, S. (2002). Ikaros is critical for B cell differentiation and function. Eur. J. Immunol. *32*, 720–730.

Kleinmann, E., Geimer Le Lay, A.-S., Sellars, M., Kastner, P., and Chan, S. (2008). Ikaros represses the transcriptional response to Notch signaling in T-cell development. Mol. Cell. Biol. *28*, 7465–7475.

Klug, C.A., Morrison, S.J., Masek, M., Hahm, K., Smale, S.T., and Weissman, I.L. (1998). Hematopoietic stem cells and lymphoid progenitors express different Ikaros isoforms, and Ikaros is localized to heterochromatin in immature lymphocytes. Proc. Natl. Acad. Sci. U. S. A. *95*, 657–662.

Koch, M.A., Tucker-Heard, G., Perdue, N.R., Killebrew, J.R., Urdahl, K.B., and Campbell, D.J. (2009). The transcription factor T-bet controls regulatory T cell homeostasis and function during type 1 inflammation. Nat. Immunol. *10*, 595–602.

Koipally, J., and Georgopoulos, K. (2000). Ikaros interactions with CtBP reveal a repression mechanism that is independent of histone deacetylase activity. J. Biol. Chem. *275*, 19594–19602.

Koipally, J., and Georgopoulos, K. (2002a). Ikaros-CtIP interactions do not require C-terminal binding protein and participate in a deacetylase-independent mode of repression. J. Biol. Chem. *277*, 23143–23149.

Koipally, J., and Georgopoulos, K. (2002b). A molecular dissection of the repression circuitry of Ikaros. J. Biol. Chem. *277*, 27697–27705.

Koipally, J., Renold, A., Kim, J., and Georgopoulos, K. (1999). Repression by Ikaros and Aiolos is mediated through histone deacetylase complexes. EMBO J. *18*, 3090–3100.

Koipally, J., Heller, E.J., Seavitt, J.R., and Georgopoulos, K. (2002). Unconventional potentiation of gene expression by Ikaros. J. Biol. Chem. *277*, 13007–13015.

Kondo, M., Weissman, I.L., and Akashi, K. (1997). Identification of clonogenic common lymphoid progenitors in mouse bone marrow. Cell *91*, 661–672.

Kullberg, M.C., Hay, V., Cheever, A.W., Mamura, M., Sher, A., Letterio, J.J., Shevach, E.M., and Piccirillo, C.A. (2005). TGF-beta1 production by CD4+ CD25+ regulatory T cells is not essential for suppression of intestinal inflammation. Eur. J. Immunol. *35*, 2886–2895.

Lafferty, K.J., and Cunningham, A.J. (1975). A new analysis of allogeneic interactions. Aust. J. Exp. Biol. Med. Sci. *53*, 27–42.

Lehmann, J., Huehn, J., de la Rosa, M., Maszyna, F., Kretschmer, U., Krenn, V., Brunner, M., Scheffold, A., and Hamann, A. (2002). Expression of the integrin alpha Ebeta 7 identifies unique subsets of CD25+ as well as CD25- regulatory T cells. Proc. Natl. Acad. Sci. U. S. A. *99*, 13031–13036.

Lemischka, I.R., Raulet, D.H., and Mulligan, R.C. (1986). Developmental potential and dynamic behavior of hematopoietic stem cells. Cell *45*, 917–927.

Lerret, N.M., Houlihan, J.L., Kheradmand, T., Pothoven, K.L., Zhang, Z.J., and Luo, X. (2012). Donor-specific CD8+ Foxp3+ T cells protect skin allografts and facilitate induction of conventional CD4+ Foxp3+ regulatory T cells. Am. J. Transplant. Off. J. Am. Soc. Transplant. Am. Soc. Transpl. Surg. *12*, 2335–2347.

Li, B., Samanta, A., Song, X., Iacono, K.T., Bembas, K., Tao, R., Basu, S., Riley, J.L., Hancock, W.W., Shen, Y., et al. (2007). FOXP3 interactions with histone acetyltransferase and class II histone deacetylases are required for repression. Proc. Natl. Acad. Sci. U. S. A. *104*, 4571–4576.

Li, Z., Perez-Casellas, L.A., Savic, A., Song, C., and Dovat, S. (2011). Ikaros isoforms: The saga continues. World J. Biol. Chem. *2*, 140–145.

Liang, B., Workman, C., Lee, J., Chew, C., Dale, B.M., Colonna, L., Flores, M., Li, N., Schweighoffer, E., Greenberg, S., et al. (2008). Regulatory T cells inhibit dendritic cells by lymphocyte activation gene-3 engagement of MHC class II. J. Immunol. *180*, 5916–5926.

Lin, W., Haribhai, D., Relland, L.M., Truong, N., Carlson, M.R., Williams, C.B., and Chatila, T.A. (2007). Regulatory T cell development in the absence of functional Foxp3. Nat. Immunol. *8*, 359–368.

Linsley, P.S., Clark, E.A., and Ledbetter, J.A. (1990). T-cell antigen CD28 mediates adhesion with B cells by interacting with activation antigen B7/BB-1. Proc. Natl. Acad. Sci. U. S. A. *87*, 5031–5035.

Linterman, M.A., Pierson, W., Lee, S.K., Kallies, A., Kawamoto, S., Rayner, T.F., Srivastava, M., Divekar, D.P., Beaton, L., Hogan, J.J., et al. (2011). Foxp3+ follicular regulatory T cells control the germinal center response. Nat. Med. *17*, 975–982.

Lio, C.-W.J., and Hsieh, C.-S. (2008). A two-step process for thymic regulatory T cell development. Immunity *28*, 100–111.

Liu, S.-Q., Jiang, S., Li, C., Zhang, B., and Li, Q.-J. (2014). miR-17-92 cluster targets phosphatase and tensin homology and Ikaros Family Zinc Finger 4 to promote TH17-mediated inflammation. J. Biol. Chem. *289*, 12446–12456.

Lo, K., Landau, N.R., and Smale, S.T. (1991). LyF-1, a transcriptional regulator that interacts with a novel class of promoters for lymphocyte-specific genes. Mol. Cell. Biol. *11*, 5229–5243.

Love, P.E., and Bhandoola, A. (2011). Signal integration and crosstalk during thymocyte migration and emigration. Nat. Rev. Immunol. *11*, 469–477.

Lu, L., Yu, Y., Li, G., Pu, L., Zhang, F., Zheng, S., and Wang, X. (2009). CD8(+)CD103(+) regulatory T cells in spontaneous tolerance of liver allografts. Int. Immunopharmacol. *9*, 546–548.

Luckheeram, R.V., Zhou, R., Verma, A.D., and Xia, B. (2012). $CD4^+$T cells: differentiation and functions. Clin. Dev. Immunol. *2012*, 925135.

Luo, X., Zhang, Q., Liu, V., Xia, Z., Pothoven, K.L., and Lee, C. (2008). Cutting edge: TGF-beta-induced expression of Foxp3 in T cells is mediated through inactivation of ERK. J. Immunol. *180*, 2757–2761.

Mahic, M., Henjum, K., Yaqub, S., Bjørnbeth, B.A., Torgersen, K.M., Taskén, K., and Aandahl, E.M. (2008). Generation of highly suppressive adaptive CD8(+)CD25(+)FOXP3(+) regulatory T cells by continuous antigen stimulation. Eur. J. Immunol. *38*, 640–646.

Maillard, I., Tu, L., Sambandam, A., Yashiro-Ohtani, Y., Millholland, J., Keeshan, K., Shestova, O., Xu, L., Bhandoola, A., and Pear, W.S. (2006). The requirement for Notch signaling at the beta-selection checkpoint in vivo is absolute and independent of the pre-T cell receptor. J. Exp. Med. *203*, 2239–2245.

Malissen, B., Grégoire, C., Malissen, M., and Roncagalli, R. (2014). Integrative biology of T cell activation. Nat. Immunol. *15*, 790–797.

Mangalam, A.K., Luckey, D., Giri, S., Smart, M., Pease, L.R., Rodriguez, M., and David, C.S. (2012). Two discreet subsets of CD8 T cells modulate PLP(91-110) induced experimental autoimmune encephalomyelitis in HLA-DR3 transgenic mice. J. Autoimmun. *38*, 344–353.

Marie, J.C., Letterio, J.J., Gavin, M., and Rudensky, A.Y. (2005). TGF-beta1 maintains suppressor function and Foxp3 expression in CD4+CD25+ regulatory T cells. J. Exp. Med. *201*, 1061–1067.

Marson, A., Kretschmer, K., Frampton, G.M., Jacobsen, E.S., Polansky, J.K., MacIsaac, K.D., Levine, S.S., Fraenkel, E., von Boehmer, H., and Young, R.A. (2007). Foxp3 occupancy and regulation of key target genes during T-cell stimulation. Nature *445*, 931–935.

Masuda, K., Kakugawa, K., Nakayama, T., Minato, N., Katsura, Y., and Kawamoto, H. (2007). T cell lineage determination precedes the initiation of TCR beta gene rearrangement. J. Immunol. *179*, 3699–3706.

Mayle, A., Luo, M., Jeong, M., and Goodell, M.A. (2013). Mouse Hematopoietic Stem Cell Identification And Analysis. Cytom. Part J. Int. Soc. Anal. Cytol. *83*, 27–37.

Mazo, I.B., Massberg, S., and von Andrian, U.H. (2011). Hematopoietic stem and progenitor cell trafficking. Trends Immunol. *32*, 493–503.

McPherson, S.W., Heuss, N.D., and Gregerson, D.S. (2013). Local “on-demand” generation and function of antigen-specific Foxp3+ regulatory T cells. J. Immunol. *190*, 4971–4981.

Miyara, M., Yoshioka, Y., Kitoh, A., Shima, T., Wing, K., Niwa, A., Parizot, C., Taflin, C., Heike, T., Valeyre, D., et al. (2009). Functional delineation and differentiation dynamics of human CD4+ T cells expressing the FoxP3 transcription factor. Immunity *30*, 899–911.

Molnár, A., and Georgopoulos, K. (1994). The Ikaros gene encodes a family of functionally diverse zinc finger DNA-binding proteins. Mol. Cell. Biol. *14*, 8292–8303.

Morgan, B., Sun, L., Avitahl, N., Andrikopoulos, K., Ikeda, T., Gonzales, E., Wu, P., Neben, S., and Georgopoulos, K. (1997). Aiolos, a lymphoid restricted transcription factor that interacts with Ikaros to regulate lymphocyte differentiation. EMBO J. *16*, 2004–2013.

Morrison, S.J., and Scadden, D.T. (2014). The bone marrow niche for haematopoietic stem cells. Nature *505*, 327–334.

Morrison, S.J., and Weissman, I.L. (1994). The long-term repopulating subset of hematopoietic stem cells is deterministic and isolatable by phenotype. Immunity *1*, 661–673.

Morrissey, P.J., Charrier, K., Braddy, S., Liggitt, D., and Watson, J.D. (1993). CD4+ T cells that express high levels of CD45RB induce wasting disease when transferred into congenic severe combined immunodeficient mice. Disease development is prevented by cotransfer of purified CD4+ T cells. J. Exp. Med. *178*, 237–244.

Mottet, C., Uhlig, H.H., and Powrie, F. (2003). Cutting edge: cure of colitis by CD4+CD25+ regulatory T cells. J. Immunol. *170*, 3939–3943.

Mucida, D., Kutchukhidze, N., Erazo, A., Russo, M., Lafaille, J.J., and Curotto de Lafaille, M.A. (2005). Oral tolerance in the absence of naturally occurring Tregs. J. Clin. Invest. *115*, 1923–1933.

Mullighan, C.G., Miller, C.B., Radtke, I., Phillips, L.A., Dalton, J., Ma, J., White, D., Hughes, T.P., Le Beau, M.M., Pui, C.-H., et al. (2008). BCR-ABL1 lymphoblastic leukaemia is characterized by the deletion of Ikaros. Nature *453*, 110–114.

Nagai, Y., Garrett, K.P., Ohta, S., Bahrun, U., Kouro, T., Akira, S., Takatsu, K., and Kincade, P.W. (2006). Toll-like receptors on hematopoietic progenitor cells stimulate innate immune system replenishment. Immunity *24*, 801–812.

Nakamura-Ishizu, A., Takizawa, H., and Suda, T. (2014). The analysis, roles and regulation of quiescence in hematopoietic stem cells. Dev. Camb. Engl. *141*, 4656–4666.

Nakase, K., Ishimaru, F., Fujii, K., Tabayashi, T., Kozuka, T., Sezaki, N., Matsuo, Y., and Harada, M. (2002). Overexpression of novel short isoforms of Helios in a patient with T-cell acute lymphoblastic leukemia. Exp. Hematol. *30*, 313–317.

Nakauchi, H., Sudo, K., and Ema, H. (2001). Quantitative assessment of the stem cell self-renewal capacity. Ann. N. Y. Acad. Sci. *938*, 18–24; discussion 24–25.

Na Nakorn, T., Traver, D., Weissman, I.L., and Akashi, K. (2002). Myeloerythroid-restricted progenitors are sufficient to confer radioprotection and provide the majority of day 8 CFU-S. J. Clin. Invest. *109*, 1579–1585.

Nichogiannopoulou, A., Trevisan, M., Neben, S., Friedrich, C., and Georgopoulos, K. (1999). Defects in hemopoietic stem cell activity in Ikaros mutant mice. J. Exp. Med. *190*, 1201–1214.

Nishizuka, Y., and Sakakura, T. (1969). Thymus and reproduction: sex-linked dysgenesia of the gonad after neonatal thymectomy in mice. Science *166*, 753–755.

Ntziachristos, P., Tsirigos, A., Van Vlierberghe, P., Nedjic, J., Trimarchi, T., Flaherty, M.S., Ferres-Marco, D., da Ros, V., Tang, Z., Siegle, J., et al. (2012). Genetic inactivation of the polycomb repressive complex 2 in T cell acute lymphoblastic leukemia. Nat. Med. *18*, 298–301.

Oberle, N., Eberhardt, N., Falk, C.S., Krammer, P.H., and Suri-Payer, E. (2007). Rapid suppression of cytokine transcription in human CD4+CD25 T cells by CD4+Foxp3+ regulatory T cells: independence of IL-2 consumption, TGF-beta, and various inhibitors of TCR signaling. J. Immunol. *179*, 3578–3587.

O'Carroll, D., Erhardt, S., Pagani, M., Barton, S.C., Surani, M.A., and Jenuwein, T. (2001). The polycomb-group gene Ezh2 is required for early mouse development. Mol. Cell. Biol. *21*, 4330–4336.

Oderup, C., Cederbom, L., Makowska, A., Cilio, C.M., and Ivars, F. (2006). Cytotoxic T lymphocyte antigen-4-dependent down-modulation of costimulatory molecules on dendritic cells in CD4+ CD25+ regulatory T-cell-mediated suppression. Immunology *118*, 240–249.

Oguro, H., Ding, L., and Morrison, S.J. (2013). SLAM family markers resolve functionally distinct subpopulations of hematopoietic stem cells and multipotent progenitors. Cell Stem Cell *13*, 102–116.

Ohkura, N., Hamaguchi, M., Morikawa, H., Sugimura, K., Tanaka, A., Ito, Y., Osaki, M., Tanaka, Y., Yamashita, R., Nakano, N., et al. (2012). T cell receptor stimulation-induced epigenetic changes and Foxp3 expression are independent and complementary events required for Treg cell development. Immunity *37*, 785–799.

Okazaki, T., Iwai, Y., and Honjo, T. (2002). New regulatory co-receptors: inducible co-stimulator and PD-1. Curr. Opin. Immunol. *14*, 779–782.

Olovnikov, A.M. (1973). A theory of marginotomy. The incomplete copying of template margin in enzymic synthesis of polynucleotides and biological significance of the phenomenon. J. Theor. Biol. *41*, 181–190.

O'Neill, D.W., Schoetz, S.S., Lopez, R.A., Castle, M., Rabinowitz, L., Shor, E., Krawchuk, D., Goll, M.G., Renz, M., Seelig, H.P., et al. (2000). An ikaros-containing chromatin-remodeling complex in adult-type erythroid cells. Mol. Cell. Biol. *20*, 7572–7582.

Oravecz A, Apostolov A, Polak K, Jost B, Le Gras S, Chan S, Kastner P. (2015) Ikaros mediates gene silencing in T cells through Polycomb repressive complex 2. Nat Commun. Nov 9;6:8823.

Orford, K.W., and Scadden, D.T. (2008). Deconstructing stem cell self-renewal: genetic insights into cell-cycle regulation. Nat. Rev. Genet. *9*, 115–128.

Orkin, S.H. (2000). Diversification of haematopoietic stem cells to specific lineages. Nat. Rev. Genet. *1*, 57–64.

Osawa, M., Hanada, K., Hamada, H., and Nakauchi, H. (1996). Long-term lymphohematopoietic reconstitution by a single CD34-low/negative hematopoietic stem cell. Science *273*, 242–245.

Ostanin, D.V., Bao, J., Koboziev, I., Gray, L., Robinson-Jackson, S.A., Kosloski-Davidson, M., Price, V.H., and Grisham, M.B. (2009). T cell transfer model of chronic colitis: concepts, considerations, and tricks of the trade. Am. J. Physiol. Gastrointest. Liver Physiol. *296*, G135–G146.

Ouyang, W., Beckett, O., Ma, Q., and Li, M.O. (2010). Transforming growth factor-beta signaling curbs thymic negative selection promoting regulatory T cell development. Immunity *32*, 642–653.

Pacholczyk, R., Ignatowicz, H., Kraj, P., and Ignatowicz, L. (2006). Origin and T cell receptor diversity of Foxp3+CD4+CD25+ T cells. Immunity *25*, 249–259.

Pan, F., Yu, H., Dang, E.V., Barbi, J., Pan, X., Grosso, J.F., Jinasena, D., Sharma, S.M., McCadden, E.M., Getnet, D., et al. (2009). Eos mediates Foxp3-dependent gene silencing in CD4+ regulatory T cells. Science *325*, 1142–1146.

Pandiyan, P., Zheng, L., Ishihara, S., Reed, J., and Lenardo, M.J. (2007). CD4+CD25+Foxp3+ regulatory T cells induce cytokine deprivation-mediated apoptosis of effector CD4+ T cells. Nat. Immunol. *8*, 1353–1362.

Papathanasiou, P., Attema, J.L., Karsunky, H., Hosen, N., Sontani, Y., Hoyne, G.F., Tunningley, R., Smale, S.T., and Weissman, I.L. (2009). Self-renewal of the long-term reconstituting subset of hematopoietic stem cells is regulated by Ikaros. Stem Cells Dayt. Ohio *27*, 3082–3092.

Passegué, E., Wagers, A.J., Giuriato, S., Anderson, W.C., and Weissman, I.L. (2005). Global analysis of proliferation and cell cycle gene expression in the regulation of hematopoietic stem and progenitor cell fates. J. Exp. Med. *202*, 1599–1611.

Paul, W.E., and Zhu, J. (2010). How are T(H)2-type immune responses initiated and amplified? Nat. Rev. Immunol. *10*, 225–235.

Payne, K.J., Huang, G., Sahakian, E., Zhu, J.Y., Barteneva, N.S., Barsky, L.W., Payne, M.A., and Crooks, G.M. (2003). Ikaros isoform x is selectively expressed in myeloid differentiation. J. Immunol. *170*, 3091–3098.

Pear, W.S., Aster, J.C., Scott, M.L., Hasserjian, R.P., Soffer, B., Sklar, J., and Baltimore, D. (1996). Exclusive development of T cell neoplasms in mice transplanted with bone marrow expressing activated Notch alleles. J. Exp. Med. *183*, 2283–2291.

Perdomo, J., and Crossley, M. (2002). The Ikaros family protein Eos associates with C-terminal-binding protein corepressors. Eur. J. Biochem. FEBS *269*, 5885–5892.

Perdomo, J., Holmes, M., Chong, B., and Crossley, M. (2000). Eos and pegasus, two members of the Ikaros family of proteins with distinct DNA binding activities. J. Biol. Chem. *275*, 38347–38354.

Powrie, F., and Mason, D. (1990). OX-22high CD4+ T cells induce wasting disease with multiple organ pathology: prevention by the OX-22low subset. J. Exp. Med. *172*, 1701–1708.

Powrie, F., Carlino, J., Leach, M.W., Mauze, S., and Coffman, R.L. (1996). A critical role for transforming growth factor-beta but not interleukin 4 in the suppression of T helper type 1-mediated colitis by CD45RB(low) CD4+ T cells. J. Exp. Med. *183*, 2669–2674.

Pui, J.C., Allman, D., Xu, L., DeRocco, S., Karnell, F.G., Bakkour, S., Lee, J.Y., Kadesch, T., Hardy, R.R., Aster, J.C., et al. (1999). Notch1 expression in early lymphopoiesis influences B versus T lineage determination. Immunity *11*, 299–308.

Purton, L.E., and Scadden, D.T. (2007). Limiting factors in murine hematopoietic stem cell assays. Cell Stem Cell *1*, 263–270.

Radtke, F., Wilson, A., Stark, G., Bauer, M., van Meerwijk, J., MacDonald, H.R., and Aguet, M. (1999). Deficient T cell fate specification in mice with an induced inactivation of Notch1. Immunity *10*, 547–558.

Radtke, F., MacDonald, H.R., and Tacchini-Cottier, F. (2013). Regulation of innate and adaptive immunity by Notch. Nat. Rev. Immunol. *13*, 427–437.

Rea, S., Eisenhaber, F., O'Carroll, D., Strahl, B.D., Sun, Z.W., Schmid, M., Opravil, S., Mechtler, K., Ponting, C.P., Allis, C.D., et al. (2000). Regulation of chromatin structure by site-specific histone H3 methyltransferases. Nature *406*, 593–599.

Rebollo, A., and Schmitt, C. (2003). Ikaros, Aiolos and Helios: transcription regulators and lymphoid malignancies. Immunol. Cell Biol. *81*, 171–175.

Rieder, S.A., Metidji, A., Glass, D.D., Thornton, A.M., Ikeda, T., Morgan, B.A., and Shevach, E.M. (2015). Eos Is Redundant for Regulatory T Cell Function but Plays an Important Role in IL-2 and Th17 Production by CD4+ Conventional T Cells. J. Immunol. *195*, 553–563.

Rifa'i, M., Kawamoto, Y., Nakashima, I., and Suzuki, H. (2004). Essential roles of CD8+CD122+ regulatory T cells in the maintenance of T cell homeostasis. J. Exp. Med. *200*, 1123–1134.

Rifa'i, M., Shi, Z., Zhang, S.-Y., Lee, Y.H., Shiku, H., Isobe, K.-I., and Suzuki, H. (2008). CD8+CD122+ regulatory T cells recognize activated T cells via conventional MHC class I-alphabetaTCR interaction and become IL-10-producing active regulatory cells. Int. Immunol. *20*, 937–947.

Robb, R.J., Lineburg, K.E., Kuns, R.D., Wilson, Y.A., Raffelt, N.C., Olver, S.D., Varelias, A., Alexander, K.A., Teal, B.E., Sparwasser, T., et al. (2012). Identification and expansion of highly suppressive CD8(+)FoxP3(+) regulatory T cells after experimental allogeneic bone marrow transplantation. Blood *119*, 5898–5908.

Roncagalli, R., Mingueneau, M., Grégoire, C., Malissen, M., and Malissen, B. (2010). LAT signaling pathology: an "autoimmune" condition without T cell self-reactivity. Trends Immunol. *31*, 253–259.

Roncagalli, R., Hauri, S., Fiore, F., Liang, Y., Chen, Z., Sansoni, A., Kanduri, K., Joly, R., Malzac, A., Lähdesmäki, H., et al. (2014). Quantitative proteomics analysis of signalosome dynamics in primary T cells identifies the surface receptor CD6 as a Lat adaptor-independent TCR signaling hub. Nat. Immunol. *15*, 384–392.

Rossi, D.J., Bryder, D., Zahn, J.M., Ahlenius, H., Sonu, R., Wagers, A.J., and Weissman, I.L. (2005). Cell intrinsic alterations underlie hematopoietic stem cell aging. Proc. Natl. Acad. Sci. U. S. A. *102*, 9194–9199.

Round, J.L., and Mazmanian, S.K. (2010). Inducible Foxp3+ regulatory T-cell development by a commensal bacterium of the intestinal microbiota. Proc. Natl. Acad. Sci. U. S. A. *107*, 12204–12209.

Rudensky, A.Y. (2011). Regulatory T cells and Foxp3. Immunol. Rev. *241*, 260–268.

Rudra, D., deRoos, P., Chaudhry, A., Niec, R.E., Arvey, A., Samstein, R.M., Leslie, C., Shaffer, S.A., Goodlett, D.R., and Rudensky, A.Y. (2012). Transcription factor Foxp3 and its protein partners form a complex regulatory network. Nat. Immunol. *13*, 1010–1019.

Sakaguchi, S., Takahashi, T., and Nishizuka, Y. (1982). Study on cellular events in post-thymectomy autoimmune oophoritis in mice. II. Requirement of Lyt-1 cells in normal female mice for the prevention of oophoritis. J. Exp. Med. *156*, 1577–1586.

Sakaguchi, S., Sakaguchi, N., Asano, M., Itoh, M., and Toda, M. (1995). Immunologic self-tolerance maintained by activated T cells expressing IL-2 receptor alpha-chains (CD25). Breakdown of a single mechanism of self-tolerance causes various autoimmune diseases. J. Immunol. *155*, 1151–1164.

Sakaguchi, S., Yamaguchi, T., Nomura, T., and Ono, M. (2008). Regulatory T Cells and Immune Tolerance. Cell *133*, 775–787.

Samstein, R.M., Arvey, A., Josefowicz, S.Z., Peng, X., Reynolds, A., Sandstrom, R., Neph, S., Sabo, P., Kim, J.M., Liao, W., et al. (2012). Foxp3 exploits a pre-existent enhancer landscape for regulatory T cell lineage specification. Cell *151*, 153–166.

Sather, B.D., Treuting, P., Perdue, N., Miazgowicz, M., Fontenot, J.D., Rudensky, A.Y., and Campbell, D.J. (2007). Altering the distribution of Foxp3(+) regulatory T cells results in tissue-specific inflammatory disease. J. Exp. Med. *204*, 1335–1347.

Sawamukai, N., Satake, A., Schmidt, A.M., Lamborn, I.T., Ojha, P., Tanaka, Y., and Kambayashi, T. (2012). Cell-autonomous role of TGFβ and IL-2 receptors in CD4+ and CD8+ inducible regulatory T-cell generation during GVHD. Blood *119*, 5575–5583.

Schjerven, H., McLaughlin, J., Arenzana, T.L., Frietze, S., Cheng, D., Wadsworth, S.E., Lawson, G.W., Bensinger, S.J., Farnham, P.J., Witte, O.N., et al. (2013). Selective regulation of lymphopoiesis and leukemogenesis by individual zinc fingers of Ikaros. Nat. Immunol. *14*, 1073–1083.

Schlenner, S.M., Madan, V., Busch, K., Tietz, A., Läufle, C., Costa, C., Blum, C., Fehling, H.J., and Rodewald, H.-R. (2010). Fate mapping reveals separate origins of T cells and myeloid lineages in the thymus. Immunity *32*, 426–436.

Schön, M.P., Arya, A., Murphy, E.A., Adams, C.M., Strauch, U.G., Agace, W.W., Marsal, J., Donohue, J.P., Her, H., Beier, D.R., et al. (1999). Mucosal T lymphocyte numbers are selectively reduced in integrin alpha E (CD103)-deficient mice. J. Immunol. *162*, 6641–6649.

Serre, K., Bénézech, C., Desanti, G., Bobat, S., Toellner, K.-M., Bird, R., Chan, S., Kastner, P., Cunningham, A.F., Maclennan, I.C.M., et al. (2011). Helios is associated with CD4 T cells differentiating to T helper 2 and follicular helper T cells in vivo independently of Foxp3 expression. PloS One *6*, e20731.

Serwold, T., Ehrlich, L.I.R., and Weissman, I.L. (2009). Reductive isolation from bone marrow and blood implicates common lymphoid progenitors as the major source of thymopoiesis. Blood *113*, 807–815.

Sharma, M.D., Huang, L., Choi, J.-H., Lee, E.-J., Wilson, J.M., Lemos, H., Pan, F., Blazar, B.R., Pardoll, D.M., Mellor, A.L., et al. (2013). An inherently bifunctional subset of Foxp3+ T helper cells is controlled by the transcription factor eos. Immunity *38*, 998–1012.

Shen, X., Liu, Y., Hsu, Y.-J., Fujiwara, Y., Kim, J., Mao, X., Yuan, G.-C., and Orkin, S.H. (2008). EZH1 mediates methylation on histone H3 lysine 27 and complements EZH2 in maintaining stem cell identity and executing pluripotency. Mol. Cell *32*, 491–502.

Shi, Z., Rifa'i, M., Lee, Y.H., Shiku, H., Isobe, K.-I., and Suzuki, H. (2008). Importance of CD80/CD86-CD28 interactions in the recognition of target cells by CD8+CD122+ regulatory T cells. Immunology *124*, 121–128.

Shrikant, P.A., Rao, R., Li, Q., Kesterson, J., Eppolito, C., Mischo, A., and Singhal, P. (2010). Regulating functional cell fates in CD8 T cells. Immunol. Res. *46*, 12–22.

Singh, B., Read, S., Asseman, C., Malmström, V., Mottet, C., Stephens, L.A., Stepankova, R., Tlaskalova, H., and Powrie, F. (2001). Control of intestinal inflammation by regulatory T cells. Immunol. Rev. *182*, 190–200.

Singh, K., Hjort, M., Thorvaldson, L., and Sandler, S. (2015). Concomitant analysis of Helios and Neuropilin-1 as a marker to detect thymic derived regulatory T cells in naïve mice. Sci. Rep. *5*, 7767.

Smith, H., Sakamoto, Y., Kasai, K., and Tung, K.S. (1991). Effector and regulatory cells in autoimmune oophoritis elicited by neonatal thymectomy. J. Immunol. *147*, 2928–2933.

Soper, D.M., Kasprowicz, D.J., and Ziegler, S.F. (2007). IL-2Rbeta links IL-2R signaling with Foxp3 expression. Eur. J. Immunol. *37*, 1817–1826.

Spangrude, G.J., Heimfeld, S., and Weissman, I.L. (1988). Purification and characterization of mouse hematopoietic stem cells. Science *241*, 58–62.

Sridharan, R., and Smale, S.T. (2007). Predominant interaction of both Ikaros and Helios with the NuRD complex in immature thymocytes. J. Biol. Chem. *282*, 30227–30238.

Starr, T.K., Jameson, S.C., and Hogquist, K.A. (2003). Positive and negative selection of T cells. Annu. Rev. Immunol. *21*, 139–176.

Stephens, G.L., Andersson, J., and Shevach, E.M. (2007). Distinct subsets of FoxP3+ regulatory T cells participate in the control of immune responses. J. Immunol. *178*, 6901–6911.

Sugimoto, N., Oida, T., Hirota, K., Nakamura, K., Nomura, T., Uchiyama, T., and Sakaguchi, S. (2006). Foxp3-dependent and -independent molecules specific for CD25+CD4+ natural regulatory T cells revealed by DNA microarray analysis. Int. Immunol. *18*, 1197–1209.

Sun, C.-M., Hall, J.A., Blank, R.B., Bouladoux, N., Oukka, M., Mora, J.R., and Belkaid, Y. (2007). Small intestine lamina propria dendritic cells promote de novo generation of Foxp3 T reg cells via retinoic acid. J. Exp. Med. *204*, 1775–1785.

Sun, L., Liu, A., and Georgopoulos, K. (1996). Zinc finger-mediated protein interactions modulate Ikaros activity, a molecular control of lymphocyte development. EMBO J. *15*, 5358–5369.

Suzuki, H., Kündig, T.M., Furlonger, C., Wakeham, A., Timms, E., Matsuyama, T., Schmits, R., Simard, J.J., Ohashi, P.S., and Griesser, H. (1995). Deregulated T cell activation and autoimmunity in mice lacking interleukin-2 receptor beta. Science *268*, 1472–1476.

Suzuki, H., Zhou, Y.W., Kato, M., Mak, T.W., and Nakashima, I. (1999). Normal regulatory alpha/beta T cells effectively eliminate abnormally activated T cells lacking the interleukin 2 receptor beta in vivo. J. Exp. Med. *190*, 1561–1572.

Tabrizifard, S., Olaru, A., Plotkin, J., Fallahi-Sichani, M., Livak, F., and Petrie, H.T. (2004). Analysis of transcription factor expression during discrete stages of postnatal thymocyte differentiation. J. Immunol. *173*, 1094–1102.

Taghon, T.N., David, E.-S., Zúñiga-Pflücker, J.C., and Rothenberg, E.V. (2005). Delayed, asynchronous, and reversible T-lineage specification induced by Notch/Delta signaling. Genes Dev. *19*, 965–978.

Tai, X., Cowan, M., Feigenbaum, L., and Singer, A. (2005). CD28 costimulation of developing thymocytes induces Foxp3 expression and regulatory T cell differentiation independently of interleukin 2. Nat. Immunol. *6*, 152–162.

Takahama, Y. (2006). Journey through the thymus: stromal guides for T-cell development and selection. Nat. Rev. Immunol. *6*, 127–135.

Takizawa, H., Regoes, R.R., Boddupalli, C.S., Bonhoeffer, S., and Manz, M.G. (2011). Dynamic variation in cycling of hematopoietic stem cells in steady state and inflammation. J. Exp. Med. *208*, 273–284.

Tang, Q., Henriksen, K.J., Boden, E.K., Tooley, A.J., Ye, J., Subudhi, S.K., Zheng, X.X., Strom, T.B., and Bluestone, J.A. (2003). Cutting edge: CD28 controls peripheral homeostasis of CD4+CD25+ regulatory T cells. J. Immunol. *171*, 3348–3352.

Tao, R., de Zoeten, E.F., Ozkaynak, E., Chen, C., Wang, L., Porrett, P.M., Li, B., Turka, L.A., Olson, E.N., Greene, M.I., et al. (2007). Deacetylase inhibition promotes the generation and function of regulatory T cells. Nat. Med. *13*, 1299–1307.

Thiault, N., Darrigues, J., Adoue, V., Gros, M., Binet, B., Perals, C., Leobon, B., Fazilleau, N., Joffre, O.P., Robey, E.A., et al. (2015). Peripheral regulatory T lymphocytes recirculating to the thymus suppress the development of their precursors. Nat. Immunol. *16*, 628–634.

Thornton, A.M., and Shevach, E.M. (1998). CD4+CD25+ immunoregulatory T cells suppress polyclonal T cell activation in vitro by inhibiting interleukin 2 production. J. Exp. Med. *188*, 287–296.

Thornton, A.M., Korty, P.E., Tran, D.Q., Wohlfert, E.A., Murray, P.E., Belkaid, Y., and Shevach, E.M. (2010). Expression of Helios, an Ikaros transcription factor family member, differentiates thymic-derived from peripherally induced Foxp3+ T regulatory cells. J. Immunol. *184*, 3433–3441.

Thorstenson, K.M., and Khoruts, A. (2001). Generation of anergic and potentially immunoregulatory CD25+CD4 T cells in vivo after induction of peripheral tolerance with intravenous or oral antigen. J. Immunol. *167*, 188–195.

Tone, Y., Furuuchi, K., Kojima, Y., Tykocinski, M.L., Greene, M.I., and Tone, M. (2008). Smad3 and NFAT cooperate to induce Foxp3 expression through its enhancer. Nat. Immunol. *9*, 194–202.

Trumpp, A., Essers, M., and Wilson, A. (2010). Awakening dormant haematopoietic stem cells. Nat. Rev. Immunol. *10*, 201–209.

Uchida, N., Aguila, H.L., Fleming, W.H., Jerabek, L., and Weissman, I.L. (1994). Rapid and sustained hematopoietic recovery in lethally irradiated mice transplanted with purified Thy-1.1lo Lin-Sca-1+ hematopoietic stem cells. Blood *83*, 3758–3779.

Ukena, S.N., Geffers, R., Buchholz, S., Stadler, M., and Franzke, A. (2012). Biomarkers for acute and chronic graft-versus-host disease in regulatory T cells. Transpl. Immunol. *27*, 179–183.

Uss, E., Rowshani, A.T., Hooibrink, B., Lardy, N.M., van Lier, R.A.W., and ten Berge, I.J.M. (2006). CD103 is a marker for alloantigen-induced regulatory CD8+ T cells. J. Immunol. *177*, 2775–2783.

Uss, E., Yong, S.-L., Hooibrink, B., van Lier, R.A.W., and ten Berge, I.J.M. (2007). Rapamycin enhances the number of alloantigen-induced human CD103+CD8+ regulatory T cells in vitro. Transplantation *83*, 1098–1106.

Verhagen, J., and Wraith, D.C. (2010). Comment on "Expression of Helios, an Ikaros transcription factor family member, differentiates thymic-derived from peripherally induced Foxp3+ T regulatory cells." J. Immunol. *185*, 7129; author reply 7130.

Wang, G., Khattar, M., Guo, Z., Miyahara, Y., Linkes, S.P., Sun, Z., He, X., Stepkowski, S.M., and Chen, W. (2010). IL-2-deprivation and TGF-beta are two non-redundant suppressor mechanisms of CD4+CD25+ regulatory T cell which jointly restrain CD4+CD25- cell activation. Immunol. Lett. *132*, 61–68.

Wang, L., Liu, Y., Han, R., Beier, U.H., Bhatti, T.R., Akimova, T., Greene, M.I., Hiebert, S.W., and Hancock, W.W. (2015). FOXP3+ regulatory T cell development and function require histone/protein deacetylase 3. J. Clin. Invest. *125*, 3304.

Waskow, C., Madan, V., Bartels, S., Costa, C., Blasig, R., and Rodewald, H.-R. (2009). Hematopoietic stem cell transplantation without irradiation. Nat. Methods *6*, 267–269.

Waterstrat, A., and Van Zant, G. (2009). Effects of aging on hematopoietic stem and progenitor cells. Curr. Opin. Immunol. *21*, 408–413.

Wei, S., Kryczek, I., and Zou, W. (2006). Regulatory T-cell compartmentalization and trafficking. Blood *108*, 426–431.

Weist, B.M., Kurd, N., Boussier, J., Chan, S.W., and Robey, E.A. (2015). Thymic regulatory T cell niche size is dictated by limiting IL-2 from antigen-bearing dendritic cells and feedback competition. Nat. Immunol. *16*, 635–641.

Weng, A.P., Ferrando, A.A., Lee, W., Morris, J.P., Silverman, L.B., Sanchez-Irizarry, C., Blacklow, S.C., Look, A.T., and Aster, J.C. (2004). Activating mutations of NOTCH1 in human T cell acute lymphoblastic leukemia. Science *306*, 269–271.

Westman, B.J., Perdomo, J., Sunde, M., Crossley, M., and Mackay, J.P. (2003). The C-terminal domain of Eos forms a high order complex in solution. J. Biol. Chem. *278*, 42419–42426.

Wilson, A., Laurenti, E., Oser, G., van der Wath, R.C., Blanco-Bose, W., Jaworski, M., Offner, S., Dunant, C.F., Eshkind, L., Bockamp, E., et al. (2008). Hematopoietic stem cells reversibly switch from dormancy to self-renewal during homeostasis and repair. Cell *135*, 1118–1129.

Winandy, S., Wu, P., and Georgopoulos, K. (1995). A dominant mutation in the Ikaros gene leads to rapid development of leukemia and lymphoma. Cell *83*, 289–299.

Wolfe, S.A., Nekludova, L., and Pabo, C.O. (2000). DNA recognition by Cys2His2 zinc finger proteins. Annu. Rev. Biophys. Biomol. Struct. *29*, 183–212.

Wong, J., Obst, R., Correia-Neves, M., Losyev, G., Mathis, D., and Benoist, C. (2007). Adaptation of TCR repertoires to self-peptides in regulatory and nonregulatory CD4+ T cells. J. Immunol. *178*, 7032–7041.

Wood, K.J., and Sakaguchi, S. (2003). Regulatory T cells in transplantation tolerance. Nat. Rev. Immunol. *3*, 199–210.

Workman, C.J., Collison, L.W., Bettini, M., Pillai, M.R., Rehg, J.E., and Vignali, D.A.A. (2011). In vivo Treg suppression assays. Methods Mol. Biol. Clifton NJ *707*, 119–156.

Wurster, A.L., and Pazin, M.J. (2012). ATP-dependent chromatin remodeling in T cells. Biochem. Cell Biol. Biochim. Biol. Cell. *90*, 1–13.

Xiao, Y., Li, B., Zhou, Z., Hancock, W.W., Zhang, H., and Greene, M.I. (2010). Histone acetyltransferase mediated regulation of FOXP3 acetylation and Treg function. Curr. Opin. Immunol. *22*, 583–591.

Xu, D., Liu, H., Komai-Koma, M., Campbell, C., McSharry, C., Alexander, J., and Liew, F.Y. (2003). CD4+CD25+ regulatory T cells suppress differentiation and functions of Th1 and Th2 cells, Leishmania major infection, and colitis in mice. J. Immunol. *170*, 394–399.

Yang, L., Bryder, D., Adolfsson, J., Nygren, J., Månsson, R., Sigvardsson, M., and Jacobsen, S.E.W. (2005). Identification of Lin(-)Sca1(+)kit(+)CD34(+)Flt3- short-term hematopoietic stem cells capable of rapidly reconstituting and rescuing myeloablated transplant recipients. Blood *105*, 2717–2723.

Yeung, F., Chung, E., Guess, M.G., Bell, M.L., and Leinwand, L.A. (2012). Myh7b/miR-499 gene expression is transcriptionally regulated by MRFs and Eos. Nucleic Acids Res. *40*, 7303–7318.

Yu, H.-C., Zhao, H.-L., Wu, Z.-K., and Zhang, J.-W. (2011). Eos negatively regulates human γ-globin gene transcription during erythroid differentiation. PloS One *6*, e22907.

Yui, M.A., and Rothenberg, E.V. (2014). Developmental gene networks: a triathlon on the course to T cell identity. Nat. Rev. Immunol. *14*, 529–545.

Zabransky, D.J., Nirschl, C.J., Durham, N.M., Park, B.V., Ceccato, C.M., Bruno, T.C., Tam, A.J., Getnet, D., and Drake, C.G. (2012). Phenotypic and functional properties of Helios+ regulatory T cells. PloS One *7*, e34547.

Zhang, J., Grindley, J.C., Yin, T., Jayasinghe, S., He, X.C., Ross, J.T., Haug, J.S., Rupp, D., Porter-Westpfahl, K.S., Wiedemann, L.M., et al. (2006). PTEN maintains haematopoietic stem cells and acts in lineage choice and leukaemia prevention. Nature *441*, 518–522.

Zhang, J., Jackson, A.F., Naito, T., Dose, M., Seavitt, J., Liu, F., Heller, E.J., Kashiwagi, M., Yoshida, T., Gounari, F., et al. (2012). Harnessing of the nucleosome-remodeling-deacetylase complex controls lymphocyte development and prevents leukemogenesis. Nat. Immunol. *13*, 86–94.

Zhang, Y., Kinkel, S., Maksimovic, J., Bandala-Sanchez, E., Tanzer, M.C., Naselli, G., Zhang, J.-G., Zhan, Y., Lew, A.M., Silke, J., et al. (2014). The polycomb repressive complex 2 governs life and death of peripheral T cells. Blood *124*, 737–749.

Zhang, Z., Swindle, C.S., Bates, J.T., Ko, R., Cotta, C.V., and Klug, C.A. (2007). Expression of a non-DNA-binding isoform of Helios induces T-cell lymphoma in mice. Blood *109*, 2190–2197.

Zhao, D., Zhang, C., Yi, T., Lin, C.-L., Todorov, I., Kandeel, F., Forman, S., and Zeng, D. (2008). In vivo-activated CD103+CD4+ regulatory T cells ameliorate ongoing chronic graft-versus-host disease. Blood *112*, 2129–2138.

Zhao, D.-M., Thornton, A.M., DiPaolo, R.J., and Shevach, E.M. (2006). Activated CD4+CD25+ T cells selectively kill B lymphocytes. Blood *107*, 3925–3932.

Zheng, Y., Josefowicz, S.Z., Kas, A., Chu, T.-T., Gavin, M.A., and Rudensky, A.Y. (2007). Genome-wide analysis of Foxp3 target genes in developing and mature regulatory T cells. Nature *445*, 936–940.

Zheng, Y., Josefowicz, S., Chaudhry, A., Peng, X.P., Forbush, K., and Rudensky, A.Y. (2010). Role of conserved non-coding DNA elements in the Foxp3 gene in regulatory T-cell fate. Nature *463*, 808–812.

Zhong, R.K., Astle, C.M., and Harrison, D.E. (1996). Distinct developmental patterns of short-term and long-term functioning lymphoid and myeloid precursors defined by competitive limiting dilution analysis in vivo. J. Immunol. *157*, 138–145.

Zhou, L., Chong, M.M.W., and Littman, D.R. (2009). Plasticity of CD4+ T cell lineage differentiation. Immunity *30*, 646–655.

Zhou, R., Horai, R., Silver, P.B., Mattapallil, M.J., Zárate-Bladés, C.R., Chong, W.P., Chen, J., Rigden, R.C., Villasmil, R., and Caspi, R.R. (2012). The living eye “disarms” uncommitted autoreactive T cells by converting them to Foxp3(+) regulatory cells following local antigen recognition. J. Immunol. *188*, 1742–1750.

De Zoeten, E.F., Wang, L., Sai, H., Dillmann, W.H., and Hancock, W.W. (2010). Inhibition of HDAC9 increases T regulatory cell function and prevents colitis in mice. Gastroenterology *138*, 583–594.

Résumé de thèse en français

La famille des facteurs de transcriptions Ikaros comprend Ikaros, Helios, Aiolos, Eos et Pegasus et est essentielle durant l'hématopoïèse. Ikaros est le membre le plus étudié de cette famille. Il joue un rôle important dans la régulation de la différenciation des lymphocytes et peut agir en tant que suppresseur de tumeur (Dumortier et al., 2006; Winandy et al., 1995). Eos est moins étudié et peut agir soit en tant que répresseur transcriptionnelle dans le système hématopoïétique (Hu R et al., 2007; Yu HC et al., 2011; Pan F et al., 2009) soit en tant qu'activateur transcriptionnelle à l'extérieur de ce système (Bao J et al., 2004; Yeung F et al., 2011).

Les séquences protéiques et les profils d'expression observés pour Eos sont très proches de ceux observés pour Helios (Honma et al., 1999). De plus, tous deux possèdent un rôle de modulateur des fonctions des cellules T régulatrices (Treg) (Sharma et al., 2013; Getnet et al., 2010; Pan et al., 2009). Leur rôle potentiel dans la biologie de ces cellules Treg reste controversé, avec des données conflictuelles publiées par plusieurs travaux indépendants utilisant différents systèmes d'étude (Rieder et al., 2015; Thornton et al., 2010; Cai et al., 2009). En particulier, le rôle d'Helios et Eos dans la maintenance des fonctions essentielles des cellules Treg reste à éclaircir *in vivo*.

Le premier objectif de ma thèse était d'étudier le rôle d'Eos dans le système hématopoïétique. J'ai tout d'abord étudié la fonction d'Eos dans le compartiment des cellules souches hématopoïétiques (CSH). A partir des résultats préliminaires et des données déjà publiées, je me suis concentrée sur l'étude du rôle d'Eos dans la biologie des cellules Treg et dans la mesure du possible, le rôle combiné d'Helios et Eos dans le lignage Treg. Durant ma première année de thèse, j'ai aussi participé à un projet sur le rôle d'Ikaros dans la régulation du complexe Polycomb (PRC2). Les résultats de ce projet ont donnée lieu à une publication où je suis co-auteur (Oravecz et al., 2015). Dans la première partie de mon résumé je vais brièvement décrire le rôle d'Ikaros et de PRC2. J'aborderai ensuite le rôle d'Eos dans le compartiment des CSH et me focaliserai sur le rôle d'Eos et Helios dans les cellules Treg entant que sujet principal de ma thèse.

1. Rôle d'Ikaros dans la régulation de la fonction Polycomb.

Le but de ce projet était d'étudier comment Ikaros régule la fonction du complexe Polycomb (PRC2) en utilisant un modèle *in vivo*. Pour répondre à cette question, nous avons généré des souris déficientes pour Ikaros et Ezh2 (un composant du complexe PRC2, déposant la marque répressive H3K27me3) (Rea et al., 2000). J'ai ensuite analysé les souris double hétérozygotes

obtenues et les résultats ne montrent aucune anomalie phénotypique, comparé aux souris de type sauvages (WT) ou simple hétérozygotes. Nous n'avons observé aucune altération de la marque H3K27me3 ni de l'expression des gènes cibles d'Ikaros dans les cellules T (Figure 1).

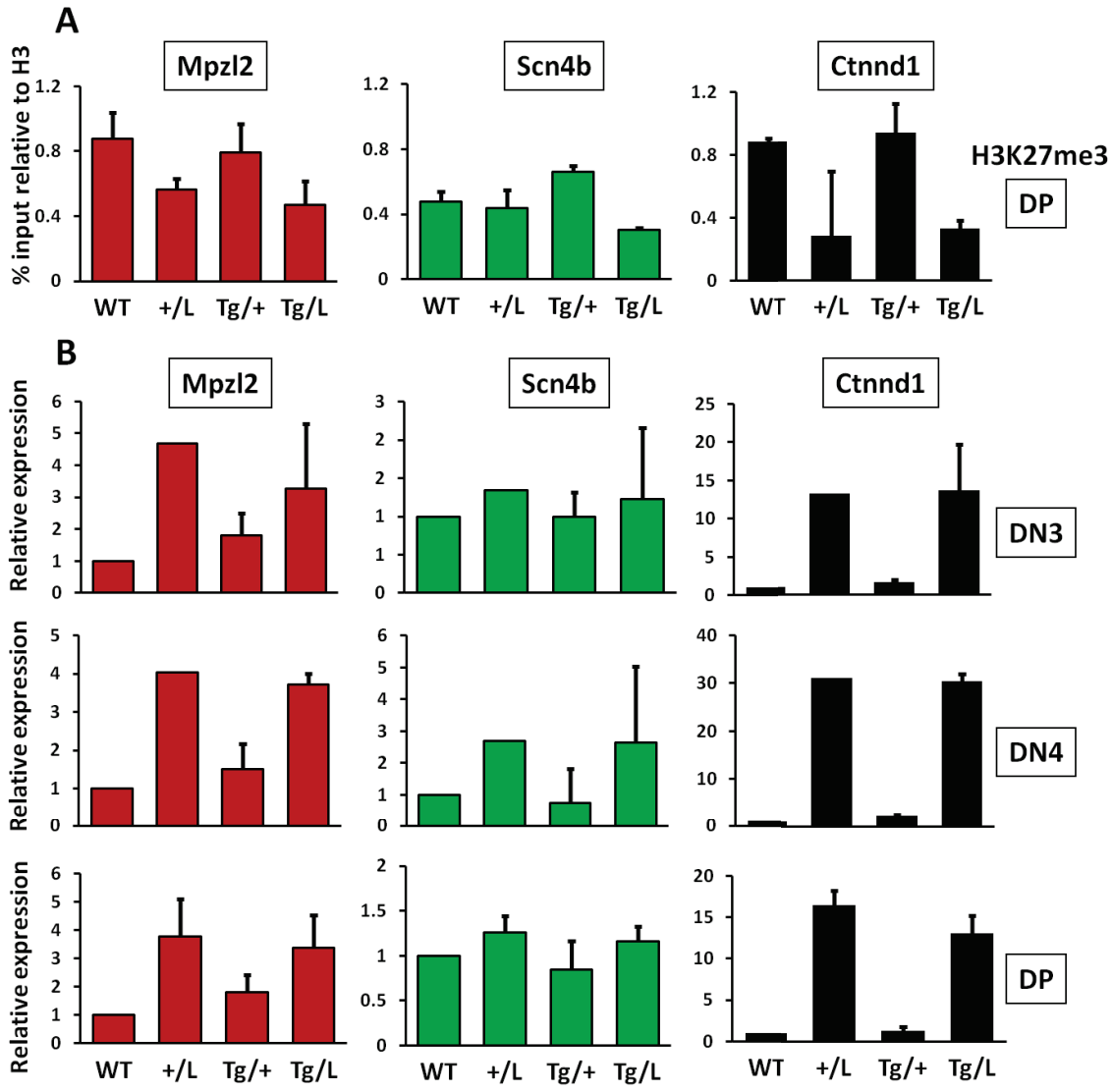

Figure 1. H3K27me3 et expression des gènes ciblés par Ikaros dans les cellules T $Ik^{+/L}Ezh2^{Tg/+}$. A. H3K27me3 ChIP-qPCR sur chromatine en cellules DP pour une séléction de 3 gènes. B. Niveau d'expression d'ARNm dans une séléction de trois gènes dans trois types cellulaires DN3, DN4 et DP. +/L ($Ik^{+/L}$), Tg/+ ($Ezh2^{Tg/+}$) and Tg/L ($Ik^{+/L}$ $Ezh2^{Tg/+}$).

Pour conclure, ce modèle murin ne démontre aucune synergie entre Ikaros et le complexe Polycomb durant le processus d''hématopoïèse et en particulier, aucun changement dans l'expression des gènes cibles d'Ikaros. However, it is clear that Ikaros represses its target genes in T cells through PRC2 complex with which it can directly interact (Oravecz et al., 2015).

2. Rôle d'Eos dans les cellules souches hématopoïétiques

L'analyse du pattern d'expression d'Eos a montré son expression dans les cellules souches hématopoïétiques avec les niveaux les plus élevés dans les CSHs à long terme (Figure 2).

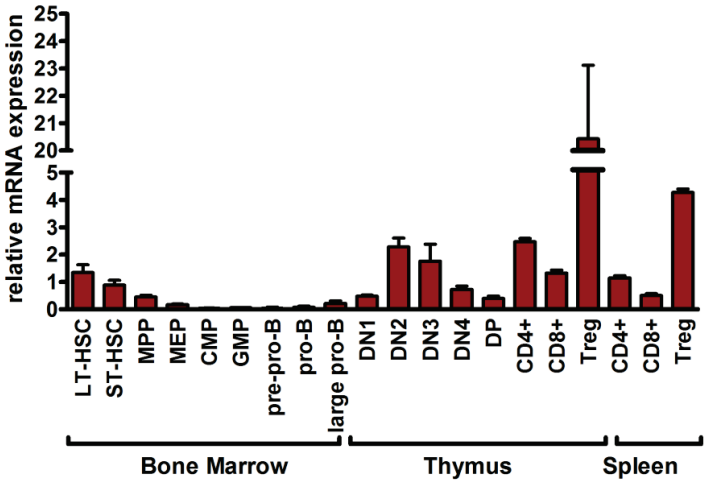

Figure 2. Eos est exprimé differentiellement durant l'hematopoiesis.

Durant l'homéostasie, les souris Eos$^{-/-}$ ont une hématopoïèse normale incluant le compartiment CSH, comme démontré par l'analyse cytométrie en flux. Dans les essais de transplantation compétitive, les CSHs Eos$^{-/-}$ semblent avoir moins d'activité biologique (Figure 3).

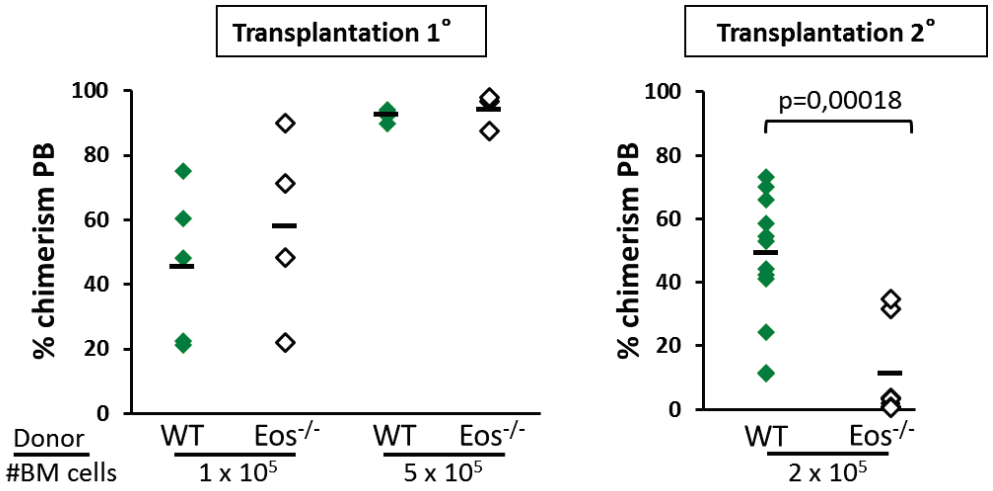

Figure 3. Les cellules Eos$^{-/-}$ de moelle osseuse reconstituent le système hematopoietic de façon similaire aux cellules WT en transplantion primaire mais pas secondaire. Le pourcentage de chimérisme en sang periphérique est estimé 6 mois après transplantation.

Cependant, elles prolifèrent avec une vigueur similaire à celle des cellules WT (Eos$^{+/+}$) et répondent normalement aux différentes conditions de stress *in vitro*. J'ai aussi réalisé des essais de formation de colonies avec les cellules Eos$^{-/-}$ pour vérifier leur production de

progéniteurs hématopoïétiques. Ces essais n'ont donné aucun résultat concluant. Nous avons finalement décidé de ne pas poursuivre cette étude et nous nous sommes concentrés sur la question suivante.

3. Rôle des facteurs de transcription Eos et Helios dans la différentiation et la fonction des cellules T régulatrices.

Pour étudier *in vivo* le rôle d'Eos dans les Treg, mon laboratoire a généré des souris $Eos^{-/-}$ en collaboration avec l'Institut Clinique de la Souris (Strasbourg). Les souris $Eos^{-/-}$ sont en bonne santé jusqu'à l'âge de 2 ans, ont une masse corporelle normale et naissent à une fréquence mendélienne. Durant l'homéostasie, les souris $Eos^{-/-}$ montrent une activité hématopoïétique normale avec les proportions attendues pour toutes les populations cellulaires majeures. Pour étudier Helios dans le compartiment des Treg, j'ai utilisée des souris préalablement générées et caractérisées dans le laboratoire (Cai et al., 2009).

L'analyse du pattern d'expression d'Eos dans différentes populations cellulaires du système hématopoïétique montre des niveaux d'expression élevés dans les cellules Treg dans la rate et le thymus (Figure 2). Cette observation supporte le rôle potentiel d'Eos dans le compartiment des Treg. L'expression de Helios a été précédemment décrite dans les Treg (Thornton et al., 2010; Gottschalk et al., 2012). Pour évaluer en détails l'expression d'Eos et Helios dans les cellules naturelles Treg $CD4^+$ et $CD8^+$ (nTreg), j'ai réalisé un marquage intracellulaire de ces protéines. Dans les Treg $CD4^+$, Eos et Helios sont tous deux hautement exprimés dans le thymus. Dans la rate, cependant seulement 70% des $CD4^+$ Treg expriment Helios et l'expression d'Eos est réduite dans l'ensemble de la rate (Figure 4).

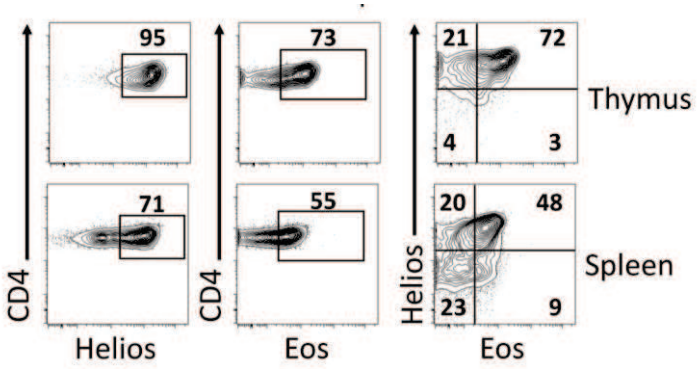

Figure 4. Expression d'Eos et d'Helios dans le thymus et la rate des souris WT. Mesuré par cytométrie en flux dans les cellules Treg $CD4^+CD25^+Foxp3^+$.

Ces résultats indiquent qu'Eos et Helios sont différemment exprimés dans les populations de cellules Treg. Pour déterminer si la perte d'Eos affecte le développement des Treg, j'ai tout d'abord analysé le compartiment des nTreg $CD4^+$ dans les souris $Eos^{-/-}$ et des souris WT. Ces expériences montrent que l'absence d'Eos n'affecte pas la fréquence et le nombre des cellules

Treg $CD4^+CD25^+Foxp3^+$ dans le thymus ou dans la rate des souris $Eos^{-/-}$, suggérant que la différenciation des nTreg $CD4^+$ durant l'homéostasie n'est pas affectée (Figure 5A). De plus, un essai de suppression *in vitro* montre que la fonction des cellules nTreg $Eos^{-/-}$ $CD4^+$ est similaire à celle des cellules WT (Figure 5B).

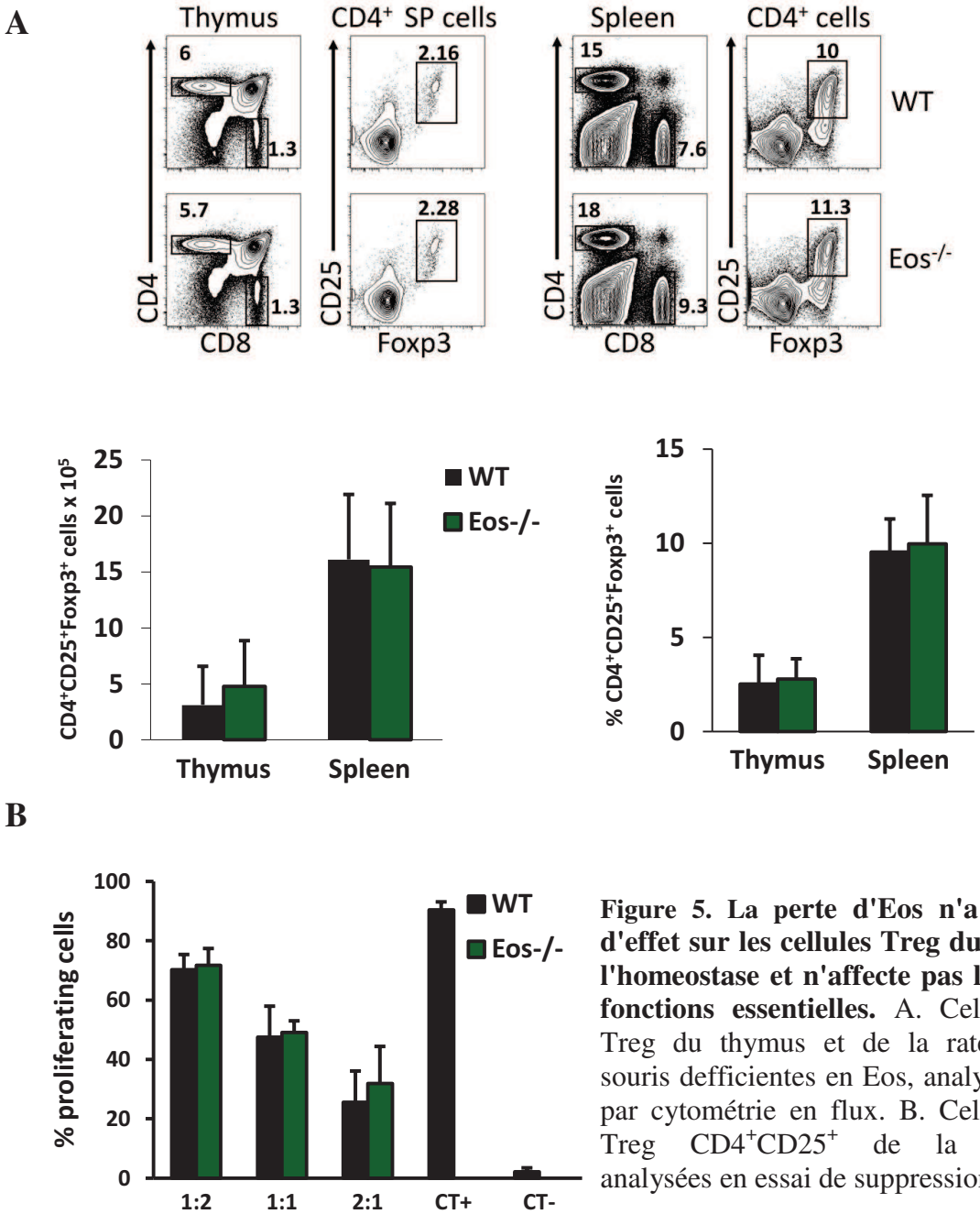

Figure 5. La perte d'Eos n'a pas d'effet sur les cellules Treg durant l'homeostase et n'affecte pas leurs fonctions essentielles. A. Cellules Treg du thymus et de la rate de souris defficientes en Eos, analysées par cytométrie en flux. B. Cellules Treg $CD4^+CD25^+$ de la rate analysées en essai de suppression.

J'ai aussi étudié les cellules Treg $CD8^+Foxp3^+$ qui n'existent pas naturellement en quantité abondante, mais peuvent être induites en présence de IL-2, de TGF-B et d'acide rétinoïque (Beres et al., 2012). J'ai alors observé le rôle d'Helios et Eos dans le développement des Treg $CD8^+$ induites (iTreg) à partir des cellules T $CD8^+$ de la rate *in vivo*. Fait intéressant, l'expression d'Helios et Eos est induite dans les cellules différenciées

$CD8^+CD25^+Foxp3^+$ WT, comme démontré par RT-qPCR et marquage intracellulaire (Figure 6A). Cependant, les iTreg $CD8^+$ se développent de manière similaire, qu'elles soient issues de cellules T WT ou $Eos^{-/-}$ (Figure 6B). Elles sont également fonctionnelles comme démontré par un essai de suppression *in vitro* (Figure 6C).

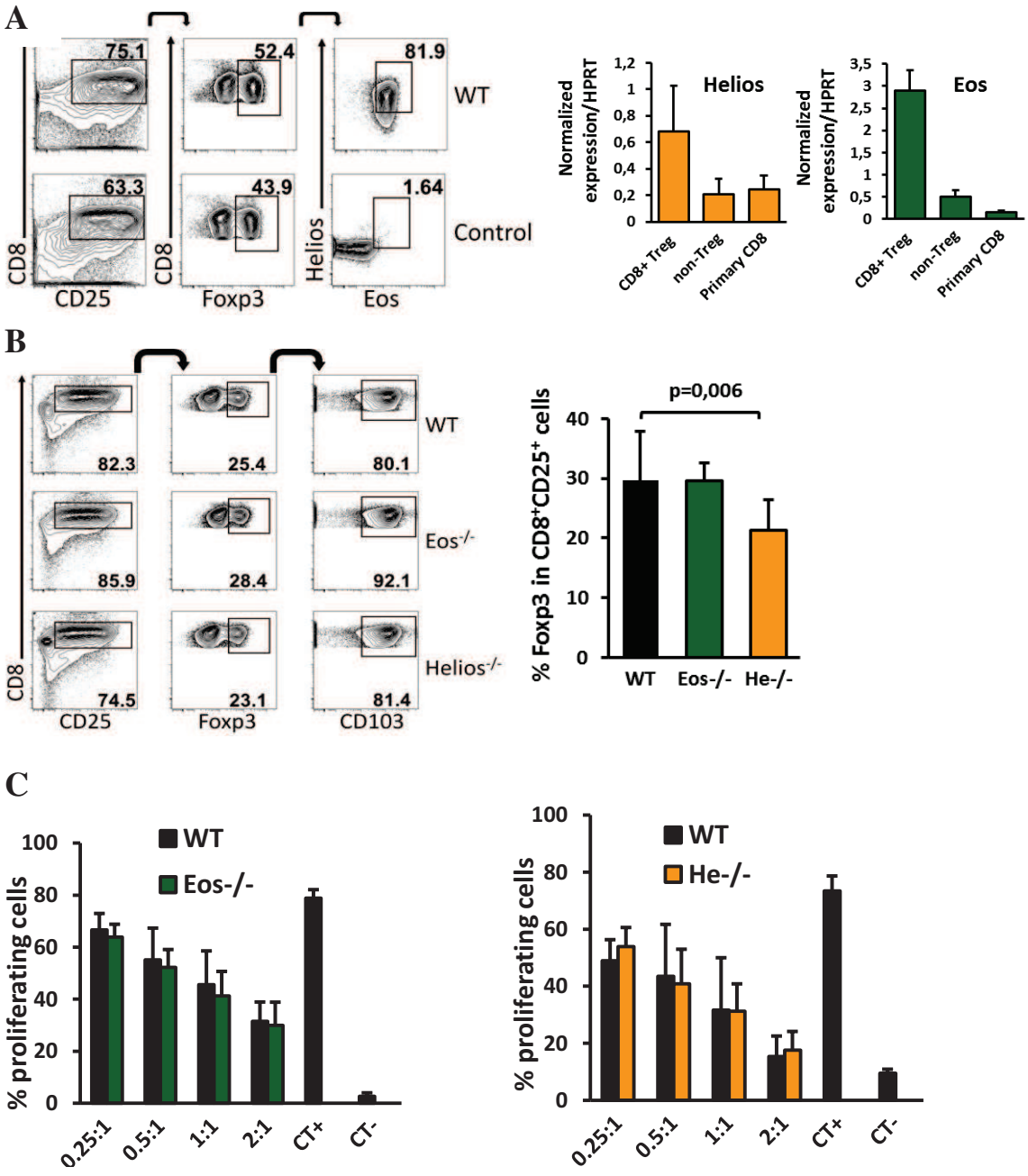

Figure 6. Role d'Eos et Helios dans la différentiation et la fonction des cellules Treg $CD8^+$. A. Eos et Helios sont exprimées dans les cellules Treg $CD8^+$ differenciée *in vitro* comme mesurée par cryométrie en flux et RT-qPCR. B. La perte d'Helios mais pas d'Eos a un effet minimal pour la différenciation des cellules Treg $CD8^+$. C. Les cellules Treg CD8+ $Helio^{s-/-}$ et $Eos^{-/-}$ sont fonctionnelles dans l'essai de suppression *in vitro*.

Seules les cellules d'origine $Helios^{-/-}$ se développent moins efficacement, mais restent également entièrement fonctionnelles (Figure 6B/C). J'ai aussi analysé le rôle de Helios et

Eos dans l'induction des cellules iTreg $CD8^+$ *in vivo* en transplantant des cellules T $CD3^+CD25^-$ spléniques des souris WT, $Helios^{-/-}$ ou $Eos^{-/-}$ et de moelle osseuse dans des souris receveuses syngéniques et allogéniques irradiées. Ces expériences montrent également que les iTreg $CD8^+Foxp3^+$ se développent normalement quel que soit leur origine (WT, $Helios^{-/-}$ ou $Eos^{-/-}$).

Comme Eos et Helios possèdent une séquence protéique similaire, l'absence de phénotype apparent dans mes expériences pourrait être due à une redondance de fonction entre Eos et Helios. Pour étudier cette hypothèse, j'ai tout d'abord analysé par un marquage intracellulaire l'expression d'Eos dans les nTreg $Helios^{-/-}$ $CD4^+$ et l'expression de Helios dans les cellules $Eos^{-/-}$ mais n'a observé aucune différence. Ce résultat indique qu'au moins au niveau de leur expression ces deux facteurs de transcription ne se compensent pas l'un et l'autre. Pour confirmer une éventuelle coopération d'Eos et Helios dans la régulation des Treg, j'ai croisé des souris $Eos^{-/-}$ et $Helios^{-/-}$ pour obtenir un double knock-out $Eos^{-/-}Helios^{-/-}$. Ce double mutant ne montre aucune anomalie phénotypique et possède une hématopoïèse normale. J'ai analysé la population des nTreg $CD4^+CD25^+Foxp3^+$ et ai trouvé un nombre similaire de cellules Treg dans tous les génotypes analysés (Figure 7).

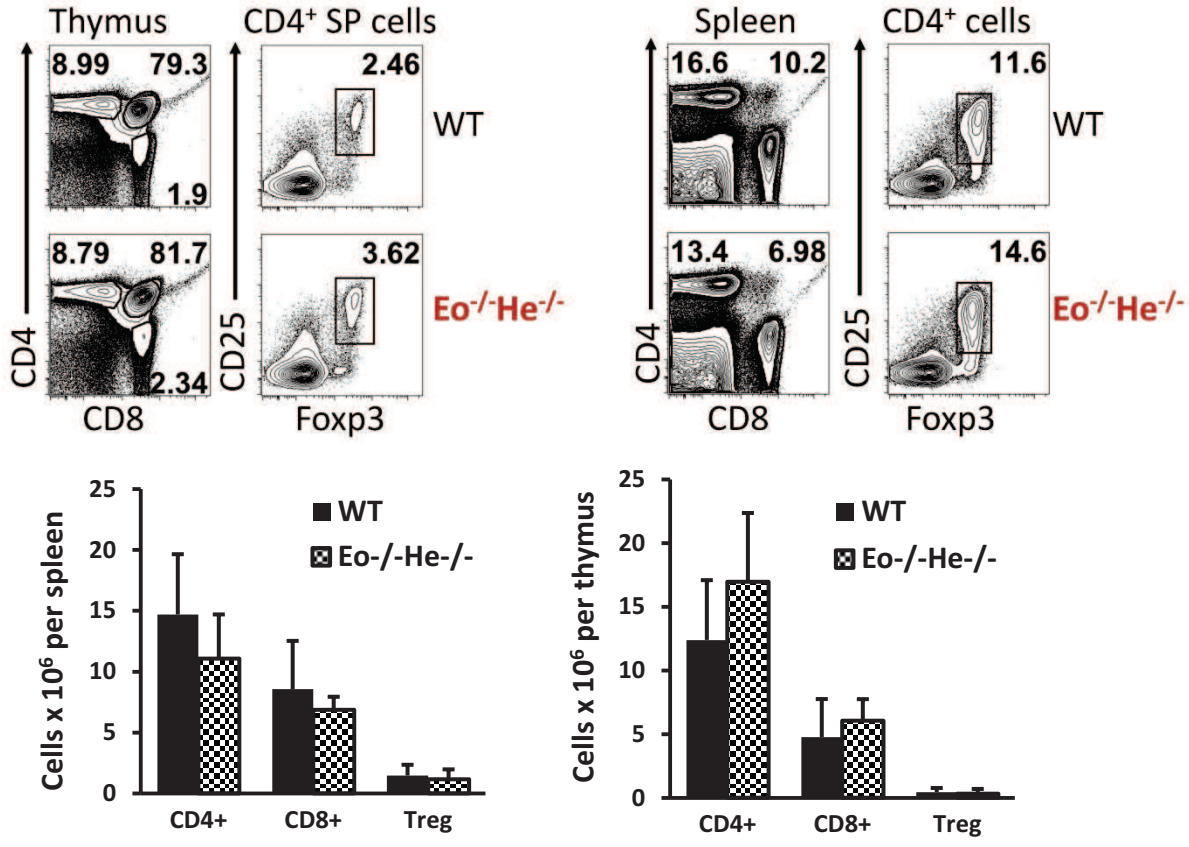

Figure 7. La perte d'Eos et d'Helios n'ont pas d'effet sur les cellules Treg durant l'homeostasise. Céllules naturelles Treg du thymus et de la rate de souris double mutant analysées par cryométrie en flux.

J'ai aussi étudié le compartiment Treg CD8$^+$ en utilisant des cellules de souris Eos$^{-/-}$Helios$^{-/-}$. Les résultats obtenus montrent que les Treg CD8$^+$ peuvent être générées *in vitro* et *in vivo*, sont fonctionnelles, mais moins efficaces que les cellules WT (Figure 8).

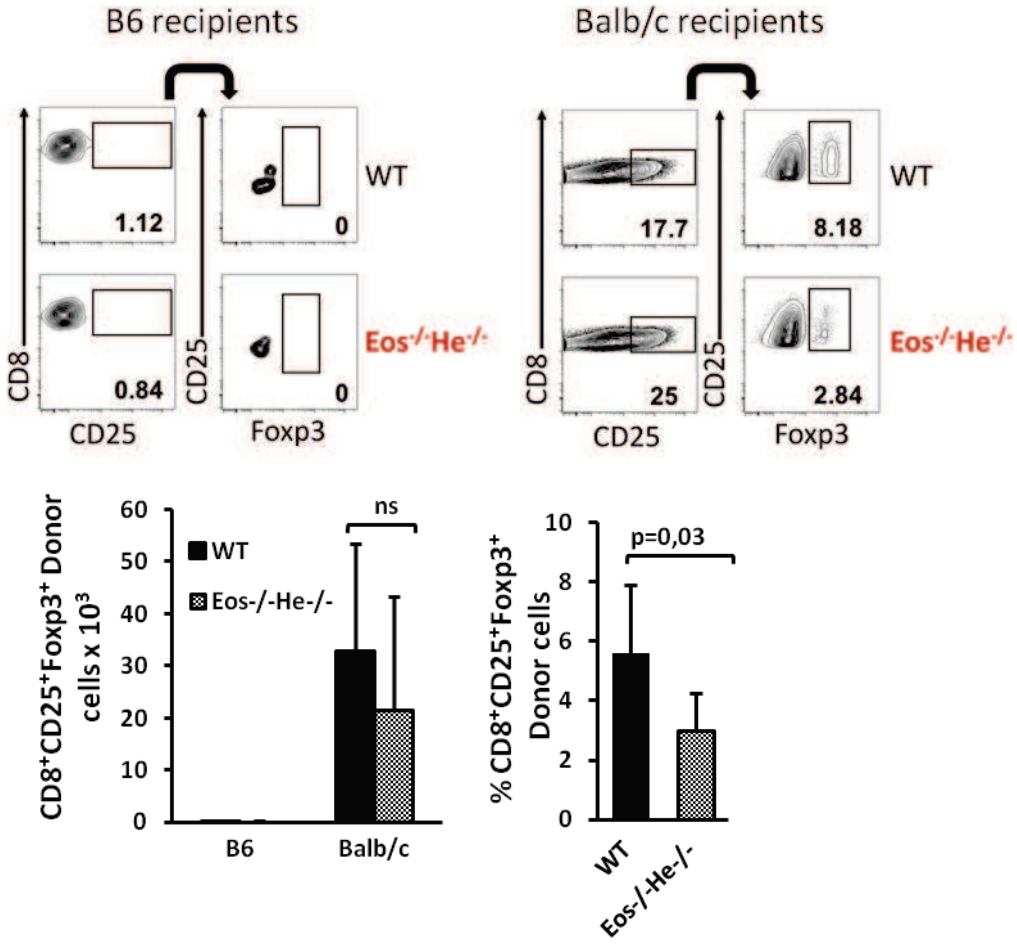

Figure 7. Cellules Eos$^{-/-}$Helios$^{-/-}$ CD8$^+$ T montrant un potentielle de différentiation diminué *in vivo*.

Pour avoir une vue globale sur les changements encourus pas les cellules Treg déficientes en Eos et Helios, j'ai également mené une analyse transcriptomique des cellules Treg mutantes. Les résultats montrent que la perte d'Eos seul a un impact minimal sur l'expression des gènes relatifs à la biologie des Treg, ce qui est en accord avec les résultats obtenus dans les essais fonctionnels. Dans les doubles mutants Eos$^{-/-}$Helios$^{-/-}$, nous avons trouvé des gènes exprimés spécifiquement dans les Treg, qui sont sur et sous exprimés. Cependant, ces gènes n'étaient différentiellement exprimés que dans les échantillons Eos$^{-/-}$Helios$^{-/-}$, indiquant qu'ils sont spécifiquement dépendant d'Helios. Ceci a été confirmé par l'analyse du transcriptome des cellules Treg Helios$^{-/-}$ et WT, où ces gènes ont aussi été identifiés (Figure 9).

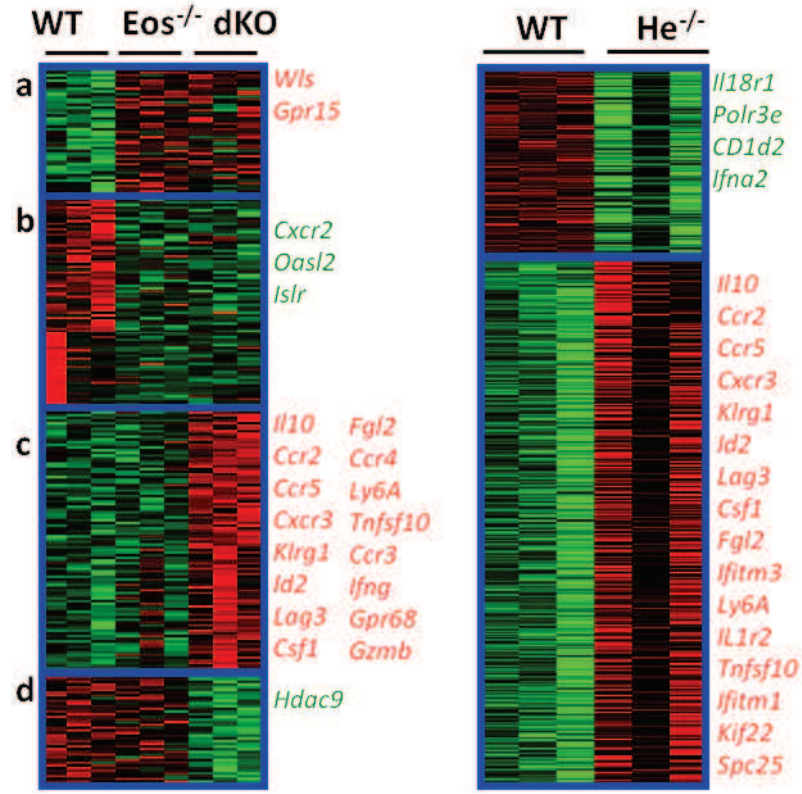

Figure 9. Profile d'expression des cellules Treg He$^{-/-}$, Eos$^{-/-}$ et dKO. a/b cluster de gènes dérégulés à la fois dans les Treg Eos KO et dKO. c/d - clusters de gènes dérégulés seulement dans les Treg dKO.

Les gènes Treg spécifiques surexprimés dans les cellules Helios$^{-/-}$ sont caractéristiques de l'activation des cellules Treg, comme démontré précédemment (Arvey et al., 2014).

Je l'ai également confirmé ces résultats *in vitro* dans un essai de suppression où des cellules Helios$^{-/-}$ étaient supérieures aux cellules WT (Figure 10). Finalement, cette analyse montre également qu'il n'y a aucune intercommunication entre Eos et Helios pour réguler la signature transcriptionnelle des cellules Treg.

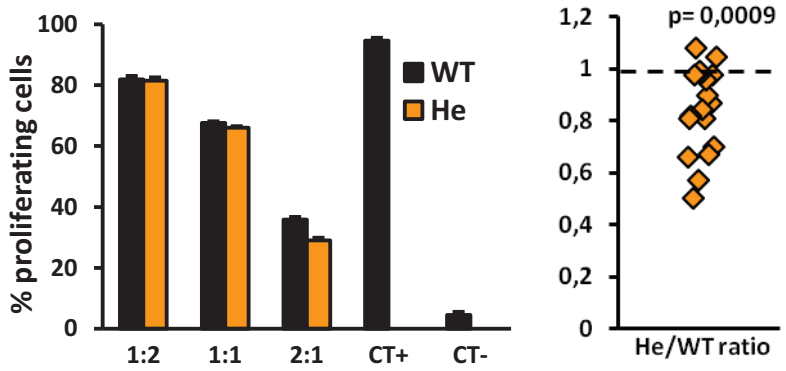

Figure 10. Les cellules Treg défficientes en Helios sont supérieures dans leur activité suppressive. Essai de suppression in vitro représentatif et ratios de prolifération des cellules T dans 6 expériences independentes dans l'étude présente et Cai et al., 2009.

Pour conclure, nos résultats montrent qu'Eos et Helios ne jouent pas un rôle dans la maintenance des fonctions essentielles des cellules Treg dans la souris, du moins pour les fonctions déjà décrites. Les deux facteurs de transcriptions sont hautement exprimés dans les Treg $CD4^+$ et peuvent être induits durant la différenciation des Treg $CD8^+$. Cependant, la perte de l'un ou l'autre n'affecte pas la différenciation et la fonction des cellules Treg $CD4^+$. Les analyses fonctionnelles et transcriptomiques des Treg dans des souris double mutantes montrent qu'Eos a un impact minimal sur l'expression des gènes liés aux cellules Treg et qu'Helios et Eos ne coopèrent pas pour réguler le compartiment des Treg $CD4^+$. Cependant, la perte de l'un ou l'autre n'affecte pas la différenciation et la fonction des cellules Treg $CD4^+$. Concernant des cellules Treg $CD8^+$, Eos et Helios semblent avoir un rôle dans leur différenciation, mais pas leur fonctionnalité.

Les résultats obtenus durant ma thèse représentent une étude compréhensive des cellules Treg dans les conditions établies et les modèles de souris utilisées. Ces travaux de thèse seront résumés dans une publication en tant que premier auteur qui est actuellement en préparation.

Bibliographie:

Arvey, A., van der Veeken, J., Samstein, R.M., Feng, Y., Stamatoyannopoulos, J.A., and Rudensky, A.Y. (2014). Inflammation-induced repression of chromatin bound by the transcription factor Foxp3 in regulatory T cells. Nat. Immunol. *15*, 580–587.

Bao, J., Lin, H., Ouyang, Y., Lei, D., Osman, A., Kim, T.-W., Mei, L., Dai, P., Ohlemiller, K.K., and Ambron, R.T. (2004). Activity-dependent transcription regulation of PSD-95 by neuregulin-1 and Eos. Nat. Neurosci. *7*, 1250–1258.

Beres, A.J., Haribhai, D., Chadwick, A.C., Gonyo, P.J., Williams, C.B., and Drobyski, W.R. (2012). CD8+ Foxp3+ regulatory T cells are induced during graft-versus-host disease and mitigate disease severity. J. Immunol. *189*, 464–474.

Cai, Q., Dierich, A., Oulad-Abdelghani, M., Chan, S., and Kastner, P. (2009). Helios deficiency has minimal impact on T cell development and function. J. Immunol. *183*, 2303–2311.

Dumortier, A., Jeannet, R., Kirstetter, P., Kleinmann, E., Sellars, M., dos Santos, N.R., Thibault, C., Barths, J., Ghysdael, J., Punt, J.A., et al. (2006). Notch activation is an early and critical event during T-Cell leukemogenesis in Ikaros-deficient mice. Mol. Cell. Biol. *26*, 209–220.

Getnet, D., Grosso, J.F., Goldberg, M.V., Harris, T.J., Yen, H.-R., Bruno, T.C., Durham, N.M., Hipkiss, E.L., Pyle, K.J., Wada, S., et al. (2010). A role for the transcription factor Helios in human CD4(+)CD25(+) regulatory T cells. Mol. Immunol. *47*, 1595–1600.

Gottschalk, R.A., Corse, E., and Allison, J.P. (2012). Expression of Helios in peripherally induced Foxp3+ regulatory T cells. J. Immunol. *188*, 976–980.

Honma, Y., Kiyosawa, H., Mori, T., Oguri, A., Nikaido, T., Kanazawa, K., Tojo, M., Takeda, J., Tanno, Y., Yokoya, S., et al. (1999). Eos: a novel member of the Ikaros gene family expressed predominantly in the developing nervous system. FEBS Lett. *447*, 76–80.

Hu, R., Sharma, S.M., Bronisz, A., Srinivasan, R., Sankar, U., and Ostrowski, M.C. (2007). Eos, MITF, and PU.1 recruit corepressors to osteoclast-specific genes in committed myeloid progenitors. Mol. Cell. Biol. *27*, 4018–4027.

Oravecz A, Apostolov A, Polak K, Jost B, Le Gras S, Chan S, Kastner P. (2015) Ikaros mediates gene silencing in T cells through Polycomb repressive complex 2. Nat Commun. Nov 9;6:8823.

Pan, F., Yu, H., Dang, E.V., Barbi, J., Pan, X., Grosso, J.F., Jinasena, D., Sharma, S.M., McCadden, E.M., Getnet, D., et al. (2009). Eos mediates Foxp3-dependent gene silencing in CD4+ regulatory T cells. Science *325*, 1142–1146.

Rea, S., Eisenhaber, F., O'Carroll, D., Strahl, B.D., Sun, Z.W., Schmid, M., Opravil, S., Mechtler, K., Ponting, C.P., Allis, C.D., et al. (2000). Regulation of chromatin structure by site-specific histone H3 methyltransferases. Nature *406*, 593–599.

Rieder, S.A., Metidji, A., Glass, D.D., Thornton, A.M., Ikeda, T., Morgan, B.A., and Shevach, E.M. (2015). Eos Is Redundant for Regulatory T Cell Function but Plays an Important Role in IL-2 and Th17 Production by CD4+ Conventional T Cells. J. Immunol. *195*, 553–563.

Sharma, M.D., Huang, L., Choi, J.-H., Lee, E.-J., Wilson, J.M., Lemos, H., Pan, F., Blazar, B.R., Pardoll, D.M., Mellor, A.L., et al. (2013). An inherently bifunctional subset of Foxp3+ T helper cells is controlled by the transcription factor eos. Immunity *38*, 998–1012.

Thornton, A.M., and Shevach, E.M. (1998). CD4+CD25+ immunoregulatory T cells suppress polyclonal T cell activation in vitro by inhibiting interleukin 2 production. J. Exp. Med. *188*, 287–296.

Winandy, S., Wu, P., and Georgopoulos, K. (1995). A dominant mutation in the Ikaros gene leads to rapid development of leukemia and lymphoma. Cell *83*, 289–299.

Yeung, F., Chung, E., Guess, M.G., Bell, M.L., and Leinwand, L.A. (2012). Myh7b/miR-499 gene expression is transcriptionally regulated by MRFs and Eos. Nucleic Acids Res. *40*, 7303–7318.

Yu, H.-C., Zhao, H.-L., Wu, Z.-K., and Zhang, J.-W. (2011). Eos negatively regulates human γ-globin gene transcription during erythroid differentiation. PloS One *6*, e22907.

APPENDIX – Oravecz et al., 2015

nature COMMUNICATIONS

ARTICLE

Received 19 Mar 2015 | Accepted 7 Oct 2015 | Published 9 Nov 2015

DOI: 10.1038/ncomms9823 OPEN

Ikaros mediates gene silencing in T cells through Polycomb repressive complex 2

Attila Oravecz[1], Apostol Apostolov[1,*], Katarzyna Polak[1,*], Bernard Jost[2], Stéphanie Le Gras[2], Susan Chan[1] & Philippe Kastner[1,3]

T-cell development is accompanied by epigenetic changes that ensure the silencing of stem cell-related genes and the activation of lymphocyte-specific programmes. How transcription factors influence these changes remains unclear. We show that the Ikaros transcription factor forms a complex with Polycomb repressive complex 2 (PRC2) in $CD4^-CD8^-$ thymocytes and allows its binding to more than 500 developmentally regulated loci, including those normally activated in haematopoietic stem cells and others induced by the Notch pathway. Loss of Ikaros in $CD4^-CD8^-$ cells leads to reduced histone H3 lysine 27 trimethylation and ectopic gene expression. Furthermore, Ikaros binding triggers PRC2 recruitment and Ikaros interacts with PRC2 independently of the nucleosome remodelling and deacetylation complex. Our results identify Ikaros as a fundamental regulator of PRC2 function in developing T cells.

[1] Functional Genomics and Cancer, Institut de Génétique et de Biologie Moléculaire et Cellulaire (IGBMC), INSERM U964, CNRS UMR 7104, Université de Strasbourg, Equipe Labellisée Ligue Contre le Cancer, 1 rue Laurent Fries, Illkirch 67404, France. [2] IGBMC Microarray and Sequencing Platform, Illkirch 67404, France. [3] Faculté de Médecine, Université de Strasbourg, Strasbourg 67000, France. * These authors contributed equally to this work. Correspondence and requests for materials should be addressed to A.O. (email: oravecz@igbmc.fr) or to S.C. and P.K. (email: scpk@igbmc.fr).

The development of a haematopoietic stem cell (HSC) into a T lymphocyte requires the loss of stem cell properties and the acquisition of T-cell characteristics, which is accompanied by changes in chromatin architecture and gene expression. Although genome-wide studies have begun to provide a detailed view of these changes and associated transcriptional regulators[1–3], the current understanding is largely correlative and the impact of a given regulator in the dynamic evolution of the transcriptional and epigenetic states remains poorly understood.

The Ikaros transcription factor is critical for T-cell development. It is important early, for lymphoid specification in haematopoietic progenitors[4], and late, to activate and repress numerous genes in thymocytes[5,6]. Ikaros shapes the timing and specificity of the Notch target gene response in double-negative (DN) $CD4^-CD8^-$ thymocytes[5], and modulates positive and negative selection in double-positive (DP) $CD4^+CD8^+$ thymocytes[7]. Further, Ikaros is implicated in peripheral T-cell functions[8–11]. At the molecular level, Ikaros acts as both transcriptional repressor or activator. It associates with the nucleosome remodelling and deacetylation (NuRD) complex[12,13], suggesting that it may repress transcription via NuRD-mediated histone deacetylation. In addition, it has been shown that Ikaros represses the expression of the Notch target gene *Hes1* in DP thymocytes[14,15], which is correlated with decreased levels of histone H3 lysine 27 trimethylation (H3K27me3) in Ikaros-deficient cells, thus suggesting a possible role for Polycomb group proteins in Ikaros-dependent gene silencing. Collectively, these studies indicate that the molecular mechanisms of Ikaros-dependent repression remain unclear.

Here we show that loss of H3K27me3 is a prominent epigenetic defect in Ikaros-deficient thymocytes, which underlies the ectopic expression of genes repressed by Ikaros, including HSC-specific genes and Notch target genes. Ikaros is required for Polycomb repressive complex 2 (PRC2) binding to target loci in DN3 cells. Ikaros associates with PRC2 in DN cells and stable Ikaros–PRC2 complexes form independently of NuRD. Thus, Ikaros mediates gene silencing in T cells in large part through PRC2.

Results

Widespread loss of H3K27me3 in Ikaros-deficient DP cells. To assess the global effect of Ikaros on the 'repressive' H3K27me3 and 'active' histone H3 lysine 4 trimethyl (H3K4me3) marks, we compared DP thymocytes from 3- to 4-week-old wild-type (WT) and $Ik^{L/L}$ mice by chromatin immunoprecipitation sequencing (ChIP-seq). $Ik^{L/L}$ mice carry a hypomorphic mutation in the *Ikzf1* gene and the levels of functional Ikaros proteins in $Ik^{L/L}$ cells are ~10% of WT[14,16]. Although $Ik^{L/L}$ mice die from T-cell acute lymphoblastic lymphomas/leukemias (ALL) at 4–6 months of age, the animals used here showed no signs of transformation in the thymus, as defined by CD4 and CD8 profiling, TCR Vα and Vβ chain usage, and the absence of intracellular Notch1 in DP thymocytes[14,15].

These experiments revealed 5,172 and 10,914 islands of enrichment for H3K27me3 and H3K4me3, respectively (Supplementary Fig. 1a). Although most were unchanged between WT and $Ik^{L/L}$ cells (<1.8-fold), 370 of the H3K27me3 islands (7.2%) were decreased in $Ik^{L/L}$ cells, many of which had high tag numbers in the WT sample (Fig. 1a). These islands could be divided into three major groups (Fig. 1b clusters *a*–*c*). Cluster *a* islands mapped mostly to intergenic regions and lacked H3K4me3 in both WT and $Ik^{L/L}$ cells. Cluster *b* islands mapped largely to promoter or intragenic regions, and also exhibited H3K4me3 marks that were unchanged between WT and $Ik^{L/L}$ cells (for example, *Ctnna1* and *Cd9*; Fig. 1c). By contrast, cluster *c* marked a small group of islands that showed a concomitant increase of H3K4me3 in the $Ik^{L/L}$ sample (for example, *Mpzl2* and *Ctnnd1*; Fig. 1c). Furthermore, increased H3K4me3 was seen at 232 regions (2.2%) where H3K27me3 was either absent or unchanged (Fig. 1b clusters *d*–*e*). Finally, we found 132 regions with increased H3K27me3 and 154 regions with decreased H3K4me3, which overlapped only marginally (Fig. 1a and Supplementary Fig. 1b). Thus, a major hallmark of the chromatin landscape in $Ik^{L/L}$ DP cells is the selective decrease of H3K27me3 at regions of 'bivalent' H3K27me3/H3K4me3 chromatin (14.5% of the 1,382 bivalent regions).

We then assessed the impact of H3K27me3 and H3K4me3 defects on gene expression in $Ik^{L/L}$ DP thymocytes, using our published microarray data (Fig. 1b and Supplementary Fig. 1b)[5]. Genes with decreased H3K27me3, and notably those with unaltered H3K4me3 (cluster *b*), were associated with increased messenger RNA expression in most cases (Fig. 1b right panels). Genes with a selective increase in H3K4me3 (Fig. 1b clusters *d*–*e*) were also associated with increased expression. In contrast, genes with increased H3K27me3, or decreased H3K4me3, were associated with slightly decreased mRNA levels (Supplementary Fig. 1b). These data indicate that diverse epigenetic changes underlie the deregulated gene expression in Ikaros-deficient DP cells. However, loss of H3K27me3 appears to be more prominent: it is the most frequent, occurs on islands with high H3K27me3 levels in WT cells and is often associated with increased gene expression regardless of H3K4me3 status. We therefore studied H3K27 trimethylation as a potential mechanism of Ikaros-mediated repression.

To determine whether the loss of H3K27me3 correlates with loss of PRC2 binding, we performed ChIP–quantitative PCR (qPCR) analysis to measure H3K27me3 levels and binding of the core PRC2 subunit Suz12 in WT and $Ik^{L/L}$ DP thymocytes, using

Figure 1 | Impaired H3K27 trimethylation is a major defect in $Ik^{L/L}$ DP thymocytes. (**a**) Scatter plots showing the $Ik^{L/L}$/WT $\log_2$ fold changes of the indicated histone modifications in DP cells. ChIP-seq tag counts in WT and $Ik^{L/L}$ are shown. Red/green values indicate the total number of chromatin marks that are >1.8× decreased/increased in the mutant. Dots highlighted in the same colours represent the corresponding individual islands. The circled area highlights decreased regions with high tag counts in WT cells. (**b**) Venn diagram showing the overlap between genomic regions with decreased H3K27me3 or increased H3K4me3 in $Ik^{L/L}$ DP thymocytes. The blue-coloured heatmap shows *k*-means clustering of the tag densities of the corresponding genomic regions for each group. The central stripe schematizes the genomic positions of the islands, with yellow, orange and black indicating promoter, intragenic and intergenic regions, respectively. The $\log_2$ expression (left) or $\log_2$ fold change (FC, right) of the matched genes is shown in the red–green heatmaps. Transcriptome data are from GSE 46090 (ref. 5). Black lines indicate intergenic regions and light blue lines indicate genes that were not represented on the microarray. For genes with multiple probe sets, we calculated a score corresponding to the product of the expression and FC values for each probe set, and selected the probe set with the highest score. (**c**) Representative UCSC Genome browser track of H3K27me3 and H3K4me3 ChIP-seq in WT and $Ik^{L/L}$ cells. *Cd3d* and the HoxA cluster served as positive controls for the H3K4me3 and H3K27me3 tracks, respectively. (**d**) H3K27me3 and Suz12 ChIP–qPCRs from WT and $Ik^{L/L}$ cells. The *x* axes indicate primer pair positions relative to the TSS of the test (*Mpzl2*, *Ctnna1*, *Ctnnd1* and *Cd9*) and control (*Cd3d* and *Hoxa13*) genes. % input = [(ab ChIP)-(IgG ChIP)]/1% input. Error bars, s.d.; $^*P<0.05$, $^{**}P<0.01$ (two-sample *t*-test); $n=3$–6 and $n=2$–3 for H3K27me3 and Suz12, respectively.

promoter-scanning primers (*Mpzl2* and *Ctnna1*) or primers specific for transcriptional start site (TSS) regions (*Cd9* and *Ctnnd1*; Fig. 1d). These experiments confirmed that the reduction of H3K27me3 is linked to decreased Suz12 binding in $Ik^{L/L}$ cells at all genes tested.

Impaired H3K27me3 and gene repression in $Ik^{L/L}$ thymocytes. To evaluate the temporal changes in H3K27me3 during T-cell differentiation, we analysed the chromatin of bone marrow-derived LSK ($Lin^-Sca1^+c\text{-}Kit^+$) cells and DN1 ($CD44^+CD25^-$), DN2 ($CD44^+CD25^+$), DN3 ($CD44^-CD25^+$), DN4

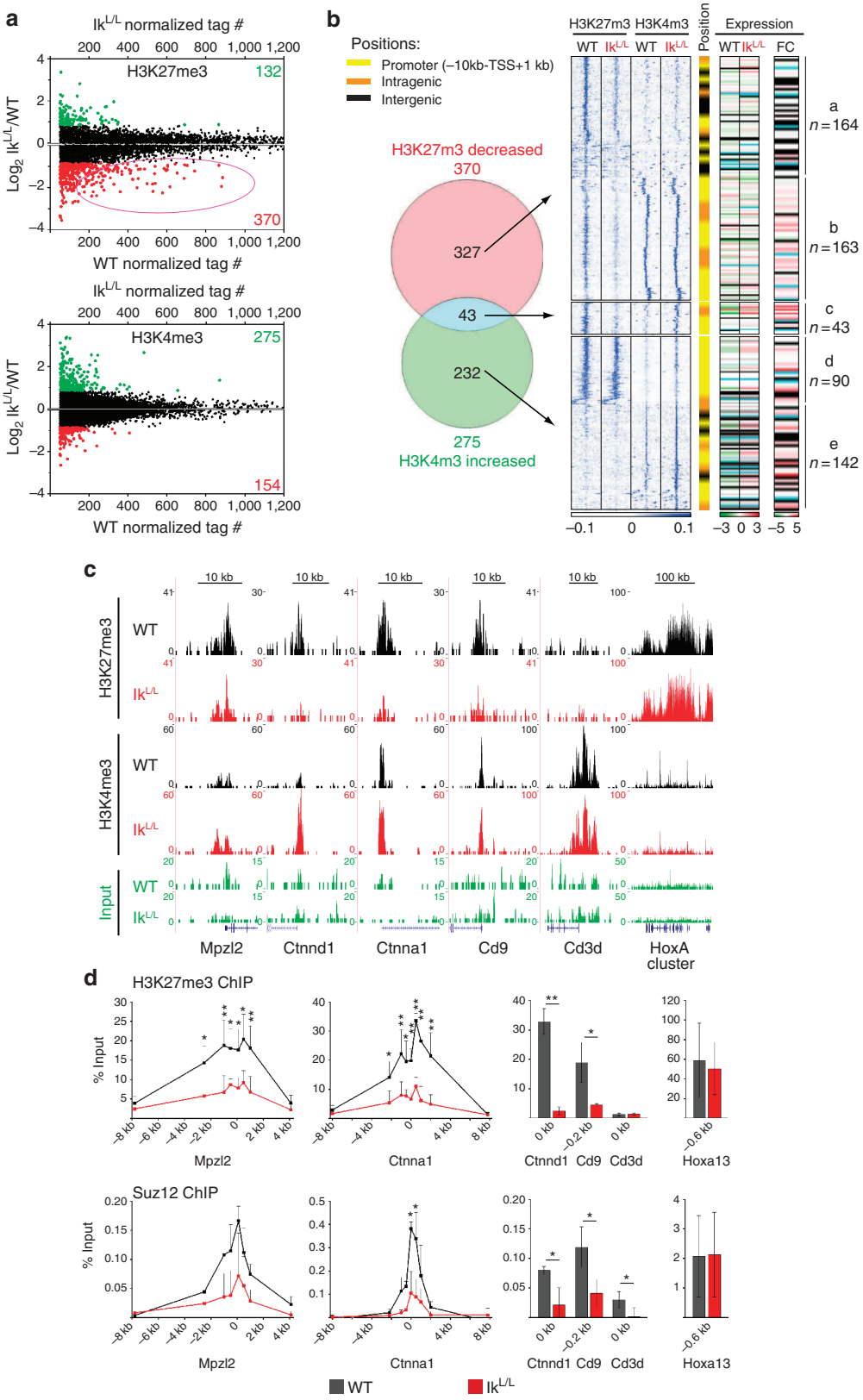

(CD44$^-$CD25$^-$) and DP thymocytes from 3- to 4-week-old WT and Ik$^{L/L}$ mice. Overall, H3K27me3 levels were similar in Ik$^{L/L}$ cells compared with WT (Supplementary Fig. 2a). By ChIP-seq, a total of 7,131 H3K27me3 islands were detected: the majority were similar between WT and Ik$^{L/L}$ cells of the same developmental stage (Supplementary Fig. 2b) and included islands that were constitutively present (for example, *Ebf1*) or dynamically regulated (for example, *Tal1*; Fig. 2a). Of the islands that were changed, few were detected in the LSK and DN1 populations, whereas the number of islands with decreased H3K27me3 gradually increased from the DN2 to the DP stage (Supplementary Fig. 2c). Increased H3K27me3 was infrequent. In all, 583 islands were reduced >1.8-fold in the mutant samples compared with WT (Fig. 2b, Supplementary Fig. 2b and Supplementary Table 1); this number is likely to be underestimated, as some regions with a clear decrease in H3K27me3 were not selected by our bioinformatic criteria (for example, *Hes1* or *Ikzf3*; Fig. 2a). The reduced H3K27me3 islands could be further divided into four groups.

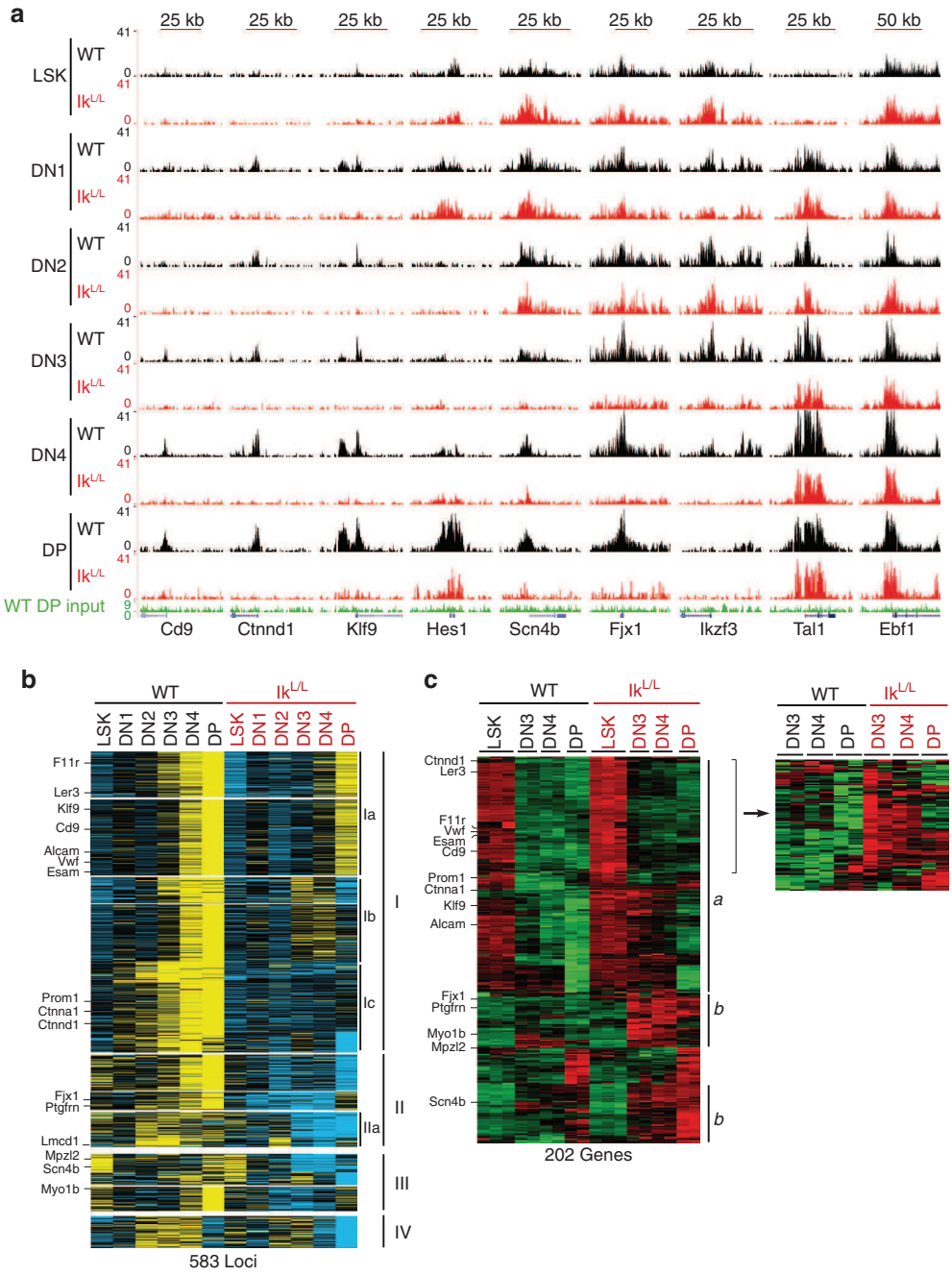

Figure 2 | Ikaros is required for the establishment and maintenance of H3K27me3 in developing T cells. (**a**) Genome browser tracks of H3K27me3 ChIP-seq data from WT and Ik$^{L/L}$ cells. (**b**) *k*-means clustering of relative normalized tag numbers (the region's normalized tag count/length of the region) in H3K27me3 enriched merged genomic regions from the indicated populations. Five hundred and eighty-three loci with >1.8 × decreased normalized tag count in at least one Ik$^{L/L}$ population are shown. Blue and yellow represent low and high levels of H3K27me3, respectively. (**c**) *k*-means clustering of microarray data from the indicated populations showing 297 probe sets (202 genes) associated with decreased H3K27me3 (>1.8 ×) and an expression change of >4 × between the lowest and highest value of the analysed samples. The right panel shows clustering without the LSK data of part of cluster *a*. Green and red represent low and high levels of gene expression, respectively.

Group I islands were small or undetectable in WT LSK cells, but increased from the DN1 to the DP stage (for example, *Cd9*, *Ctnnd1*, *Klf9*, *Ctnna1*, *Ier3*, *Vwf* and *Alcam*; Fig. 2a,b and Supplementary Fig. 2d); they were similar in $Ik^{L/L}$ LSK cells, but did not increase (Fig. 2b subgroup Ic), or increased slightly in DP (subgroup Ia) or DN3 and DN4 (subgroup Ib) cells. Group II islands were constitutively present in WT LSK cells and thymocytes (for example, *Fjx1* and *Ptgfrn*); they were similarly observed in $Ik^{L/L}$ LSK cells, but were undetectable in thymocytes after the DN2 and DN3 stages. Group III islands were present in LSK cells of both genotypes. In WT thymocytes, they were transiently reduced between the DN1 and DN3 stages, and increased in DN4 and DP cells. In $Ik^{L/L}$ cells, these islands were also decreased from the DN1 stage, but did not increase afterwards, or increased only slightly in DP cells. Group III islands mapped to genes activated by Notch signalling (for example, *Mpzl2*, *Scn4b*, *Hes1* and *Myo1b* in Fig. 2a,b and Supplementary Fig. 2d)[5] among others. Group IV islands were detected mainly between the DN2 and DN4 stages in WT cells; they were inconsistently detected in $Ik^{L/L}$ LSK and DN cells, and were prematurely lost in DN4 cells (for example, *Ikzf3* and *Rorc* in Fig. 2a and Supplementary Fig. 2d).

To equate the H3K27me3 changes with gene expression in the above populations, we compared the mRNA expression of the associated genes between WT and $Ik^{L/L}$ cells (LSK data from this study and thymocyte data from GSE 46090)[5]. Four hundred and forty-nine of the 583 H3K27me3 islands from Fig. 2b were associated with 444 genes, of which 392 were represented on the microarrays. Decreased H3K27me3 correlated with increased gene expression in each population by scatter plot analyses (Supplementary Fig. 3a). Indeed, 202 (52%) of the genes were dynamically regulated from the LSK to the DP stage, and 178 (88%) of these showed increased mRNA expression in the $Ik^{L/L}$ cells compared with WT (Fig. 2c). Group *a* genes ($n=114$) were expressed in WT LSK cells and silenced during thymocyte differentiation (Supplementary Fig. 3b); these genes were also expressed in $Ik^{L/L}$ LSK cells but were not silenced, or silenced less efficiently, in DN cells (group *a* and highlighted right panel in Fig. 2c). Group *a* included genes with important functions in HSC and progenitor cells (for example, *Cd9*, *Alcam*, *Ier3*, *F11r*, *Vwf*, *Esam* and *Prom1*)[17–23] (Fig. 2a and Supplementary Fig. 2d for selected H3K27me3 profiles). Most group *a* genes ($n=105$) were associated with group I H3K27me3 islands (similarly represented among subgroups I, a–c in Fig. 2b). Group *b* genes ($n=64$) were not expressed in WT and $Ik^{L/L}$ LSK cells, or in WT thymocytes, but were ectopically expressed in $Ik^{L/L}$ thymocytes. These genes were associated in similar numbers with H3K27me3 islands from groups I ($n=24$), II ($n=20$) and III ($n=20$). Certain Notch-activated genes ectopically increased at the mRNA level in $Ik^{L/L}$ thymocytes were found in group *b* (for example, *Myo1b*, *Lmcd1* and *Fjx1*)[5].

Collectively, these analyses indicate that Ikaros deficiency results in the reduction or disappearance of >500 H3K27me3 islands during thymocyte development, and that this is correlated with ectopic expression of genes normally expressed in HSCs.

Ikaros acts in DN cells to establish and maintain H3K27me3. To address the role of Ikaros in H3K27me3 regulation, we first studied Ikaros binding in WT DP cells by ChIP-seq. Unexpectedly, little or no Ikaros binding was detected at loci where H3K27me3 was reduced in $Ik^{L/L}$ DP cells, although Ikaros bound to other places in the genome (Supplementary Fig. 4a). Given that H3K27me3 changes were also detected in $Ik^{L/L}$ DN cells, we hypothesized that Ikaros influenced H3K27 trimethylation at earlier stages. Indeed, Ikaros proteins were abundant in DN2–DN4 cells (Supplementary Fig. 4b).

Ikaros binding was studied in WT DN3, DN4 and DP cells by ChIP-seq (DN1 and DN2 cells were not analysed due to their low numbers). We found 37,050 Ikaros peaks in DN3, 23,656 in DN4 and only 5,351 in DP cells. The majority of the regions bound by Ikaros in DP cells (4,689, 87.6%) were also bound in DN3 and DN4 cells, and only a small number (132, 2.5%) were specific to DP cells, suggesting that Ikaros binds most of its target genes at the DN stage (Supplementary Fig. 4c). Interestingly, the proportion of promoter-associated peaks increased, whereas those at intergenic regions or gene bodies decreased, during differentiation (Supplementary Fig. 4d). The AGGAA motif was highly enriched among Ikaros peaks (Supplementary Fig. 4e), consistent with previous results[5,6,24–26]. Ikaros peaks were also enriched for Ctcf sites, as described[6]. Additional enriched motifs included E-boxes as well as those specific for Sp1, Runx1, Ets1, Nrf1, Zbtb33, Bhlhb2 and Nfya. We then compared the H3K27me3 profiles with Ikaros binding and found that the majority of the H3K27me3 islands (322/583) reduced in $Ik^{L/L}$ thymocytes (Fig. 2b) overlapped with Ikaros binding in WT cells (331 peaks, $P\leq10^{-7}$; Fig. 3a groups 1 and 3, and Fig. 3b). Ikaros binding was most pronounced in DN3 and DN4 cells, and was faint or absent in DP cells. An additional 179 H3K27me3 islands showed clear Ikaros enrichment even though they were not identified bioinformatically (group 2). In contrast, little Ikaros binding was detected at regions where the H3K27me3 profiles were more dispersed (group 4 in Fig. 3a, which corresponded mostly to groups IIa and IV in Fig. 2b). Thus, nearly all of the H3K27me3 islands that increased with differentiation in WT cells show concomitant Ikaros binding in DN3 and DN4 cells. However, there was no correlation between the size of Ikaros peaks and the magnitude of H3K27me3 changes (Supplementary Fig. 4f).

To determine whether Ikaros is required in DN thymocytes for H3K27 trimethylation at these genes, we studied two T-cell-specific conditional Ikaros-null mouse models: $Ik^{f/f}$ Lck-Cre^{+} mice, in which Ikaros proteins were undetectable from the DN3 stage (Fig. 3c and Supplementary Fig. 5a), and $Ik^{f/f}$ CD4-Cre^{+} mice, in which Ikaros expression was lost from the DP stage[5]. As these mice developed T-ALL with similar kinetics as $Ik^{L/L}$ animals (Supplementary Fig. 5b–d)[5], DP cells were purified from

Figure 3 | Ikaros binds to target genes and regulates H3K27me3 in DN3 cells. (**a**) Comparison of H3K27me3 profiles and Ikaros binding. The 583 H3K27me3 islands from Fig. 2 were first divided into those with increasing H3K27me3 from the DN3 to DP stage (groups 1 and 2) or not (groups 3 and 4). They were then further divided into groups with significant Ikaros binding ($P\leq10^{-7}$; groups 1 and 3) or not (groups 2 and 4). The H3K27me3 profiles of each group were clustered (*k*-means, left panels). Tag density heatmaps of the Ikaros ChIP-seq data centred around the corresponding H3K27me3 islands (±10 kb) were calculated for each group and clustered (*k*-means; right panels). (**b**) Representative genome browser tracks showing Ikaros binding. (**c**) Deletion of Ikaros in DN3 cells. Immunoblots of whole-cell lysates from DN1 (2×10^4) and DN2–4 (5×10^4) cells from $Ik^{f/f}$ Lck-Cre^{-} and $Ik^{f/f}$ Lck-Cre^{+} mice. The two bands detected with the anti-Ikaros antibody represent the predominant Ik1 and Ik2 isoforms. Representative of three independent experiments. (**d**) Ikaros deletion in DN3, but not DP, cells results in the loss of H3K27me3 at Ikaros target genes. Hoxa13 and Tubb2a are positive and negative controls, respectively. H3K27me3 ChIP–qPCRs on chromatin from DP cells of $Ik^{f/f}$ Lck-Cre^{-} versus $Ik^{f/f}$ Lck-Cre^{+} ($n=2$), $Ik^{f/f}$ CD4-Cre^{-} versus $Ik^{f/f}$ CD4-Cre^{+} ($n=2$) mice. The values indicate [(H3K27me3 ChIP)-(IgG ChIP)]/[(H3 ChIP)-(IgG ChIP)]. Cre^{-} over Cre^{+} fold changes are shown at the bottom. Error bars, s.d.; *$P<0.05$ (two-sample *t*-test).

3- to 4-week-old mice and studied for H3K27me3 at select loci by ChIP–qPCR analysis (Fig. 3d). We analysed *Ctnna1*, *Cd9* and *Ctnnd1*, because these loci gradually acquire H3K27me3 from the DN1 stage on in WT but not $Ik^{L/L}$ cells, and *Mpzl2*, *Scn4b*, *Fjx1*, *Tbx21*, *Prom1* and *Zfp334*, because they are constitutively marked with H3K27me3 in all WT populations, but lose this mark in $Ik^{L/L}$ DN cells at various stages (Fig. 2a and Supplementary Fig. 2d). We found that H3K27me3 levels were similar to WT at all genes in $Ik^{f/f}$ CD4-Cre^{+} DP cells, but were lower in $Ik^{f/f}$ Lck-Cre^{+} DP cells, except for *Prom1* and *Zpf334*. Interestingly, *Zfp334* and

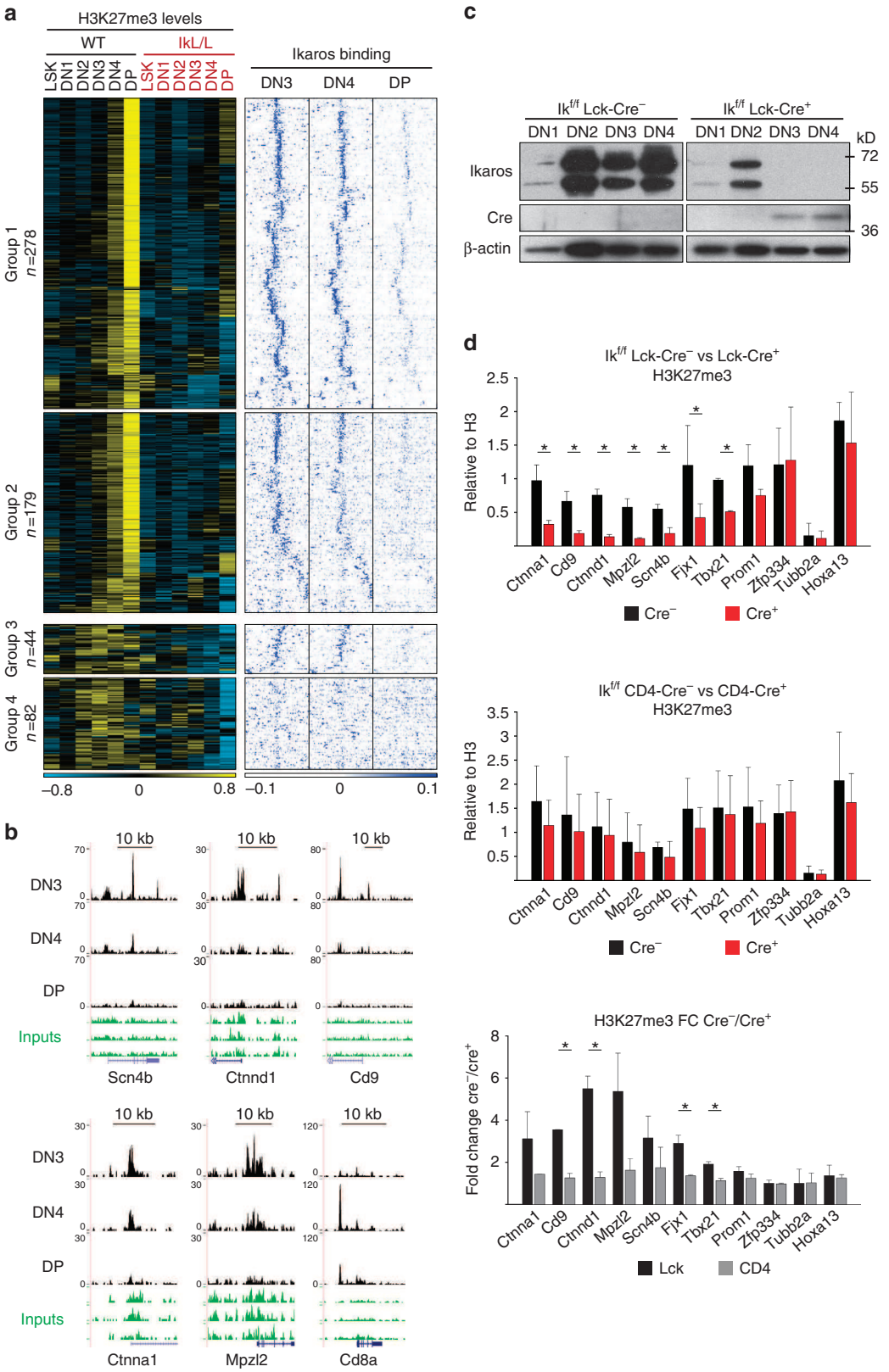

Prom1 lost H3K27me3 early during differentiation in $Ik^{L/L}$ cells (in DN1 and DN2 cells, respectively; Supplementary Fig. 2d). These results demonstrate that Ikaros acts in DN cells in a stage- and locus-specific manner, to initiate and/or maintain H3K27me3.

Reduced PRC2 binding to specific loci in $Ik^{L/L}$ DN3 cells. To determine the impact of Ikaros on PRC2 recruitment, we first evaluated Ezh2 protein levels in thymocytes. Ezh2 was detected in both WT and $Ik^{L/L}$ DN subsets (Supplementary Fig. 6a), indicating that the decrease in H3K27me3 in Ikaros-deficient thymocytes is not due to a decrease in PRC2 activity.

We then evaluated Suz12 binding by ChIP-seq in DN3 cells, where Ikaros binding was best detected, and identified 9,541 Suz12 peaks ($P \leq 10^{-7}$) in the WT and $Ik^{L/L}$ samples. Although most Suz12 peaks were comparable between WT and mutant, the majority of the 583 loci, characterized by reduced H3K27me3 in $Ik^{L/L}$ cells, showed a striking overlap between Ikaros and Suz12 binding on WT chromatin and a marked decrease in Suz12 enrichment on $Ik^{L/L}$ chromatin (Fig. 4a,b). Of these, we focused on 216 Suz12 peaks that overlapped with Ikaros binding using

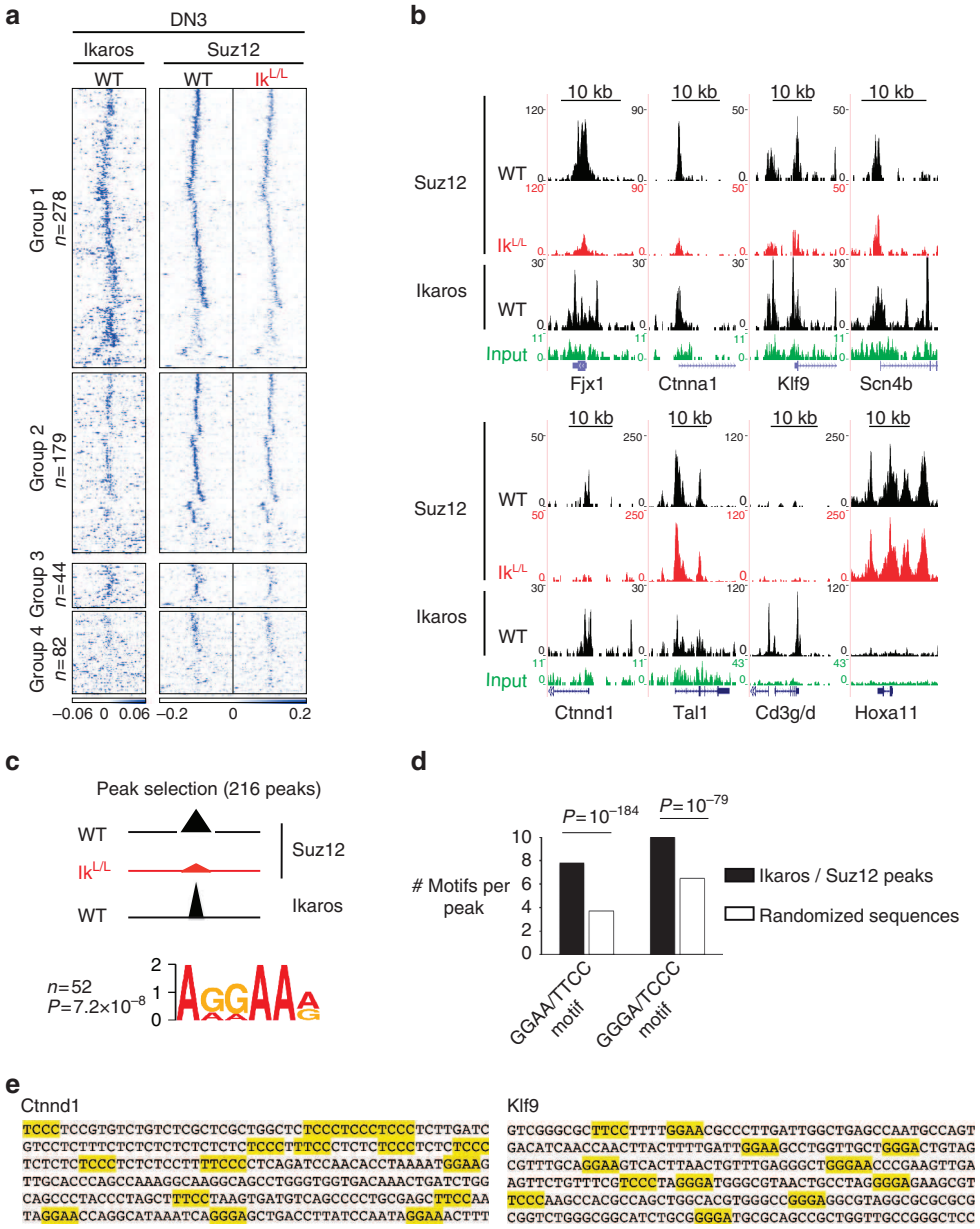

Figure 4 | Ikaros is required for PRC2 targeting in DN3 cells. (**a**) *k*-means clustering of Ikaros and Suz12 tag density heatmaps on the 583 regions that showed decreased H3K27me3 in $Ik^{L/L}$ DN3 cells. Groups 1–4 are identical to those in Fig. 3a. (**b**) Representative genome browser tracks showing Suz12 and Ikaros ChIP-seq in WT and $Ik^{L/L}$ cells. WT DP input controls in green. (**c**) The Ikaros peaks associated with the 216 Suz12 peaks (from Supplementary Fig. 5b left) were selected and motif enrichment near the peak centre (± 40 bp from the summit) was analysed with MEME. The AGGAA motif was significantly enriched. (**d**) Enrichment of the GGGA and GGAA motifs near the Ikaros/Suz12 peaks. The average number of GGGA and GGAA motifs (or their complementary motifs) were determined within 150 bp of the peak summits defined in Supplementary Fig. 5b, as well as in nucleotide sequences of randomized permutations. The *P*-value was calculated with the χ^2-test. (**e**) Examples of sequences where the putative Ikaros target motifs GGGA and GGAA have been highlighted.

stringent bioinformatic criteria ($P \leq 10^{-7}$; Supplementary Fig. 6b left). The genes associated with these peaks exhibited a clear bias towards activation in $Ik^{L/L}$ DN3 cells (Supplementary Fig. 6c), compared with other groups. The Ikaros motif (AGGAAa/g) was the only known motif detected under the Ikaros/Suz12 peaks and it was located within 40 bp of the centre of the Ikaros peaks (Fig. 4c). The regions surrounding the Ikaros peaks (± 150 bp of the summit) also contained a high number of GGAA or GGGA motifs (Fig. 4d,e), previously shown to bind Ikaros[27–29], when compared with control sequences with random nucleotide permutations, suggesting a functional importance. Thus, Ikaros is required for PRC2 binding to a specific set of target genes in DN3 cells.

Ikaros is required for PRC2 binding and H3K27 trimethylation. To determine how Ikaros induces PRC2 binding, we established a gain-of-function system with the ILC87 Ikaros-null T-cell line, derived from a lymphoma of an $Ik^{f/f}$ Lck-Cre^{+} mouse (Supplementary Fig. 7a). ILC87 cells were stably transduced to express an inducible full-length Ikaros1 isoform fused to the ligand-binding domain of the oestrogen receptor (Ik1-ER) and green fluorescent protein (GFP). Upon treatment with the ER ligand 4-hydroxytamoxifen (4OHT), for 1–3 days, GFP^{+} cells showed enhanced nuclear translocation of Ik1-ER (Supplementary Fig. 7b)[5]. The differentiation markers CD4, CD8 and CD3 showed little change in 4OHT-treated ILC87-Ik1-ER cells after 1 day (Supplementary Fig. 7c), although their expression increased at later timepoints.

We analysed the genomic localization of Ikaros, Suz12 and H3K27me3 in 4OHT-treated ILC87-Ik1-ER cells by ChIP-seq. Ikaros was studied after 24 h of treatment, and Suz12 and H3K27me3 after 72 h. Although Ikaros binding was nearly absent in vehicle-treated cells, 4OHT induced binding to 8,017 regions (Supplementary Fig. 8a). We identified 61 sites with increased H3K27me3 that correlated with a 4OHT-dependent increase of Ikaros and/or Suz12 binding (Fig. 5, Supplementary Fig. 8b and Supplementary Table 2). Importantly, 40 of these sites mapped to genes that showed decreased H3K27me3 in primary Ikaros-deficient thymocytes (Fig. 5a, Supplementary Fig. 8b and Supplementary Table 2). Thus, gain of Ikaros function in ILC87 cells rescues H3K27me3 at genes that had lost the mark in Ikaros-deficient thymocytes. These data were validated by ChIP–qPCR analysis at the *Scn4b* locus (Supplementary Fig. 8c). Similar

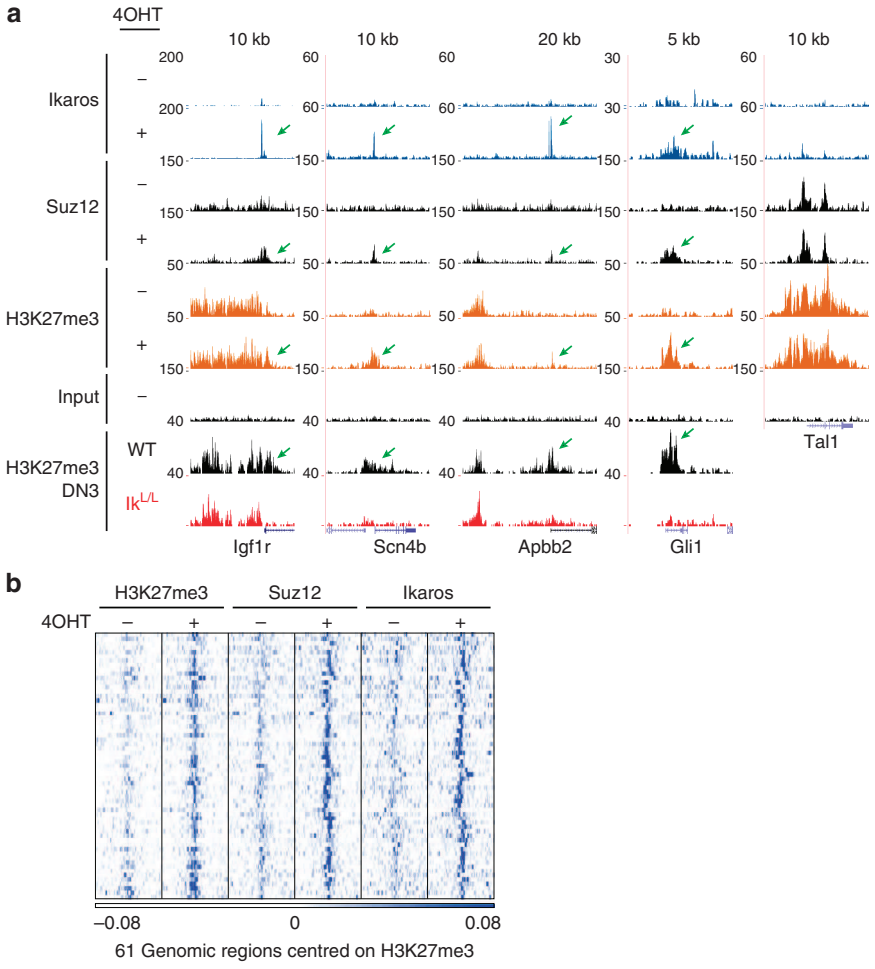

Figure 5 | Ikaros induces PRC2 targeting and H3K27 trimethylation. ChIP-seq of Ikaros, Suz12 and H3K27me3 on ILC87-Ik1-ER cells treated with 4OHT (+) or ethanol (−) for 1 day (Ikaros) or 3 days (Suz12 and H3K27me3). (**a**) Representative genome browser tracks. Green arrows depict induced Ikaros, Suz12 and H3K27me3. Corresponding H3K27me3 tracks from primary WT and $Ik^{L/L}$ DN3 thymocytes are shown at the bottom. Tal1 is shown as positive control. Vertical scales indicate tag numbers. (**b**) *k*-means clustering of H3K27me3-centred (± 10 kb) Ikaros, Suz12 and H3K27me3 tag density heatmaps on the 61 regions with increased H3K27me3 in 4OHT-treated samples. Selected regions were identified bioinformatically (as having an Ikaros peak in 4OHT-treated cells, which overlapped with a H3K27me3 island that increased >1.8 × between ethanol- and 4OHT-treated cells), or by visual scanning of the tracks.

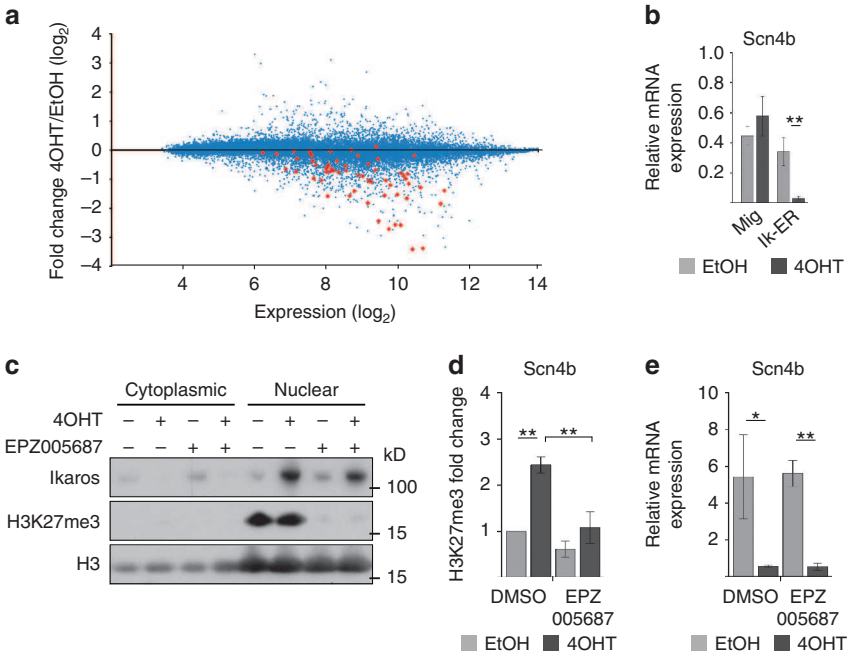

Figure 6 | Impact of Ikaros-induced PRC2 activity on gene expression. (**a**) MA plot depicting the expression (in ethanol-treated samples) versus fold change of all the probe sets of the Mouse Gene ST 1.0 array in ILC87-Ik1-ER cells treated with ethanol or 4OHT for 1 day. Probe sets highlighted in red represent the 61 genes with 4OHT-induced H3K27me3 from Fig. 5b. (**b**) Reverse transcriptase–qPCR (RT–qPCR) analysis of *Scn4b* expression in ILC87-Ik1-ER and control (Mig) cells treated with ethanol or 4OHT for 1 day. (**c**) Western blotting of H3K27me3 and Ikaros in ILC87-Ik1-ER cells treated with the Ezh2 inhibitor EPZ005687 or vehicle (dimethyl sulphoxide (DMSO)) for 2 days. During day 2, cells were also treated with 4OHT or ethanol. Histone H3 is shown as loading control. (**d**,**e**) H3K27me3 ChIP–qPCR (**d**) and RT–qPCR (**e**) analysis of the *Scn4b* gene in cells treated as in **c**. Expression data are normalized to Hprt. Error bars, s.d. ($n=3$); $^{*}P<0.05$, $^{**}P<0.01$ (two-sample *t*-test).

results were obtained with ILC87 cells transduced to constitutively express non-tagged Ikaros (Supplementary Fig. 8d).

To determine whether increased H3K27me3 correlates with decreased gene expression, we generated microarray data from ILC87-Ik1-ER cells treated with 4OHT or vehicle and evaluated the mRNA level of the 61 genes that exhibited increased H3K27me3. Most of the genes showed reduced mRNA expression (Fig. 6a), which was confirmed by reverse transcriptase–qPCR analysis for *Scn4b* (Fig. 6b), suggesting a correlation between H3K27me3 and gene repression. To determine whether increased H3K27me3 is required, we analysed 4OHT-treated ILC87-Ik1-ER cells treated with an Ezh2 inhibitor. This strongly reduced both the global H3K27me3 levels and the 4OHT-induced H3K27me3 increase at *Scn4b* (Fig. 6c,d), but *Scn4b* expression was still repressed (Fig. 6e). Thus, Ikaros is associated with PRC2 binding and H3K27me3, but these events are not required to initiate Ikaros-mediated repression of this gene.

Ikaros interacts with PRC2 independently of NuRD. The above results suggested that Ikaros may recruit PRC2 to its target genes. To determine whether Ikaros forms a complex with PRC2, we performed a glutathione *S*-transferase (GST) pull-down assay. Ikaros–GST fusion proteins were captured with glutathione beads and were incubated with nuclear extracts from ILC87 cells. Ikaros–GST, but not GST or empty glutathione beads, precipitated the PRC2 components Ezh2 and Suz12 (Fig. 7a). Furthermore, immunoprecipitation (IP) of nuclear extracts from ILC87 cells constitutively expressing Ikaros, with an anti-Ikaros antibody, led to the co-IP of Ezh2 and Suz12 (Fig. 7b). Conversely, IP of either Suz12 or Ezh2 led to the co-IP of Ikaros. As a positive control, the NuRD complex proteins Mi2β and Mta2 were also found to co-IP with Ikaros. Importantly, Mi2β and Mta2 did not co-IP with Suz12 or Ezh2, indicating that the interaction between PRC2 and Ikaros is specific. To assess the stability of the Ikaros–PRC2 interaction, the extracts were immunoprecipitated with the anti-Ikaros antibody in the presence of high salt concentrations (Fig. 7c); this showed that Ikaros could associate with Ezh2 and Mta2 in the presence of 0.3 or 0.5 M NaCl. In a second experiment, the extracts immunoprecipitated with anti-Ikaros were subsequently washed with increasing salt concentrations, which revealed that the interaction of Ikaros with Ezh2 and Mta2 remained stable at up to 1 M NaCl (Fig. 7d), although the Ikaros–Mta2 interaction appeared to be more resistant. Thus, Ikaros forms stable complexes with PRC2. To determine whether specific Ikaros domains were required for interaction with PRC2, we generated ILC87 cells constitutively expressing Ikaros proteins deleted for the amino-terminal domain (ΔN, aa1–114), the DNA-binding domain (ΔDBD, aa119–223) or the dimerization domain (ΔDIM, aa457–508). After IP with anti-Ikaros, the ΔN and ΔDBD, but not the ΔDIM, proteins interacted with Ezh2 (Fig. 7e), suggesting that dimerization may be important for PRC2 interaction.

To determine whether Ikaros interacts with PRC2 in primary thymocytes, nuclear extracts from WT DN thymocytes were immunoprecipitated with antibodies against Ikaros or Suz12 and analysed for Ikaros, Ezh2 and Suz12 (Fig. 7f). Both Ezh2 and Suz12 co-immunoprecipitated with Ikaros, whereas Ikaros and Ezh2 co-immunoprecipitated with Suz12. These results demonstrate that Ikaros interacts with PRC2 in DN thymocytes.

The NuRD complex has been reported to be important for PRC2 recruitment and activity in other systems[30–34]. Our data, however, suggest that PRC2 does not interact with NuRD in the present system. We further evaluated whether the Ikaros–PRC2

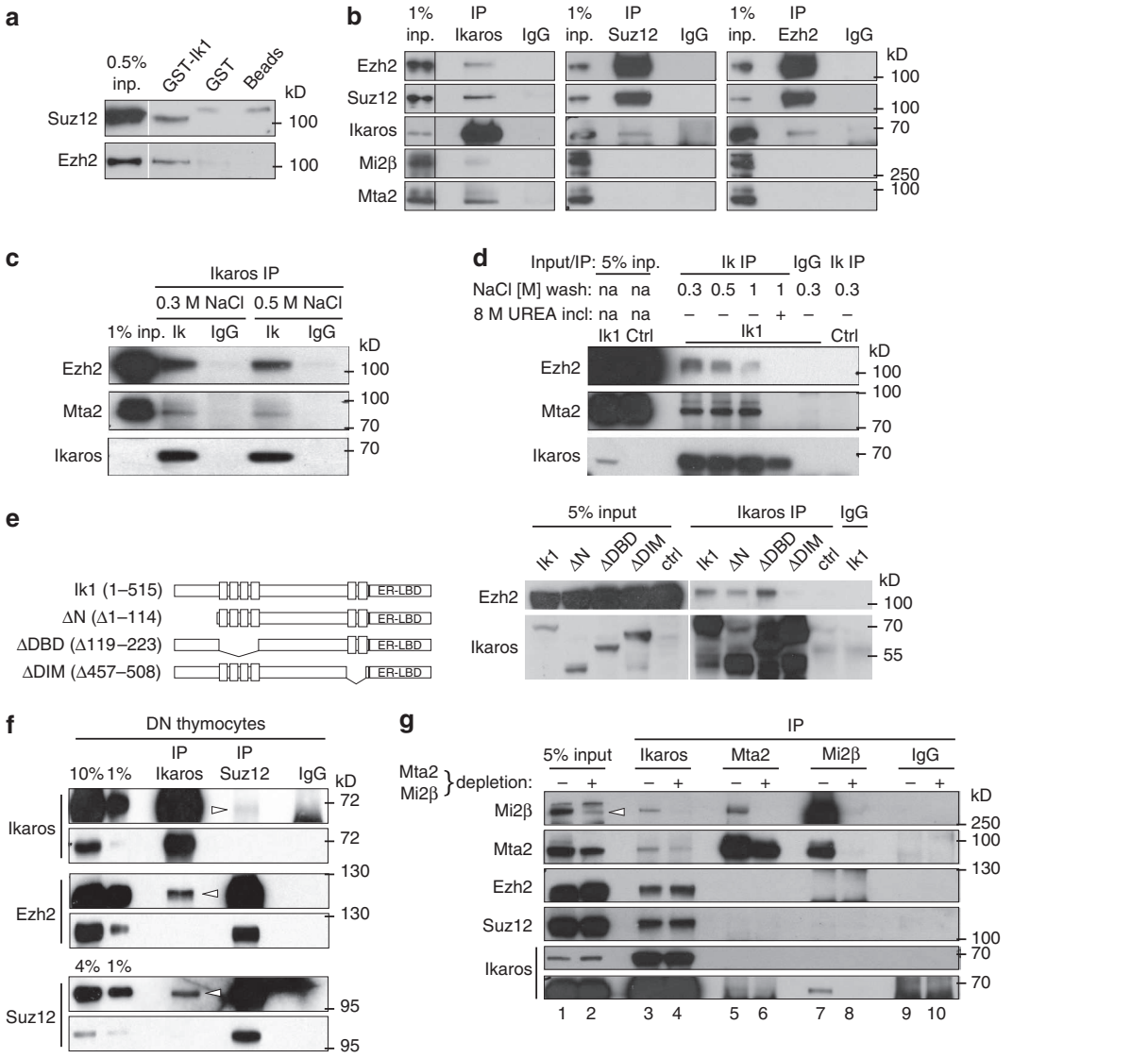

Figure 7 | Ikaros forms a complex with PRC2 independent of NuRD. (**a**) GST-Ikaros binds PRC2. Bacterially expressed Ik1-GST fusion protein was immobilized on glutathione-agarose beads and incubated with ILC87 nuclear extracts. Bound proteins were analysed by western blotting. Immobilized GST protein alone, or glutathione-agarose beads alone were used as negative controls. (**b**) Ikaros interacts with PRC2 in ILC87 cells. Western blottings for the indicated proteins after IP of Ikaros, Suz12, Ezh2 or IgG. One per cent inputs from the nuclear extracts of ILC87-Ik1-Bcl2 cells are shown. (**c**) Western blottings for the indicated proteins after IP of Ikaros (Ik) or IgG from nuclear extracts as in **b**, except that the IPs and washing steps were performed in the presence of 0.3 or 0.5 M NaCl as indicated. (**d**) Ikaros (Ik) or IgG IPs from nuclear extracts as in **b**. Immune complexes were washed in the presence of 0.3, 0.5 or 1 M NaCl, or 1 M NaCl plus 8 M urea, as indicated. The ctrl sample is an Ikaros IP performed on nuclear extracts of ILC87-Bcl2 cells transduced with the empty MigR1 vector. Five per cent inputs are shown. (**e**) Right: analysis of the interaction of Ikaros deletion mutants with Ezh2 by co-IP. As in **b**, except that ILC87-Bcl2 cells expressing the indicated Ikaros mutants were analysed. Five per cent input controls are shown. Left: schematic representation of the Ikaros deletion constructs. (**f**) Ikaros interacts with PRC2 in primary WT DN cells. Western blottings for the indicated proteins after IP of Ikaros, Suz12 or IgG on ~333 μg nuclear extracts from WT $CD4^-CD8^-CD3^-$ thymocytes. (**g**) NuRD depletion does not affect the Ikaros–PRC2 interaction. Nuclear extracts of ILC87-Ik1-Bcl2 cells were incubated in three consecutive steps with IgG- (−), or anti-Mta2- and anti-Mi2β-coupled (+), Protein A/G Sepharose beads. Resulting supernatants (shown as 5% inputs) were subjected to Ikaros, Mta2, Mi2β or IgG IPs and immunoblotted as indicated. Arrowhead indicates the Mi2β-specific signal. Short and long exposures of the Ikaros blot are shown. (**b**) Representative of ≥5, (**c**) 1, (**d**) 2, (**a**,**e**–**g**) 3 independent experiments.

interaction required NuRD, by first depleting nuclear extracts from ILC87 cells constitutively expressing Ikaros of NuRD-associated proteins, or not, with antibodies against Mta2 and Mi2β (Fig. 7g). Although Mi2β was nearly absent from the depleted extracts, Mta2 was reduced approximately twofold (Supplementary Fig. 9 lane 3). Samples were then immunoprecipitated with antibodies specific for Ikaros, Mta2 or Mi2β and analysed for Ezh2, Suz12, Mta2, Mi2β or Ikaros. As expected, depletion of Mta2 and Mi2β diminished the abundance of these proteins in the precipitated samples (Fig. 7g lanes 4, 6 and 8). However, the Ezh2 and Suz12 levels in the anti-Ikaros precipitated samples were unaffected by the Mta2/Mi2β depletion (Fig. 7g lanes 3 and 4), indicating that the Ikaros–PRC2 interaction was still intact. In addition, Ezh2 and Suz12 were not detected in the anti-Mta2 or anti-Mi2β precipitated samples (Fig. 7g lanes 5–8), suggesting a lack of interaction between PRC2 and NuRD proteins. These results indicate that Ikaros forms distinct complexes with PRC2 and NuRD.

Ikaros and PRC2 co-localize at genomic sites lacking NuRD. To determine whether Ikaros co-localizes with PRC2 independently of NuRD *in vivo*, we evaluated Mta2 and Mi2β binding, along with H3K4me3 (which co-localizes with NuRD in DP cells)[6], in DN3 thymocytes and compared these with Ikaros, Suz12 and H3K27me3. Mta2 and Mi2β overlapped at 19,747 sites (hereafter referred to as NuRD sites) and were detected alone at 9,177 regions for Mta2 and 2,055 regions for Mi2β (Fig. 8a). Most of the NuRD-bound regions were also bound by Ikaros ($n=16,378$), in agreement with published data[6]. H3K4me3 frequently co-localized with NuRD (10,466 sites, 70% of H3K4me3 islands), but H3K27me3 and NuRD co-localization was remarkably less frequent (803 sites, 23% of H3K27me3 islands) and occurred almost exclusively on bivalent H3K4me3/H3K27me3 domains (749 sites; Fig. 8b). Similarly, NuRD was observed at only 25% of Suz12 sites (2,259 of 8,792 regions; Fig. 8c). Importantly, Ikaros co-localized with Suz12 on 755 regions that lacked detectable NuRD. These results support our biochemical data that Ikaros interacts with PRC2 independently of NuRD.

Finally, we asked whether NuRD co-localizes with Ikaros and Suz12 at loci that were dependent on Ikaros for H3K27 trimethylation (Fig. 8d,e). Of the 213 loci where overlapping Ikaros/Suz12 binding was detected, 153 were occupied by NuRD

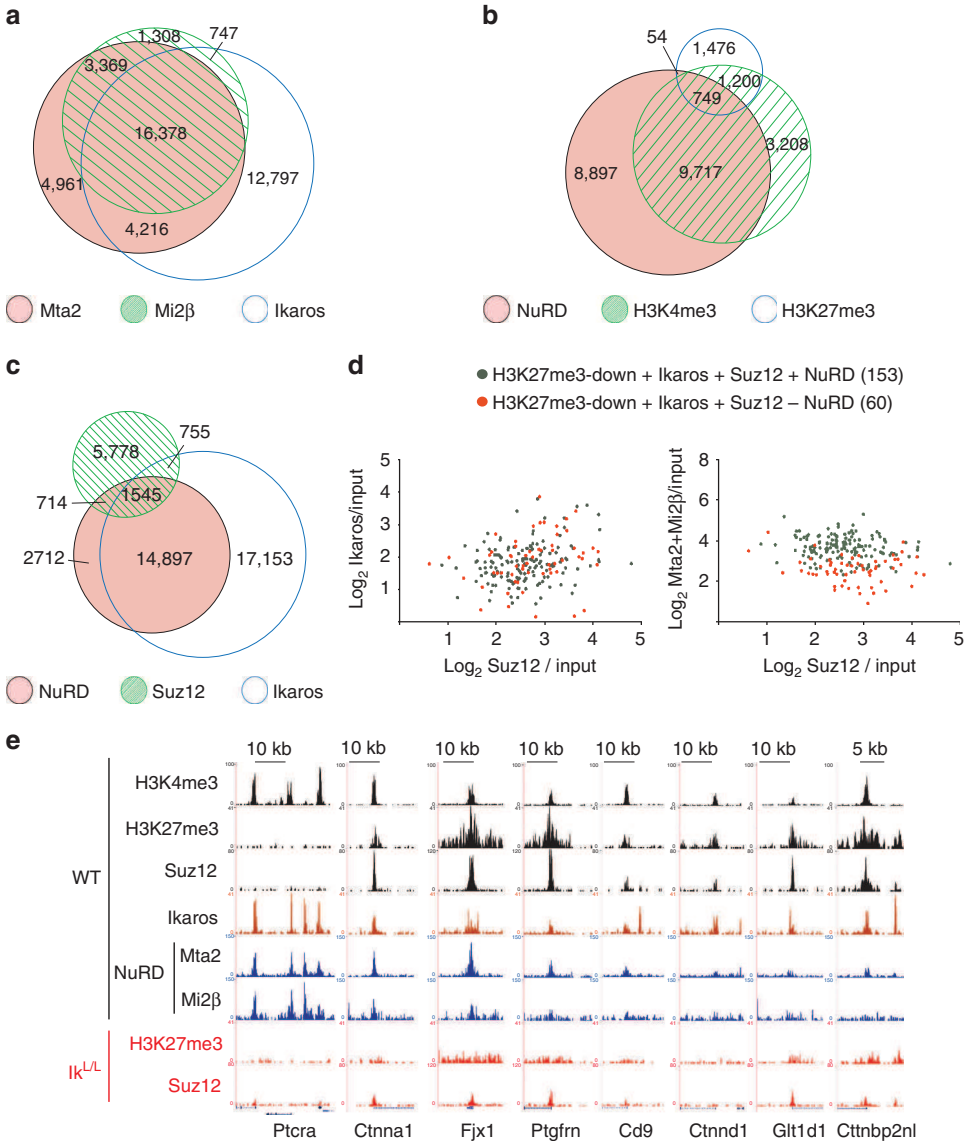

Figure 8 | Ikaros and PRC2 co-localize at genomic regions devoid of NuRD. ChIP-seq analysis of Mta2, Mi2β, H3K4me3 and H3K27me3 (Fig. 2), Ikaros (Fig. 3) and Suz12 (Fig. 4) in WT DN3 thymocytes. Venn diagrams of (**a**) 43,776 merged genomic regions bound by Mta2, Mi2β and Ikaros; (**b**) 25,301 merged genomic regions occupied by NuRD (that is, Mta2 and Mi2β), H3K4me3 and H3K27me3; (**c**) 43,554 merged genomic regions bound by NuRD, Ikaros and Suz12. It is noteworthy that each merged genomic region may comprise several overlapping binding sites from the different samples. (**d**) Scatter plot comparisons of Ikaros (left) and NuRD (right) binding to 213 Suz12- and Ikaros-bound regions that exhibit decreased H3K27me3 in $Ik^{L/L}$ thymocytes (Supplementary Fig. S6b,c; it is noteworthy that 3 of the 213 common Ikaros/Suz12-bound regions considered here had 2 distinct Suz12 peaks, of which only the ones with higher tag numbers were kept for this analysis). Binding intensities are expressed as $\log_2$ FC over input. Regions bound or not by NuRD are shown in grey and red, respectively. (**e**) Representative genome browser tracks illustrating occupancy by Ikaros, Suz12 and NURD, as well as H3K4me3 and H3K27me3 levels of selected loci. H3K27me3 and Suz12 tracks from $Ik^{L/L}$ DN3 thymocytes are shown at the bottom. The *Ptcra* locus is shown as an active gene with high levels of NURD, Ikaros and H3K4me3.

(for example, *Ctnna1*, *Fjx1* and *Ptgfrn*), whereas 60 were not (for example, *Cd9*, *Ctnnd1*, *Glt1d1* and *Cttnbp2nl*). In addition, there was no correlation between the presence or absence of NuRD and the intensity of Ikaros or Suz12 binding. Thus, Ikaros can act independently of NuRD to regulate PRC2 activity on a number of target genes, to establish the H3K27me3 mark in DN3 cells.

Discussion

We show that Ikaros regulates the epigenetic silencing of >500 developmentally regulated loci in $CD4^-CD8^-$ thymocytes via PRC2, which include genes specifically expressed in HSCs or activated by Notch. Many genes affected by Ikaros exhibit bivalent epigenetic marks in WT cells and are derepressed in Ikaros-deficient cells through the selective loss of H3K27me3. Ikaros binding results in PRC2 recruitment and H3K27 trimethylation. Further, Ikaros complexes with PRC2 in T-cell lines and primary thymocytes, independently of NuRD. These results identify a fundamental mechanism of Ikaros as a regulator of PRC2 function in T lymphocytes.

Interestingly, our data suggest that PRC2 activity is not required for the downregulation of Ikaros target gene expression, which occurs in the presence of a PRC2 inhibitor. As most genes with Ikaros-dependent H3K27me3 increases also showed decreased expression, it is possible that transcriptional repression is a prerequisite for PRC2 tethering, as was recently suggested[35]. Ikaros target genes may require PRC2 and H3K27 trimethylation to maintain repression through epigenetic memory, in particular in DP thymocytes where Ikaros can no longer be detected at the DNA. Nonetheless, repression alone does not ensure PRC2 recruitment, as Ikaros represses the expression of other genes that do not gain H3K27me3, suggesting a role for additional mechanisms.

The majority of the genes affected by the loss of H3K27me3 are normally expressed in HSCs and silenced during T-cell differentiation, and the top biological functions associated with them are cell/organ morphology and development (Supplementary Table 3). These data implicate Ikaros as a negative regulator of the HSC gene expression programme in early T cells. Interestingly, HSC-specific genes were previously found to be inefficiently silenced in lymphoid-committed progenitors of Ikaros-null mice[4], but only 3 (*Ppic*, *Rhoj* and *Socs2*) of the 22 genes identified in that report were deregulated in our study, suggesting that Ikaros regulates distinct target gene repertoires in progenitor cells versus thymocytes. The persistent expression of a stem cell gene repertoire may also be associated with the tumour suppressor function of Ikaros. *IKZF1* mutations are found in 12% of early T-cell precursor ALL, which are also characterized by mutations in PRC2 genes (*SUZ12*, *EZH2* or *EED*) in 42% of cases[36]. Transcriptomic signatures of human B-ALL or myeloid leukemias associated with *IKZF1* mutations have also been shown to be enriched in HSC-related genes[37,38].

Ikaros and PRC2 also repress the expression of some Notch target genes (*Hes1*, *Mpzl2* and *Scn4b*), which are transiently induced in DN2 and DN3 cells, and require Ikaros to be efficiently silenced in DN4 and DP cells[5]. Ikaros binds to these genes in DN3 cells (see Fig. 3b for *Mpzl2* and *Scn4b*), perhaps setting the stage for later PRC2 recruitment in DN4 and DP cells when Notch signalling is no longer required. Intriguingly, genes (*Lmcd1*, *Fjx1* and *Myo1b*) activated by Notch only in the context of Ikaros deficiency[5] show striking decreases in H3K27me3, suggesting that loss of this mark defines a permissive epigenetic state in the mutant cells.

Given the various facets of PRC2 regulation by Ikaros, it will be important to investigate whether Ikaros influences PRC2 function during peripheral T-cell development. For example, Ikaros has been reported to positively regulate T-helper 2 (Th2) polarization[8], in part by repressing *Tbx21* expression[9], which is required for Th1 development. Interestingly, PRC2 has been shown to bind and prevent the ectopic expression of *Tbx21* in differentiating Th2 cells[39]. As H3K27me3 levels are strongly decreased at the *Tbx21* locus in $Ik^{L/L}$ DN and DP cells (Supplementary Fig. 2b), epigenetic regulation of *Tbx21* by Ikaros via PRC2 might also control its function in Th cell differentiation. In addition, Ikaros may influence PRC2 activity in other cell types, as some of the genes identified here (*Ctnnd1*, *Mmp14*, *Vwf*, *Dock1* and *Hes1*) are strongly upregulated in Ikaros-deficient dendritic cells[40] and Ikaros is important for PRC2 recruitment to *Hes1* in erythrocytes[41].

Our data shed light on how PRC2 is targeted to chromatin. This question remains poorly understood and several mechanisms including transcription regulators, non-coding RNAs and non-methylated non-transcribed CpG regions have been implicated[42]. The most compelling evidence for a role of transcription factors was obtained in *Drosophila*, where factors such as pleiohomeotic and sex-comb-on-midlegs target PRC2 to DNA[43]. Nonetheless, several studies have also implicated DNA-binding factors in mammalian cells, notably: YY1 in mesenchymal stem cells[44], REST in neuronal progenitors[45,46] and Foxp3 in regulatory T cells[47]. We propose that Ikaros mediates PRC2 recruitment in thymocytes.

One common feature of the Ikaros–PRC2 binding sites is the absence of motifs for other regulators, such as E2A, Runx1 and Ets1, which are often found near Ikaros motifs. This lack of recognition sequences was previously suggested to be an important property of the GC-rich sequences responsible for PRC2 binding[48]. Ikaros binding at these regions was also different, as it was spread over long stretches of DNA rather than a short distance typical of other Ikaros peaks. Indeed, these regions were characterized by numerous Ikaros motifs, suggesting that they contain low affinity binding sites. It is worth noting that, even though the number of loci at which Ikaros controls PRC2 recruitment may be low when compared with the total Ikaros sites, it is in the same range as the number of loci affected by Foxp3 or REST[46,47]. Ikaros may also act redundantly with other factors or gene-specific features to modulate PRC2 binding. For example, Ikaros and Suz12 both bind to *Lmo2* and *Tal1* in DN3 cells, but Suz12 binding is unaffected by Ikaros deficiency.

Previous studies have implicated the NuRD complex in Polycomb function[30–34]. Our results, however, suggest that Ikaros can mediate PRC2 binding independently of NuRD, as we show a strong functional interaction between Ikaros and PRC2, the existence of distinct Ikaros–NuRD and Ikaros–PRC2 complexes, and the absence of NuRD at ~30% of common Ikaros–PRC2 target sites. Further investigation will be required to clarify the relevance of NuRD at other sites.

Loss of H3K27me3 was previously observed in Ikaros-null DP cells[6]. However, as Ikaros did not bind the affected loci in WT DP thymocytes and as *de novo* Mi-2β binding was observed for many of these sites in mutant cells, it was concluded that the reduction in H3K27me3 was an indirect consequence of NuRD redistribution in the absence of Ikaros. In contrast, our results suggest that Ikaros directly affects PRC2 binding and the appearance of H3K27me3 marks in DN cells, the latter of which is maintained in DP thymocytes even after Ikaros binding is no longer detected. It remains unknown whether other Ikaros family members can contribute to H3K27me3 maintenance, in particular Aiolos, which is induced in DP cells. Interestingly, the published Aiolos ChIP-seq data from Ikaros-null thymocytes[6] showed Aiolos binding to ~50% of the affected loci identified in our study, suggesting that Aiolos cannot rescue H3K27 trimethylation in DP cells.

In conclusion, our study reveals a novel mechanism by which Ikaros represses gene expression in T cells. We anticipate that the Ikaros–PRC2 interaction will play a major role in lymphoid differentiation and tumour suppression.

Methods

Cell lines. The ILC87 cell line was previously described[5]. To retrovirally express inducible forms of the full-length or truncated Ikaros proteins, the ERT2 complementary DNA encoding the ligand-binding domain of the ER[49] was fused to the 3′-ends of the cDNAs encoding the Ikaros1 isoform (Ik1)[5] or Ik1 proteins lacking residues 1–114 (ΔN), 119–223 (ΔDBD) or 457–508 (ΔDIM) and cloned into the MigR1 vector upstream of the internal ribosome entry site that precedes a GFP coding sequence. ILC87 cells were transduced and GFP$^+$ cells were sorted to generate stable cell lines. 4OHT (Sigma) was used at a final concentration of 100 nM and the Ezh2 inhibitor EPZ005687 (Selleckchem) at 2.5 μM. To generate ILC87 cells constitutively expressing Ik1, Ik1 cDNA was cloned into the MigR1 vector and ILC87 cells were first transduced with pMCSV-mBcl2-DsRed[50] to increase cell survival, and then with the MigR1 constructs, and DsRed$^+$ GFP$^+$ cells were sorted and stable cultures were established.

Mice. Ik$^{L/L}$ and Ik$^{f/f}$ CD4-Cre tg mice were described previously[5,16]. Ik$^{f/f}$ mice[51] were also crossed with Lck-Cre tg mice[52]. Ik$^{L/L}$ mice were on the C57Bl/6 background, whereas Ik$^{f/f}$ CD4-Cre$^+$ and Ik$^{f/f}$ Lck-Cre$^+$ animals were on a mixed C57Bl/6-129Sv background. All mice used here were 3–4 weeks old and were both male or female. All animal experiments were approved by the IGBMC ethical committee (Com'Eth #2012-092).

Cell purification. Thymocytes were depleted of CD4$^+$ and CD8$^+$ cells using sheep anti-rat IgG-conjugated Dynabeads (Invitrogen). The remaining cells were stained for lineage (Lin) markers (CD4, CD8, CD3, B220, CD11b, Gr1 and NK1.1), CD44, CD25 and 4,6-diamidino-2-phenylindole (DAPI). DAPI$^-$ DN1 (Lin$^-$ CD25$^-$CD44$^+$), DN2 (Lin$^-$CD25$^+$CD44$^+$), DN3 (Lin$^-$CD25$^+$CD44$^-$) and DN4 (Lin$^-$CD25$^-$CD44$^-$) cells were sorted. To isolate DP cells, DAPI$^-$ CD4$^+$CD8$^+$CD3^{low} cells were sorted.

For LSK cells, bone marrow cells were depleted for Lin$^+$ (B220, CD11b, Gr1 and Ter119) cells with anti-rat IgG-conjugated Dynabeads. The remaining cells were first stained for CD16/CD32, Lin, Sca1, c-Kit and DAPI. DAPI$^-$ LSK cells were sorted. Cell sorting was performed on a FACSAria II SORP (BD Biosciences). Purity was >98%.

DP thymocytes were also isolated by positive selection of CD8$^+$ cells (Mitenyi Biotech). Ninety-two to 95% of the isolated cells were CD4$^+$CD8$^+$. Similar results were obtained using DP populations purified by cell sorting or by magnetic bead selection. Total DN thymocytes were depleted for CD4-, CD8- and Ter119-positive cells, and then further depleted for CD4-, CD8-, CD3-, B220-, CD11b-, Gr1-, NK1.1- and Ter119-positive cells with anti-rat IgG-conjugated Dynabeads. Isolated cells contained 70–80% cells with a DN1–4 profile. Antibodies were from BD Biosciences and eBioscience.

Antibodies. The purified rabbit polyclonal carboxy terminus-specific anti-Ikaros antibody and the mouse monoclonal anti-ER and anti-Cre antibodies were generated in-house. The N terminus-specific anti-Ikaros (sc-13039, Santa Cruz), anti-Suz12 (3737, Cell Signaling; sc46264, Santa Cruz), anti-Ezh2 (3147S, Cell Signaling), anti-Mta2 (ab8106, Abcam), anti-Mi2β (CHD4; ab70469, Abcam), anti-H3K27me3 (07-449, Millipore), anti-H3K4me3 (ab8580, Abcam), anti-H3 (06-755, Millipore; ab1791 Abcam), anti-H4 (ab7311, Abcam) and anti-β-actin (A5441; Sigma) antibodies were purchased.

Chromatin immunoprecipitation. The ChIP protocol was adapted from the Millipore ChIP Assay Kit (17-295) with minor modifications. Cells were washed in PBS and 2–6 × 10^7 cells were cross-linked at 37 °C for 10 min in 5 ml PBS/0.5% BSA/1% ultra-pure formaldehyde (Electron Microscopy Sciences). Quenching with 125 mM glycine and a cold PBS wash (containig 1 × protease inhibitor cocktail (PIC); Roche) was followed by cell lysis in 5 ml of 1% Triton X-100, 50 mM $MgCl_2$, 100 mM Tris-HCl pH 7.1, 11% sucrose, 1 × PIC for 10 min on ice. Nuclei were pelleted and were lysed in 500 μl of 1% SDS, 50 mM Tris-HCl, 10 mM EDTA, 1 × PIC. Chromatin was sonicated to 500–300 bp using a Bioruptor 200 (Diagenode), cleared by centrifugation and sonication efficiency was verified. Sonicated chromatin diluted 4 × with 0.01% SDS, 1.1% Triton X-100, 1.2 mM EDTA, 16.7 mM Tris-HCl pH 8.1, 167 mM $NaCl_2$, 1 × PIC was pre-cleared with 100 μl protein A sepharose 50% slurry or with 50 μl Magna ChIP Protein A Magnetic Beads (Millipore) previously blocked with 0.5% BSA. Cell equivalents (2.5 × 10^5–30 × 10^6) were diluted 2.5 × in the same buffer and incubated overnight (ON) with 5 μg (for anti-Ikaros (home-made), anti-Mta2 (ab8106), anti-Mi2β (ab70469), anti-H3K27me3 (07-449), anti-H3K4me3 (ab8580), anti-H3 (06-755)) or 5 μl (for anti-Suz12 (3737)) test antibodies, or 5 μg IgG control, except for Fig. 3d, where 1.5 × 10^5 cell equivalents were incubated with 2 μg anti-H3K27me3 (07-449), anti-H3 (06-755)) or IgG. Protein–DNA complexes were bound to 75 μl 50% protein A slurry or 30 μl Protein A Magnetic Beads for 5–6 h at 4 °C and washed 1 × with low-salt buffer (20 mM Tris-HCl pH 8.1, 150 mM $NaCl_2$, 2 mM EDTA, 1% Triton X-100, 0.1% SDS), high-salt buffer (20 mM Tris-HCl pH 8.1, 500 mM $NaCl_2$, 2 mM EDTA, 1% Triton X-100, 0.1% SDS), LiCl buffer (10 mM Tris-HCl pH 8.1, 1 mM EDTA, 1% deoxycholate, 1% NP40, 0.25 M LiCl) and Tris EDTA (10 mM Tris-HCl pH 8, 1 mM EDTA). Samples were eluted, cross-linking was reversed and DNA was purified using the iPure Kit (Diagenode).

ChIP sequencing. Libraries were prepared according to standard Illumina protocols and were validated with the Agilent Bioanalyzer. Single, 36-bp read sequencing runs were performed on an Illumina GAIIx, except for the Suz12, Mta2 and Mi2β ChIP-seq for which single, 50-bp reads were sequenced on a HiSeq2000. Image analysis and base calling was performed with the Illumina pipeline and reads were aligned to the mm9 mouse genome with Bowtie[53]. ChIP-seq tag libraries from two experiments were combined for the analysis of WT DN3, DN4 and DP H3K27me3, and input samples. For visualization in the UCSC genome browser, either Wig files were generated by extending the reads to 200 bp length and the read densities in 25 bp bins were normalized to the library size, or quantile-normalized 200 bp binned BedGraph tracks were used. All analyses were performed with unique reads that did not overlap with >5 bp with known short or long interspersed nuclear elements, long terminal repeats and satellites. Wig tracks of the Suz12 data in ILC87-Ik1-ER cells (Fig. 5a) were also normalized by the 10% trimmed mean peak-tag counts.

Peak callings and filtering. All peak calling analyses were performed with unique reads that did not overlap with >5 bp with known short or long interspersed nuclear elements, long terminal repeats and satellites. H3K27me3 and H3K4me3 peak callings were performed using SICER v1.1 (ref. 54) with the following settings for the analysis of DP cells (Fig. 1 and Supplementary Fig. 1): window size = 200; fragment length = 200, *E*-value = 100, window *P*-value = 0.02, false discovery rate = 10^{-3} and gap size set to 1,400 for H3K27me3 and 800 for H3K4me3, respectively. For the analysis of H3K27me3 on thymocyte subsets, LSK cells (Fig. 2 and Supplementary Fig. 2) and ILC87-Ik1-ER cells (Fig. 5), window size = 200; fragment length = 300, *E*-value = 0.1, window *P*-value = 0.004, false discovery rate = 10^{-3} and gap size = 1,200 were used. The same settings, except for gap size = 600, were used for the H3K4me3 data from DN3 cells (Fig. 8). For the data from DP cells (Fig. 1 and Supplementary Fig. 1), eligible islands were required to be min 800 bp for H3K27me3 and 400 bp for H3K4me3, to have >50 tags and a tag number/island length value >0.03 for H3K27me3 and >0.04 for H3K4me3 in the merged genomic regions. Only the most TSS-proximal islands were considered per gene. For primary thymocyte subsets and LSK cells (Figs 2 and 8, and Supplementary Fig. 2; H3K27me3 and H3K4me3), islands identified by SICER were further filtered to be ≥800 bp long, with SICER island scores >45 and the tag/length ratio >0.04. H3K27me3 islands corresponding to merged regions with the following characteristics were excluded from further analysis: regions ≤1.2 kb that are >5 kb away from the closest TSS (to eliminate small intergenic 'islands' that probably result from sequencing noise), regions <2 kb that are in close vicinity (<5 kb) to a longer (≥3 ×) island (to prevent the selection of island 'tails' as separate islands) and merged regions in which the input's normalized tag/length ratio is >0.024. MACS v1.4 (ref. 55) was used for peak calling on Ikaros, Suz12, Mta2 and Mi2β ChIP-seq samples using default parameters with the following modifications: band width was provided as the fragment length of the libraries according to the Agilent Bioanalyzer and *P*-value cutoff was set to 10^{-7}.

Annotation, quantification and normalization. Merged genomic regions of overlapping peaks across samples were created using mergeBed from the BEDTools suite (2.16.2)[56]. The annotations and tag numbers were determined by the HOMER software[57]. Promoters were defined as regions between −10 and 1 kb relative to TSS; other annotated features (untranslated regions, introns, exons, transcription termination sites and non-coding) downstream of the 1 kb position were commonly referred to as gene body (intragenic) regions; and all other genomic positions were labelled intergenic. Tag numbers for all data sets were normalized to the library sizes. For fold-change comparisons, pairwise normalization between WT and mutant samples were done as follows: for DP samples (Fig. 1 and Supplementary Fig. 1), the 10% trimmed means were used to normalize the larger data set; for the data in Fig. 2 and Supplementary Fig. 2, linear regression lines were calculated for each WT/mutant pair, and the equation of the line was used for normalization. HOMER was used to generate coverage plots and the data matrices for tag density heatmaps that were normalized using the 10% trimmed-mean for Figs 1b, 3a and 4a, and Supplementary Fig. 1a. Clustering was performed using Cluster 3.0 and visualized with Java Tree View. For motif analysis of Ikaros peaks, enriched motifs were identified with the MEME software and matched to transcription factor-binding sites in the Jaspar data base with the Tomtom algorithm. The labelling of GGAA-containing motifs as Ikaros motifs derives from ChIP-seq studies for Ikaros in T and B cells[5,6,24–26]. The identity of the Ets1 motif was inferred from the study by Hollenhorst *et al.*[58].

IP of nuclear extracts and western blot analysis. Cells were incubated in hypotonic buffer (10 mM HEPES pH 7.3, 1.5 mM $MgCl_2$, 10 mM KCl, 0.5 mM dithiothreitol (DTT), 1 × PIC, 1 × phosphatase inhibitor cocktail (Sigma), 1 mM NaF, 0.5 mM phenylmethyl sulphonyl fluoride) on ice and pelleted. Nuclei were lysed in RIPA buffer (50 mM Tris pH 8.1, 150 mM $NaCl_2$, 2 mM EDTA, 1% NP40,

0.5% Na-deoxycholate, 0.1% SDS, 0.5 mM DTT, 1 × PIC, 1 × phosphatase inhibitor cocktail, 1 mM NaF, 0.5 mM phenylmethyl sulphonyl fluoride) for 30 min at 4 °C. Nuclear extracts were cleared by centrifugation. For each IP reaction, 500 µl extract was pre-cleared with 50 µl Protein A Sepharose 50% bead slurry that was previously washed and blocked with 0.5 mg ml^{-1} BSA. Pre-cleared extracts were incubated with 2.5–5 µg anti-Ikaros or 5 µl anti-Suz12 antibodies, or 5 µg rabbit IgG ON at 4 °C. Antibody–protein complexes were captured with 100 µl 50% bead slurry for 5–6 h and washed 5 × at 4 °C with RIPA buffer containing 300 mM $NaCl_2$, and subsequently denatured by boiling with SDS–PAGE loading buffer.

To deplete NuRD, a 2.4-ml BSA-blocked half-and-half mix of Protein A and Protein G Sepharose 50% bead slurry was coated with 60 µg anti-Mta2 and 40 µg anti-Mi2β ON at 4 °C and washed 5 × with RIPA buffer (without DTT). Another 2.4 ml Protein A + G mix was coated with 100 µg rabbit IgG as negative control. Two millilitres of nuclear extracts were incubated in three consecutive steps with 0.8 ml of antibody- or 0.8 ml of control IgG-coupled beads for 3 h 2 × and ON 1 × at 4 °C. After incubating with 200 µl BSA-blocked Protein A + G 50% bead slurry for an additional 1 h at 4 °C, supernatants from each were recovered, sampled for input and split into four. IPs on 'depleted' and control nuclear extracts were performed for 8 h at 4 °C using 100 µl BSA blocked Protein A bead slurry coated with either 5 µg anti-Ikaros, anti-Mta2 or rabbit IgG, or 100 µl Protein G slurry coated with 5 µg anti-Mi2β. Beads were then washed 5 × at 4 °C with RIPA containing 300 mM $NaCl_2$ and subsequently denatured by boiling with SDS–PAGE loading buffer.

Proteins were separated on SDS polyacrylamide gels, transferred to polyvinylidene difluoride membranes (Millipore) and detected using horseradish-peroxidase-conjugated secondary antibodies and chemiluminescence (Pierce, Millipore). Primary antibodies were used at 1:1,000 dilution. Western blot images were cropped for presentation. Full-size images are presented in Supplementary Figs 10 and 11.

Transcriptome analysis. LSK cells were sorted from 6- to 7-week-old WT and $Ik^{L/L}$ mice. RNA was extracted from 5×10^4 cells and used for transcriptome analysis with Affymetrix 430 2.0 arrays using standard amplification methods. LSK transcriptome data were normalized with those from DN3, DN4 and DP cells (GSE 46090) with the Robust Multiarray Average algorithm. K-means clustering was performed using Cluster 3. Transcriptome analysis of the ILC87-Ik1-ER cells treated with ethanol or 4OHT for 24 h was performed with the Affymetrix Gene ST 1.0 arrays.

GST pull-down assay. The full-length Ik1 isoform was cloned into the pGEXT2 plasmid downstream of the GST tag. *E. coli* BL21 was transformed with pGEX2T-Ik1 or the empty vector expressing GST alone. ON cultures were initiated from single colonies, diluted 50 ×, expanded for ~2 hours until $OD_{600} = 0.5–0.6$ and induced with 1 µM isopropyl-β-D-thiogalactoside at 16 °C for 13 h. Bacteria were pelleted at 5,000*g* for 5 min and lysed in 400 µl per 5 ml of the original culture volume of lysis buffer (50 mM NaH_2PO_4 pH 8.0, 300 mM NaCl containing 1 × PIC, 1 mM DTT, 1 mg ml^{-1} lysozyme) for 30 min on ice and sonicated. Lysates were cleared by centrifugation at 14,000 r.p.m. for 20 min at 4 °C and the SN was saved as the soluble protein extract. Glutathione agarose beads (Thermo Scientific) were washed 5 × with 50 mM NaH_2PO_4 pH 8.0, 300 mM NaCl and 50 µl of the 50% bead slurry was incubated with 400 µl protein extract for 3 h at 4 °C and washed again 5 ×. The recovery of the GST-Ik1 and GST proteins in the soluble protein extracts and their efficient capture on the beads was validated by SDS–PAGE and Coomassie Blue staining. Fifty microlitres of the 50% bead slurry with immobilized GST-Ik1 or GST, or beads alone, were then incubated with nuclear extracts of Ikaros-null ILC87 cells ON at 4 °C. Beads were washed 5 × with RIPA buffer containing 300 mM NaCl and analysed by western blotting.

PCR primers. Primers used for ChIP–qPCR and reverse transcriptase-qPCR are listed in Supplementary Table 4.

References

1. Zhang, J. A., Mortazavi, A., Williams, B. A., Wold, B. J. & Rothenberg, E. V. Dynamic transformations of genome-wide epigenetic marking and transcriptional control establish T cell identity. *Cell* **149,** 467–482 (2012).
2. Mingueneau, M. *et al.* The transcriptional landscape of alphabeta T cell differentiation. *Nat. Immunol.* **14,** 619–632 (2013).
3. Vigano, M. A. *et al.* An epigenetic profile of early T-cell development from multipotent progenitors to committed T-cell descendants. *Eur. J. Immunol.* **44,** 1181–1193 (2014).
4. Ng, S. Y., Yoshida, T., Zhang, J. & Georgopoulos, K. Genome-wide lineage-specific transcriptional networks underscore Ikaros-dependent lymphoid priming in hematopoietic stem cells. *Immunity* **30,** 493–507 (2009).
5. Geimer Le Lay, A. S. *et al.* The tumor suppressor Ikaros shapes the repertoire of Notch target genes in T cells. *Sci. Signal.* **7,** ra28 (2014).
6. Zhang, J. *et al.* Harnessing of the nucleosome-remodeling-deacetylase complex controls lymphocyte development and prevents leukemogenesis. *Nat. Immunol.* **13,** 86–94 (2012).
7. Urban, J. A. & Winandy, S. Ikaros null mice display defects in T cell selection and CD4 versus CD8 lineage decisions. *J. Immunol.* **173,** 4470–4478 (2004).
8. Quirion, M. R., Gregory, G. D., Umetsu, S. E., Winandy, S. & Brown, M. A. Ikaros is a regulator of Th2 cell differentiation. *J. Immunol.* **182,** 741–745 (2009).
9. Thomas, R. M. *et al.* Ikaros silences T-bet expression and interferon-gamma production during T helper 2 differentiation. *J. Biol. Chem.* **285,** 2545–2553 (2010).
10. Wong, L. Y., Hatfield, J. K. & Brown, M. A. Ikaros sets the potential for Th17 lineage gene expression through effects on chromatin state in early T cell development. *J. Biol. Chem.* **288,** 35170–35179 (2013).
11. Avitahl, N. *et al.* Ikaros sets thresholds for T cell activation and regulates chromosome propagation. *Immunity* **10,** 333–343 (1999).
12. Kim, J. *et al.* Ikaros DNA-binding proteins direct formation of chromatin remodeling complexes in lymphocytes. *Immunity* **10,** 345–355 (1999).
13. Sridharan, R. & Smale, S. T. Predominant interaction of both Ikaros and Helios with the NuRD complex in immature thymocytes. *J. Biol. Chem.* **282,** 30227–30238 (2007).
14. Dumortier, A. *et al.* Notch activation is an early and critical event during T-cell leukemogenesis in Ikaros-deficient mice. *Mol. Cell. Biol.* **26,** 209–220 (2006).
15. Kleinmann, E., Geimer Le Lay, A. S., Sellars, M., Kastner, P. & Chan, S. Ikaros represses the transcriptional response to Notch signaling in T-cell development. *Mol. Cell. Biol.* **28,** 7465–7475 (2008).
16. Kirstetter, P., Thomas, M., Dierich, A., Kastner, P. & Chan, S. Ikaros is critical for B cell differentiation and function. *Eur. J. Immunol.* **32,** 720–730 (2002).
17. Karlsson, G. *et al.* The tetraspanin CD9 affords high-purity capture of all murine hematopoietic stem cells. *Cell Rep.* **4,** 642–648 (2013).
18. Jeannet, R., Cai, Q., Liu, H., Vu, H. & Kuo, Y. H. Alcam regulates long-term hematopoietic stem cell engraftment and self-renewal. *Stem Cells* **31,** 560–571 (2013).
19. de Laval, B. *et al.* Thrombopoietin promotes NHEJ DNA repair in hematopoietic stem cells through specific activation of Erk and NF-kappaB pathways and their target, IEX-1. *Blood* **123,** 509–519 (2014).
20. Sugano, Y. *et al.* Junctional adhesion molecule-A, JAM-A, is a novel cell-surface marker for long-term repopulating hematopoietic stem cells. *Blood* **111,** 1167–1172 (2008).
21. Sanjuan-Pla, A. *et al.* Platelet-biased stem cells reside at the apex of the haematopoietic stem-cell hierarchy. *Nature* **502,** 232–236 (2013).
22. Ooi, A. G. *et al.* The adhesion molecule esam1 is a novel hematopoietic stem cell marker. *Stem Cells* **27,** 653–661 (2009).
23. Yin, A. H. *et al.* AC133, a novel marker for human hematopoietic stem and progenitor cells. *Blood* **90,** 5002–5012 (1997).
24. Ferreiros-Vidal, I. *et al.* Genome-wide identification of Ikaros targets elucidates its contribution to mouse B-cell lineage specification and pre-B-cell differentiation. *Blood* **121,** 1769–1782 (2013).
25. Schjerven, H. *et al.* Selective regulation of lymphopoiesis and leukemogenesis by individual zinc fingers of Ikaros. *Nat. Immunol.* **14,** 1073–1083 (2013).
26. Schwickert, T. A. *et al.* Stage-specific control of early B cell development by the transcription factor Ikaros. *Nat. Immunol.* **15,** 283–293 (2014).
27. Molnar, A. & Georgopoulos, K. The Ikaros gene encodes a family of functionally diverse zinc finger DNA-binding proteins. *Mol. Cell. Biol.* **14,** 8292–8303 (1994).
28. Hahm, K. *et al.* Helios, a T cell-restricted Ikaros family member that quantitatively associates with Ikaros at centromeric heterochromatin. *Genes Dev.* **12,** 782–796 (1998).
29. Cobb, B. S. *et al.* Targeting of Ikaros to pericentromeric heterochromatin by direct DNA binding. *Genes Dev.* **14,** 2146–2160 (2000).
30. Kehle, J. *et al.* dMi-2, a hunchback-interacting protein that functions in polycomb repression. *Science* **282,** 1897–1900 (1998).
31. Zhang, H. *et al.* The CHD3 remodeler PICKLE promotes trimethylation of histone H3 lysine 27. *J. Biol. Chem.* **283,** 22637–22648 (2008).
32. Zhang, H., Bishop, B., Ringenberg, W., Muir, W. M. & Ogas, J. The CHD3 remodeler PICKLE associates with genes enriched for trimethylation of histone H3 lysine 27. *Plant Physiol.* **159,** 418–432 (2012).
33. Reynolds, N. *et al.* NuRD-mediated deacetylation of H3K27 facilitates recruitment of Polycomb repressive complex 2 to direct gene repression. *EMBO J.* **31,** 593–605 (2012).
34. Sparmann, A. *et al.* The chromodomain helicase Chd4 is required for Polycomb-mediated inhibition of astroglial differentiation. *EMBO J.* **32,** 1598–1612 (2013).
35. Riising, E. M. *et al.* Gene silencing triggers polycomb repressive complex 2 recruitment to CpG islands genome wide. *Mol. Cell* **55,** 347–360 (2014).
36. Zhang, J. *et al.* The genetic basis of early T-cell precursor acute lymphoblastic leukaemia. *Nature* **481,** 157–163 (2012).
37. Mullighan, C. G. *et al.* Deletion of IKZF1 and prognosis in acute lymphoblastic leukemia. *N. Engl. J. Med.* **360,** 470–480 (2009).

38. Theocharides, A. P. *et al.* Dominant-negative Ikaros cooperates with BCR-ABL1 to induce human acute myeloid leukemia in xenografts. *Leukemia* **29,** 177–187 (2015).
39. Tumes, D. J. *et al.* The polycomb protein Ezh2 regulates differentiation and plasticity of CD4(+) T helper type 1 and type 2 cells. *Immunity* **39,** 819–832 (2013).
40. Allman, D. *et al.* Ikaros is required for plasmacytoid dendritic cell differentiation. *Blood* **108,** 4025–4034 (2006).
41. Ross, J., Mavoungou, L., Bresnick, E. H. & Milot, E. GATA-1 utilizes Ikaros and polycomb repressive complex 2 to suppress Hes1 and to promote erythropoiesis. *Mol. Cell. Biol.* **32,** 3624–3638 (2012).
42. Di Croce, L. & Helin, K. Transcriptional regulation by Polycomb group proteins. *Nat. Struct. Mol. Biol.* **20,** 1147–1155 (2013).
43. Brown, J. L. & Kassis, J. A. Architectural and functional diversity of polycomb group response elements in *Drosophila*. *Genetics* **195,** 407–419 (2013).
44. Woo, C. J., Kharchenko, P. V., Daheron, L, Park, P. J. & Kingston, R. E. Variable requirements for DNA-binding proteins at polycomb-dependent repressive regions in human HOX clusters. *Mol. Cell. Biol.* **33,** 3274–3285 (2013).
45. Arnold, P. *et al.* Modeling of epigenome dynamics identifies transcription factors that mediate Polycomb targeting. *Genome Res.* **23,** 60–73 (2013).
46. Dietrich, N. *et al.* REST-mediated recruitment of polycomb repressor complexes in mammalian cells. *PLoS Genet.* **8,** e1002494 (2012).
47. Arvey, A. *et al.* Inflammation-induced repression of chromatin bound by the transcription factor Foxp3 in regulatory T cells. *Nat. Immunol.* **15,** 580–587 (2014).
48. Mendenhall, E. M. *et al.* GC-rich sequence elements recruit PRC2 in mammalian ES cells. *PLoS Genet.* **6,** e1001244 (2010).
49. Indra, A. K. *et al.* Temporally-controlled site-specific mutagenesis in the basal layer of the epidermis: comparison of the recombinase activity of the tamoxifen-inducible Cre-ER(T) and Cre-ER(T2) recombinases. *Nucleic Acids Res.* **27,** 4324–4327 (1999).
50. Gachet, S. *et al.* Leukemia-initiating cell activity requires calcineurin in T-cell acute lymphoblastic leukemia. *Leukemia* **27,** 2289–2300 (2013).
51. Heizmann, B., Kastner, P. & Chan, S. Ikaros is absolutely required for pre-B cell differentiation by attenuating IL-7 signals. *J. Exp. Med.* **210,** 2823–2832 (2013).
52. Lee, P. P. *et al.* A critical role for Dnmt1 and DNA methylation in T cell development, function, and survival. *Immunity* **15,** 763–774 (2001).
53. Langmead, B. Aligning short sequencing reads with Bowtie. *Curr. Protoc. Bioinformatics* **32,** 11.7.1–11.7.14 (2010).
54. Zang, C. *et al.* A clustering approach for identification of enriched domains from histone modification ChIP-Seq data. *Bioinformatics* **25,** 1952–1958 (2009).
55. Zhang, Y. *et al.* Model-based analysis of ChIP-Seq (MACS). *Genome Biol.* **9,** R137 (2008).
56. Quinlan, A. R. & Hall, I. M. BEDTools: a flexible suite of utilities for comparing genomic features. *Bioinformatics* **26,** 841–842 (2010).
57. Heinz, S. *et al.* Simple combinations of lineage-determining transcription factors prime cis-regulatory elements required for macrophage and B cell identities. *Mol. Cell* **38,** 576–589 (2010).
58. Hollenhorst, P. C. *et al.* Oncogenic ETS proteins mimic activated RAS/MAPK signaling in prostate cells. *Genes Dev.* **25,** 2147–2157 (2011).

Acknowledgements

We thank J. Ghysdael for the pMCSV-mBcl2-DsRed vector and discussions; W. Pear for the MigR1 vector; G. Nolan for the Eco-Phoenix cells; A.S. Geimer Le Lay for the Ik1-ER vector; P. Marchal for technical support; members of the Kastner/Chan lab for help and discussions; C. Thibault for the IGBMC microarray and sequencing platform; M. Gendron and S. Falcone for animal husbandry; and C. Ebel for cell sorting. S.C. and P.K. received grants from the Agence Nationale de la Recherche (ANR-11-BSV3-018), La Ligue Contre le Cancer (Equipe Labellisée 2006-2012, 2015-2017), the Institut National du Cancer (INCa #2011-144), the Fondation ARC (SFI20101201884, CR309/8511) and Institute Funding from INSERM, CNRS, Université de Strasbourg and the ANR-10-LABX-0030-INRT grant. A.O. received postdoctoral fellowships from INCa and the Fondation pour la Recherche Médicale, and further support from the ANR grant. A.A. received a predoctoral fellowship from the Ministère de la Recherche et de la Technologie. K.P. received a predoctoral fellowship from a European Initial Training Network (HEM-ID).

Author contributions

A.O. designed and performed most of the experiments and analysed the data. A.A. generated constructs and K.P. analysed mutant strains. B.J. and S.L.G. provided support for the high-throughput experiments and analyses. S.C. and P.K. supervised the research. A.O., S.C. and P.K. wrote the paper.

Additional information

Accession numbers: Microarray and ChIP-seq data generated in this study are available from the GEO database under the accession number GSE 61149.

Supplementary Information accompanies this paper at http://www.nature.com/naturecommunications

Competing financial interests: The authors declare no competing financial interests.

Reprints and permission information is available online at http://npg.nature.com/reprintsandpermissions/

How to cite this article: Oravecz, A. *et al.* Ikaros mediates gene silencing in T cells through Polycomb repressive complex 2. *Nat. Commun.* 6:8823 doi: 10.1038/ncomms9823 (2015).

Katarzyna POLAK

Role of the Eos and Helios transcription factors in regulatory T cell biology

Résumé

Les cellules T régulatrices (Treg) sont responsables de la maintenance de l'homéostasie immunitaire. Les facteurs de transcription Eos et Helios ont été décrits comme étant des modulateurs des fonctions des cellules Treg. Ils sont impliqués dans la régulation de Foxp3 qui est un marqueur clé et un facteur fonctionnel des cellules Treg $CD4^+$ régulatrices. Néanmoins, leur potentiel rôle dans la biologie des cellules Treg reste controversé. En effet, l'utilisation de différents systèmes ont produits des données contradictoires. Pour clarifier si Eos et Helios peuvent réguler les cellules Treg *in vivo*, nous avons dans un premier temps étudié les souris déficientes pour l'un ou l'autre de ces facteurs. Nous avons montré qu'Eos et Helios sont différemment exprimés dans les cellules Treg. Nos résultats suggèrent qu'Eos et Helios ne sont pas nécessaires, ni pour la différenciation, ni pour les principales fonctions des cellules Treg $CD4^+$. Cependant, les cellules $Helios^{-/-}$ présentent une meilleure activité suppressive comparée aux cellules contrôles et à un profil transcriptomique de cellules Treg activées. Pour tester si Eos et Helios coopèrent pour réguler les fonctions des cellules Treg, nous avons, dans un second temps, analysé les souris doubles mutantes. Nos découvertes indiquent que la perte combinée d'Eos et d'Helios n'a pas d'effet sur la biologie des cellules Treg dans des conditions homéostatiques. De plus, nous avons montré qu'Eos et Helios sont induits dans les cellules Treg $CD8^+$. Néanmoins, seule la perte d'Helios ou celle combinée d'Eos et d'Helios affectent leur différenciation. Tous ces résultats suggèrent donc qu'Eos et Helios ne sont pas requis et ne coopèrent pas pour réguler les fonctions essentielles des cellules Treg $CD4^+$. Toutefois, l'absence d'Helios pourrait avoir un impact sur leur niveau d'activation. Finalement, nous avons mis en évidence un potentiel rôle d'Helios et d'Eos dans le compartiment de cellules Treg $CD8^+$.

Mots clés: facteurs de transcription, Eos, Helios, cellules T régulatrices, Treg

Summary

Regulatory T cells (Treg) are responsible for the maintenance of immune homeostasis. The transcription factors Eos and Helios have been described as modulators of Treg cell functions. They are involved in the regulation of Foxp3, a key marker and functional factor for $CD4^+$ regulatory T cells. Nonetheless, their potential roles in Treg cell biology remain controversial as conflicting data has been published depending on the system used. To clarify if Eos and Helios can regulate Treg cells, we first studied mice deficient for one or the other of these factors. We showed that Eos and Helios are differentially expressed in Treg cells. Our results suggest that Eos and Helios are not necessary for the differentiation and essential functions of $CD4^+$ Treg cells. However, $Helios^{-/-}$ cells present a superior suppressive activity compared to control cells and a transcriptional profile of activated Treg cells. To test if Eos and Helios can cooperate to regulate Treg cell functions, we then analyzed double null mice. Our findings indicate that loss of both Eos and Helios has no effect on Treg cell biology during homeostasis. In addition, we showed that Eos and Helios are induced in $CD8^+$ Treg cells. However, only loss of Helios, or both Helios and Eos, affect their differentiation. Altogether, these results suggest that Eos and Helios are not required and do not cooperate to regulate essential $CD4^+$ Treg cell functions, but the absence of Helios may have an impact on their level of activation. Finally, we showed a potential role of Helios and Eos in the $CD8^+$ Treg cell compartment.

Key words: transcription factors, Eos, Helios, regulatory T cells, Treg